UNDERSTANDING SOURCES AND CYCLING OF MERCURY USING MERCURY STABLE ISOTOPES

by

Laura S. Sherman

A dissertation submitted in partial fulfillment
of the requirements for the degree of
Doctor of Philosophy
(Earth and Environmental Sciences)
in The University of Michigan
2012

Doctoral Committee:

Professor Joel D. Blum, Chair
Professor Rodney C. Ewing
Professor Gerald J. Keeler (Deceased)
Professor Kyger C. Lohmann
Assistant Professor Niladri Basu
Assistant Professor J. Timothy Dvonch

© Laura S. Sherman
2012

To my parents
for their support and encouragement

and in memory of my friend and mentor
Dr. Jerry Keeler

ACKNOWLEDGEMENTS

The research presented in this dissertation was made possible by funding from the National Science Foundation, the National Aeronautic and Space Administration, Environment Canada, the Florida Department of Environmental Protection, the John D. MacArthur Professorship at the University of Michigan to Joel D. Blum, and a Scott Turner research award through the University of Michigan Earth and Environmental Sciences Department. Additional funding for my graduate studies was provided by a National Defense Science and Engineering Graduate Fellowship (DOD-ONR) and a Graham Environmental Sustainability Institute Doctoral Fellowship. I am grateful for these fellowships and the numerous opportunities that this funding has given me.

I would like to acknowledge my collaborators and co-authors. This research would not have been possible without their assistance with study design, sample collection and analysis, data interpretation, and manuscript preparation. Joel Blum, Kirk Nordstrom, Blaine McCleskey, Tamar Barkay, and Costa Ventriani are co-authors on Chapter 2 (published in *Earth and Planetary Science Letters*); Joel Blum, Kelsey Johnson, Jerry Keeler, Jim Barres, and Tom Douglas are co-authors on Chapter 3 (published in *Nature Geoscience*); Joel Blum, Tom Douglas, and Sandy Steffen are co-authors on Chapter 4 (published in the *Journal of Geophysical Research*); Joel Blum, Jerry Keeler, Jason Demers, and Tim Dvonch are co-authors on Chapter 5 (published in *Environmental*

Science and Technology); and Joel Blum is a co-author on Chapter 6 (in review at *Science of the Total Environment*).

I would also like to thank my dissertation committee members: Rod Ewing, Jerry Keeler, Kacey Lohmann, Nil Basu, and Tim Dvonch. Their input throughout my graduate studies has helped to improve this dissertation and expand my scientific knowledge. I would especially like to thank and remember Jerry Keeler. He was devoted to the production of scientifically sound data and to the thoughtful interpretation of those data. Jerry and his former graduate students, Lynne Gratz and Tim Dvonch, taught me everything that I know about atmospheric science. During the months before he passed away, we met every two weeks to jointly interpret isotopic, trace metal, and meteorological data (presented in Chapter 5). Even when he could barely get out of bed, he managed to devote entire afternoons to my research. I will be forever grateful for his mentorship, generosity, humor, and long, tangential stories.

In addition to my committee members, I would like to specifically thank my advisor and chair, Joel Blum. I chose the University of Michigan for graduate school specifically to work with Joel and I have never once regretted that decision. Joel has always listened to my ideas (even when they were wrong), treated me with respect, and pushed me to reach my potential. He has also always been available (even when I bother him multiple times a day) and always returns my work promptly with constructive comments. I have learned a great deal from Joel and I know that I will be well prepared to tackle future challenges thanks to his mentorship.

I would also like to thank Marcus Johnson and Jim Barres for teaching me so much about trace element sample collection, laboratory work, and sample analysis.

During many long hours in the University of Michigan Air Quality Laboratory (UMAQL) and on field trips to Florida, Jim was always ready to lend me a hand or at least ready to make me laugh and take a photograph of the situation. I will always be grateful for his help with my fieldwork preparations and sample collection in Florida. Marcus has been my constant guide, mentor, and friend in the University of Michigan Biogeochemistry and Environmental Isotope Geochemistry Laboratory (UM BEIGL). We have spent many hours scheming over analytical methods and pouring through data. He has never hesitated to drop whatever he is doing to help me and I will be forever thankful.

Thank you also to my fellow graduate students and postdocs. I would especially like to thank Lynne Gratz, Jason Demers, Gretchen Gehrke, Kelsey Johnson, Patrick Donovan, and Sae Yon Kwon in UM BEIGL and UMAQL. Their company, assistance, and humor made many long hours in the lab and in Florida enjoyable. Thank you to my other friends in the Earth and Environmental Science Department, especially Jessica Malone, Alison Duvall, Dan Horton, Louise Jeffrey, and Laura Waters. I would also like to thank to all of my friends in the Graham Environmental Sustainability Institute, especially Laura Smith, Krista Badiane, Paul Coseo, and Darshan Karwat for the wonderful discussions and friendship over the last two years.

Finally, I would like to thank my family and friends outside of the University of Michigan. Thank you to my Dad and Janet for always supporting me and reminding me that "[I] can do anything I put my little mind to." Thank you to Peter for making me laugh and reminding me never to take myself too seriously. Thank you to my Mom for teaching me never to give up and for all of her love. I only wish that she could be here to

share in this accomplishment. I would also like to thank my large extended hockey family for keeping me sane and healthy throughout this journey. Finally, I would like to extend a heartfelt thank you to Shawna and Chelsea for keeping me happy, well fed, wrapped in love, and covered in puppy kisses when I have most needed it.

TABLE OF CONTENTS

DEDICATION……...…ii

ACKNOWLEDGEMENTS…….iii

LIST OF FIGURES……...x

LIST OF TABLES……...xii

ABSTRACT……....xiii

CHAPTER 1 Introduction……..……...1
1.1 Mercury as a hazardous pollutant 1
1.2 Mercury speciation.....2
1.3 Sources of mercury 3
1.4 Mercury stable isotope ratios 4
1.5 Applications of Hg stable isotopes: Dissertation structure 6

CHAPTER 2 Mercury isotopic composition of hydrothermal systems in the Yellowstone volcanic field and Guaymas Basin sea-floor rift.....18
2.1 Introduction.....19
2.2 Description of sampling localities 22
2.2.1 Yellowstone Plateau volcanic field.....22
2.2.2 Guaymas Basin 23
2.3 Methods.....24
2.3.1 Sample collection.....24
2.3.2 Sample processing 25
2.3.2.1 Liquid samples 27
2.3.2.2 Solid samples 27
2.3.3 Mineralogical characterization.....27
2.3.4 Isotopic analyses 28
2.4 Results.....29
2.4.1 Sample characterization 29
2.4.2 Mercury concentrations and recovery.....30
2.4.3 Mercury isotopic compositions.....31
2.5 Mercury isotopes in hydrothermal systems 34
2.5.1 Mass-dependent fractionation.....34
2.5.2 Mass-independent fractionation.....38
2.6 Conclusions and implications 40

CHAPTER 3 Mass-independent fractionation of mercury isotopes in Arctic snow driven by sunlight 57
3.1 Introduction 57
3.2 Main text 58
3.3 Methods 64

CHAPTER 4 Frost flowers growing in the Arctic ocean-atmosphere-sea ice-snow interface: 2. Mercury exchange between the atmosphere, snow, and frost flowers 75
4.1 Introduction 76
4.2 Mercury stable isotopes 78
4.3 Methods 80
4.3.1 Sample collection 80
4.3.2 Analytical methods 82
4.4 Results 84
4.5 Discussion 86
4.6 Conclusions 91

CHAPTER 5 Investigation of local mercury deposition from a coal-fired power plant using mercury isotopes 106
5.1 Introduction 107
5.1.1 Mercury stable isotopes 108
5.2 Experimental 109
5.2.1 Site descriptions 109
5.2.2 Sample collection 111
5.2.3 Meteorological analysis 111
5.2.4 Sample processing and analysis 112
5.3 Results and discussion 114
5.3.1 Precipitation events 114
5.3.2 Mercury concentrations 116
5.3.3 Mercury isotopic compositions 117
5.3.3.1 Factors influencing Hg isotopic composition 119
5.3.3.1.1 Source isotopic composition 119
5.3.3.1.2 In-system fractionation 120
5.3.3.1.3 Post-emission atmospheric fractionation 121
5.4 Supplemental information 135
5.4.1 Experimental 135
5.4.1.1 Sample collection 135
5.4.1.2 Meteorological analysis 135
5.4.1.3 Statistical analysis 136
5.4.1.4 Sample processing and analysis 136
5.4.1.5 Field blanks 138
5.4.1.6 Procedural standards 139
5.4.2 Results and discussion 140

5.4.2.1 MIF of ^{200}Hg 140

CHAPTER 6 Mercury stable isotopes in sediments and largemouth bass (*Micropterus salmoides*) in Florida lakes 152
6.1 Introduction 153
6.2 Materials and methods 157
6.2.1 Sample collection 157
6.2.2 Sample processing 159
6.2.3 Stable isotope ratio analyses 161
6.3 Results and discussion 162
6.3.1 Water quality parameters 162
6.3.2 Mercury concentrations 163
6.3.3 Carbon and nitrogen isotope ratios 165
6.3.4 Mercury stable isotope ratios 166
6.3.4.1 Lakes closer to (<50 km) the Crystal River CFUB 167
6.3.4.2 Lakes farther from (>50 km) the Crystal River CFUB 170
6.4 Conclusions 177
6.5 Supplemental information 201
6.5.1 Water quality parameters 201
6.5.2 Supplemental data 202
6.5.3 Photochemical demethylation calculations 206

CHAPTER 7 Conclusions 210
7.1 Summary of key findings 211
7.1.1 Methodological advancements 211
7.1.2 Mercury stable isotope fractionation 212
7.1.3 Sources and fate of atmospherically deposited Hg 216
7.2 Future work 219

LIST OF FIGURES

Figure

2.1 Map of Yellowstone National Park boundary with the rim of the Yellowstone Caldera outlined and study areas indicated....48

2.2 Map indicating location of Guaymas Basin in the Gulf of California....49

2.3 Aerial view schematic of Ojo Caliente with sampling locations indicated....50

2.4 Plot of Si/Cl ratios and Hg/Cl ratios in Ojo Caliente from the source pool (OC-1) to the end of the outflow channel (OC-6)....51

2.5a Plot of δ^{202}Hg versus the fraction of Hg remaining in each fluid sample from Ojo Caliente with respect to the Hg concentration in the original vent fluid (f_R)....52

2.5b Same data as Figure 2.5a plotted on a log-log plot....52

2.6 Δ^{199}Hg versus δ^{202}Hg measured in the fluid and sinter samples from Yellowstone National Park and vent precipitates from Guaymas Basin....53

3.1 Mercury isotopic compositions of snow samples, chamber experiment samples, and gaseous samples....71

3.2 Mass-independent fractionation of snow samples and chamber experiment samples....72

3.3 Rayleigh fractionation models showing mercury isotope changes in snow and emitted gas....73

4.1 Map of frost flower sampling area near Barrow, AK with inset map of Alaska....99

4.2 Isotopic composition (δ^{202}Hg versus Δ^{199}Hg) of frost flower, surface snow, and brine samples....100

4.3 Mercury concentration (ng/L) versus Δ^{199}Hg (‰) for frost flower, surface snow, and brine samples....101

4.4 Atmospheric TGM concentrations were measured continuously using a Tekran 2537A at the Barrow Arctic Science Consortium (BASC) located ~4 km north of Barrow, AK....102

4.5 Hypothesized isotopic evolution of frost flower samples, surface snow, and emitted GEM.....103

5.1 Map of Hg emissions sources and sample collection sites with inset showing sites surrounding Crystal River utility.....131

5.2 Precipitation depth (cm) versus log Hg concentration (ng/L).....132

5.3 δ^{202}Hg (‰) versus Δ^{199}Hg (‰) measured in precipitation and coal samples...133

5.4 Δ^{201}Hg (‰) versus Δ^{199}Hg (‰) in precipitation and coal samples.....134

6.1 Map of sample collection sites.....193

6.2 Mercury isotopic composition of sediment and largemouth bass samples.....194

6.3 Mass-independent fractionation of Hg in largemouth bass.....195

6.4 Light penetration depth and DOC concentration versus MIF in largemouth bass.....196

6.5 Bulk sediment isotopic composition versus estimated sediment MeHg isotopic composition.....198

LIST OF TABLES

Table

2.1 Water chemistry properties and solute concentrations measured in fluid samples from Yellowstone National Park 54

2.2 Mercury concentrations, percent recovery, and summary of measured $\delta^{202}Hg$ and $\Delta^{199}Hg$ for all of the fluid and solid samples in this study collected from Yellowstone National Park and Guaymas Basin 55

2.SI-1 Mercury isotopic composition of standards, fluid and sinter samples from Yellowstone National Park, and vent precipitates from Guaymas Basin 56

3.1 Mercury isotopic compositions of standards, snow samples and chamber experiment samples.....74

4.1 Mercury concentrations in frost flower, surface snow, and brine samples.....104

4.2 Mercury isotopic compositions of standards and samples.....105

5.SI-1 Precipitation collection sites in Crystal River and in other FL locations with site descriptions, site IDs, and site locations (i.e., nearest city).....144

5.SI-2 Characteristics of the coal-fired power plants in FL emitting >1 kg of Hg per year.....145

5.SI-3 Meteorological characteristics of precipitation events.....146

5.SI-4 Mercury concentrations and isotopic compositions of standards and samples.....148

6.1 Water quality parameters 200

6.SI-1 Complete concentration and isotopic data 202

6.SI-2 Estimated percent photochemical demethylation of MeHg from FL lakes.....209

ABSTRACT

Mercury (Hg) is a neurotoxin that humans are exposed to primarily through consumption of fish. Significant gaps remain in our knowledge of Hg biogeochemistry and measurement of natural abundance Hg stable isotopes is beginning to answer some of the outstanding questions. Mass-dependent fractionation (MDF, reported as δ^{202}Hg) and mass-independent fractionation (MIF, reported as Δ^{199}Hg) of Hg isotopes occur during many biogeochemical processes.

To better understand Hg cycling in volcanic systems we first investigated the isotopic composition of Hg emissions from Yellowstone volcanic field. We found that the light isotopes of Hg were preferentially emitted as $Hg^0_{(g)}$ from hydrothermal waters, suggesting that natural $Hg^0_{(g)}$ emissions may display negative δ^{202}Hg values.
Next, we used Hg isotopes to explore the role of photochemical reactions in Arctic atmospheric mercury depletion events. We found that a significant percentage of the Hg deposited during these events is subsequently photochemically reduced and lost, producing negative MIF of Hg remaining in the snow. We also found that a portion of the reemitted Hg accumulates on nearby ice crystals. These results suggest that although a large percentage of the Hg deposited during these events is lost from the snow, a portion of the Hg is retained locally and may enter local aquatic ecosystems. Finally, we investigated whether Hg isotopes could be used to trace anthropogenic Hg emissions to deposition sites and ultimately into fish populations. We found that Hg in precipitation

collected downwind of a coal-fired power plant in Florida displayed anomalously negative δ^{202}Hg values. We then explored whether this isotopic signature could be used to trace Hg emitted by the power plant into local sport fish. Instead, we found that Hg in largemouth bass was largely derived from accumulated Hg in lake sediments.

This dissertation demonstrates that measurement of natural Hg isotopes in environmental samples is a powerful tool that can be used to gain greater understanding of complex Hg biogeochemistry. This relatively new technique may allow us to answer difficult questions about Hg atmospheric chemistry and biogeochemistry, to trace natural and anthropogenic Hg emissions, and to better understand pathways of human exposure to this hazardous trace metal.

CHAPTER 1

Introduction

1.1 Mercury as a hazardous pollutant

Mercury (Hg) is a hazardous toxin that can damage the human central nervous system causing severe neurological and developmental defects (*1, 2*). Fetal exposure to monomethylmercury (MeHg) can lead to brain damage, decreased motor skills, and impaired language cognition (*2-4*). Adult exposure to moderate amounts of MeHg may cause elevated risk of cardiovascular disease (*1*) while higher levels of exposure can cause muscle spasms, corrode mucous membranes, damage the immune system, and affect the central nervous system (*5, 6*). Monomethylmercury can also have adverse reproductive effects on piscivorous birds and can cause neurotoxicity and death in mammals that feed on fish (e.g., otter and mink) (*7-9*).

The toxicity of Hg was first widely recognized in the 1950s when fishermen and their families near Minamata Bay, Japan exhibited signs of severe neurological damage (*1, 10, 11*). A local chemical company producing acetaldehyde using Hg as a catalyst released vast quantities of MeHg directly to the bay (*10, 11*). The MeHg subsequently bioaccumulated through the aquatic food web and reached toxic levels in local marine organisms. Although the morbidity and mortality observed at Minamata Bay characterize very high levels of MeHg exposure, such mass poisonings are rare and direct releases of MeHg to waterbodies are uncommon. Today, humans can be exposed to inorganic Hg

occupationally, through deterioration of dental amalgams, and during precious metal mining operations (*1*). However, exposure to significant quantities of inorganic Hg is less common than exposure to organic MeHg through consumption of high trophic level fish (*1, 2*). Monomethylmercury contamination in fish is widespread and all 50 states in the U.S. have issued at least one fish consumption advisory (*12*).

1.2 Mercury speciation

Mercury can exist in the environment in solid, aqueous, and gaseous forms. The biogeochemical cycling of Hg is complex and includes reductive-oxidative reactions, biological processes, and photochemical reactions. As a solid, Hg is usually found in conjunction with sulfides (e.g., cinnabar, HgS) (*13*). In the atmosphere, Hg exists in three operationally defined forms: gaseous elemental Hg ($Hg^0_{(g)}$ or GEM), reactive gaseous Hg (Hg^{2+} or RGM), and fine particle bound Hg ($Hg_{(p)}$). Mercury speciation is important to studies of Hg contamination not only because sources emit varying percentages of each species (see Section 1.3), but also, because these species are deposited from the atmosphere on different spatial and temporal scales. Because $Hg^0_{(g)}$ is a relatively inert gas, it has a long atmospheric residence time (~1-2 years) and can be transported globally (*14, 15*). In contrast, the oxidized forms of Hg (RGM and $Hg_{(p)}$) are water-soluble and highly particle reactive. As a result, these Hg species are rapidly scavenged from the atmosphere and deposited to surface environments (*16, 17*). Mercury deposition can be enhanced near point sources and urban areas because RGM and $Hg_{(p)}$ are often emitted in higher relative proportions from anthropogenic sources (*17-22*). However, Hg deposition is influenced by a variety of factors including local meteorology,

atmospheric oxidants, emission of co-pollutants, and gas-particle interactions (*17, 22, 23*). After it is deposited to the Earth's surface, Hg can be reduced and reemitted to the atmosphere as $Hg^0_{(g)}$ (*15, 24, 25*). Mercury that remains in aquatic ecosystems can be biotically methylated in surface sediments, wetlands, and within anoxic zones in the water column (*26-28*). Because MeHg is rapidly assimilated and slowly eliminated by organisms, it bioaccumulates through food webs reaching hazardous levels in higher order consumers (*29-33*).

1.3 Sources of mercury

Mercury is emitted to the atmosphere by a variety of natural and anthropogenic sources. Natural sources include volcanoes, geothermal systems, wildfires, and evasion from terrestrial and aquatic surfaces (*16, 17, 34-36*). Anthropogenic sources include fossil fuel combustion, caustic soda manufacturing (i.e., the chlor-alkali process), metal smelting, iron and steel manufacturing, waste incineration, cement manufacturing, and precious metal mining (*17, 37, 38*). In the late 1800s, gold and silver mining in the western U.S. resulted in a Hg emissions peak of more than ~2.5 Gg per year (*38, 39*). Currently, fossil fuel combustion (primarily coal) accounts for between one-half and two-thirds of total anthropogenic emissions (*37, 38*). As discussed above, although natural sources of Hg emit primarily $Hg^0_{(g)}$, anthropogenic sources often emit higher proportions of oxidized Hg species that are rapidly deposited (*18-22*). For example, Hg emissions from point sources such as coal-fired power plants and waste incinerators can be 75-95% RGM and $Hg_{(p)}$ (*20, 40*).

Estimates of natural Hg emissions are highly uncertain and complicated by the reemission of previously deposited Hg. Natural processes such as forest fires, emission from soils, and evasion from waterbodies often emit Hg that was originally anthropogenic in origin (*17, 41*). In fact, it is estimated that half of the current 'naturally-emitted' Hg was originally emitted by anthropogenic sources (*42*). Some estimates suggest that natural and anthropogenic emissions of Hg to the atmosphere are roughly equivalent (*16, 17*), whereas others, which attempt to exclude reemission of previously deposited Hg, estimate that anthropogenic emissions are approximately four times greater than natural emissions (*38*). Historic records of Hg deposition based on lake sediments, peat cores, and ice cores indicate that atmospheric deposition of Hg has increased significantly (by 3-11 times) since the Industrial Revolution (*17, 39, 43, 44*).

1.4 Mercury stable isotope ratios

There are seven stable isotopes of Hg with varying natural abundances: ^{196}Hg (0.16%), ^{198}Hg (10.0%), ^{199}Hg (16.9%), ^{200}Hg (23.1%), ^{201}Hg (13.2%), ^{202}Hg (29.7%), ^{204}Hg (6.8%) (*45*). Recent advances in multi-collector inductively-coupled plasma mass spectrometry, including the ability to introduce Hg as a cold vapor and improved methods of instrumental mass bias correction, now allow the precise measurement of Hg stable isotope ratios. In addition, improvements in laboratory methods (including those outlined in this dissertation) now allow reliable measurement of Hg isotope ratios in a wide variety of environmental samples including biological tissues, soils and sediments, gaseous atmospheric samples, and low concentration precipitation samples (*46-51*).

Mercury isotope ratios are reported using delta notation as

$$\delta^{xxx}Hg\ (‰) = ([(^{xxx}Hg/^{198}Hg)_{sample}/(^{xxx}Hg/^{198}Hg)_{SRM\ 3133}] - 1) * 1000 \quad (1)$$

where ^{xxx}Hg is an isotope of Hg and SRM 3133 is a NIST Hg standard (*45*). Significant variations in isotopic composition have been observed in reservoirs including fossil fuels (*47, 52, 53*), the atmosphere and precipitation (*47, 48, 50*), sediments (*46, 51, 54*), and fish (*51, 55-62*). Mass-dependent fractionation (MDF) of Hg stable isotopes occurs during a number of processes including volatilization of $Hg^0_{(aq)}$ from aqueous solutions (*63, 64*), photochemical reduction of Hg from aqueous solutions and snow surfaces (*48, 55*), methylation of inorganic Hg (*65, 66*), and photochemical degradation of MeHg (*55, 67*). Mercury can also undergo mass-independent fractionation (MIF) during both kinetic and equilibrium reactions wherein the odd-mass-number isotopes are either enriched or depleted relative to the even-mass-number isotopes. Mass-independent fractionation is reported as the deviation of a measured isotope ratio from that theoretically predicted to result due to MDF as

$$\Delta^{xxx}Hg = \delta^{xxx}Hg - (\delta^{202}Hg * \beta) \quad (2)$$

For kinetic reactions, β is equal to 0.252 for ^{199}Hg, 0.502 for ^{200}Hg, and 0.752 for ^{201}Hg (*45*). There are currently two mechanisms that are hypothesized to cause MIF of the odd-mass-number isotopes of Hg: the nuclear volume (or nuclear field shift) effect and the magnetic isotope effect (*55, 64, 68, 69*). The nuclear volume effect occurs during equilibrium reactions whereas the magnetic isotope effect is a kinetic phenomenon (*70*). The nuclear volume effect has been predicted theoretically and shown experimentally to cause small amounts of MIF (< ~0.3‰) due to differences in the effective nuclear charge radii between Hg isotopes (*69, 71, 72*). In contrast, high levels of MIF are thought to occur due to the magnetic isotope effect during spin-selective photochemical reactions

that involve the creation of long-lived radical pairs (*55, 73, 74*). Because only the odd-mass-number isotopes of Hg are magnetic and have unpaired nuclear spin, radical pairs involving odd-mass-number isotopes of Hg can recombine at different rates than those with even-mass-number isotopes of Hg. As a result, during reactions that cause MIF, the odd-mass-number isotopes of Hg preferentially accumulate in the products or reactants relative to the even-mass-number isotopes of Hg. Recent studies suggest that MIF of the even-mass-number isotopes of Hg is also possible. There are no currently proposed mechanisms that satisfactorily explain this phenomenon, but it is likely to be an area of active future study (*47, 50*).

1.5 Applications of Hg stable isotopes: Dissertation structure

Although many aspects of Hg biogeochemical cycling are well studied, many questions remain to be explored. Differences in isotopic composition between environmental samples and fractionation of Hg stable isotopes during reactions of interest enable the use of Hg isotopes to better understand Hg biogeochemical cycling and to trace Hg emissions. Over the last five years, as a result of advances in analytical methods and increasing scientific interest, the field of Hg stable isotope geochemistry has significantly expanded. This dissertation begins to answer some of the questions that are now within reach of this exciting field of study and raises additional questions that may be addressed in future investigations (Chapter 7).

In Chapter 2 (published in *Earth and Planetary Science Letters*) we explore the isotopic composition of geothermal Hg emissions. We measured Hg stable isotope ratios in hydrothermal waters and sinters from a large continental hydrothermal system

(Yellowstone Plateau volcanic field) and a sea-floor rift system in the Gulf of California (Guaymas Basin). We found that the light isotopes of Hg were preferentially emitted as $Hg^0_{(g)}$ from the hydrothermal waters of Yellowstone volcanic field (*63*). Coupled with previous studies of Hg isotope systematics in hydrothermal systems (*75, 76*), these data suggest that natural $Hg^0_{(g)}$ emissions from hydrothermal systems are characterized by negative $\delta^{202}Hg$ values. We also observed small positive $\Delta^{199}Hg$ values in the hydrothermal waters but did not observe MIF of Hg isotopes in samples collected at depth in Guaymas Basin (*63*). This finding supports the hypothesis that photochemical reactions cause MIF of Hg isotopes.

After investigating the isotopic composition of Hg emissions from volcanic systems, we used some of the same analytical methods to explore Hg cycling in the Arctic (Chapters 3 and 4). After Polar sunrise, atmospheric mercury depletion events (AMDEs) occur repeatedly until snowmelt. During these events, photochemically initiated reactions involving halogen radicals oxidize $Hg^0_{(g)}$ in the lower atmospheric boundary layer to RGM compounds that are rapidly deposited to the snowpack (*24, 77-79*). This process results in near complete loss of $Hg^0_{(g)}$ from the atmosphere and elevated Hg concentrations in surface snow (*24, 80*). Mercury in the snow can subsequently be photochemically reduced and emitted back to the atmosphere as $Hg^0_{(g)}$. It is unclear how much Hg is photochemically lost from the snowpack and how much remains at the time of snowmelt (*48, 78, 81, 82*).

Chapters 3 (published in *Nature Geoscience*) and 4 (published in *Journal of Geophysical Research*) explore this question using Hg stable isotopes. We observed extreme negative MIF of Hg isotopes in surface snow samples and determined that this

MIF was caused by photochemical loss of up to ~75% Hg from the snow (*48*). In a follow-up study (Chapter 4), we found that a percentage of the Hg that was photochemically emitted from the snow was reoxidized and accumulated on nearby ice crystals (*49*). This suggests that Hg deposited during AMDEs is actively cycled by photochemical reactions and, depending on the conditions, may be lost as $Hg^0_{(g)}$ or retained at the surface and ultimately enter the aquatic food web.

After studying Hg cycling in the remote Arctic, we shifted focus to a polluted urban setting to investigate whether Hg isotopes could be used to link anthropogenic sources of Hg to deposition sites and ultimately to aquatic ecosystems. Elevated levels of Hg have been found across Florida in fish (*83, 84*), wading birds (*85*), and precipitation (*86, 87*). In Chapter 5 (published in *Environmental Science and Technology*) we use Hg stable isotopes to trace local deposition of Hg emitted by a large coal-fired power plant (*47*). We found that Hg in precipitation collected directly downwind of the Crystal River, Florida power plant displayed extreme negative δ^{202}Hg values. Precipitation samples collected at other sites in central Florida that were not strongly influenced by coal combustion displayed δ^{202}Hg values close to 0‰. We suggest that the isotopic composition of the combusted coal powder coupled with partial removal of Hg by air pollution control devices resulted in the emission of isotopically distinct Hg from the power plant.

In Chapter 6 (in review at *Science of the Total Environment*) we explore whether this distinct isotopic signature can be used to trace Hg emitted by the coal-fired power plant into nearby aquatic ecosystems. We measured the Hg isotopic composition of surface sediments and largemouth bass from lakes in central Florida including several

that were close to the Crystal River power plant. Although some studies suggest that recently deposited Hg is preferentially methylated and bioaccumulated compared to previously accumulated Hg in lake sediments, we found no evidence of the extreme negative δ^{202}Hg values observed in Crystal River precipitation in largemouth bass from the nearby lakes. Instead, we hypothesize that MeHg in the largemouth bass is largely derived from the large reservoir of accumulated Hg in the upper lake sediments. In addition to these findings, we observed that the degree of MIF of Hg isotopes in fish tissue was correlated to light penetration depth in each lake. This supports the hypothesis that photochemical degradation of MeHg prior to incorporation of the remaining MeHg into the food web causes MIF. Overall, these data suggest that Hg concentrations in fish populations may remain elevated for decades to centuries after Hg emissions regulations successfully result in decreased Hg deposition.

References

(1) Mergler, D.; Anderson, H. A.; Chan, L. H. M.; Mahaffey, K. R.; Murray, M.; Sakamoto, M.; Stern, A. H.; Methylmercury exposure and health effects in humans: A worldwide concern. *Ambio* **2007,** *36* (1), 3-11.

(2) Clarkson, T. W.; Magos, L.; The toxicology of mercury and its chemical compounds. *Crit. Rev. Toxicol.* **2006,** *36*, 609-662.

(3) Fitzgerald, W. F.; Lamborg, C. H., Geochemistry of Mercury in the Environment. In *Treatise on Geochemistry 9*, Holland, H. D., and Turekian, K.K., Ed. Elsevier Oxford, **2003**; Vol. 9, pp 107-148.

(4) U.S. Environmental Protection Agency, **2012**. *Mercury: Human Exposure*. access via http://www.epa.gov/hg/exposure.htm. Accessed March 25, 2012.

(5) U.S. Environmental Protection Agency, *EPA's Roadmap for Mercury: Executive Summary* EPA-HQ-2005-0013: Washington, D.C., **2006**.

(6) Krabbenhoft, D. P.; Rickert, D. A.; Mercury Contamination of Aquatic Ecosystems. *United States Geological Survey Fact Sheet* **1995,** *216-95*.

(7) Facemire, C.; Auspurger, T.; Bateman, D.; Brim, M.; Conzelmann, P.; Delchamps, S.; Douglas, E.; Inomn, L.; Looney, K.; Lopez, F.; Masson, G.; Morrison, D.; Morse, N.; Robison, A.; Impacts of mercury contamination in the southeastern United States. *Water, Air, Soil Pollut.* **1995,** *80*, 923-926.

(8) Scheuhammer, A. M.; Meyer, M. W.; Sandheinrich, M. B.; Murray, M. W.; Effects of environmental methylmercury on the health of wild birds, mammals, and fish. *Ambio: A Journal of the Human Environment* **2007,** *36* (1), 12-19.

(9) Heinz, G.; Effects of low dietary levels of methylmercury on mallard reproduction. *Bulletin of Environmental Contamination and Toxicology* **1974,** *11* (4), 386-392.

(10) Harada, M.; Minamata disease: Methylmercury poisoning in Japan caused by environmental pollution. *Crit. Rev. Toxicol.* **1995,** *25*, 1-24.

(11) McAlpine, D.; Araki, S.; Minamata disease: An unusual neurological disorder caused by contaminated fish. *The Lancet* **1958,** *2*, 629-631.

(12) U.S. Environmental Protection Agency, *2008 Biennial National Listing of Fish Advisories* EPA-823-F-09-007: Washington, D.C., **2009**.

(13) Krupp, R.; Physicochemical aspects of mercury metallogenesis. *Chem. Geol.* **1988,** *69*, 345-356.

(14) Lin, C.-J.; Pehkonen, S. O.; The chemistry of atmospheric mercury: A review. *Atmos. Environ.* **1999,** *33*, 2067-2079.

(15) Schroeder, W. H., Munthe, J.; Atmospheric mercury - An overview. *Atmos. Environ.* **1998,** *32* (5), 809-822.

(16) Mason, R. P.; Sheu, G.-R.; Role of the ocean in the global mercury cycle. *Global Biogeochem. Cycles* **2002,** *16* (4), 1-14.

(17) Lindberg, S.; Bullock, R.; Ebinghaus, R.; Engstrom, D.; Feng, X.; Fitzgerald, W.; Pirrone, N.; Prestbo, E.; Seigneur, C.; A synthesis of progress and uncertainties in attributing the sources of mercury in deposition. *Ambio* **2007,** *36* (1), 19-32.

(18) Landis, M. S.; Vette, A. F.; Keeler, G. J.; Atmospheric mercury in the Lake Michigan Basin: Influence of the Chicago/Gary urban area. *Environ. Sci. Technol.* **2002,** *36*, 4508-4517.

(19) U.S. Environmental Protection Agency, **2005**. *National Emissions Inventory for Mercury Point Sources in the State of Florida*. access via http://www.epa.gov/ttn/chief/net/2005inventory.html - inventorydata. Accessed November 15, 2010.

(20) Dvonch, J. T.; Graney, J. R.; Keeler, G. J.; Stevens, R. K.; Use of elemental tracers to source apportion mercury in south Florida precipitation. *Environ. Sci. Technol.* **1999,** *33*, 4522-4527.

(21) Lohman, K.; Seigneur, C.; Edgerton, E.; Jansen, J.; Modeling mercury in power plant plumes. *Environ. Sci. Technol.* **2006,** *40*, 3848-3854.

(22) White, E. M.; Keeler, G. J.; Landis, M. S.; Spatial variability of mercury wet deposition in eastern Ohio: Summertime meteorological case study analysis of local source influences. *Environ. Sci. Technol.* **2009,** *43*, 4946-4953.

(23) Expert Panel on Mercury Atmospheric Processes, *Mercury Atmospheric Processes: A Synthesis Report, TR-104214*. Tampa, FL, **1994**.

(24) Johnson, K. P.; Blum, J. D.; Keeler, G. J.; Douglas, T. A.; Investigation of the deposition and emission of mercury in arctic snow during an atmospheric mercury depletion event. *Journal of Geophysical Research* **2008,** *113*, D17304.

(25) Kirk, J. L.; St. Louis, V. L.; Sharp, M. J.; Rapid reduction and reemission of mercury deposited into snowpacks during atmospheric mercury depletion events at Churchill, Manitoba, Canada. *Environ. Sci. Technol.* **2006,** *40*, 7590-7596.

(26) Ullrich, S. M.; Tanton, T. W.; Abdrashitova, S. A.; Mercury in the aquatic environment: A review of factors affecting methylation. *Critical Reviews in Environmental Science and Technology* **2001,** *31* (3), 241-293.

(27) Gilmour, C. C.; Henry, E. A.; Mercury methylation in aquatic systems affected by acid deposition. *Environmental Pollution* **1991,** *71*, 131-169.

(28) Eckley, C. S.; Hintelmann, H.; Determination of mercury methylation potentials in the water column of lakes across Canada. *Science of the Total Environment* **2006,** *368* (1), 111-125.

(29) Wang, W.-X.; Wong, R. S. K.; Bioaccumulation kinetics and exposure pathways of inorganic mercury and methylmercury in a marine fish, the sweetlips *Plectorhinchus gibbosus*. *Marine Ecology Progress Series* **2003,** *261*, 257-268.

(30) Trudel, M.; Rasmussen, J. B.; Modeling the elimination of mercury by fish. *Environmental Science and Technology* **1997,** *31* (6), 1716-1722.

(31) Pickhardt, P. C.; Stepanova, M.; Fisher, N. S.; Contrasting uptake routes and tissue distributions of inorganic and methylmercury in mosquitofish (*Gambusia affinis*) and redear sunfish (*Lepomis microlophus*). *Environmental Toxicology and Chemistry* **2006,** *25* (8), 2132-2142.

(32) Bloom, N. S.; On the chemical form of mercury in edible fish and marine invertebrate tissue. *Canadian Journal of Fisheries and Aquatic Sciences* **1992,** *49* (5), 1010-1017.

(33) Pentreath, R. J.; The accumulation of mercury from food by the plaice, *Pleuronectes platessa* L. *Journal of Experimental Marine Biology and Ecology* **1976,** *25* (1), 51-65.

(34) Engle, M. A.; Gustin, M. S.; Goff, F.; Counce, D. A.; Janik, C. J.; Bergfeld, D.; Rytuba, J. J.; Atmospheric mercury emissions from substrates and fumaroles associated with three hydrothermal systems in the western United States. *J. Geophys. Res.* **2006,** *111*, D17304.

(35) Pyle, D. M.; Mather, T. A.; The importance of volcanic emissions for the global atmospheric mercury cycle. *Atmos. Environ.* **2003,** *37*, 5115-5124.

(36) Gustin, M. S.; Lindberg, S. E.; Weisberg, P. J.; An update on the natural sources and sinks of atmospheric mercury. *Appl. Geochem.* **2008,** *23* (3), 482-493.

(37) Pacyna, E. G.; Pacyna, J. M.; Steenhuisen, F.; Wilson, S.; Global anthropogenic mercury emission inventory for 2000. *Atmos. Environ.* **2006,** *40*, 4048-4063.

(38) Streets, D. G.; Devane, M. K.; Lu, Z.; Bond, T. C.; Sunderland, E. M.; Jacob, D. J.; All-time releases of mercury to the atmosphere from human activities. *Environ. Sci. Technol.* **2011,** *45* (24), 10485-10491.

(39) Schuster, P. F.; Krabbenhoft, D. P.; Naftz, D. L.; Cecil, L. D.; Olson, M. L.; Dewild, J. F.; Susong, D. D.; Green, J. R.; Abbott, M. L.; Atmospheric mercury deposition during the last 270 years: A glacial ice core record of natural and anthropogenic sources. *Environ. Sci. Technol.* **2002,** *36* (11), 2303-2310.

(40) Galbreath, K. C.; Zygarlicke, C. J.; Mercury speciation in coal combustion and gasification flue gases. *Environ. Sci. Technol.* **1996,** *30*, 2421-2426.

(41) Bargagli, R.; Barghigiani, C.; Lichen biomonitoring of mercury emission and deposition in mining, geothermal and volcanic areas of Italy. *Environ. Monit. Assess.* **1991,** *16*, 265-275.

(42) Fitzgerald, W. F.; Lamborg, C. H.; Hammerschmidt, C. R.; Marine biogeochemical cycling of mercury. *Chem. Rev.* **2007,** *107*, 641-662.

(43) Lamborg, C. H.; Fitzgerald, W. F.; Damman, A. W. H.; Benoit, J. M.; Balcom, P. H.; Engstrom, D. R.; Modern and historic atmospheric mercury fluxes in both hemispheres: Global and regional mercury cycling implications. *Global Biogeochem. Cycles* **2002,** *16* (4), 1-11.

(44) Bindler, R.; Renberg, I.; Appleby, P. G.; Anderson, N. J.; Rose, N. L.; Mercury accumulation rates and spatial patterns in lake sediments from West Greenland: A coast to ice margin transect. *Environ. Sci. Technol.* **2001,** *35* (9), 1736-1741.

(45) Blum, J. D.; Bergquist, B. A.; Reporting the variations in the natural isotopic composition of mercury. *Anal. Bioanal. Chem.* **2007,** *388* (2), 353-359.

(46) Gehrke, G. E.; Blum, J. D.; Marvin-DePasquale, M.; Sources of mercury to San Francisco Bay surface sediment as revealed by mercury stable isotopes. *Geochim. Cosmochim. Acta* **2010,** *75* (3), 691-705.

(47) Sherman, L. S.; Blum, J. D.; Keeler, G. J.; Demers, J. D.; Dvonch, J. T.; Investigation of local mercury deposition from a coal-fired power plant using mercury isotopes. *Environ. Sci. Technol.* **2012,** *46* (1), 382-390.

(48) Sherman, L. S.; Blum, J. D.; Johnson, K. P.; Keeler, G. J.; Barres, J. A.; Douglas, T. A.; Mass-independent fractionation of mercury isotopes in Arctic snow driven by sunlight. *Nature Geoscience* **2010,** *3* (3), 173-177.

(49) Sherman, L. S.; Blum, J. D.; Douglas, T. A.; Steffen, A.; Frost flowers growing in the Arctic ocean-atmosphere-sea ice-snow interface: 2. Mercury exchange

between the atmosphere, snow, and frost flowers. *Journal of Geophysical Research* **2012,** *117*, D00R10.

(50) Gratz, L. E.; Keeler, G. J.; Blum, J. D.; Sherman, L. S.; Isotopic composition and fractionation of mercury in Great Lakes precipitation and ambient air. *Environ. Sci. Technol.* **2010,** *44*, 7764-7770.

(51) Sherman, L. S.; Blum, J. D.; Mercury stable isotopes in sediments and largemouth bass (*Micropterus salmoides*) from Florida lakes. *Science of the Total Environment***, in review**.

(52) Biswas, A.; Blum, J. D.; Bergquist, B. A.; Keeler, G. J.; Zhouqing, X.; Natural mercury isotope variation in coal deposits and organic soils. *Environ. Sci. Technol.* **2008,** *42* (22), 8303-8309.

(53) Lefticariu, L.; Blum, J. D.; Gleason, J. D.; Mercury isotopic evidence for multiple mercury sources in coal from the Illinois Basin. *Environ. Sci. Technol.* **2011,** *45* (4), 1724-1729.

(54) Senn, D. B.; Chesney, E. J.; Blum, J. D.; Bank, M. S.; Maage, A.; Shine, J. P.; Stable isotope (N, C, Hg) study of methylmercury sources and trophic transfer in the northern Gulf of Mexico. *Environ. Sci. Technol.* **2010,** *44* (5), 1630-1637.

(55) Bergquist, B. A.; Blum, J. D.; Mass-dependent and mass-independent fractionation of Hg isotopes by photo-reduction in aquatic systems. *Science* **2007,** *318* (5849), 417-420.

(56) Gehrke, G. E.; Blum, J. D.; Slotton, D. G.; Greenfield, B. K.; Mercury isotopes link mercury in San Francisco Bay forage fish to surface sediments. *Environmental Science and Technology* **2011,** *45* (4), 1264-1270.

(57) Gantner, N.; Hintelmann, H.; Zheng, W.; Muir, D. C.; Variations in stable isotope fractionation of Hg in food webs of Arctic lakes. *Environmental Science and Technology* **2009,** *43*, 9148-9154.

(58) Perrot, V.; Epov, V. N.; Pastukhov, M. V.; Grebenshchikova, V. I.; Zouiten, C.; Sonke, J. E.; Husted, S.; Donard, O. F. X.; Amouroux, D.; Tracing sources and bioaccumulation of mercury in fish of Lake Baikal - Angara River using Hg isotopic composition. *Environmental Science and Technology* **2010,** *44* (21), 8030-8037.

(59) Das, R.; Salters, V. J. M.; Odem, A. L.; A case for in vivo mass-independent fractionation of mercury isotopes in fish. *Geochemistry Geophysics Geosystems* **2009,** *10*, Q11012.

(60) Kwon, S. Y.; Blum, J. D.; Carvan, M. J.; Basu, N.; Head, J. A.; Madenjian, C. P.; David, S. R.; Absence of fractionation of mercury isotopes during trophic transfer of methylmercury to freshwater fish in captivity. *Environmental Science and Technology* **2012,** *46* (14), 7527-7534.

(61) Point, D.; Sonke, J. E.; Day, R. D.; Roseneau, D. G.; Hobson, K. A.; Vander Pol, S. S.; Moors, A. J.; Pugh, R. S.; Donard, O. F. X.; Becker, P. R.; Methylmercury photodegradation influenced by sea-ice cover in Arctic marine ecosystems. *Nature Geoscience* **2011,** *4*, 188-194.

(62) Laffont, L.; Sonke, J. E.; Maurice, L.; Hintelmann, H.; Pouilly, M.; Bacarreza, Y. S.; Perez, T.; Behra, P.; Anomalous mercury isotopic compositions of fish and human hair in the Bolivian Amazon. *Environ. Sci. Technol.* **2009,** *43*, 8985-8990.

(63) Sherman, L. S.; Blum, J. D.; Nordstrom, D. K.; McCleskey, R. B.; Barkay, T.; Vetriani, C.; Mercury isotopic composition of hydrothermal systems in the Yellowstone Plateau volcanic field and Guaymas Basin sea-floor rift. *Earth. Planet. Sci. Lett.* **2009,** *279*, 86-96.

(64) Zheng, W.; Foucher, D.; Hintelmann, H.; Mercury isotope fractionation during volatilization of Hg(0) from solution into the gas phase. *J. Anal. Atomic Spectro.* **2007,** *22*, 1097-1104.

(65) Rodriguez-Gonzalez, P.; Epov, V. N.; Bridou, R.; Tessier, E.; Guyoneaud, R.; Monperrus, M.; Amouroux, D.; Species-specfic stable isotope fractionation of mercury during Hg(II) methylation by an anaerobic bacteria (*Desulfobulbus propionicus*) under dark conditions. *Environ. Sci. Technol.* **2009**.

(66) Malinovsky, D.; Vanhaecke, F.; Mass-independent isotope fractionation of heavy elements measured by MC-ICPMS: A unique probe in environmental sciences. *Anal. Bioanal. Chem.* **2011,** *400*, 1619-1624.

(67) Kritee, K.; Barkay, T.; Blum, J. D.; Mass dependent stable isotope fractionation of mercury during *mer* mediated microbial degradation of monomethylmercury. *Geochim. Cosmochim. Acta* **2009,** *73*, 1285-1296.

(68) Zheng, W.; Hintelmann, H.; Isotope fractionation of mercury during its photochemical reduction by low-molecular-weight organic compounds. *J. Phys. Chem. A* **2010,** *114* (12), 4246-4253.

(69) Estrade, N.; Carignan, J.; Sonke, J. E.; Donard, O. F. X.; Mercury isotope fractionation during liquid-vapor evaporation experiments. *Geochim. Cosmochim. Acta* **2009,** *73*, 2693-2711.

(70) Ghosh, S.; Schauble, E. A.; Couloume, G. L.; Blum, J. D.; Bergquist, B. A.; Estimation of nuclear volume dependent fractionation of mercury isotopes in equilibrium liquid-vapor evaporation experiments. *Chem. Geol.* **2012**.

(71) Schauble, E. A.; Role of nuclear volume in driving equilibrium stable isotope fractionation of mercury, thallium, and other very heavy elements. *Geochim. Cosmochim. Acta* **2007,** *71*, 2170-2189.

(72) Zheng, W.; Hintelmann, H.; Nuclear field shift effect in isotope fractionation of mercury during abiotic reduction in the absence of light. *The Journal of Physical Chemistry A* **2010,** *114* (12), 4238-4245.

(73) Buchachenko, A. L.; Magnetic isotope effect: Nuclear spin control of chemical reactions. *J. Phys. Chem.* **2001,** *105* (44), 9995-10011.

(74) Turro, N. J.; Influence of nuclear spin on chemical reactions: Magnetic isotope and magnetic field effects. *Proceedings of the National Academy of Sciences* **1983,** *80*, 609-621.

(75) Smith, C. N.; Kesler, S. E.; Blum, J. D.; Rytuba, J. J.; Isotope geochemistry of mercury in source rocks, mineral deposits and spring deposits of the California Coast Ranges, USA. *Earth Planet. Sci. Lett.* **2008,** *269*, 399-407.

(76) Smith, C. N.; Kesler, S. E.; Klaue, B.; Blum, J. D.; Mercury isotope fractionation in fossil hydrothermal systems. *Geology* **2005,** *33* (10), 825-828.

(77) Lindberg, S. E.; Brooks, S.; Lin, C.-J.; Scott, K. J.; Landis, M. S.; Stevens, R. K.; Goodsite, M.; Richter, A.; Dynamic oxidation of gaseous mercury in the troposphere at polar sunrise. *Environ. Sci. Technol.* **2002,** *36*, 1245-1256.

(78) Lu, J. Y.; Schroeder, W. H.; Barrie, L. A.; Steffen, A.; Welch, H. E.; Martin, K.; Lockhart, L.; Hunt, R. V.; Boila, G.; Richter, A.; Magnification of atmospheric mercury deposition to polar regions in springtime: the link to tropospheric ozone depletion chemistry. *Geophys. Res. Lett.* **2001,** *28* (17), 3219-3222.

(79) Tackett, P. J.; Cavender, A. E.; Keil, A. D.; Shepson, P. B.; Bottenheim, J. W.; Morin, S.; Deary, J.; Steffen, A.; Doerge, C.; A study of the vertical scale of halogen chemistry in the Arctic troposphere during Polar Sunrise at Barrow, Alaska. *J. Geophys. Res.* **2007,** *112*, D07306.

(80) Douglas, T. A.; Sturm, M.; Simpson, W. R.; Brooks, S.; Lindberg, S. E.; Perovich, D. K.; Elevated mercury measured in snow and frost flowers near Arctic sea ice leads. *Geophys. Res. Lett.* **2005,** *32*.

(81) Larose, C.; Dommergue, A.; De Angelis, M.; Cossa, D.; Averty, B.; Marusczak, N.; Soumis, N.; Schneider, D.; Ferrari, C.; Springtime changes in snow chemistry

lead to new insights into mercury methylation in the Arctic. *Geochim. Cosmochim. Acta* **2010,** *74*, 6263-6275.

(82) Dommergue, A.; Ferrari, C. P.; Gauchard, P.-A.; Boutron, C. F.; The fate of mercury species in a sub-arctic snowpack during snowmelt. *Geophys. Res. Lett.* **2003,** *30* (12).

(83) Axelrad, D. M.; Lange, T.; Gabriel, M. C.; Aiken, G. R.; Brandon, A.; Cunningham, M. W.; DeBusk, T.; Dierberg, F.; Donner, B. A.; Frederick, P.; Gilmour, C.; Harris, R.; Jansen, D.; Krabbenhoft, D. P.; McCray, J. M.; Orem, W. H.; Oronato, D. P.; Pollman, C. D.; Rumbold, D. G.; White, G.; Wright, A. L.; Ye, R., 2011 South Florida Environmental Report: Chapter 3B Mercury and Sulfur Monitoring, Research and Environmental Assessment in South Florida. South Florida Water Management District: **2011**; Vol. I, p 53.

(84) Hand, J.; Friedemann, M., Mercury, largemouth bass, and water quality: A preliminary report. Florida Department of Environmental Regulation: Talahassee, FL, **1990**.

(85) Frederick, P. C.; Spalding, M. G.; Dusek, R.; Wading birds as bioindicators of mercury contamination in Florida: Annual and geographic variation. *Environ. Toxicol. Chem.* **2002,** *21* (1), 163-167.

(86) Dvonch, J. T.; Graney, J. R.; Marsik, F. J.; Keeler, G. J.; Stevens, R. K.; An investigation of source-receptor relationships for mercury in south Florida using event precipitation data. *Sci. Total Environ.* **1998,** *213*, 95-108.

(87) Dvonch, J. T.; Keeler, G. J.; Marsik, F. J.; The influence of meteorological conditions on the wet deposition of mercury in southern Florida. *JApMe* **2005,** *44*, 1421-1435.

CHAPTER 2

Mercury isotopic composition of hydrothermal systems in the Yellowstone Plateau volcanic field and Guaymas Basin sea-floor rift[1]

Abstract

To characterize mercury (Hg) isotopes and isotopic fractionation in hydrothermal systems we analyzed fluid and precipitate samples from hot springs in the Yellowstone Plateau volcanic field and vent chimney samples from the Guaymas Basin sea-floor rift. These samples provide an initial indication of the variability in Hg isotopic composition among marine and continental hydrothermal systems that are controlled predominantly by mantle-derived magmas. Fluid samples from Ojo Caliente hot spring in Yellowstone range in δ^{202}Hg from -1.02‰ to 0.58‰ (± 0.11‰, 2 s.d.) and solid precipitate samples from Guaymas Basin range in δ^{202}Hg from -0.37‰ to -0.01‰ (± 0.14‰, 2 s.d.). Fluid samples from Ojo Caliente display mass-dependent fractionation (MDF) of Hg from the vent (δ^{202}Hg = 0.10 ± 0.11‰, 2 s.d.) to the end of the outflow channel (δ^{202}Hg = 0.58 ± 0.11‰, 2 s.d.) in conjunction with a decrease in Hg concentration from 46.6 pg/g to 20.0 pg/g. Although a small amount of Hg is lost from the fluids due to co-precipitation with siliceous sinter, we infer that the majority of the observed MDF and Hg loss from waters in Ojo Caliente is due to volatilization of $Hg^0_{(aq)}$ to $Hg^0_{(g)}$ and the preferential loss of Hg

[1]Sherman, L. S., Blum, J. D., Nordstrom, D. K., McCleskey, R. B., Barkay, T., Vetriani, C. Mercury isotopic composition of hydrothermal systems in the Yellowstone Plateau volcanic field and Guaymas Basin sea-floor rift. *Earth and Planetary Science Letters* **2009**, *279*, 86-96.

with a lower δ^{202}Hg value to the atmosphere. A small amount of mass-independent fractionation (MIF) was observed in all samples from Ojo Caliente (Δ^{199}Hg = 0.13 ± 0.06‰, 2 s.d.) but no significant MIF was measured in the sea-floor rift samples from Guaymas Basin. This study demonstrates that several different hydrothermal processes fractionate Hg isotopes and that Hg isotopes may be used to better understand these processes.

Keywords

Mercury, isotope fractionation, hydrothermal, Yellowstone, Guaymas Basin

2.1 Introduction

Mercury (Hg) is a redox-active metal with gaseous, aqueous, and solid forms in the environment. Mercury isotope variations have the potential to inform studies of global metal cycling, paleo-redox conditions, ore deposit formation, and environmental contamination (*1-6*). As a neurotoxic element, Hg poses serious threats to human health largely through the consumption of fish that bioaccumulate monomethylmercury (MeHg) (*7*). Anthropogenic activities such as fossil fuel combustion and natural processes such as volcanic activity and Hg evasion from geothermally enriched regions contribute Hg to the environment (*8-13*). However, because the biogeochemical cycling of Hg through different Earth reservoirs is complex, it is often difficult to directly link Hg sources to human and wildlife Hg exposure (*9, 10, 14*).

Several recent studies demonstrate that potential sources of Hg emissions may be isotopically distinct (*2, 3, 5, 15, 16*). As a result, it may be possible to use Hg isotopes to

trace Hg from a variety of sources into environmental reservoirs. Measurements of the isotopic composition of anthropogenic Hg emissions from some ore deposits and fossil fuels are now available (*3, 5, 6*), but the Hg isotopic composition of natural volcanic emissions have only been reported from one volcano in Italy (Vulcano, Aeolian Islands) (*17*). Additionally, although recent investigations have measured Hg isotopes in crustal rocks and sediments (*1, 6, 15*), very little work has been done to describe the Hg isotopic composition of mantle-derived materials. It is of fundamental importance to characterize mantle-derived Hg because mantle materials represent an important source of Hg to other Earth reservoirs.

Mantle-derived Hg can enter the surface environment in many tectonic settings including hot spots and oceanic spreading centers. In these regions, meteoric water and seawater percolates through crustal rocks and is conductively heated (*18, 19*). The hot fluid then leaches, concentrates, and transports Hg and other metals from the volcanic rocks (*5, 20, 21*). As the fluids move upward, the changing temperature and pressure conditions cause the solubility of Hg to decrease and Hg can precipitate in Hg minerals (e.g. cinnabar, HgS), in solid solution with sulfides, or as impurities in other minerals (*5, 20, 21*). Additionally, $Hg^0_{(aq)}$ in fluids can be volatilized to $Hg^0_{(g)}$ and subsequently lost to the atmosphere (*11, 22*). These processes produce economically viable Hg deposits, may cause the export of Hg to marine environments, and can result in substantial gaseous Hg emissions from geothermally enriched continental regions (*11, 21, 23-26*).

It is likely that some of the hydrothermal processes that lead to the formation of Hg-enriched deposits and Hg emissions cause isotope fractionation (*5, 6, 27*). Because Hg has seven stable isotopes (196, 198, 199, 200, 201, 202, and 204 amu) and active

redox chemistry, it is fractionated during a wide variety of reactions (*2, 4, 5, 16, 28*). For example, Hg isotope fractionation has been observed in fossil hydrothermal systems due to the preferential vapor phase transport of isotopically light Hg (*5*) and in laboratory experiments during volatilization of $Hg^0_{(aq)}$ to $Hg^0_{(g)}$ (*27*). However, minimal Hg isotope fractionation occurs during the hydrothermal leaching of Hg from source-rocks (*6*) and, by analogy to other heavy metals (*29, 30*), we expect that magmatic processes such as partial melting and magma cooling should fractionate Hg to a lesser degree than lower temperature processes. We hypothesize that the Hg isotopic composition of hydrothermal fluids and precipitates is determined by the original composition of the mantle-derived materials and processes occurring in the hydrothermal systems. To date, no studies have measured Hg isotope fractionation in active hydrothermal systems to characterize the processes that affect the Hg isotopic composition of fluids, precipitates, and gaseous emissions.

For this initial investigation of Hg isotopes in modern hydrothermal systems we studied a large continental magmatic-hydrothermal system (Yellowstone Plateau volcanic field, Wyoming, U.S.A.) and a sea-floor rift magmatic-hydrothermal system (Guaymas Basin, East Pacific Rise, Gulf of California). Both regions are associated with shallow magma bodies that provide heat and a source of Hg to extensive and active hydrothermal systems (*31-33*). As a result, these hydrothermal systems contain elevated concentrations of Hg and contribute Hg to precipitates and to the atmosphere or ocean (*11, 26, 34, 35*). The present study aims to describe Hg fractionation in hydrothermal systems and to begin to characterize the Hg isotopic composition of mantle-derived materials.

2.2 Description of sampling localities

2.2.1 Yellowstone Plateau volcanic field

The Yellowstone Plateau volcanic field has produced more than 6,000 km^3 of volcanic ash and lavas over the last 2.2 million years as a result of hot spot emplacement of shallow magma bodies beneath the region (*31-33, 36*). The youngest caldera produced by this volcanism, Yellowstone Caldera, is located in the center of Yellowstone National Park (YNP) (Figure 2.1) (*31*). The downward percolation and subsequent heating of meteoric water to temperatures up to 350 °C sustains a large number of active hydrothermal systems in YNP (*31, 32, 37, 38*). When the fluids in these systems reach the surface, they emit gases to the atmosphere and precipitate carbonaceous travertine and siliceous sinter on the margins of hot spring pools and geysers (*39-42*). These emissions and precipitates contain elevated concentrations of Hg (*34, 35, 43*).

Samples for this study were collected at several locations across YNP. Individual fluid samples were collected in the Washburn area from Inkpot #3 and in the Mud Volcano Area from Turbulent Pool and Sulfur Cauldron (Figure 2.1). The hydrothermal fluids collected from these areas were acidic, non-boiling, and contained high concentrations of sulfur and organic carbon (Table 2.1). Fluids and siliceous sinter samples were also collected along a downstream transect through Ojo Caliente hot spring in the Lower Geyser Basin. In contrast to the other hydrothermal systems, Ojo Caliente has a neutral pH, boiling source pool (~94 °C), and low concentrations of sulfur and organic carbon (Table 2.1). For several reasons, Ojo Caliente hot spring is a good location to study Hg isotope fractionation during specific hydrothermal processes. First, fluids in hot springs such as Ojo Caliente do not have high concentrations of suspended

solid precipitates. The physical separation of fluids and precipitates in Ojo Caliente enables observation of fractionation between the two phases. Second, Ojo Caliente's neutral pH promotes the precipitation of siliceous sinters (*41*) and its boiling source pool enhances the phase transfer of $Hg^0_{(aq)}$ to $Hg^0_{(g)}$. These conditions allow the observation of Hg fractionation both during mineral precipitation and Hg vapor phase separation. Third, the chemistry of Ojo Caliente has not changed significantly for over a century (*41, 44, 45*). We can therefore assume that the measurements made during this study are representative of the long-term conditions in Ojo Caliente.

2.2.2 Guaymas Basin

Guaymas Basin (Figure 2.2) encompasses a pair of en echelon sediment-covered rift valleys at approximately 2000 m water depth in the Gulf of California (*46-48*). Heat flow measurements indicate that an actively circulating hydrothermal system is maintained by shallow magmatic intrusions and a deep magma chamber (*47*). Metal-enriched hydrothermal fluids vent to the ocean both directly through hydrothermal chimneys and via diffuse dissemination through the organic-rich sediment cover (*47, 49*). The vent chimneys are composed primarily of anhydrite, calcite, and sulfides including sphalerite, pyrrhotite, pyrite, and galena (*46, 50*). Samples for this study were collected from two of these chimneys.

2.3 Methods

2.3.1 Sample collection

During September of 2006, in YNP, fluid and sinter samples were collected using Hg-clean methods. All fluid samples were collected via pumping through a 0.1 μm filter; samples were not retained until at least 0.5 L of fluid passed through the filter. Samples were collected into acid-washed Teflon bottles and immediately acidified with 1% (v/v) HCl (Fisher, Trace Metal Grade). Two separate Teflon bottles of deionized water were processed in the same manner as 'sampling blanks' and replicate fluid samples were collected at each site to measure water chemistry properties and solute concentrations (Table 2.1). Fluid samples were collected in the Washburn Area from Inkpot #3 ('YNP-1') and in the Mud Volcano Area from Turbulent Pool ('YNP-2') and Sulfur Cauldron ('YNP-3'). In addition, during the course of one sampling day, fluid and sinter samples were collected in the Lower Geyser Basin from Ojo Caliente. Fluid samples were collected from the hot spring along a downstream transect through the longest outflow channel (Figure 2.3). These samples were collected at the hot spring vent ('OC-1' from 5.7 m depth and 'OC-2' from 30 cm depth), in the middle of the source pool ('OC-3'), at the pool's outflow ('OC-4'), and along the outflow channel ('OC-5', 'OC-6'). Sample OC-3 is expected to represent a mixture of OC-1 and OC-2. Sinter samples from Ojo Caliente were collected at the vent pool's edge ('OC-S-2') and at the same approximate downstream locations as the corresponding fluid samples ('OC-S-4', 'OC-S-5', 'OC-S-6'). Two of these samples, OC-S-2 and OC-S-4, were broken from a cohesive sinter rim. In contrast, the other two sinter samples, OC-S-5 and OC-S-6, were unattached pieces of

sinter sampled from the outflow channel. It is possible, therefore, that samples OC-S-5 and OC-S-6 were not composed entirely of silica that precipitated in situ.

In October of 2007, during an oceanographic expedition of the R/V *Atlantis*, three samples were collected from the "Rebecca's Roost" area of the Southern Trough of Guaymas Basin using the manipulator arms of the DSV *Alvin* (Cruise AT 15-25A). Two solid chimney samples were collected from the top of the Pink Flamingo chimney ('GB-1') and from a flange located at the base of another unnamed chimney ('GB-3'). These samples were wrapped in aluminum foil and immediately frozen upon transport to the surface. Hydrothermal fluid was also collected from the Pink Flamingo chimney with a titanium sampler using Hg-clean methods (*51*) and this fluid was stored at the surface at 4ºC for 18 hours. The resulting precipitates were filtered from solution using a pre-burned glass fiber filter, stored frozen, and analyzed as sample 'GB-2.'

2.3.2 Sample processing

Prior to isotopic analyses, fluid and solid samples were processed in the University of Michigan Biogeochemistry and Environmental Isotope Geochemistry Laboratory. To facilitate the oxidation of dissolved Hg species in fluid samples, 2% (v/v) BrCl was added to each sample and the fluids were heated in an oven for 8 h at 60 °C. Precipitates were dried in an oven for 6 h at 60 °C and then crushed to a fine powder using an agate mortar and pestle. The mortar and pestle were cleaned between samples with 5% (v/v) HNO_3 (Fisher, Trace Metal Grade) and CH_3OH (Fisher). To minimize carryover, pure quartz sand was crushed between samples. None of this crushed sand contained any detectable Hg. One of the chimney samples from Guaymas Basin (GB-3)

was composed of two distinct mineral phases. By separating the two phases, we determined using atomic absorption spectroscopy (see below) that the darker, sulfide-rich phase contained nearly all of the Hg in the sample. This sulfide-rich sub-sample was subsequently processed as GB-3.

Mercury concentrations in fluid and solid samples were determined using atomic absorption spectroscopy (Nippon Instruments, MA 2000). Sub-samples of the fluids were analyzed via Hg reduction with $SnCl_2$ (Alfa Aesar) followed by concentration of the released $Hg^0_{(g)}$ onto a gold trap. Approximately 0.5 to 1 g of each solid sample was placed in a ceramic boat with activated alumina, sodium carbonate, and calcium hydroxide powders (Nippon Instruments). Hg in solid samples was then released by combustion in a tube furnace at 800 °C for 4 minutes and concentrated onto a gold trap. Hg from both solid and liquid samples was subsequently thermally desorbed from the gold traps and quantified by comparison to an 8-point calibration curve with $r^2 \geq 0.99$. Typical precision calculated by replicate analyses of NIST SRM 3133 (Mercury Standard Solution) was ± 4% (1 s.d.) for liquid samples and ± 8% (1 s.d.) for solid samples. Replicate sample analyses agreed to within 5%. The detection limit, estimated as 3 s.d. of blank analyses, was 1.54 pg/g for liquid samples and 7.43 ng/g for solid samples. All samples and standards contained concentrations of Hg above these detection limits.

After sample Hg concentrations were determined, Hg was liberated from the samples and concentrated into 8 g of an acidic 2% $KMnO_4$ (Alfa Aesar, low Hg, w/w) oxidizing solution using the following methods.

2.3.2.1 Liquid samples

Each 1 L liquid sample was chemically reduced in a sealed Pyrex bottle using 100 mL of 20% $SnCl_2$ (w/v), 100 mL of 50% H_2SO_4 (v/v), and 5 mL of 30% NH_2OH (w/v). The solution was stirred and $Hg^0_{(g)}$ was purged from the liquid with Ar gas. The effluent gas was then bubbled into the 2% $KMnO_4$ (w/v) solution. Procedural blanks, sampling blanks, and process standard solutions containing NIST SRM 3133 were processed in the same manner.

2.3.2.2 Solid samples

Depending on the measured Hg concentration, ~0.5 to ~2 g of sample was weighed into a quartz boat with activated alumina, sodium carbonate, and calcium hydroxide powders (Nippon Instruments). The filter sample from Guaymas Basin (GB-2) was cut into 0.5 cm wide strips and placed into a quartz boat with the same powders. Hg was liberated from all samples by combustion for 3 hours in a two-stage flow-through tube furnace (Thermo Electron Corporation). The temperature of the first furnace was incrementally increased to 900 °C and the second furnace was held at 1000 °C. The evolved Hg was swept by Ar gas into the $KMnO_4$ solution. Procedural blanks and replicates of NIST SRM 2711 (Montana Soil) were processed in the same manner.

2.3.3 Mineralogical characterization

The mineralogy of the solid samples was characterized using reflected and transmitted light microscopy and scanning electron microscopy-energy dispersive spectroscopy (SEM-EDS) (Hitachi S3200N, Noran UTW SiLi detector). The sinter samples from Ojo Caliente were further characterized using powder X-ray diffraction

(XRD) (Scintag Powder XRD). The bulk mineralogy of the sinter samples was determined using whole-sample powders and the clay mineralogy was determined using clay-size fraction powder separates.

2.3.4 Isotopic analyses

Multi-collector inductively coupled plasma mass spectrometry (MC-ICP-MS) was used to measure the Hg isotopic composition of the hydrothermal samples. The methods involved in these continuous-flow cold vapor generation measurements have been described in detail previously (*2, 5, 6, 52*). Briefly, the oxidizing $KMnO_4$ solutions were partially reduced with NH_2OH and the samples were matched in solution matrix and Hg concentration to a bracketing standard (NIST SRM 3133) to within 5%. The $Hg^{2+}_{(aq)}$ in the fluids was then reduced to $Hg^0_{(g)}$ with 10% $SnCl_2$ (w/v), separated from the fluid using a frosted-tip gas-liquid separator, and mixed with a Tl internal standard (NIST SRM 997) that was introduced as an aerosol using an Aridus desolvating nebulizer (CETAC). This mixture of $Hg^0_{(g)}$ and Tl was then introduced into a Nu Instruments MC-ICP-MS. Corrections for mass bias were made using the Tl internal standard and measurements of bracketing standards. On-peak zero corrections were applied to each measurement. Analytical uncertainty was determined based on replicate measurements of an in-house UM Almadén secondary standard as well as analyses of procedural standards (i.e., NIST SRM 3133 and 2711).

2.4 Results

2.4.1 Sample characterization

Concentrations of dissolved solutes in fluid samples from YNP were measured volumetrically and are presented in Table 2.1. In general, fluids in these hot springs are highly reducing and redox sensitive species (such as Fe, As, and Hg) are present in their reduced forms. As previously noted, hydrothermal fluids in Washburn Inkpot #3 (YNP-1), Turbulent Pool (YNP-2), and Sulfur Cauldron (YNP-3) were more acidic, lower in temperature, and generally contained higher concentrations of dissolved solutes than fluids collected in Ojo Caliente. During sampling, temperatures in Ojo Caliente decreased from 93 °C (boiling) at the vent (OC-1) to 75 °C approximately 21 m down the outflow channel (OC-6). The pH of the fluids increased slightly from 7.44 at the vent (OC-1) to 7.61 in the outflow channel (OC-5). All samples from Ojo Caliente contained similar Si/Cl ratios but Hg/Cl ratios decreased from the pool to the end of the outflow channel (Figure 2.4). Assuming that Cl behaves conservatively, this suggests that although Hg is lost from the fluids along the downstream transect, no measurable Si loss occurs.

During sampling in Guaymas Basin, we made several measurements to characterize the hydrothermal fluids exiting the vent chimneys. The hydrothermal fluid exiting the Pink Flamingo chimney was 305 °C. Preserved sub-samples of this fluid had a pH of 5.44 and total Hg concentrations of 2200 pg/g. During collection of the solid chimney sample from the unnamed vent (GB-3), the temperature measured below the flange was 281 °C and the temperature above the flange was ~65 °C.

The mineral phases present in the solid samples from Guaymas Basin and Ojo Caliente were characterized using SEM-EDS (Hitachi S3200N, Noran SiLi detector) and the sinter samples from Ojo Caliente were further examined using powder XRD (Scintag Powder XRD). The sinter samples from Ojo Caliente were composed primarily of finely laminated amorphous opaline silica and quartz. These samples also contained smectite (<5 wt.%) and minor (<1 wt.%) inclusions of pyrite and iron oxides in vugs in the silica matrix. The vent precipitates from Guaymas Basin were composed primarily of calcite and sulfides including pyrrhotite, pyrite, sphalerite, and galena. These results agree with those of previous studies (*39, 46, 53, 54*). No primary Hg phases (e.g., cinnabar) were observed in any of the solid samples from Ojo Caliente or Guaymas Basin. It is most likely that Hg is present as impurities in the sulfide phases (*19*).

2.4.2 Mercury concentrations and recovery

Mercury concentrations were measured gravimetrically and are reported as pg of Hg per g of sample (Table 2.2). Hg concentrations in all sampling and procedural blanks were below detection limits and are thus negligible. Hg concentrations in hydrothermal fluids from YNP ranged from 25.8 pg/g (± 1 pg/g) in Washburn Inkpot #3 (YNP-1) to 132 pg/g (±5 pg/g) in Sulfur Cauldron (YNP-3). Hg concentrations in fluids from Ojo Caliente ranged from 46.6 pg/g (± 2 pg/g) at the vent (OC-1) to 20.0 pg/g (± 1 pg/g) along the outflow channel (OC-6) and concentrations in the sinters ranged from 2040 ng/g (± 163 ng/g) at the edge of the main pool (OC-S-1) to 215 ng/g (± 17 ng/g) along the outflow channel (OC-S-6). The Hg concentrations of the Pink Flamingo chimney sample

(GB-1) and the other solid chimney sample (GB-3) were 39.5 ng/g (± 3 ng/g) and 111 ng/g (± 9 ng/g), respectively.

Also shown in Table 2.2 is the percentage of Hg originally measured in each sample that was retained after separation and re-capture in solution for isotopic analysis. Because preferential loss of light or heavy isotopes during sample processing could cause secondary fractionation, complete Hg recovery ensures that the sample's original isotopic composition is retained. For most of the samples, Hg recoveries were 95% to 100%. However, possibly due to leaks or incomplete Hg trapping efficiency, Hg recoveries were less than 95% for one fluid sample (OC-1), two solid samples (OC-S-2 and OC-S-6), and several process standards (NIST SRM 3133 and NIST SRM 2711). To determine if these losses could have caused Hg fractionation, we measured Hg isotopes in process standards with a range of Hg recoveries from 50% to 100%. δ^{202}Hg (‰) (see Section 2.4.3) in these standards does not systematically increase or decrease. The mean δ^{202}Hg for NIST SRM 3133 was -0.02‰ (± 0.11‰, 2SD, n = 9) and mean δ^{202}Hg for NIST SRM 2711 was -0.08‰ (± 0.15‰, 2SD, n = 15). These data suggest that the processes contributing to loss from our sample processing systems do not preferentially remove Hg isotopes according to mass. For these reasons we suggest that all of the isotopic compositions presented in this paper are accurate within the analytical precision determined by analysis of procedural standards.

2.4.3 Mercury isotopic compositions

Mercury isotopic compositions of samples and standards are reported using delta notation according to Eq. (1). Sample isotopic compositions are reported as deviations

from the average isotope ratios of bracketing standards (NIST SRM 3133) analyzed directly prior to and after each sample.

$$\delta^{xxx}Hg\ (‰) = ([(^{xxx}Hg/^{198}Hg)_{unknown}/(^{xxx}Hg/^{198}Hg)_{SRM\ 3133}] - 1) * 1000 \quad (1)$$

where

$(^{xxx}Hg/^{198}Hg)_{unknown}$ = Hg isotope ratio of the sample

$(^{xxx}Hg/^{198}Hg)_{SRM\ 3133}$ = Average Hg isotope ratio of bracketing standards

A summary of measured sample isotopic compositions is shown in Table 2.2; complete isotopic data are presented in the supplementary material. Mass-independent fractionation (MIF) is calculated according to Eqs. (2)-(4) as the deviation in the measured isotope ratio from that theoretically predicted by mass-dependent fractionation (MDF) and is reported using "capital delta" notation (e.g., $\Delta^{xxx}Hg$) (*2, 52*).

$$\Delta^{199}Hg = \delta^{199}Hg - (\delta^{202}Hg * 0.252) \quad (2)$$

$$\Delta^{200}Hg = \delta^{200}Hg - (\delta^{202}Hg * 0.502) \quad (3)$$

$$\Delta^{201}Hg = \delta^{201}Hg - (\delta^{202}Hg * 0.752) \quad (4)$$

MIF is considered significant if it is greater than 2 s.d. of that measured in the bracketing standards (i.e., >~0.08‰). Uncertainty in isotopic measurements are presented as the larger of the 2 s.e. reproducibility of repeated analyses of the sample, 2 s.d. of the long-term external reproducibility of the in-house UM Almadén standard, or 2 s.d. of the external reproducibility of procedural standards (*52*).

Measured $\delta^{202}Hg$ values in fluid samples from Ojo Caliente are presented in Figures 2.5a and 2.5b. Figure 2.5a depicts $\delta^{202}Hg$ from the vent (OC-1) down the outflow channel (to OC-6) versus the fraction of Hg remaining in the sample with respect to the original Hg concentration at OC-1 ('f_R'). The decrease in Hg concentration from

OC-1 to OC-6 is accompanied by an increase in δ^{202}Hg from 0.10‰ to 0.58‰ (± 0.11‰, 2SD). Figure 2.5b shows the same data on a log-log plot. Assuming that the loss of Hg at Ojo Caliente involves complete separation of the Hg without back-reaction, the increase in δ^{202}Hg can be modeled as a kinetic fractionation process using a Rayleigh distillation equation (*55, 56*). This model defines the kinetic fractionation factor ($^{xxx/198}\alpha$) as

$$^{xxx/198}\alpha = (^{xxx}Hg/^{198}Hg)_{\text{instantaneous reactant}}/(^{xxx}Hg/^{198}Hg)_{\text{instantaneous product}} \quad (5)$$

By plotting the left hand side of Eq. (6) versus $\ln(f_R)$, $^{202/198}\alpha$ can be estimated from the slope of a linear regression through the data points (Figure 2.5b) (*2, 4, 55*).

$$\ln[(1000+ \delta^{202}Hg)/(1000+ \delta^{202}Hg_i)] = [(1/^{202/198}\alpha)-1]*\ln(f_R) \quad (6)$$

where

$\delta^{202}Hg_i$ = isotopic composition of OC-1

Based on this relationship, the estimated fractionation factor describing the loss of Hg from fluids in Ojo Caliente is 1.00059 ± 0.00016 (1 s.d.). The uncertainty in this estimate was calculated using a York regression (*57*) and includes the uncertainty in both f_R and δ^{202}Hg.

A compilation of the Hg isotopic compositions of fluid and solid samples from YNP and Guaymas Basin is presented in Figure 2.6. MDF (represented by δ^{202}Hg) is plotted versus MIF (represented by Δ^{199}Hg). Measured δ^{202}Hg of fluid samples from YNP ranges from -1.02‰ to 0.58‰ (± 0.11‰, 2 s.d.). Individual fluid samples collected in the Washburn and Mud Volcano areas (YNP-1, YNP-2, and YNP-3) have lower δ^{202}Hg than fluid samples collected from Ojo Caliente and only one sample (YNP-1) displays significant MIF (Δ^{199}Hg = 0.09‰±0.06‰, 2 s.d.). Although these data provide

a preliminary estimate of the isotopic variability of Hg in YNP hydrothermal fluids, without a more detailed study of these hot springs, we cannot determine the reasons for this variability. Δ^{199}Hg values of all of the fluid samples from Ojo Caliente are the same within analytical error (0.13 ± 0.06‰, 2 s.d.). δ^{202}Hg of sinter samples from Ojo Caliente ranges from -0.50‰ to 0.36‰ (± 0.14‰, 2 s.d.) and Δ^{199}Hg of these samples ranges from 0.07‰ to 0.27‰ (± 0.08‰, 2 s.d.).

δ^{202}Hg of the solid chimney piece (GB-1) and fluid precipitate sample (GB-2) from the Pink Flamingo chimney in Guaymas Basin are indistinguishable (-0.31‰ and -0.37‰; ± 0.14‰, 2 s.d.). However, the solid chimney sample from the unnamed vent (GB-3) is isotopically distinct (δ^{202}Hg = -0.01 ± 0.14‰, 2 s.d.). No significant MIF is observed in any of the samples from Guaymas Basin (average Δ^{199}Hg = 0.02 ± 0.08‰, 2 s.d.).

2.5 Mercury isotopes in hydrothermal systems

2.5.1 Mass-dependent fractionation

Previous measurements of δ^{202}Hg in siliceous sinters from modern hot springs range from -3.42‰ to -0.21‰ (± 0.08‰, 2 s.d.) (*6*) and a study from Vulcano Island in Italy reported δ^{202}Hg of -0.74‰ (± 0.23‰, 2 s.d.) in volcanic fumerolic gas (*58*). The data reported in this study indicate that hydrothermal Hg isotopic compositions are variable within individual hydrothermal systems and are controlled by multiple processes. Data from this study do not allow us to predict the Hg isotopic composition of hydrothermal fluids or emissions on a regional scale. However, it is clear that Hg

isotopes can be used to better understand the processes that cause Hg fractionation in individual hydrothermal systems.

Mass-dependent fractionation of Hg isotopes observed in fluids from Ojo Caliente indicates that light isotopes of Hg are preferentially lost from the hydrothermal fluids. As shown in Figure 2.5b, this fractionation can be modeled using a Rayleigh distillation equation with a kinetic fractionation factor of 1.00059 ± 0.00016. There are two possible explanations for this observation: 1) isotopically light Hg is preferentially incorporated into precipitates (i.e., sinter) or 2) isotopically light Hg is preferentially lost to the atmosphere as $Hg^0_{(g)}$.

If Hg in the hydrothermal fluids of Ojo Caliente were primarily lost due to co-precipitation with sinters, it would seem reasonable that this process might preferentially incorporate isotopically light Hg into the solid phase. Such MDF has been observed during the disequilibrium precipitation of other metal-sulfides such as FeS (*59*). As shown in Figure 2.6, three of the four sinters collected from Ojo Caliente have substantially lower δ^{202}Hg values than the corresponding fluid samples. Because OC-S-5 and OC-S-6 may not have precipitated in situ, they may not accurately reflect the δ^{202}Hg of sinters precipitating from solution at those locations (see Section 2.3.1). Based on the other two liquid-solid sample pairs (i.e., OC-2 with OC-S-2 and OC-4 with OC-S-4), the co-precipitation of Hg in siliceous sinters appears to cause MDF with isotopically light Hg preferentially incorporated into the solid phase. Measured δ^{202}Hg of the sinters is 0.65‰ and 0.58‰ lower than the corresponding fluid. It is worth considering, therefore, whether loss of Hg by this mechanism could result in the observed MDF in the hydrothermal fluids.

Given that Hg is present at relatively low concentrations in these sinters, it is important to consider the absolute amount of Hg that could be lost to sinter precipitation and whether this quantity is of the appropriate magnitude to explain the observed fluid isotopic compositions. To this end, we present the following calculation based on two assumptions: (1) that all of the measured Hg loss from hydrothermal fluids at Ojo Caliente (26.6 pg/g) is due to sinter precipitation, and (2) that all of the sinter precipitating in the system contains between the minimum (197 ng/g) and maximum (2040 ng/g) measured Hg concentrations. Given these assumptions, between ~13.1 µg and ~135 µg of sinter would need to precipitate from each gram of water to account for the measured Hg loss from Ojo Caliente fluids. Given a measured pool outflow cross-sectional area of ~77 cm^2 and a flow rate of 0.286 m/s, we estimate that the discharge rate from Ojo Caliente is ~133 L/min. To account for the measured Hg loss, between 910 and 9400 kg of sinter would have to precipitate every year at Ojo Caliente. Spread over a stream outflow surface area of ~25 m^2, and assuming a sinter density of ~2.2 g/cm^3 (*60*), this would represent deposition of between 16 and 171 mm of sinter across the entire area per year. Although we have not explicitly measured the sinter surface elevation through time, based on annual observations and historical photos, we are confident that this is more precipitation than occurs on a yearly basis. In addition, sinter is deposited abiotically much more slowly than would be required to precipitate this quantity of material (*53*) and no measurable silica is lost from the hydrothermal fluids (Figure 2.4). Although these calculations are highly simplified, they demonstrate that Hg incorporation into siliceous sinters can probably only account for a small amount of the Hg lost from hydrothermal fluids at Ojo Caliente.

We suggest, instead, that isotopically light Hg is primarily lost from this hydrothermal system due to evasion of $Hg^0_{(g)}$ to the atmosphere. Gaseous evasion of Hg from the Yellowstone Plateau volcanic field is a measurable natural source of Hg to the environment (*11*). If all of the Hg lost from fluids in Ojo Caliente does evade to the atmosphere, we estimate that this hot spring produces Hg emissions of approximately 1.9 g/yr. This estimate is reasonable when compared to previous measurements of Hg emissions from geothermal regions (*11, 61*).

Recent studies suggest that the preferential loss of isotopically light Hg due to volatilization of $Hg^0_{(aq)}$ to $Hg^0_{(g)}$ results in MDF in fossil hydrothermal systems, ore deposits, and modern hot springs (*5, 6*). Zambardi et al. (*58*) found that volcanic emissions of $Hg^0_{(g)}$ are enriched in light isotopes of Hg relative to the magmatic source. In addition, recent laboratory experiments by Zheng et al. (*27*) demonstrated that significant (~1‰) Hg fractionation is caused by the volatilization of $Hg^0_{(aq)}$ at 25 °C from aqueous solutions. During these experiments, Zheng et al. (*27*) separated the evolved $Hg^0_{(g)}$ from the system and estimated a kinetic fractionation factor of 1.00047 ± 0.00002. This fractionation factor is similar to the fractionation factor that we estimate to describe Hg loss from Ojo Caliente (1.00059 ± 0.00016, Figure 2.5b). We suggest that although substantial fractionation of Hg does occur during the precipitation of Hg as an impurity in siliceous sinter, the increase in δ^{202}Hg observed in fluids from Ojo Caliente is primarily caused by volatilization of $Hg^0_{(aq)}$ to $Hg^0_{(g)}$.

Mass-dependent fractionation during vent chimney formation may occur in a similar manner in the Guaymas Basin hydrothermal system. Assuming that little Hg fractionation occurs during magmatic processes and leaching of Hg from volcanic source

rocks (*6*), we expect that the Hg isotopic composition of hydrothermal vent fluids is representative of the composition of mantle-derived materials. Because we were able to collect measurable quantities of Hg (~2200 pg/g) in hydrothermal vent fluids exiting the Pink Flamingo chimney, it is unlikely that Hg precipitation occurs as a result of complete loss from the hydrothermal fluids. Instead, the Hg in the vent chimneys probably precipitates via incomplete precipitation and incremental separation of Hg into the solid phase without back-reaction. Based on our observations in Ojo Caliente, and assuming that precipitation of Hg in hydrothermal vent chimneys operates in a similar manner to precipitation of Hg in siliceous sinter, we suggest that the hydrothermal vent fluids and magmas at Guaymas Basin may have higher δ^{202}Hg values than the vent chimney precipitates.

2.5.2 Mass-independent fractionation

Mass-independent fractionation (MIF) of Hg has now been observed in a wide range of natural samples (*1-3, 16, 62, 63*). However, previous studies of Hg isotopes in hydrothermal systems either did not investigate MIF (*5, 6*) or found no evidence for MIF (*58*). Experimental evidence indicates that MIF can occur during photochemical reduction of Hg^{2+} and demethylation of MeHg (*2*). During processes that cause MIF, odd isotopes react at slightly different rates than even isotopes, most likely due to mechanisms related to the magnetic isotope effect or the nuclear volume effect (*2, 16, 63-65*).

A small but significant positive MIF signature (Δ^{199}Hg = 0.13 ± 0.06‰ 2 s.d.) was measured in all of the fluid and sinter samples from Ojo Caliente and in one of the

additional samples from YNP (Figure 2.6). No Hg MIF was observed in any of the samples from Guaymas Basin. If it is assumed that photochemical reactions are the primary cause of Hg MIF, these data suggest that photochemical reduction has affected Hg in some of the hot springs in YNP but has not affected Hg in vent chimneys isolated from light in Guaymas Basin.

Photochemical reduction of $Hg^{2+}_{(aq)}$ to $Hg^{0}_{(g)}$ preferentially retains the odd isotopes of Hg in the aqueous phase and releases the even isotopes of Hg as $Hg^{0}_{(g)}$ (*2*). As a result, as photochemical reduction occurs in an aqueous system, Δ^{199}Hg in the fluid becomes increasingly higher and Δ^{199}Hg in the released gas becomes increasingly lower. In Ojo Caliente, because all of the samples measured exhibit approximately the same degree of MIF, it is not likely that measurable MIF of Hg is occurring in this system on the short timescale of outflow from the hot spring to the Firehole River. Instead, it is likely that either some portion of the Hg currently dissolved in these hydrothermal fluids was photochemically reduced at some stage in its geological history and re-mixed into the hydrothermal system or that Hg containing a MIF signature was leached directly from the volcanic source rocks.

The lack of MIF observed in vent chimney samples from Guaymas Basin suggests that Hg in that sea-floor rift hydrothermal system may not be of sedimentary origin. In Guaymas Basin, a portion of the hydrothermal fluids circulate through the thick organic-rich sediments that cover the sea-floor (*48, 49*). It is possible that Hg measured in the vent precipitates could have been leached from those sediments and not from mantle-derived materials. For example, studies of lead isotopes indicate that some of the lead in hydrothermal fluids at sediment-covered ridges is derived from the sediments (*66*).

However, based on limited data, we suggest that Hg in marine sediments generally displays MIF (*1, 62*) and we suggest that this is due to photochemical reactions near the Earth's surface. Therefore, if a large portion of the Hg precipitated in vent chimneys is affected by secondary circulation and was leached from the sediments, we might expect to observe MIF of Hg isotopes in solid chimney samples. Because no such MIF was observed in samples from Guaymas Basin, we speculate that the Hg in the vent chimneys of Guaymas Basin is most likely to have been sourced from mantle-derived materials rather than from sediments.

2.6 Conclusions and Implications

Mercury concentrations are elevated in hydrothermal systems due to the leaching of Hg-containing materials by hot fluids. The results of this study indicate that substantial MDF of Hg isotopes occurs in hydrothermal systems during several processes including the precipitation of Hg in siliceous sinters and during the volatilization of $Hg^0_{(aq)}$ to $Hg^0_{(g)}$. Additionally, the presence of MIF in samples from YNP and the absence of MIF in samples from Guaymas Basin is consistent with the hypothesis that MIF occurs where light is present to facilitate photochemical reactions.

Hg isotopes in geothermal emissions may allow us to trace these emissions through the terrestrial and aquatic environments that they impact. In order to accurately accomplish this goal, more research is needed to fully characterize the isotopic variability in Hg emissions from hydrothermal systems and in mantle-derived materials. The results of this study indicate that it is possible to effectively use Hg stable isotopes to understand

hydrothermal Hg processes that fractionate Hg and to characterize Hg export from active hydrothermal systems.

Acknowledgements

The funding for this research was provided by NSF Grant EAR-0433772 to J. D. Blum, EAR-0433793 to T. Barkay, and NSF Grant MCB 04-56676 to C. Vetriani. L. S. Sherman is funded by a National Defense Science and Engineering Graduate Research Fellowship from the Office for Naval Research. We thank the crew of R/V *Atlantis* and the crew and pilots of the deep-submergence vehicle *Alvin* for their skillful operations at sea. We are grateful to M. W. Johnson for his laboratory expertise, to S. E. Kesler for his mineralogical knowledge and advice, to A. Schleicher for her laboratory assistance, to P. W. Sherman for thoughtful suggestions, and to the members of the University of Michigan Biogeochemistry and Environmental Isotope Geochemistry Laboratory for many inspiring discussions. We also thank J. Sonke and an anonymous reviewer for comments that improved the manuscript. Any use of trade, firm, or product names is for descriptive purposes only and does not imply endorsement by the U.S. Government.

References

(1) Gehrke, G. E.; Blum, J. D.; Meyers, P. A.; The geochemical behavior and isotopic composition of Hg in a mid-Pleistocene western Mediterranean sapropel. *Geochim. Cosmochim. Acta* **2009,** *73*, 1651-1665.

(2) Bergquist, B. A.; Blum, J. D.; Mass-dependent and mass-independent fractionation of Hg isotopes by photo-reduction in aquatic systems. *Science* **2007,** *318* (5849), 417-420.

(3) Biswas, A.; Blum, J. D.; Bergquist, B. A.; Keeler, G. J.; Zhouqing, X.; Natural mercury isotope variation in coal deposits and organic soils. *Environ. Sci. Technol.* **2008,** *42* (22), 8303-8309.

(4) Kritee, K.; Blum, J. D.; Johnson, M. W.; Bergquist, B. A.; Barkay, T.; Mercury stable isotope fractionation during reduction of Hg(II) to Hg(0) by mercury resistant microorganisms. *Environ. Sci. Technol.* **2007,** *41*, 1889-1895.

(5) Smith, C. N.; Kesler, S. E.; Klaue, B.; Blum, J. D.; Mercury isotope fractionation in fossil hydrothermal systems. *Geology* **2005,** *33* (10), 825-828.

(6) Smith, C. N.; Kesler, S. E.; Blum, J. D.; Rytuba, J. J.; Isotope geochemistry of mercury in source rocks, mineral deposits and spring deposits of the California Coast Ranges, USA. *Earth Planet. Sci. Lett.* **2008,** *269*, 399-407.

(7) Clarkson, T. W.; Magos, L.; The toxicology of mercury and its chemical compounds. *Crit. Rev. Toxicol.* **2006,** *36*, 609-662.

(8) Mason, R. P.; Fitzgerald, W. F.; Morel, F. M. M.; The biogeochemical cycling of elemental mercury: Anthropogenic influences. *Geochim. Cosmochim. Acta* **1994,** *58* (15), 3191-3198.

(9) Mason, R. P.; Sheu, G.-R.; Role of the ocean in the global mercury cycle. *Global Biogeochem. Cycles* **2002,** *16* (4), 1-14.

(10) Gustin, M. S.; Lindberg, S. E.; Weisberg, P. J.; An update on the natural sources and sinks of atmospheric mercury. *Appl. Geochem.* **2008,** *23* (3), 482-493.

(11) Engle, M. A.; Gustin, M. S.; Goff, F.; Counce, D. A.; Janik, C. J.; Bergfeld, D.; Rytuba, J. J.; Atmospheric mercury emissions from substrates and fumaroles associated with three hydrothermal systems in the western United States. *J. Geophys. Res.* **2006,** *111*, D17304.

(12) Nacht, D. M.; Gustin, M. S.; Engle, M. A.; Zehner, R. E.; Giglini, A. D.; Atmospheric mercury emissions and speciation at the Sulphur Bank mercury mine superfund site, northern California. *Environ. Sci. Technol.* **2004,** *38*, 1977-1983.

(13) Pyle, D. M.; Mather, T. A.; The importance of volcanic emissions for the global atmospheric mercury cycle. *Atmos. Environ.* **2003,** *37*, 5115-5124.

(14) Morel, F. M. M.; Kraepiel, A. M. L.; Amyot, M.; The chemical cycle and bioaccumulation of mercury. *Annu. Rev. Ecol. Syst.* **1998,** *29*, 543-566.

(15) Hintelmann, H.; Lu, S.; High precision isotope ratio measurements of mercury isotopes in cinnabar ores using multi-collector inductively coupled plasma mass spectrometry. *Analyst* **2003,** *128*, 635-639.

(16) Jackson, T. A.; Whittle, D. M.; Evans, M. S.; Muir, D. C. G.; Evidence for mass-independent and mass-dependent fractionation of the stable isotopes of mercury by natural processes in aquatic ecosystems. *Appl. Geochem.* **2008,** *23* (3), 547-571.

(17) Zambardi, T.; Sonke, J. E.; Toutain, J. P.; Sortino, F.; Shinohara, H.; Mercury emissions and stable isotopic compositions at Vulcano Island (Italy). *Earth. Planet. Sci. Lett.* **2009,** *277*, 236-243.

(18) German, C. R.; Von Damm, K. L., Hydrothermal processes. In *Treatise on Geochemistry*, Holland, H. D., and Turekian, K.K., Ed. Elsevier: Oxford, **2004**; Vol. 6, pp 182-222.

(19) Barnes, H. L.; Seward, T. M., Geothermal systems and mercury deposits. In *Geochemistry of Hydrothermal Ore Deposits*, Barnes, H. L., Ed. John Wiley: New York, **1997**; pp 699-736.

(20) Krupp, R.; Physicochemical aspects of mercury metallogenesis. *Chem. Geol.* **1988,** *69*, 345-356.

(21) Varekamp, J. C.; Buseck, P. R.; The speciation of mercury in hydrothermal systems with applications to ore deposition. *Geochim. Cosmochim. Acta* **1984,** *48*, 177-185.

(22) Spycher, N. F.; Reed, M. H.; Evolution of a broadlands-type epithermal ore fluid along alternative P-T paths: Implications for the transport and deposition of base, precious, and volatile metals. *Econom. Geol.* **1989,** *84*, 328-359.

(23) Kraepiel, A. M. L.; Keller, K.; Chin, H. B.; Malcolm, E. G.; Morel, F. M. M.; Sources and variations of mercury in tuna. *Environ. Sci. Technol.* **2003,** *37*, 5551-5558.

(24) Zehner, R. E.; Gustin, M. S.; Estimation of mercury vapor flux from natural substrate in Nevada. *Environ. Sci. Technol.* **2002,** *36*, 4039-4045.

(25) Stoffers, P.; Hannington, M.; Wright, I.; Herzig, P., Ronde, C. de., Shipboard Scientific Party; Elemental mercury at submarine hydrothermal vents in the Bay of Plenty, Taupo volcanic zone, New Zealand. *Geology* **1999,** *27* (10), 931-934.

(26) Lamborg, C. H.; Von Damm, K. L.; Fitzgerald, W. F.; Hammerschmidt, C. R.; Zierenberg, R.; Mercury and monomethylmercury in fluids from Sea Cliff submarine hydrothermal field, Gorda Ridge. *Geophys. Res. Lett.* **2006,** *33*, 4 pp.

(27) Zheng, W.; Foucher, D.; Hintelmann, H.; Mercury isotope fractionation during volatilization of Hg(0) from solution into the gas phase. *J. Anal. Atomic Spectro.* **2007,** *22*, 1097-1104.

(28) Foucher, D.; Hintelmann, H.; High-precision measurement of mercury isotope ratios in sediments using cold-vapor generation multi-collector inductively coupled plasma mass spectrometry. *Anal. Bioanal. Chem.* **2006,** *384*, 1470-1478.

(29) Johnson, C. M.; Beard, B. L.; Biogeochemical cycling of iron isotopes. *Science* **2005,** *309*, 1025-1027.

(30) Beard, B. L.; Johnson, C. M.; Fe isotope variations in the modern and ancient Earth and other planetary bodies. *Reviews in Mineralogy and Geochemistry* **2004,** *55*, 319-357.

(31) Christiansen, R. L.; The Quaternary and Pliocene Yellowstone Plateau Volcanic Field of Wyoming, Idaho, and Montana. *U.S. Geol. Surv. Prof. Pap.* **2001**, 145.

(32) Fournier, R. O.; Geochemistry and dynamics of the Yellowstone National Park hydrothermal system. *Annu. Rev. Earth Planet. Sci.* **1989,** *17*, 13-53.

(33) Eaton, G. P.; Christiansen, R. L.; Iyer, H. M.; Pitt, A. M.; Mabey, D. R.; Blank Jr., H. R.; Zietz, I.; Gettings, M. E.; Magma beneath Yellowstone National Park. *Science* **1975,** *188* (4190), 787-796.

(34) King, S. A.; Behnke, S.; Slack, K.; Krabbenhoft, D. P.; Nordstrom, D. K.; Burr, M. D.; Striegl, R. G.; Mercury in water and biomass of microbial communities in hot springs of Yellowstone National Park, USA. *Appl. Geochem.* **2006,** *21*, 1868-1879.

(35) Phelps, D.; Buseck, P. R.; Distribution of soil mercury and the development of soil mercury anomalies in the Yellowstone geothermal area, Wyoming. *Econom. Geol.* **1980,** *75*, 730-741.

(36) Hildreth, W.; Halliday, A. N.; Christiansen, R. L.; Isotopic and chemical evidence concerning the genesis and contamination of basaltic and rhyolitic magma beneath the Yellowstone Plateau Volcanic Field. *Journal of Petrology* **1991,** *32*, 63-138.

(37) Truesdell, A. H.; Fournier, R. O.; Conditions in the deeper parts of the hot spring systems of Yellowstone National Park, Wyoming. *U.S. Geol. Surv. Open-File Rep.* **1976**, 32.

(38) Craig, H., The isotopic geochemistry of water and carbon in geothermal areas. In *Nuclear Geology of Geothermal Areas*, Tongiorgi, E., Ed. Consiglio Nazionale delle Richerche, Laboratorio de Geologia Nucleate, Pisa: Spoleto, **1963**; pp 17-53.

(39) Braunstein, D.; Lowe, D. R.; Relationship between spring and geyser activity and the deposition and morphology of high temperature (>73°C) siliceous sinter, Yellowstone National Park, Wyoming, USA. *Journal of Sedimentary Research* **2001,** *71* (5), 747-763.

(40) Guidry, S. A.; Chafetz, H. S.; Anatomy of siliceous hot springs: examples from Yellowstone National Park, Wyoming, USA. *Sediment. Geol.* **2003,** *157*, 71-106.

(41) Nordstrom, D. K.; Ball, J. W.; McCleskey, R. B., Ground water to surface water: Chemistry of thermal outflows in Yellowstone National Park. In *Geothermal Biology and Geochemistry of Yellowstone National Park*, Inskeep, W. P., McDermott, T.R., Ed. Thermal Biology Institute: Bozeman, Montana, **2005**; pp 73-94.

(42) Fouke, B. W.; Farmer, J. C.; Des Marais, D. J.; Pratt, L.; Sturchio, N. C.; Burns, P. C.; Discipulo, M. K.; Depositional facies and aqueous-solid geochemistry of travertine-depositing hot springs (Angel Terrace, Mammoth Hot Springs, Yellowstone National Park, U.S.A.). *Journal of Sedimentary Research* **2000,** *70* (3), 565-585.

(43) Bennett, J. P.; Wetmore, C. M.; Geothermal elements in lichens of Yellowstone National Park, USA. *Environ. Exp. Bot.* **1999,** *42*, 191-200.

(44) Ball, J. W.; Nordstrom, D. K.; Cunningham, K. M.; Schoonen, M. A. A.; Xu, Y.; DeMonge, J. M.; Water-chemistry and on-site sulfur-speciation data for selected springs in Yellowstone National Park, Wyoming, 1994-1995. *U.S. Geol. Surv. Open-File Rep.* **1998**, 40.

(45) Gooch, F. A.; Whitfield, J. E.; Analyses of waters of the Yellowstone National Park. *U.S. Geol. Surv. Bull.* **1888,** *47*.

(46) Peter, J. M.; Scott, S. D.; Mineralogy, composition, and fluid-inclusion microthermometry of seafloor hydrothermal deposits in the Southern Trough of Guaymas Basin, Gulf of California. *Can. Mineral.* **1988,** *26*, 567-587.

(47) Lonsdale, P.; Becker, K.; Hydrothermal plumes, hot springs, and conductive heat flow in the Southern Trough of the Guaymas Basin. *Earth Planet. Sci. Lett.* **1985,** *73*, 211-225.

(48) Lonsdale, P.; Lawver, L. A.; Immature plate boundary zones studied with a submersible in the Gulf of California. *Geo. Soc. Amer. Bull.* **1980,** *91*, 555-569.

(49) Sturz, A. A.; Sturdivant, A. E.; Leif, R. N.; Simoneit, B. R. T.; Gieskes, J. M.; Evidence for retrograde hydrothermal reactions in near surface sediments of Guaymas Basin, Gulf of California. *Appl. Geochem.* **1996,** *11*, 645-665.

(50) Lonsdale, P.; Hydrothermal plumes and baritic sulfide mounds at a Gulf of California spreading center. *EOS Trans. Am. Geophys. Union* **1980,** *61*, 995.

(51) Crespo-Medina, M.; Chatziefthimiou, A. D.; Bloom, N. S.; Luther III, G. W.; Wright, D. D.; Reingelder, J. R.; Vetriani, C.; Barkay, T.; Adaptation of chemosynthetic microorganisms to elevated mercury concentrations in deep-sea hydrothermal vents. *Limnol. Oceanogr.* **2009,** *54* (1), 41-49.

(52) Blum, J. D.; Bergquist, B. A.; Reporting the variations in the natural isotopic composition of mercury. *Anal. Bioanal. Chem.* **2007,** *388* (2), 353-359.

(53) Bryan, T. S., The Geysers of Yellowstone. 3rd ed.; University Press of Colorado: Colorado, **1995**; p 463.

(54) Jones, B.; Renaut, R. W.; Water content of opal-A: Implications for the origin of laminae in geyserite and sinter. *Journal of Sedimentary Research* **2004,** *74* (1), 117-128.

(55) Mariotti, A.; Germon, J. C.; Hubert, P.; Kaiser, P.; Letolle, R.; Tardieux, A.; Tardieux, P.; Experimental determination of nitrogen kinetic isotope fractionation: Some principles; illustration for the denitrification and nitrification processes. *Plant Soil* **1981,** *62*, 413-430.

(56) Scott, K. M.; Lu, X.; Cavanaugh, C. M.; Liu, J. S.; Optimal methods for estimating kinetic isotope effects from different forms of the Rayleigh distillation equation. *Geochim. Cosmochim. Acta* **2004,** *68* (3), 433-442.

(57) York, D.; Least-squares fitting of a straight line. *Can. J. Phys.* **1966,** *44*, 1076-1086.

(58) Zambardi, T.; Sonke, J. E.; Toutain, J. P.; Sortino, F.; Shinohara, H.; Mercury emissions and stable isotopic compositions at Vulcano Island (Italy). *Geophys. Res. Abstr.* **2008,** *10*, EGU General Assembly.

(59) Butler, I. B.; Archer, C.; Vance, D.; Oldroyd, A.; Rickard, D.; Fe isotope fractionation on FeS formation in ambient aqueous solution. *Earth Planet. Sci. Lett.* **2005,** *236*, 430-442.

(60) Campbell, K. A.; Sannazzaro, K.; Rodgers, K. A.; Herdianita, N. R.; Browne, P. R. L.; Sedimentary facies and mineralogy of the late Pleistocene Umukuri silica sinter, Taupo Volcanic Zone, New Zealand. *Journal of Sedimentary Research* **2001,** *71* (5), 727-746.

(61) Varekamp, J. C.; Buseck, P. R.; Global mercury flux from volcanic and geothermal sources. *Appl. Geochem.* **1986,** *1*, 65-73.

(62) Hintelmann, H.; Foucher, D.; Telmer, K.; Zheng, J.; Yamada, M.; Hg isotope fractionation in sediment cores. *Geochim. Cosmochim. Acta* **2008,** *72* (12S), A379.

(63) Ghosh, S.; Xu, Y.; Humayun, M.; Odom, L.; Mass-independent fractionation of mercury isotopes in the environment. *Geochem. Geophys. Geosyst.* **2008,** *9*, Q03004, doi: 10.1029/2007/GC001827.

(64) Buchachenko, A. L.; Ivanov, V. L.; Roznyatovskii, V. A., Vorob'ev, A.Kh., Ustynyuk, Yu.A.; Inversion of the sign of the magnetic isotope effect of mercury in photolysis of substituted dibenzylmercury. *Doklady Phys. Chem.* **2008,** *420* (1), 85-87.

(65) Schauble, E. A.; Role of nuclear volume in driving equilibrium stable isotope fractionation of mercury, thallium, and other very heavy elements. *Geochim. Cosmochim. Acta* **2007,** *71*, 2170-2189.

(66) Fouquet, Y.; Marcoux, E.; Lead isotope systematics in Pacific hydrothermal sulfide deposits. *J. Geophys. Res.* **1995,** *100* (B4), 6025-6040.

(67) Xu, Y.; Schoonen, M. A. A.; Nordstrom, D. K.; Cunningham, K. M.; Ball, J. W.; Sulfur geochemistry of hydrothermal waters in Yellowstone National Park: I. The origin of thiosulfate in hot spring waters. *Geochim. Cosmochim. Acta* **1998,** *62*, 3729-3743.

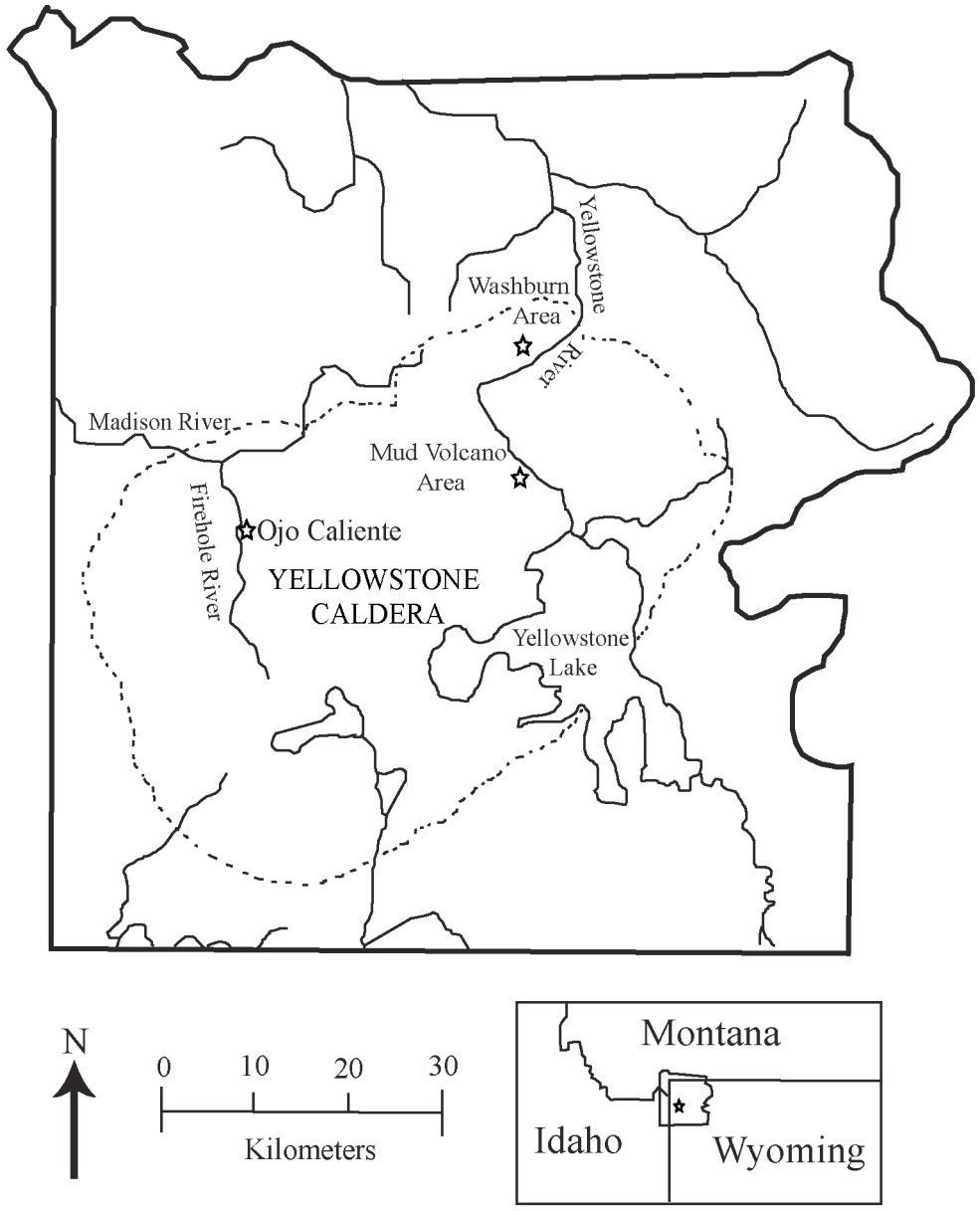


Figure 2.1 Map of Yellowstone National Park boundary with the rim of the Yellowstone Caldera outlined and study areas indicated. Adapted from (*31, 44, 67*).

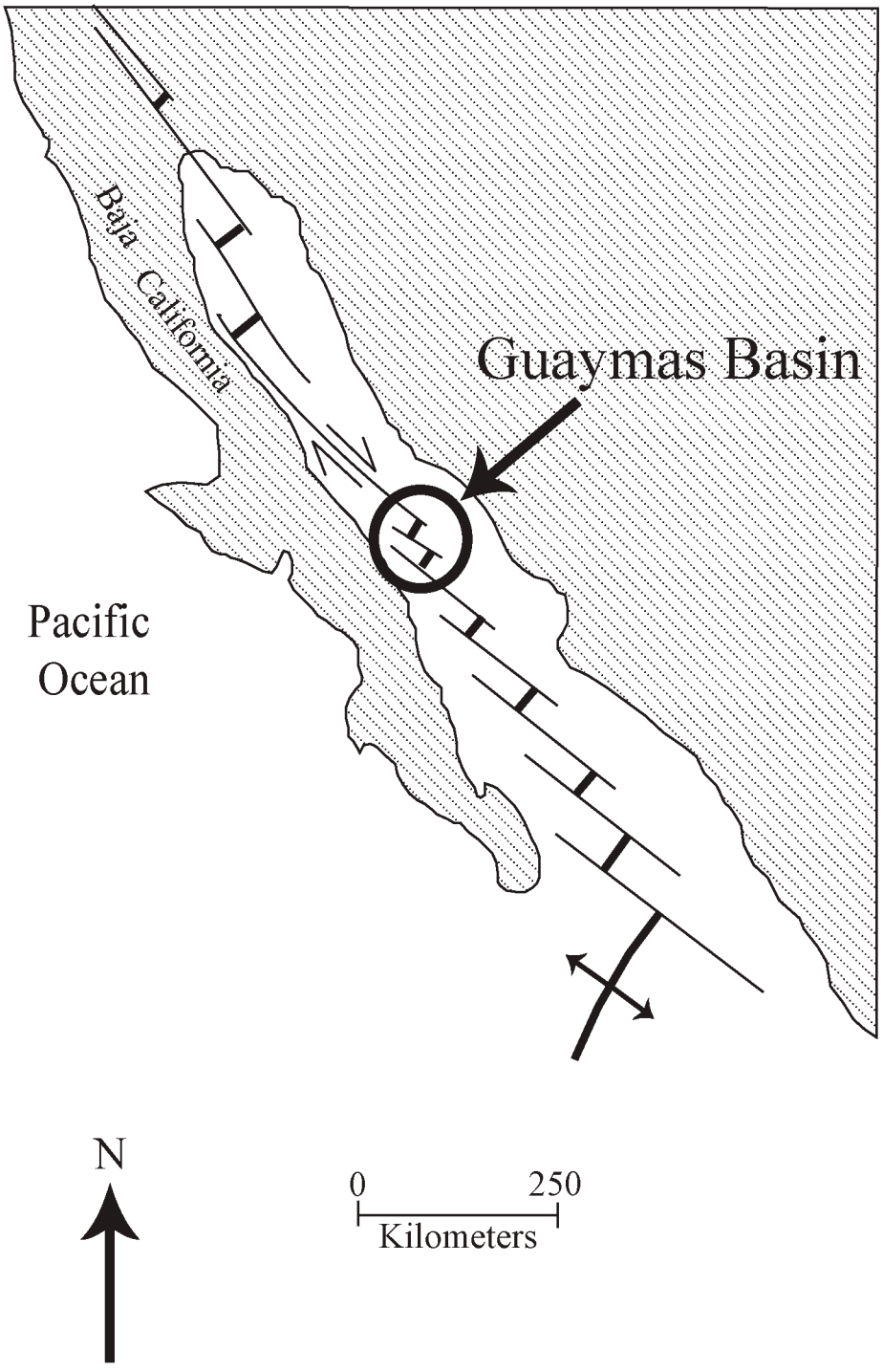


Figure 2.2 Map indicating location of Guaymas Basin in the Gulf of California. Axial spreading ridges are shown. Adapted from (*46*).

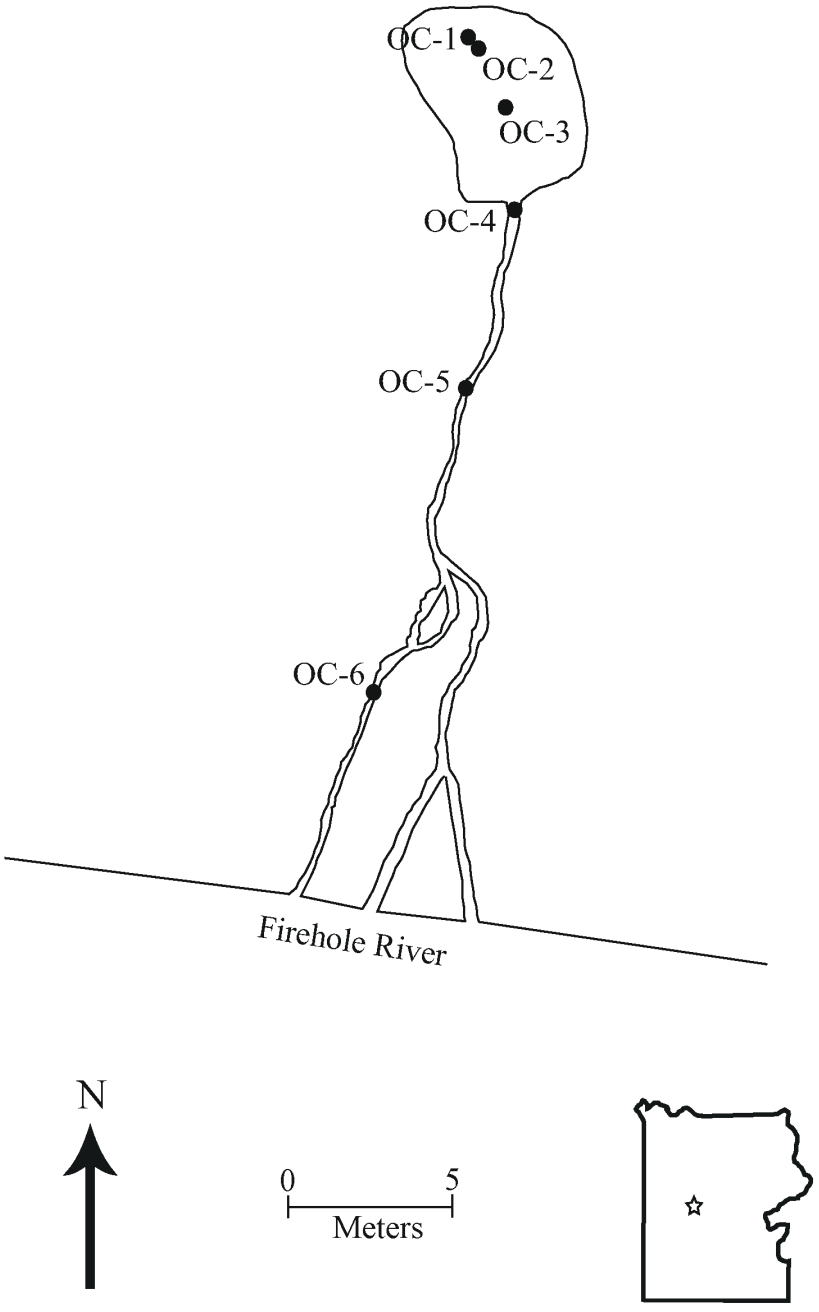


Figure 2.3 Aerial view schematic of Ojo Caliente with sampling locations indicated. Water sample OC-1 was taken at the vent location (5.7 m below the surface); water sample OC-2 was taken near the surface at the same location (~30 cm depth); water sample OC-3 was taken in the middle of the source pool near the surface (~30 cm depth). Sinter samples (OC-S-2, OC-S-4, OC-S-5, and OC-S-6) were collected at the same approximate distances downstream as the corresponding liquid samples. Adapted from (*44*).

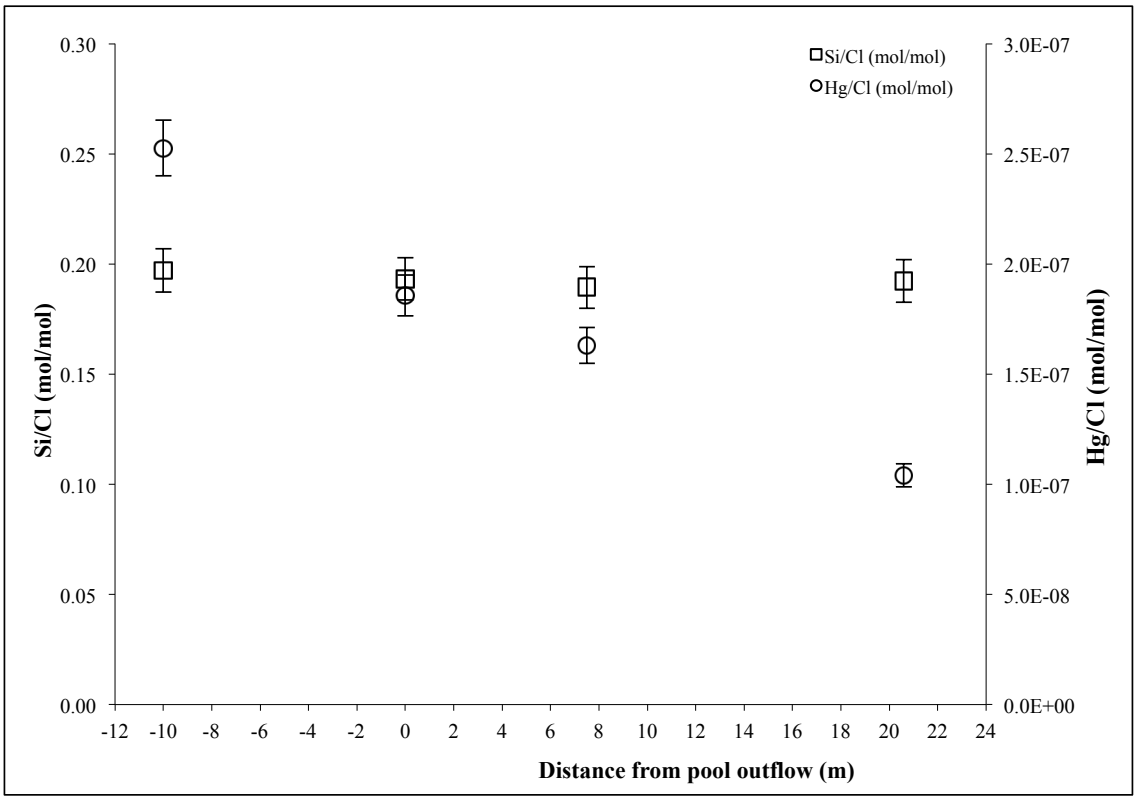
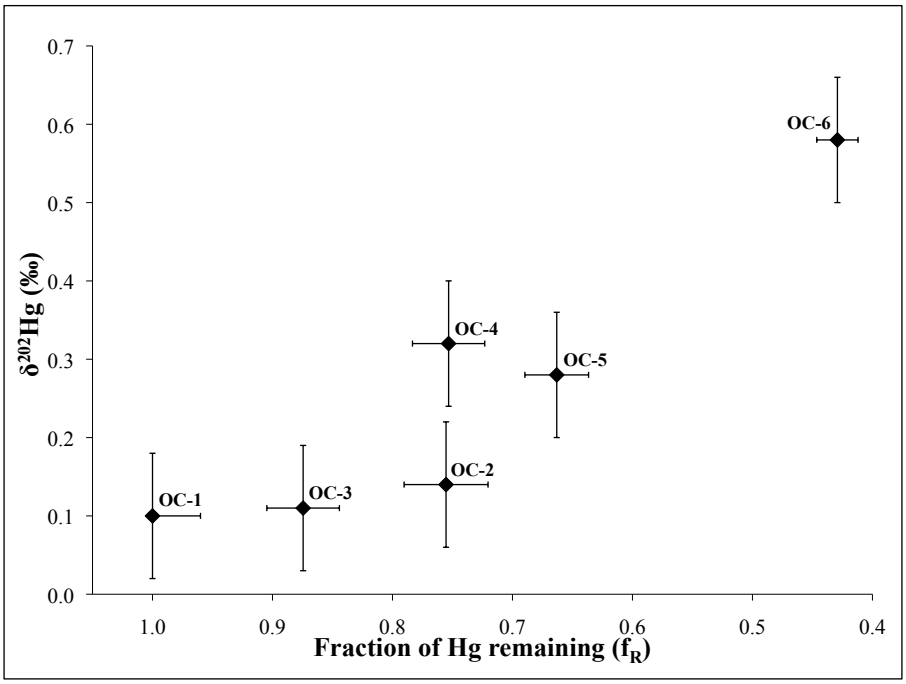


Figure 2.4 Plot of Si/Cl ratios and Hg/Cl ratios in Ojo Caliente from the source pool (OC-1) to the end of the outflow channel (OC-6). Analytical uncertainties (± 5%) are shown.

a.



b.

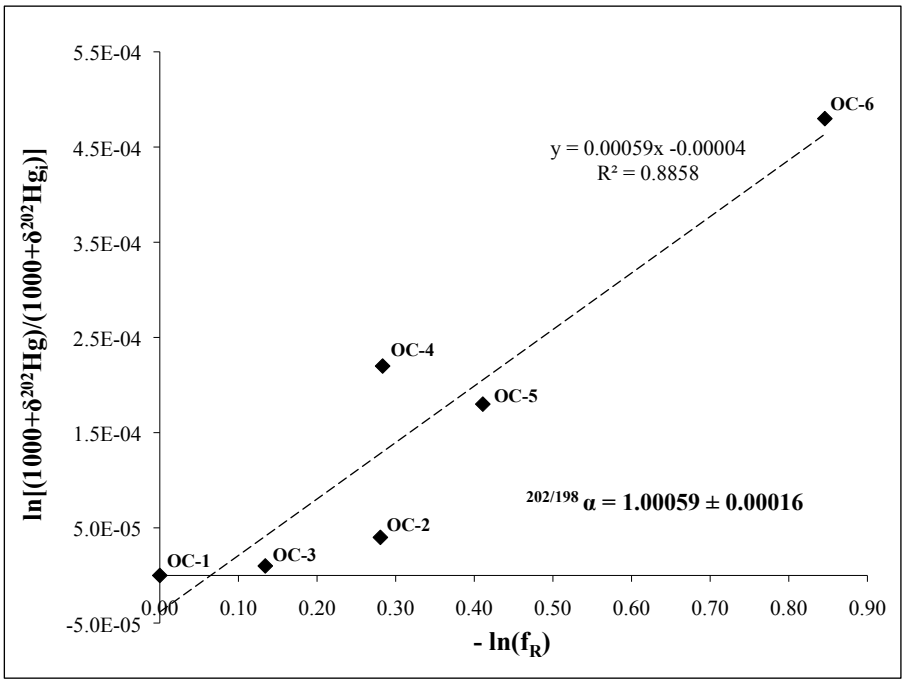


Figure 2.5 a. Plot of δ^{202}Hg versus the fraction of Hg remaining in each fluid sample from Ojo Caliente with respect to the Hg concentration in the original vent fluid (f_R). Analytical uncertainties, based on replicate analyses of procedural standards and in-house UM Almadén standard, are depicted for each data point. **b.** Same data as Figure 2.5a plotted on a log-log plot. A kinetic fractionation factor ($^{202/198}\alpha$) of 1.00059 ± 0.00016 (1 s.d.) is estimated for this relationship.

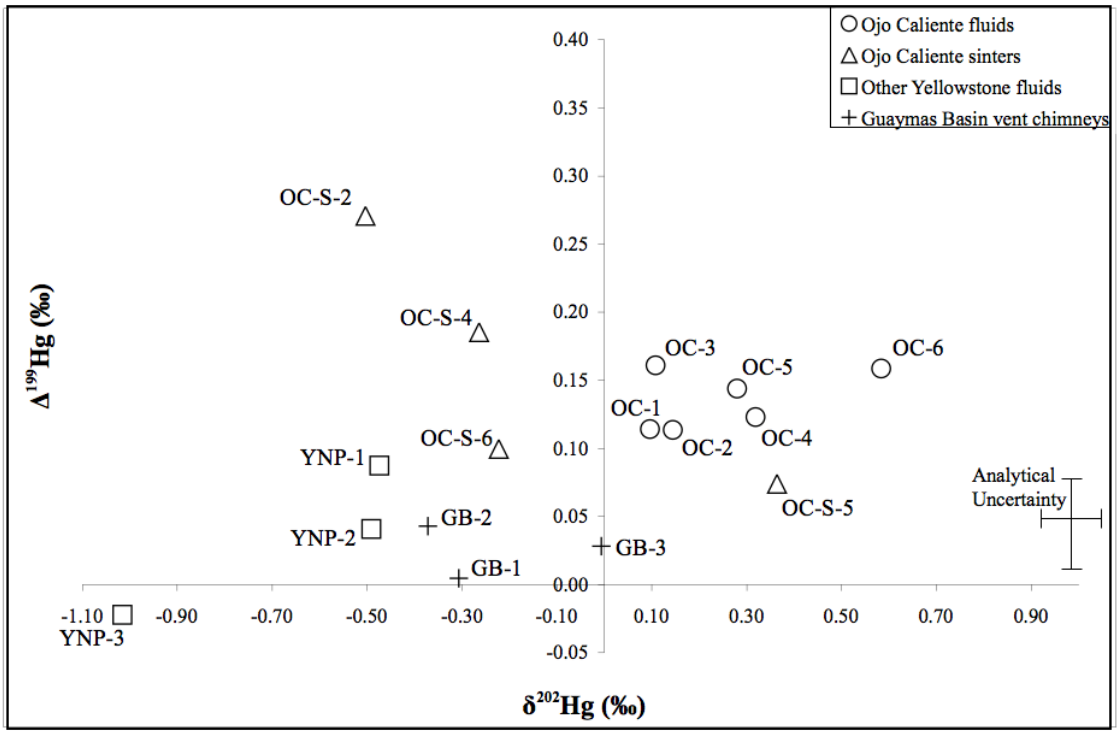


Figure 2.6 Δ^{199}Hg versus δ^{202}Hg measured in the fluid and sinter samples from Yellowstone National Park and vent precipitates from Guaymas Basin. Fluid samples from Ojo Caliente are shown as open circles, sinter samples from Ojo Caliente are shown as open triangles, fluid samples from other locations in YNP are shown as open squares, and vent precipitates from Guaymas Basin are shown as plus symbols. Representative error bars based on replicate analyses of procedural standards are depicted in the lower right corner of the plot.

Table 2.1 Water chemistry properties and solute concentrations measured in fluid samples from Yellowstone National Park. Samples measured include four from Ojo Caliente (OC-2, OC-4, OC-5, and OC-6) and individual samples from the Washburn Area (Inkpot #3 = YNP-1) and Mud Volcano area (Turbulent Pool = YNP-2, Sulfur Cauldron = YNP-3). Properties that were not analyzed are shown as "---."

Sample location	**Sample ID**	**Temp (°C)**	**pH**	**DOC (mg/L)**	**SC (µS/cm)**	**HCO_3^- (mg/L)**	**Ca (mg/L)**	**Mg (mg/L)**	**Na (mg/L)**	**K (mg/L)**	**SO_4 (mg/L)**	**Cl (mg/L)**	**SiO_2 (mg/L)**
Ojo Caliente	OC-1	93.2	7.44	0.86	1470	231	0.85	<0.007	318	9.3	22.6	326	233
Ojo Caliente	OC-4	91.4	7.52	0.50	1500	232	0.87	<0.007	323	9.2	22.2	334	234
Ojo Caliente	OC-5	86.8	7.61	0.51	1530	235	0.83	<0.007	326	9.4	22.0	335	230
Ojo Caliente	OC-6	74.8	---	0.56	1590	239	0.85	<0.007	336	9.3	23.4	340	237
Washburn area: Inkpot #3	YNP-1	70.9	3.25	5.43	5750	---	53.4	26.9	37.8	14.4	3090	1.56	251
Mud Volcano area: Turbulent Pool	YNP-2	58.5	1.89	3.98	4360	---	11.6	3.8	15.5	13.9	1710	5.04	234
Mud Volcano area: Sulfur Cauldron	YNP-3	73.5	2.02	7.74	3950	---	26.5	8.9	21.0	19.0	2660	4.33	406

Table 2.2 Mercury concentrations, percent recovery, and summary of measured δ^{202}Hg and Δ^{199}Hg for all of the fluid and solid samples in this study collected from Yellowstone National Park and Guaymas Basin.

Sample location	**Sample type**	**Sample ID**	**Hg concentration**	**Hg Recovery (%)**	**δ^{202}Hg (‰)**	**Δ^{199}Hg (‰)**
			(pg/g)			
Ojo Caliente	fluid	OC-1	46.6	48	0.10	0.11
Ojo Caliente	fluid	OC-2	35.1	100	0.14	0.11
Ojo Caliente	fluid	OC-3	40.7	100	0.11	0.16
Ojo Caliente	fluid	OC-4	35.1	95	0.32	0.12
Ojo Caliente	fluid	OC-5	30.9	100	0.28	0.14
Ojo Caliente	fluid	OC-6	20.0	100	0.58	0.16
Washburn Inkpot #3	fluid	YNP-1	25.8	100	-0.47	0.09
Turbulent Pool	fluid	YNP-2	66.8	97	-0.49	0.04
Sulfur Cauldron	fluid	YNP-3	132	98	-1.02	-0.02
			(ng/g)			
Ojo Caliente	sinter	OC-S-2	2040	75	-0.50	0.27
Ojo Caliente	sinter	OC-S-4	197	100	-0.26	0.19
Ojo Caliente	sinter	OC-S-5	161	100	0.36	0.07
Ojo Caliente	sinter	OC-S-6	215	72	-0.22	0.10
Guaymas Basin	chimney piece	GB-1	39.5	100	-0.31	0.00
Guaymas Basin	fluid precipitate	GB-2	N/A	N/A	-0.37	0.04
Guaymas Basin	chimney piece	GB-3	111	100	-0.01	0.03

Table 2.SI-1 Mercury isotopic composition of standards, fluid and sinter samples from Yellowstone National Park, and vent precipitates from Guaymas Basin. Average values presented for the in-house UM Almadén standard are from measurements made from September 2007 to March 2008. Uncertainties are presented as twice the standard error (2 s.e.) of sample replicates and the larger of the 2SE of sample replicates or twice the standard deviation (2 s.d.) of replicate measurements of the in-house UM Almadén standard or procedural standards.

Sample location	Sample type	Sample ID	n	δ^{202}Hg (‰)	2 s.e.	2 s.d.	δ^{201}Hg (‰)	2 s.e	2 s.d.	δ^{200}Hg (‰)	2 s.e	2 s.d.	δ^{199}Hg (‰)	2 s.e	2 s.d.	Δ^{201}Hg (‰)	2 s.e	2 s.d.	Δ^{200}Hg (‰)	2 s.e	2 s.d.	Δ^{199}Hg (‰)	2 s.e	2 s.d.
UM Almadén standard			117	-0.55	0.08		-0.46	0.07		-0.27	0.05		-0.16	0.04		-0.05	0.03		0.01	0.02		-0.02	0.03	
NIST SRM 3133 (liquid process std)			15	-0.02	0.11		0.01	0.11		0.03	0.07		0.03	0.06		0.02	0.08		0.00	0.04		0.04	0.06	
NIST SRM 2711 (Montana Soil)			44	-0.11	0.14		-0.26	0.15		-0.06	0.09		-0.22	0.10		-0.17	0.07		0.00	0.04		-0.20	0.08	
Ojo Caliente	fluid	OC-1	1	0.10		0.11	0.19		0.11	0.04		0.07	0.14		0.06	0.12		0.08	0.00		0.04	0.11		0.06
Ojo Caliente	fluid	OC-2	1	0.14		0.11	0.16		0.11	0.05		0.07	0.15		0.06	0.05		0.08	-0.02		0.04	0.11		0.06
Ojo Caliente	fluid	OC-3	1	0.11		0.11	0.15		0.11	0.04		0.07	0.19		0.06	0.07		0.08	-0.02		0.04	0.16		0.06
Ojo Caliente	fluid	OC-4	1	0.32		0.11	0.29		0.11	0.17		0.07	0.20		0.06	0.06		0.08	0.01		0.04	0.12		0.06
Ojo Caliente	fluid	OC-5	1	0.28		0.11	0.28		0.11	0.16		0.07	0.21		0.06	0.07		0.08	0.02		0.04	0.14		0.06
Ojo Caliente	fluid	OC-6	1	0.58		0.11	0.52		0.11	0.31		0.07	0.30		0.06	0.08		0.08	0.02		0.04	0.16		0.06
Washburn Inkpot #3	fluid	YNP-1	1	-0.47		0.11	-0.28		0.11	-0.20		0.07	-0.03		0.06	0.08		0.08	-0.01		0.04	0.09		0.06
Turbulent Pool	fluid	YNP-2	2	-0.49	0.04	0.11	-0.42	0.08	0.11	-0.25	0.08	0.07	-0.08	0.08	0.06	-0.05	0.04	0.08	-0.01	0.12	0.06	0.04	0.08	0.06
Sulfur Cauldron	fluid	YNP-3	1	-1.02		0.11	-0.72		0.11	-0.52		0.07	-0.28		0.06	0.04		0.08	-0.01		0.04	-0.02		0.06
Ojo Caliente	sinter	OC-S-2	2	-0.50	0.02	0.14	-0.24	0.01	0.15	-0.24	0.05	0.09	0.14	0.10	0.10	0.14	0.02	0.07	0.01	0.04	0.04	0.27	0.09	0.08
Ojo Caliente	sinter	OC-S-4	2	-0.26	0.04	0.14	-0.08	0.09	0.15	-0.14	0.02	0.09	0.12	0.02	0.10	0.11	0.05	0.07	-0.01	0.04	0.04	0.19	0.03	0.08
Ojo Caliente	sinter	OC-S-5	1	0.36		0.14	0.29		0.15	0.21		0.09	0.17		0.10	0.01		0.07	0.03		0.04	0.07		0.08
Ojo Caliente	sinter	OC-S-6	2	-0.22	0.10	0.14	-0.08	0.10	0.15	-0.08	0.08	0.09	0.04	0.12	0.10	0.09	0.02	0.07	0.03	0.03	0.04	0.10	0.09	0.08
Guaymas Basin	chimney piece	GB-1	1	-0.31		0.14	-0.18		0.15	-0.15		0.09	-0.07		0.10	0.05		0.07	0.00		0.04	0.00		0.08
Guaymas Basin	fluid precipitate	GB-2	2	-0.37	0.07	0.14	-0.22	0.03	0.15	-0.17	0.05	0.09	-0.05	0.06	0.10	0.06	0.02	0.07	0.01	0.02	0.04	0.04	0.04	0.08
Guaymas Basin	chimney piece	GB-3	3	-0.01	0.02	0.14	0.00	0.11	0.15	0.03	0.06	0.09	0.03	0.12	0.10	0.00	0.10	0.07	0.03	0.06	0.04	0.03	0.12	0.08

CHAPTER 3

Mass-independent fractionation of mercury isotopes in Arctic snow driven by sunlight[1]

3.1 Introduction

After polar sunrise in Arctic regions, sunlight-induced reactions convert gaseous elemental mercury into compounds that are rapidly deposited to the snowpack. These atmospheric mercury depletion events occur repeatedly until snowmelt (*1, 2*). Following deposition, the mercury can be reduced by sunlight-inducted reactions and emitted as a gas (*3-6*), or can be retained in the snowpack (*7, 8*), where it may affect Arctic ecosystems following snowmelt. However, the proportion of mercury that remains in the snowpack is uncertain. Here, we measured the mercury isotopic composition of snow samples collected during an atmospheric mercury depletion event in Barrow, Alaska. We report large negative mass-independent fractionation of mercury isotopes in the Arctic snow. Results from a flux chamber experiment suggest that mass-independent fractionation is coupled to the re-emission of elemental mercury to the atmosphere, and is triggered by sunlight-induced reactions. On the basis of the above, we estimate that photochemical reactions triggered the release of a significant portion of the mercury deposited during this atmospheric mercury depletion event.

[1]Sherman, L. S., Blum, J. D., Johnson, K. P., Keeler, G. J., Barres, J. A., Douglas, T. A. Mass-independent fractionation of mercury isotopes in Arctic snow driven by sunlight. *Nature Geoscience* **2010**, *3*, 173-177.

3.2 Main Text

As a result of active redox chemistry, occurrence in several physical states and seven stable isotopes (196, 198, 199, 200, 201, 202, and 204 amu), mercury (Hg) isotopes are fractionated during a wide range of reactions. Mass-dependent fractionation (MDF) of Hg can occur as a result of processes such as volatilization from aqueous solutions (*9, 10*) and microbial reduction (*11*). MDF is described using delta notation according to equation (1) where $(^{xxx}Hg/^{198}Hg)_{NIST\ SRM\ 3133}$ is the average Hg isotope ratio of bracketing standards (*12*).

$$\delta^{xxx}Hg\ (‰) = ([(^{xxx}Hg/^{198}Hg)_{unknown}/(^{xxx}Hg/^{198}Hg)_{NIST\ SRM\ 3133}] - 1) * 1000 \qquad (1)$$

Recent data indicate that Hg isotopes can also undergo mass-independent fractionation (MIF) in which the even and odd mass number isotopes fractionate from each other (*13-17*). MIF of Hg isotopes has been observed in a variety of natural samples including sediments, hydrothermal waters and fish tissue (*10, 13, 16, 17*). MIF is described using capital delta notation (for example, $\Delta^{199}Hg$) as the difference between the measured $\delta^{xxx}Hg$ value and that predicted on the basis of kinetic MDF (*12*).

Although the processes that cause MIF are not fully understood, MIF of Hg isotopes is believed to occur during both reactions at equilibrium (for example, as a result of the nuclear volume effect) (*18, 19*) and kinetically-driven processes (for example, as a result of the magnetic isotope effect) (*20*). The magnetic isotope effect occurs during reactions involving long-lived radical pairs as a result of the influence of hyperfine coupling between unpaired nuclear spins and electronic spins on the rate of triplet to singlet spin conversion (*13, 20*). Because only odd mass number isotopes of Hg have unpaired nuclear spins, even- and odd-mass-number isotopes can react at different rates.

Bergquist and Blum (*13*) demonstrated that photochemical reduction of Hg^{2+} and degradation of methylmercury from aqueous solutions containing dissolved organic carbon can cause the preferential reduction and evasion of the even-mass-number isotopes of Hg. As a result, increasingly positive $\Delta^{199}Hg$ values (up to 2.1 ± 0.05‰, 2 s.d.) were observed in aqueous solutions following reduction and evasion. A similar degree of positive MIF was measured in fish tissues and it was suggested that the MIF signature was passed through the aquatic food web during bioaccumulation (*13*).

During polar atmospheric mercury depletion events (AMDEs), photochemically initiated reactions involving halogen and halogen oxide radicals oxidize $Hg^0_{(g)}$ in the lower atmospheric boundary layer to compounds that are rapidly deposited to the snowpack (*1, 21-23*). As a result, atmospheric $Hg^0_{(g)}$ concentrations decrease significantly (to <0.5 ng/m^3) and surface snow inorganic Hg concentrations increase (up to >250 pg/m^3) (*1, 21*). Previous studies of Hg deposition and measurements of vertical $Hg^0_{(g)}$ profiles during AMDEs indicate that nearly total depletion of Hg occurs in the atmospheric boundary layer from the snow surface up to ~200-1000 m elevation (*21, 23, 24*). Nearly complete deposition should preserve the gaseous Hg isotope composition in deposited Hg even if fractionation occurs during oxidation.

On the basis of measurements of Hg sources to the atmosphere, we expected that atmospheric Hg would not show significant MIF (*10, 14*). To test this we collected total gaseous Hg (Hg_T, which is predominantly $Hg^0_{(g)}$) (*25*) near Barrow, Alaska in June 2008 by pumping filtered ambient air through gold traps. Although we did not collect gaseous samples at the same time as snow sample collection (March 2006), these atmospheric samples give us an indication of the gaseous Hg_T isotope composition in the spring near

Barrow, Alaska. As expected, the Hg_T samples show very little MIF ($\Delta^{199}Hg$ = -0.11 to -0.22‰ ± 0.08‰, 2 s.e.; Figure 3.1 and Table 3.1). If removal of Hg from the boundary layer was incomplete and Hg fractionation occurs during oxidation, we cannot eliminate the possibility that the isotopic composition of deposited Hg could be different from that of Hg_T. Isotopic measurements of atmospherically deposited Hg in Spanish moss and tree lichens suggest that Hg deposited in other regions may show some negative MIF ($\Delta^{199}Hg$ = -0.03 to -1‰, 2 s.d. = <0.16‰) (*15, 26*). On the basis of these data, we allow for the possibility that AMDE-deposited Hg may initially show small negative MIF ($\Delta^{199}Hg$ = 0 to -1‰).

After deposition, Hg can be photochemically reduced and subsequently re-oxidized within the snow (*4, 27*) or released to the atmosphere as $Hg^0_{(g)}$ (*3-6*). To investigate Hg fractionation during photochemical reduction and emission of $Hg^0_{(g)}$, we collected snowfall, surface snow, and drifted snow samples during a nine-day AMDE near Barrow, Alaska in March 2006. All samples were collected using Hg-clean methods; sample collection procedures have been previously published (*21*). Briefly, to avoid incorporation of saltating snow grains, snowfall was collected in trays elevated 1.5 m above the ground (*21*). Newly fallen precipitation in these trays was sampled every 24 h. Surface snow was collected from the upper 1 cm of the snowpack and represents recently deposited snow that was exposed to sunlight for at least several days. Drifted snow was collected downwind of a wooden snow fence from the upper 2 cm of the snowpack. These samples primarily represent a mixture of snow crystals that were transported across the tundra by saltation (for an unknown distance and time period).

Snowfall samples contained the highest observed inorganic Hg concentrations (>350 ng/L) and concentrations were lower (~100 ng/L) in drifted snow samples (Table 3.1).

After pre-concentration, the Hg isotopic compositions of these samples were measured using cold-vapor multi-collector inductively coupled plasma mass spectrometry (*12, 13*) (Table 3.1 and Figure 3.1). The amount of negative MIF increased from snowfall (Δ^{199}Hg = -0.95 to -1.20‰, 2 s.d = 0.09‰) to surface snow (Δ^{199}Hg = -2.41 to -2.63‰, 2 s.d. = 0.09‰) to drifted snow (Δ^{199}Hg = -3.84 to -5.08‰, 2 s.d. = 0.09‰). This degree of negative MIF is an order of magnitude greater than previously observed in natural samples of any type (*14-16, 28*).

These data indicate that with exposure to sunlight, Hg is lost from surface snow (*21*) and undergoes MIF, wherein the odd-mass-number isotopes of Hg are preferentially reduced and emitted. To further investigate the fractionation of Hg isotopes during photochemical reduction from the snowpack, we analyzed the isotopic compositions of the products of a controlled flux chamber experiment. The rates of photochemical reduction for this and similar experiments were published previously (*21*). On 27 March 2006, a 40 L polypropylene flux chamber with a transparent Teflon window was filled with snow from the drift site to a depth of 11.5 cm. Before starting the experiment, duplicate snow samples were taken from the chamber. Over a 10.5 h period, sunlight entered the chamber through the Teflon window and ambient air was pulled into the chamber through a Teflon inlet tube. Photochemically reduced Hg was simultaneously sampled into a Tekran 2537A gaseous Hg analyzer and onto an in-line gold trap at a combined rate of 2.5 L/min. After the experiment, duplicate samples were taken of the

chamber snow (0-6 cm depth). The isotopic composition of volatilized $Hg^0_{(g)}$ collected on the gold trap was also analyzed.

Photochemical reduction of Hg from the snow surface in the chamber caused both emission of $Hg^0_{(g)}$ (~6% of total Hg in the snow; (*21*) and significant fractionation of Hg isotopes (Figure 3.1 and Table 3.1). The measured isotopic compositions of the duplicate surface snow samples taken before the experiment were the same within measurement error (δ^{202}Hg = 0.40 and 0.44‰, 2 s.d. = 0.17‰; Δ^{199}Hg = -4.93 and -5.08‰, 2 s.d. = 0.09‰). During the experiment, the light isotopes of Hg were preferentially lost from the snow surface (final δ^{202}Hg = 0.73 and 0.70‰, 2 s.d. = 0.17‰) and collected onto the gold trap (δ^{202}Hg = -0.38 ± 0.16‰, 2 s.d.). Similar MDF caused by the preferential loss of light Hg isotopes has been observed during photochemical reduction of Hg from aqueous solutions (*9, 10, 13*). In addition to MDF, MIF was observed as a result of the preferential loss of the odd-mass-number isotopes of Hg. Δ^{199}Hg became more negative in the remaining surface snow (Δ^{199}Hg = -5.34 and -5.52‰, 2 s.d. = 0.09‰) and Δ^{199}Hg of the emitted $Hg^0_{(g)}$ was less negative than that of the original snow (Δ^{199}Hg = -1.87 ± 0.09‰, 2 s.d.).

We suggest that MIF observed in the chamber experiment and in the natural snow samples may be caused by photochemically driven radical-pair reactions. The ratio of Δ^{199}Hg to Δ^{201}Hg for all flux chamber experiment samples and natural snow samples was 1.07 ± 0.02 (1 s.e.) (Figure 3.2). This value is much lower than predicted to result due to nuclear volume effects (~2.47(*15, 18, 28*). Instead, we suggest that MIF in these samples is the result of a kinetic photochemical process involving Hg-halogen radical pair intermediates in which compounds containing odd-mass-number isotopes of Hg

recombine with halogen radicals at a different rate from those containing even-mass-number isotopes. This process is similar to that observed during photochemical reduction of Hg^{2+} associated with dissolved organic matter in aquatic systems for which the measured ratio of $\Delta^{199}Hg$ to $\Delta^{201}Hg$ is 1.00 ± 0.02 (2 s.e.) (*13*). The MIF in snow samples is, however, different because the odd-mass-number isotopes of Hg are preferentially reduced and emitted rather than retained in the oxidized form. Although we are unable to determine the specific reaction mechanisms causing the observed MIF, we suggest that multi-step heterogeneous redox reactions are involved, likely focused in the quasi-liquid layer on the surfaces of snow crystals (*29*).

Photochemical reduction observed during the chamber experiment can be modeled using a Rayleigh-type fractionation model (*13*) in which the Hg retained in the snow and the Hg emitted as $Hg^0_{(g)}$ form complementary reservoirs (Figure 3.3). Although we cannot eliminate the possibility that back-reactions may affect the results of this simplistic model, we suggest that this model can provide useful insight into this complex system. To calculate a kinetic fractionation factor for this process it is necessary to know the fraction of Hg lost from the chamber snow. Previous experiments determined an e-folding depth for ultraviolet radiation in uniform Arctic coastal snow of 5-6 cm (*30*). On the basis of this we calculate a kinetic fractionation factor ($\Delta^{199}\alpha_{snow\text{-}air}$) of between 0.99660 and 0.99665. If the e-folding depth was greater and ultraviolet radiation penetrated to the bottom of the chamber, the calculated fractionation factor would increase only slightly to 0.99676. Assuming that AMDE-deposited Hg shows only small negative MIF ($\Delta^{199}Hg$ = 0 to -1‰), the Rayleigh fractionation model can be used to determine the relative amount of Hg loss that has occurred (Figure 3.3). We estimate that

photochemical reduction caused loss of ~5-30% of the Hg originally in snowfall samples, ~35-50% of the Hg originally in surface snow samples and ~65-75% of the Hg in drifted snow samples.

This study demonstrates that Hg can undergo significant MIF during photochemically driven reactions in snow. Future experiments are needed to fully understand the reaction pathways involved, to explore the isotopic composition of Hg in snow during non-AMDE periods and to expand these results to other Arctic locations. We suggest that the negative MIF signature measured in AMDE-deposited Hg can be used to approximate the amount of AMDE-deposited Hg lost from the snowpack. If the remaining AMDE-deposited Hg subsequently enters Arctic ecosystems, its isotopic composition should be retained through methylation and bioaccumulation processes and would be identifiable in higher organisms.

3.3 Methods

Collection of snow samples near Barrow, AK (71.32°N, 156.5°W) and details of the flux chamber experiments have been described previously (*21*). Snow samples and procedural standards (NIST SRM 3133 in 1% BrCl) were processed according to the following methods. BrCl (1%, v/v) was added to the frozen samples and the snow was allowed to melt in a clean room. Inorganic Hg concentrations in the liquid snow samples were determined using atomic absorption spectroscopy (Nippon Instruments, MA 2000) according to previously described methods (*21*). For these analyses, the detection limit was 1.0 ng/L (3 s.d. of blank analyses) and analytical uncertainty was ± 2.5% (1 s.d.).

Before isotopic analyses it was necessary to concentrate each sample into an 8 g solution with a Hg concentration of at least 2 ng/g. Hg in the samples was reduced to $Hg^0_{(g)}$ by means of simultaneous introduction of the sample and a reagent mixture (equal parts 10% $SnCl_2$ and 25% H_2SO_4 plus 1% by volume of 30% NH_2OH) at a rate of 0.8 ml/min each onto a frosted-tip gas-liquid separator. A counter-flow of $Ar_{(g)}$ (0.9 L/min) bubbled the resulting $Hg^0_{(g)}$ into 25 g of an acidic 2% $KMnO_4$ solution (Alfa Aesar, low Hg, w/w). Each 25 g solution was further concentrated by means of reduction in 5 ml aliquots with 20 µl 30% NH_2OH, 250 µl 20% $SnCl_2$ and 250 µl 50% H_2SO_4. The resulting $Hg^0_{(g)}$ in these aliquots was bubbled into 8 g of 2% $KMnO_4$ solution using an automatic sample changer (Nippon Instruments, SC-3).

Two total gaseous Hg (Hg_T) samples were collected as part of this study (from 14 June 2008 to 16 June 2008 and from 18 June 2008 to 21 June 2008). Ambient air was pumped through eight ~15 cm glass tubes containing gold beads ('gold traps') that were mounted on a polyvinyl chloride manifold and maintained at 55-65 °C to prevent condensation. Quartz-fiber filter packs were attached to the intake end of each gold trap and the flow through each gold trap was maintained at 1.8 L/min. Hg_T samples collected on gold traps and procedural standards (NIST SRM 3133 amalgamated to gold beads) were processed according to the following methods. Using a programmable heating coil, Hg was thermally desorbed from the gold beads (heat from 20 to 100 °C over 10 min; 100 to 300 °C over 90 min; 300 to 500 °C over 40 min; 500 °C for 10 min; cool). The released $Hg^0_{(g)}$ was bubbled into 25 g of 2% $KMnO_4$ solution with $Ar_{(g)}$ at a rate of 50 ml/min. Each 25 g solution was further concentrated into 8 g using an automatic sample changer as described above.

The Hg isotope compositions of samples and procedural standards were measured according to previously published methods via continuous-flow cold-vapor generation multi-collector inductively coupled plasma mass spectrometry (*12, 13*). Analytical uncertainties in these measurements are reported as the largest of 2 s.d. of the long-term reproducibility of the in-house UM-Almadén standard, 2 s.d. of the reproducibility of procedural standards, or 2 s.e. reproducibility of replicate sample analyses (*13*). All samples reported in this study had Hg recoveries greater than 70% and procedural standards with similar Hg recoveries were not isotopically fractionated. We suggest, therefore, that all of the isotopic compositions reported in this manuscript are accurate within the reported analytical uncertainty.

MIF is described using capital delta notation according to equations (2)-(4). MIF is considered significant if it is greater than 2 s.d. of that measured in the bracketing standards (NIST SRM 3133).

$$\Delta^{199}Hg = \delta^{199}Hg - (\delta^{202}Hg * 0.252) \quad (2)$$

$$\Delta^{200}Hg = \delta^{200}Hg - (\delta^{202}Hg * 0.502) \quad (3)$$

$$\Delta^{201}Hg = \delta^{201}Hg - (\delta^{202}Hg * 0.752) \quad (4)$$

Acknowledgements

Funding for this research was provided by the National Science Foundation Office of Polar Programs (Grants ARC-0435989 and ARC-0435893). L.S. Sherman is funded by a National Defense Science and Engineering Graduate Fellowship through the Department of Defense, Office of Naval Research. We are grateful to M.W. Johnson, L. Alvarez-Aviles, M. Sturm, R. Prevost, P.W. Sherman and the members of BEIGL for

assistance and helpful discussions. Four anonymous reviewers provided comments that improved this manuscript.

Author Contributions

J.D.B. initiated this study along with T.A.D. and G.J.K. K.P.J., J.D.B., T.A.D., J.A.B. and G.J.K. collected the snow samples and conducted the chamber experiment. L.S.S. and K.P.J. conducted the laboratory analyses and L.S.S. wrote the manuscript. All authors contributed to discussions of results and conclusions.

References

(1) Lindberg, S. E.; Brooks, S.; Lin, C.-J.; Scott, K. J.; Landis, M. S.; Stevens, R. K.; Goodsite, M.; Richter, A.; Dynamic oxidation of gaseous mercury in the troposphere at polar sunrise. *Environ. Sci. Technol.* **2002,** *36*, 1245-1256.

(2) Steffen, A.; Schroeder, W.; Macdonald, R.; Poissant, L.; Konoplev, A.; Mercury in the Arctic atmosphere: An analysis of eight years of measurements on GEM at Alert (Canada) and a comparison with observations at Amderma (Russia) and Kuujjuarapik (Canada). *Sci. Total Environ.* **2005,** *342*, 185-198.

(3) Lalonde, J.; Poulain, A. J.; Amyot, M.; The role of mercury redox reactions in snow on snow-to-air mercury transfer. *Environ. Sci. Technol.* **2002,** *36*, 174-178.

(4) Poulain, A. J.; Lalonde, J. D.; Amyot, M.; Shead, J. A.; Raofie, F.; Ariya, P. A.; Redox transformations of mercury in an Arctic snowpack at springtime. *Atmos. Environ.* **2004,** *38*, 6763-6774.

(5) Steffen, A.; Schroeder, W.; Bottenheim, J.; Narayan, J.; Fuentes, J. D.; Atmospheric mercury concentrations: measurements and profiles near snow and ice surfaces in the Canadian Arctic during Alert 2000. *Atmos. Environ.* **2002,** *36*, 2653-2661.

(6) Kirk, J. L.; St. Louis, V. L.; Sharp, M. J.; Rapid reduction and reemission of mercury deposited into snowpacks during atmospheric mercury depletion events at Churchill, Manitoba, Canada. *Environ. Sci. Technol.* **2006,** *40*, 7590-7596.

(7) Dommergue, A.; Ferrari, C. P.; Gauchard, P.-A.; Boutron, C. F.; The fate of mercury species in a sub-arctic snowpack during snowmelt. *Geophys. Res. Lett.* **2003,** *30* (12).

(8) St. Louis, V. L.; Hintelmann, H.; Graydon, J. A.; Kirk, J. L.; Barker, J.; Dimock, B.; Sharp, M. J.; Lehnherr, I.; Methylated mercury species in Canadian High Arctic marine surface waters and snowpacks. *Environ. Sci. Technol.* **2007,** *41*, 6433-6441.

(9) Zheng, W.; Foucher, D.; Hintelmann, H.; Mercury isotope fractionation during volatilization of Hg(0) from solution into the gas phase. *J. Anal. Atomic Spectro.* **2007,** *22*, 1097-1104.

(10) Sherman, L. S.; Blum, J. D.; Nordstrom, D. K.; McCleskey, R. B.; Barkay, T.; Vetriani, C.; Mercury isotopic composition of hydrothermal systems in the Yellowstone Plateau volcanic field and Guaymas Basin sea-floor rift. *Earth. Planet. Sci. Lett.* **2009,** *279*, 86-96.

(11) Kritee, K.; Blum, J. D.; Johnson, M. W.; Bergquist, B. A.; Barkay, T.; Mercury stable isotope fractionation during reduction of Hg(II) to Hg(0) by mercury resistant microorganisms. *Environ. Sci. Technol.* **2007,** *41*, 1889-1895.

(12) Blum, J. D.; Bergquist, B. A.; Reporting the variations in the natural isotopic composition of mercury. *Anal. Bioanal. Chem.* **2007,** *388* (2), 353-359.

(13) Bergquist, B. A.; Blum, J. D.; Mass-dependent and mass-independent fractionation of Hg isotopes by photo-reduction in aquatic systems. *Science* **2007,** *318* (5849), 417-420.

(14) Biswas, A.; Blum, J. D.; Bergquist, B. A.; Keeler, G. J.; Zhouqing, X.; Natural mercury isotope variation in coal deposits and organic soils. *Environ. Sci. Technol.* **2008,** *42* (22), 8303-8309.

(15) Ghosh, S.; Xu, Y.; Humayun, M.; Odom, L.; Mass-independent fractionation of mercury isotopes in the environment. *Geochem. Geophys. Geosyst.* **2008,** *9*, Q03004, doi: 10.1029/2007/GC001827.

(16) Hintelmann, H.; Foucher, D.; Telmer, K.; Zheng, J.; Yamada, M.; Hg isotope fractionation in sediment cores. *Geochim. Cosmochim. Acta* **2008,** *72* (12S), A379.

(17) Jackson, T. A.; Whittle, D. M.; Evans, M. S.; Muir, D. C. G.; Evidence for mass-independent and mass-dependent fractionation of the stable isotopes of mercury by natural processes in aquatic ecosystems. *Appl. Geochem.* **2008,** *23* (3), 547-571.

(18) Schauble, E. A.; Role of nuclear volume in driving equilibrium stable isotope fractionation of mercury, thallium, and other very heavy elements. *Geochim. Cosmochim. Acta* **2007,** *71*, 2170-2189.

(19) Bigeleisen, J.; Nuclear size and shape effects in chemical reactions. Isotope chemistry of the heavy elements. *J. Am. Chem. Soc.* **1996,** *118*, 3676-3680.

(20) Buchachenko, A. L.; Magnetic isotope effect: Nuclear spin control of chemical reactions. *J. Phys. Chem.* **2001,** *105* (44), 9995-10011.

(21) Johnson, K. P.; Blum, J. D.; Keeler, G. J.; Douglas, T. A.; Investigation of the deposition and emission of mercury in arctic snow during an atmospheric mercury depletion event. *Journal of Geophysical Research* **2008,** *113*, D17304.

(22) Lu, J. Y.; Schroeder, W. H.; Barrie, L. A.; Steffen, A.; Magnification of atmospheric mercury deposition to polar regions in springtime: The link to tropospheric ozone depletion chemistry. *Geophys. Res. Lett.* **2001,** *28* (17), 3219-3222.

(23) Tackett, P. J.; Cavender, A. E.; Keil, A. D.; Shepson, P. B.; Bottenheim, J. W.; Morin, S.; Deary, J.; Steffen, A.; Doerge, C.; A study of the vertical scale of halogen chemistry in the Arctic troposphere during Polar Sunrise at Barrow, Alaska. *J. Geophys. Res.* **2007,** *112*, D07306.

(24) Banic, C. M.; Beauchamp, S. T.; Tordon, R. J.; Schroeder, W. H.; Steffen, A.; Anlauf, K. A.; Wong, H. K. T.; Vertical distribution of gaseous elemental mercury in Canada. *J. Geophys. Res.* **2003,** *108* (D9).

(25) Douglas, T. A.; Sturm, M.; Simpson, W. R.; Blum, J. D.; Alvarez-Aviles, L.; Keeler, G. J.; Perovich, D. K.; Biswas, A.; Johnson, K.; Influence of snow and ice crystal formation and accumulation on mercury deposition to the Arctic. *Environ. Sci. Technol.* **2008,** *42*, 1542-1551.

(26) Carignan, J.; Estrade, N.; Sonke, J. E.; Donard, O. F. X.; Odd Isotope Deficits in Atmospheric Hg Measured in Lichens. *Environ. Sci. Technol.* **2009,** *43* (15), 5660-5664.

(27) Lalonde, J. D.; Amyot, M.; Doyon, M.-R.; Auclair, J.-C.; Photo-induced Hg(II) reduction in snow from the remote and temperate Experimental Lakes Area (Ontario, Canada). *J. Geophys. Res.* **2003,** *108* (D6).

(28) Estrade, N.; Carignan, J.; Sonke, J. E.; Donard, O. F. X.; Mercury isotope fractionation during liquid-vapor evaporation experiments. *Geochim. Cosmochim. Acta* **2009,** *73*, 2693-2711.

(29) Ferrari, C. P.; Gauchard, P.-A.; Aspmo, K.; Dommergue, A.; Magand, O.; Bahlmann, E.; Nagorski, S.; Temme, C.; Ebinghaus, R.; Steffen, A.; Banic, C.; Berg, T.; Planchon, F.; Barbante, C.; Cescon, P.; Boutron, C. F.; Snow-to-air exchanges of mercury in an Arctic seasonal snow pack in Ny-Alesund, Svalbard. *Atmos. Environ.* **2005,** *39*, 7633-7645.

(30) King, M. D.; Simpson, W. R.; Extinction of UV radiation in Arctic snow at Alert, Canada (82°N). *J. Geophys. Res.* **2001,** *106* (D12), 12499-12507.

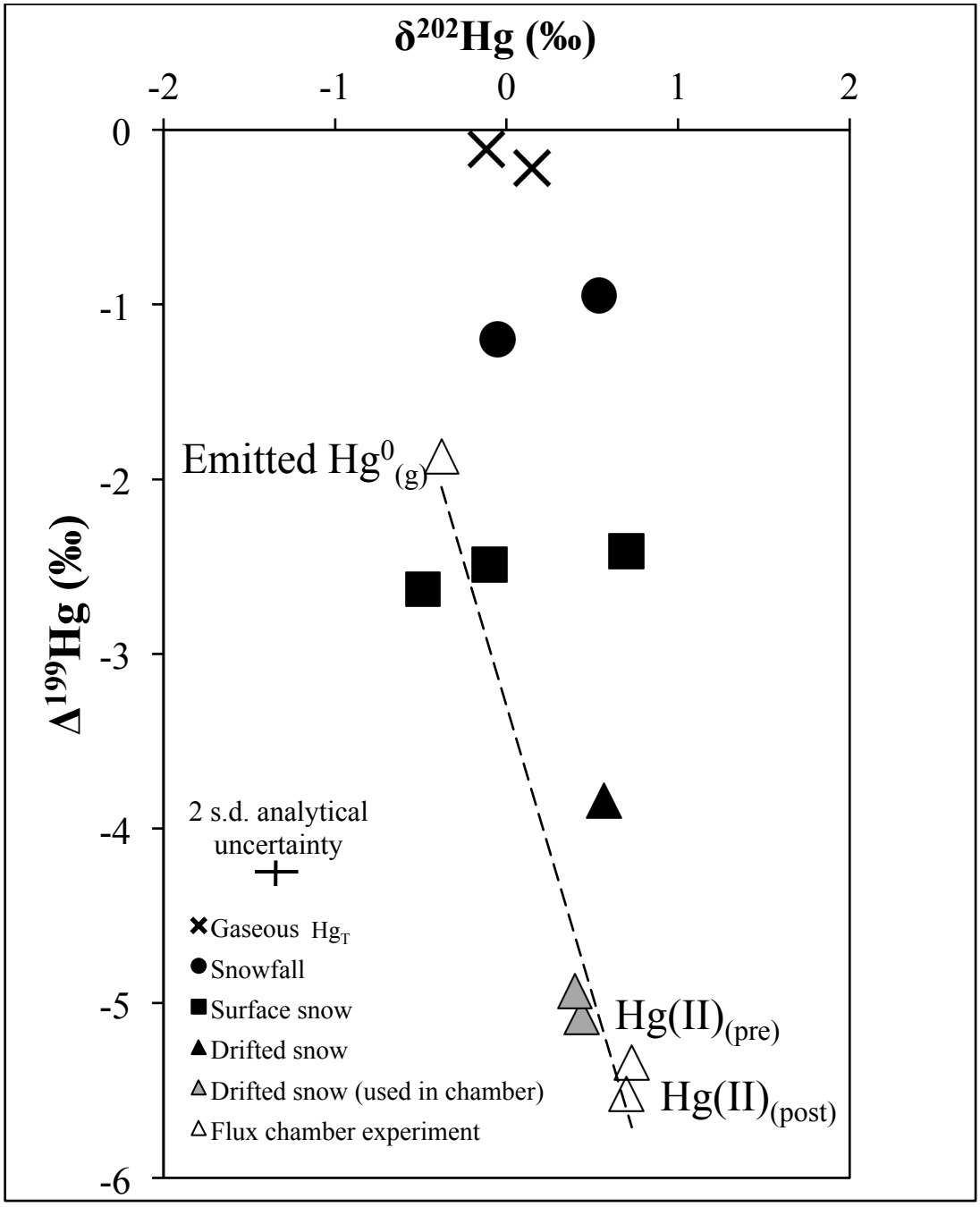


Figure 3.1 Mercury isotopic compositions of snow samples, chamber experiment samples, and gaseous samples. Snowfall, surface and drifted snow samples are represented by filled symbols. Drifted snow samples used in chamber are represented by grey triangles ($Hg(II)_{(pre)}$). Samples of snow post-experiment ($Hg(II)_{(post)}$) and $Hg^0_{(g)}$ released during the chamber experiment (Emitted $Hg^0_{(g)}$) are represented by open triangles. Gaseous Hg_T samples are represented by crosses. A linear regression based on the chamber experiment ($y = -3.30x - 3.30$; $r^2 = 0.96$) is shown as a dashed line. Representative 2 s.d. analytical uncertainty based on replicate analyses of process standards is shown.

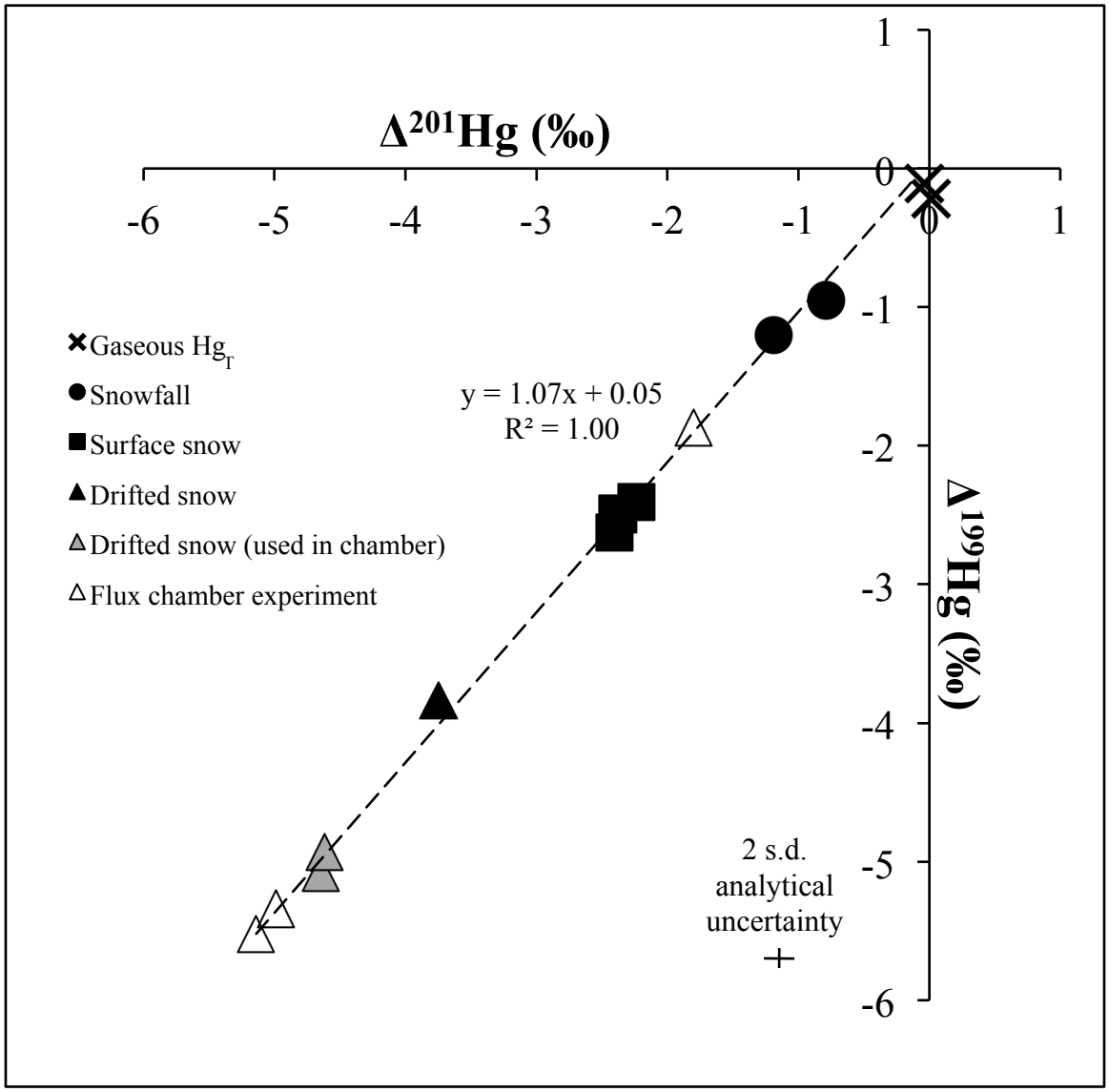


Figure 3.2 Mass-independent fractionation of snow samples and chamber experiment samples. Snowfall, surface and drifted snow samples are represented by filled symbols. Drifted snow samples used to fill the chamber are represented by grey triangles; samples of the snow in the chamber after the experiment and the $Hg^0_{(g)}$ released during the experiment are represented by open triangles. A linear regression based on all of the data is shown as a dashed line. Representative 2 s.d. analytical uncertainty based on replicate analyses of process standards is shown.

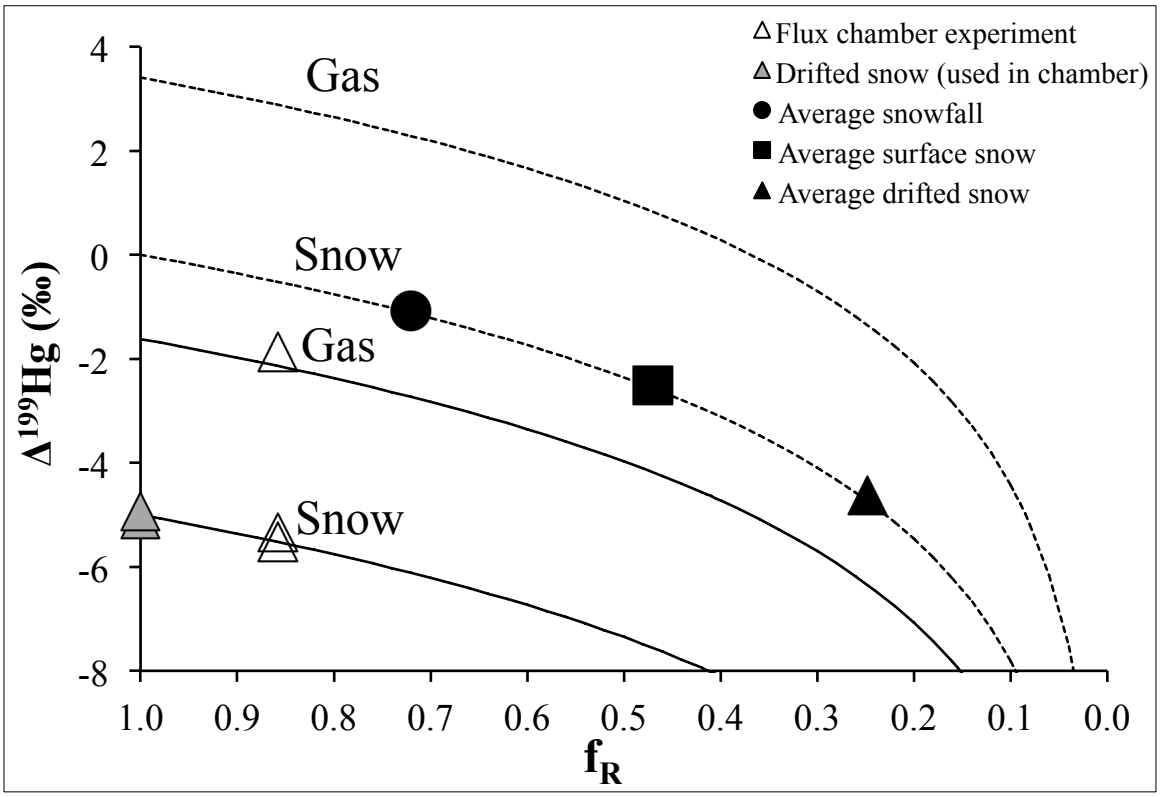


Figure 3.3 Rayleigh fractionation models showing mercury isotope changes in snow and emitted gas. Flux chamber experiment samples are shown as open and grey triangles and average Hg isotopic compositions of natural snow samples are shown as filled black symbols. Models based on chamber experiment are represented with solid lines and models of natural snow samples are represented with dashed lines. The depicted model of natural snow samples assumes that AMDE-deposited Hg does not originally display MIF (that is, $\Delta^{199}Hg \approx 0‰$).

Table 3.1 Mercury isotopic compositions of standards, snow samples and chamber experiment samples. Average values presented for the UM-Almadén standard are based on measurements made from September 2007 to February 2009. Reported 2σ uncertainties for the UM-Almadén standard and NIST SRM 3133 process standards are 2 s.d. of multiple measurements. Reported 2σ uncertainties for gaseous Hg_T samples are 2 s.e. of the mean of replicate analyses. None of the snow samples contained enough Hg for Hg isotope ratios to be analyzed more than once.

Sample type	Hg concentration (ng/L)	n	δ^{202}Hg (‰)	2σ (‰)	δ^{201}Hg (‰)	2σ (‰)	δ^{200}Hg (‰)	2σ (‰)	δ^{199}Hg (‰)	2σ (‰)	Δ^{201}Hg (‰)	2σ (‰)	Δ^{200}Hg (‰)	2σ (‰)	Δ^{199}Hg (‰)	2σ (‰)
UM-Almadén standard		151	-0.53	0.16	-0.44	0.13	-0.26	0.08	-0.15	0.08	-0.04	0.08	0.01	0.03	-0.02	0.06
NIST SRM 3133 (snow process std)		11	-0.16	0.17	-0.14	0.19	-0.09	0.11	-0.07	0.12	-0.02	0.07	-0.01	0.03	-0.03	0.09
NIST SRM 3133 (Hg_T process std)		5	-0.01	0.07	-0.03	0.08	-0.04	0.06	-0.02	0.05	-0.02	0.03	-0.03	0.05	-0.02	0.05
Gaseous Hg_T		2	-0.12	0.28	-0.13	0.32	-0.17	0.34	-0.14	0.12	-0.04	0.10	-0.11	0.20	-0.11	0.04
Gaseous Hg_T		2	0.15	0.16	0.12	0.32	0.06	0.16	-0.18	0.12	0.01	0.20	-0.01	0.08	-0.22	0.08
Snowfall	360	1	0.54		-0.38		0.19		-0.81		-0.79		-0.08		-0.95	
Snowfall	416	1	-0.05		-1.23		-0.02		-1.21		-1.19		0.00		-1.20	
Surface snow	199	1	0.70		-1.71		0.24		-2.23		-2.24		-0.12		-2.41	
Surface snow	81.2	1	-0.10		-2.45		-0.04		-2.52		-2.38		0.01		-2.49	
Surface snow	85.1	1	-0.49		-2.77		-0.26		-2.76		-2.40		-0.01		-2.63	
Drifted snow	94.5	1	0.57		-3.33		0.22		-3.70		-3.75		-0.06		-3.84	
Drifted snow	109	1	0.40		-4.32		0.12		-4.83		-4.62		-0.08		-4.93	
Drifted snow	109	1	0.44		-4.32		0.16		-4.97		-4.65		-0.06		-5.08	
Chamber expt: $Hg(II)_{(pre)}$	109	1	0.40		-4.32		0.12		-4.83		-4.62		-0.08		-4.93	
Chamber expt: $Hg(II)_{(pre)}$	109	1	0.44		-4.32		0.16		-4.97		-4.65		-0.06		-5.08	
Chamber expt: $Hg(II)_{(post)}$	96.4	1	0.73		-4.44		0.21		-5.16		-4.99		-0.16		-5.34	
Chamber expt: $Hg(II)_{(post)}$	96.4	1	0.70		-4.61		0.35		-5.34		-5.14		0.00		-5.52	
Chamber expt: Emitted $Hg^0_{(g)}$		1	-0.38		-2.08		-0.24		-1.97		-1.80		-0.05		-1.87	

CHAPTER 4

Frost flowers growing in the Arctic ocean-atmosphere-sea ice-snow interface: 2. Mercury exchange between the atmosphere, snow and frost flowers[1]

Abstract

Frost flowers are ice crystals that grow on refreezing sea ice leads in Polar Regions by wicking brine from the sea ice surface and accumulating vapor phase condensate. These crystals contain high concentrations of mercury (Hg) and are believed to be a source of reactive halogens, but their role in Hg cycling and impact on the fate of Hg deposited during atmospheric mercury depletion events (AMDEs) are not well understood. We collected frost flowers growing on refreezing sea ice near Barrow, Alaska (U.S.A.) during an AMDE in March 2009 and measured Hg concentrations and Hg stable isotope ratios in these samples to determine the origin of Hg associated with the crystals. We observed decreasing Δ^{199}Hg values in the crystals as they grew from new wet frost flowers (mean Δ^{199}Hg = 0.77 ± 0.13‰, 1 s.d.) to older dry frost flowers (mean Δ^{199}Hg = 0.10 ± 0.05‰, 1 s.d.). Over the same time period, mean Hg concentrations in these samples increased from 131 ± 6 ng/L (1 s.d.) to 180 ± 28 ng/L (1 s.d.). Coupled with a previous study of Hg isotopic fractionation during AMDEs, these results suggest that Hg initially deposited to the local snowpack was subsequently reemitted during photochemical reduction reactions and ultimately accumulated on the

[1] Sherman, L. S., Blum, J. D., Douglas, T. A., Steffen, A. Frost flowers growing in the Arctic ocean-atmosphere-sea ice-snow interface: 2. Mercury exchange between the atmosphere, snow and frost flowers. *Journal of Geophysical Research* **2012**, *117*, D00R10.

frost flowers. As a result of this process, frost flowers may lead to enhanced local retention of Hg deposited during AMDEs and may increase Hg loading to the Arctic Ocean.

4.1 Introduction

During spring in Polar Regions, chemical reactions involving reactive halogens cause atmospheric boundary layer ozone depletion and the oxidation of gaseous elemental mercury (GEM) to reactive gaseous mercury (RGM) and particle-bound mercury (PHg) compounds that are rapidly deposited to the snowpack (*1-9*). During these atmospheric mercury depletion events (AMDEs), atmospheric boundary layer concentrations of GEM decrease from ~1.6 ng/m^3 to well below 1.0 ng/m^3 for hours to days (*2, 4, 5, 10*). When these events occur due to local GEM oxidation and deposition rather than influx of a previously depleted air mass (*11*), mercury (Hg) concentrations in surface snow can increase by more than an order of magnitude to values as high as 400 ng/L (*12, 13*). Recent studies including several conducted in Barrow, Alaska (AK) (U.S.A.) (*2, 12, 14, 15*) suggest that a significant portion of the Hg deposited during AMDEs is subsequently reduced during photochemical reactions and reemitted as GEM (*16-19*). However, the percent of AMDE-deposited Hg remaining in the snowpack at the time of snowmelt has been debated (*6, 14, 20, 21*). A more complete understanding of Hg cycling at snow and sea ice surfaces during these events is crucial to determining the potential impact of AMDEs on Arctic ecosystems.

The occurrence of locally produced AMDEs requires sunlight, relatively calm meteorological conditions and elevated levels of tropospheric halogens such as bromine

(Br) (*4, 22, 23*). While the exact mechanisms that cause the production of large quantities of sea salt aerosols during these events remain unclear (*24*), it has been suggested that first-year sea ice (*25*), blowing snow (*26*), halogen reactivation and emission from snow surfaces (*27*), and frost flowers (*28, 29*) are potential sources of the gas-phase halogens. Frost flowers are ice crystals that commonly develop on the surface of new sea ice that is refreezing over lead (*29-32*). Brine is wicked upward into the newly forming "wet" frost flowers until it is depleted from the ice surface (*32, 33*). The then "dry" frost flowers continue to grow via condensation of water vapor from the supersaturated air directly above the sea ice (*33, 34*). This vapor phase deposition onto the frost flowers generally dilutes the concentrations of major elements (including Cl, Br, Na, K, Mg, and Ca) in the crystals (*32*). Frost flowers are eventually buried by blowing snow, flooded with seawater (*31*), or redistributed onto the ice and snowpack by strong winds (*29*).

In addition to potentially enhancing the production of gas-phase halogens during AMDEs, frost flowers may play other important roles in Arctic Hg cycling. High Hg concentrations have been measured in frost flowers (>150 ng/L) (*13, 35*) and it has been suggested that the high halogen concentrations in these ice crystals (*29*) cause them to scavenge atmospheric Hg (*13*). The extent to which frost flowers impact the cycling of Hg between snow, the atmosphere, and sea ice during AMDEs is not well understood. Measurement of Hg stable isotope fractionation has been shown to be an effective tool to study the transfer of Hg between snow and the atmosphere in Arctic regions (*14*). As part of the 2009 Ocean-Atmosphere-Sea Ice-Snow (OASIS) field campaign, we measured Hg stable isotope ratios in samples collected near Barrow, AK to investigate

the transfer of Hg between frost flowers, surface snow, and the atmospheric boundary layer during polar springtime.

4.2 Mercury stable isotopes

The measurement of Hg stable isotope ratios in natural samples has recently provided insight into Arctic Hg cycling (*14, 36*). There are seven stable isotopes of Hg (196, 198, 199, 200, 201, 202, and 204 amu) and isotopic fractionation can occur during a variety of biotic and abiotic reactions. Mercury isotope ratios are reported using delta notation as

$$\delta^{xxx}\text{Hg}\ (‰) = ([(^{xxx}\text{Hg}/^{198}\text{Hg})_{sample}/(^{xxx}\text{Hg}/^{198}\text{Hg})_{SRM\ 3133}] - 1) * 1000 \quad (1)$$

where ^{xxx}Hg is a given isotope of Hg and SRM 3133 is a NIST Hg standard (*37*). Mass-dependent fractionation (MDF) of Hg can occur during processes such as microbial reduction (*38*) and photochemical reduction and loss from aqueous solutions and snow (*14, 39, 40*). Mercury can also undergo mass-independent fractionation (MIF), which is reported as the deviation of a measured ratio from that theoretically predicted to result due to kinetic MDF as

$$\Delta^{xxx}\text{Hg} = \delta^{xxx}\text{Hg} - (\delta^{202}\text{Hg} * \beta) \quad (2)$$

where β is equal to 0.252 for ^{199}Hg and 0.752 for ^{201}Hg (*37*). MIF can occur during photochemical reactions (due to the "magnetic isotope effect") and to a lesser extent (<~0.5‰) primarily during equilibrium reactions due to differences in the nuclear charge radii between Hg isotopes (the "nuclear field shift effect") (*39, 41-43*). High levels of MIF occur due to the magnetic isotope effect (MIE) during kinetic photolysis reactions that are spin-selective and involve the creation of long-lived spin-related radical pairs

(*39, 44, 45*). Because only the odd-mass-number isotopes of Hg are magnetic and have unpaired nuclear spin, radical pairs involving an odd-mass-number isotope of Hg can recombine at different rates than those with an even-mass-number isotope of Hg. This process has been shown experimentally to produce $\Delta^{199}Hg/\Delta^{201}Hg$ ratios of between 1.0 and 1.3 (*39, 40*). During reactions in which radical pairs are generated in the triplet state, triplet to singlet conversion is enhanced by magnetic isotopes. As a result, radical pairs that include odd-mass-number isotopes of Hg recombine at a faster rate and the odd-mass-number isotopes of Hg are preferentially retained as reactants (*42*). Bergquist and Blum (*39*) observed this effect during the photochemical reduction of Hg^{2+} from aqueous solutions containing dissolved organic carbon. Because the odd-mass-number isotopes of Hg were preferentially retained in the oxidizing reservoir, positive MIF of ^{199}Hg and ^{201}Hg was observed in the aqueous solutions ($\Delta^{199}Hg$ values up to 2.1 ± 0.05‰, 2 s.d.) (*39*). It is also possible under different bonding conditions for radical pairs that involve Hg to be generated in the singlet state (*42*). During these reactions, singlet to triplet conversion is enhanced by magnetic isotopes and the recombination of radical pairs that include magnetic isotopes of Hg becomes spin forbidden. This results in the preferential accumulation of the odd-mass-number isotopes of Hg in the reaction products (*42*). Sherman et al. (*14*) observed MIF of this character in Arctic snow during an AMDE. Preferential photochemical reduction and loss of the odd-mass-number isotopes of Hg from surface snow resulted in the observation of extreme negative MIF of ^{199}Hg and ^{201}Hg in the snow ($\Delta^{199}Hg$ values down to -5.08 ± 0.09‰, 2 s.d.) (*14*). This suggests that the measurement of MIF of Hg stable isotopes in Arctic snow and ice samples may help to elucidate the fate of AMDE-deposited Hg.

4.3 Methods

4.3.1 Sample collection

All of the samples described in this study were collected into Teflon bottles (PTFE) using acid-cleaned Teflon scoops. The bottles were acid washed in a clean room in the Biogeochemistry and Environmental Isotope Geochemistry Laboratory at the University of Michigan (UM BEIGL). The bottles were fully submerged in a hot 5% HNO_3 (v/v) bath for 48 h and then filled with 5% BrCl (v/v) for 48 h. After being thoroughly rinsed with deionized water, the bottles were dried and a subset were filled with 1% BrCl (v/v), allowed to react for 24 h, and analyzed for Hg concentrations using atomic absorption spectrometry (AAS; Nippon Instruments, MA 2000). Mercury concentrations in these bottle blanks were below the method detection limit (MDL) for these analyses (i.e., <0.76 ng/L, see section 4.3.2).

As described by Douglas et al. (*32*), frost flower, snow, and brine samples were collected in March 2009 from two sites located approximately 7 km apart at the edge of the land-fast ice north of Barrow, AK (Figure 4.1). Site A was located ~3 km northwest of Barrow (71.306433N, 156.807159W) and Site B was located ~8.5 km northeast of Barrow (71.35385N, 156.688171W). Based on analysis of Moderate Resolution Imaging Spectroradiometer (MODIS) imagery (see Douglas et al., 2012, Figure 1), repeat visits to the sea ice sites, and calm meteorological conditions during the study period, we believe that the frost flowers at the two sites were part of a single large field. This frost flower field was several kilometers long and the ice crystals began growing either in the evening of March 13 or in the morning of March 14 (*32*). We collected samples from this field over time to represent a continuum from wet, brine-rich flowers to dry flowers coated

with an increasing amount of vapor phase condensate. To ensure collection of sufficient Hg for isotopic analyses, large volume samples were collected at each site when possible. To determine whether AMDEs were occurring during the study period, atmospheric total gaseous Hg (TGM) was measured continuously at the Barrow Arctic Science Consortium (BASC) ~4 km north of Barrow (Figure 4.1) using a Tekran 2537A. In remote areas such as Barrow where there are no significant local anthropogenic sources of Hg, TGM is predominantly composed of GEM (*35, 46*).

On March 14, 2009, actively growing wet frost flowers were collected at Site A. Based on MODIS imagery, we believe that these frost flowers were less than 24 h old (*32*). We also collected frozen surface brine (~3 mm thickness) from an area near these wet frost flowers and older dry frost flowers from a location ~300 m inland. There was no liquid brine at the surface near the dry frost flowers and the crystals were no longer wicking up brine. Finally, we collected surface snow samples (~1 cm in depth) from an ice block elevated 1 m above the sea ice surface near the frost flowers. Although we do not know exactly when this snow began accumulating, clear skies and low winds persisted for several days prior to March 14. Under these cold, clear sky conditions at sites immediately adjacent to open leads and actively refreezing leads, vapor phase deposition of diamond dust and surface hoar can add millimeters to a centimeter of ice crystals to the snowpack surface in a period of less than 24 h (*35*). We suggest, therefore, that this snow probably represents a mixture of diamond dust and surface hoar that was less than 24 h old at the time of collection. On March 16, 2009, we returned to Site A and resampled the frost flowers that had been wet and actively taking up brine two days

earlier. These frost flowers were dry and had substantially gained in ice volume due to the deposition of vapor phase condensate.

On March 20, 2009, we traveled to Site B and collected dry frost flowers, surface snow and brine samples. As previously discussed, based on MODIS imagery (*32*), we believe that these frost flowers were part of the same large field as the frost flowers collected at Site A. Therefore, we suggest that these frost flowers were approximately six days old. Finally, in the morning of March 25, 2009 we collected dry frost flowers and brine from a site approximately 1 km south of Site B.

4.3.2 Analytical methods

After collection, snow and frost flower samples were kept frozen until they were processed for analysis. At the UM BEIGL, 1% BrCl (v/v) was added to the samples and they were allowed to melt in a clean room. Prior to concentration analysis, 5 ml aliquots of the frost flower and brine samples were treated with ultraviolet light (UV) for three to four days in sealed quartz tubes to release any Hg that was strongly bound to ligands (*47*). Procedural standards (10 pg of SRM NIST 3133 in 1% BrCl) and blanks were treated with UV light in the same manner. Mercury concentrations were then measured using AAS. Variations in the means of concentration measurements are reported as 1 s.d. The MDL for these analyses was 0.76 ng/L (3 s.d. of blank analyses) and all sample replicates were within 11.8% relative percent difference (RPD) (mean RPD = 2.79 ± 2.88%, n = 40). Mercury in procedural standards treated with UV light was consistently recovered after treatment (mean recovery = 100 ± 6%, n = 5) and Hg concentrations in the procedural blanks treated with UV light were below the MDL (n = 5). Two acid-

cleaned bottles were transported to the sampling sites as process bottle blanks and remained closed during the sampling period. These bottles were filled with 200 ml of 1% BrCl (v/v) in a clean room and were found to contain small amounts of Hg (mean = 0.59 ± 0.26 ng per bottle). Although these bottle blanks contained more Hg than the laboratory bottle blanks (which did not contain detectable quantities of Hg), this amount of Hg represents only an average of 2.1 ± 1.1% of the Hg in samples analyzed for isotopic composition and thus is negligible.

After Hg concentration analysis, those samples with sufficient Hg for isotopic analysis (i.e., >8 ng) were concentrated into acidic 1% $KMnO_4$ (w/w) solutions (Alfa Aesar) as follows. Each sample was poured into a 2 L Pyrex bottle and 0.3 mL of 30% $NH_2OH \cdot HCl$ (w/v) was added and allowed to react for 30 min. A peristaltic pump was then used to add 100 ml of 5% $SnCl_2$ (w/v) to the solution at a rate of 10 ml/min. Mercury-free air was pulled through the sample and carried the resulting GEM into the trapping solution at a rate of 0.7 L/min for four hours. Procedural standards (25 to 50 ng of NIST SRM 3133 in 1% BrCl) and blanks were processed in the same manner. Mercury in these standards was consistently recovered in the final solutions (mean recovery = 91 ± 6%). The small amount of Hg measured in the procedural blanks (mean = 0.22 ± 0.12 ng per blank, n = 3) was attributable to the $KMnO_4$ solutions. The Hg isotopic compositions of samples and procedural standards were measured using continuous-flow cold vapor generation multi-collector inductively coupled plasma mass spectrometry (MC-ICP-MS) according to previously published methods (*37, 39*).

4.4 Results

Mercury concentrations measured in frost flower, surface snow, and brine samples are presented in Table 4.1. Frost flowers at Site A increased in Hg concentration as they grew: new wet frost flowers collected on March 14, 2009 contained an average of 131 ± 6 ng/L of Hg, older dry frost flowers collected the same day contained an average 157 ± 35 ng/L of Hg, and dry frost flowers that were ~48 h old (collected on March 16) contained an average of 180 ± 28 ng/L of Hg. Surface snow collected on March 14 contained an average of 89.3 ± 16 ng/L of Hg and brine samples scraped from the ice surface on the same day contained lower Hg concentrations (mean = 41.5 ± 3 ng/L). The samples collected from Site B on March 20 contained lower Hg concentrations than the samples collected previously at Site A (dry frost flowers: mean = 49.4 ± 5 ng/L; snow: mean = 11.4 ± 0.2 ng/L; brine: mean = 52.7 ± 11 ng/L). Five days later, Hg concentrations were higher in the dry frost flower samples collected at Site B (mean = 82.2 ± 13 ng/L) but the associated surface brine contained lower Hg concentrations (mean = 16.0 ± 0.1 ng/L).

The isotopic compositions of frost flower, surface snow, and brine samples that contained >8 ng of Hg are presented in Table 4.2 along with measured isotopic compositions of the UM-Almadén secondary standard and procedural standards. Variations in mean isotope ratios are reported as 1 s.d. As depicted in Figure 4.2, frost flowers collected at Site A exhibited decreasing Δ^{199}Hg values and slightly increasing δ^{202}Hg values from new wet frost flowers (mean Δ^{199}Hg = 0.77 ± 0.13‰; mean δ^{202}Hg = 0.42 ± 0.08‰) to dry frost flowers that were ~48 h old (mean Δ^{199}Hg = 0.10 ± 0.05‰; mean δ^{202}Hg = 0.51 ± 0.03‰). The dry frost flowers collected on March 14, 2009 (mean

Δ^{199}Hg = 0.15 ± 0.13‰; mean δ^{202}Hg = 0.55 ± 0.06‰) were isotopically similar to the dry (~48 h old) frost flowers collected two days later. As discussed previously, the frost flowers at Site A also increased in Hg concentration as they grew (Figure 4.3). In contrast, surface snow samples collected at Site A displayed negative Δ^{199}Hg values (mean Δ^{199}Hg = -0.99 ± 0.03‰) that were similar to those observed in snowfall samples collected during an AMDE in March 2006 (*14*) (Figure 4.2). Frost flowers and brine samples collected at Site B on March 20, 2009 exhibited negative Δ^{199}Hg values (frost flowers: mean Δ^{199}Hg = -0.32 ± 0.06‰; brine: mean Δ^{199}Hg = -0.40 ± 0.01‰) and negative δ^{202}Hg values (frost flowers: mean δ^{202}Hg = -0.29 ± 0.01‰; brine: mean δ^{202}Hg = -0.29 ± 0.14‰).

Interpretation of these data is aided by knowledge of atmospheric TGM concentrations during the study period. Figure 4.4 depicts TGM concentrations and average net solar radiation measured at BASC between March 12 and March 25, 2009. Although TGM measurements made at BASC are likely representative of regional atmospheric TGM concentrations, it is possible that TGM concentrations at the sampling sites on the sea ice were somewhat different. However, based on the observed meteorological conditions at BASC, it is likely that the air masses sampled at BASC also impacted the collection sites. From March 14 through March 16 surface winds at BASC were from the east-northeast toward Site A and on March 20 and during the morning of March 25 surface winds at BASC were from the south toward Site B. AMDE conditions existed at BASC while the frost flowers were growing from March 14 to March 16, 2009. During this time period, atmospheric TGM concentrations were highest concurrent with peak solar radiation (Figure 4.4). This may have occurred due to photochemical

reduction and reemission of GEM from the surface snow during the AMDE (*2, 12*). Atmospheric TGM concentrations began to return to typical background levels (~1.6 ng/m^3) on March 16, 2009 and largely remained at those concentrations until March 19, 2009 when they dropped below 1 ng/m^3 for less than one day. TGM concentrations returned to background concentrations on March 20, 2009 and then oscillated daily between background concentrations and concentrations less than 1 ng/m^3 for the duration of the study period.

4.5 Discussion

As frost flowers grow, deposition of water vapor condensate causes dilution of major anions and cations in the ice crystals (*32*). Our observations of Hg concentrations in frost flowers do not follow this trend. In contrast, as major element concentrations decreased in the frost flowers growing at Site A from March 14 through March 16, 2009 (*32*), Hg concentrations increased (Figure 4.3). Previous studies have similarly observed increasing Hg concentrations in frost flowers over time from new wet frost flowers to older dry frost flowers (*13, 35*). Because Hg concentrations are reported as ng of Hg per liter of melted sample, increases in Hg concentration can be the result either of addition of Hg or loss of ice. However, because vapor phase condensate was added to frost flowers collected at Site A as they grew (*32*), the observed increases in Hg concentration must have been due to the addition of Hg to the frost flowers.

New wet frost flowers collected at Site A on March 14, 2009 displayed positive $\Delta^{199}Hg$ values (mean $\Delta^{199}Hg = 0.77 \pm 0.13‰$). It is unlikely that adsorption of RGM to the frost flowers caused MIF via the MIE because photochemical reactions and long-

lived radical pairs are not believed to be involved in this process (*35*). Although the nuclear field shift (NFS) effect has been observed to cause MIF of Hg during equilibrium reactions, this effect has not been predicted or observed to produce MIF greater than ~0.5‰ (*43, 48-50*). In addition, the NFS effect has been theoretically predicted and experimentally demonstrated to produce a $\Delta^{199}Hg/\Delta^{201}Hg$ ratio between 1.6 and 2.5 (*40, 43, 49, 50*). Based on a York regression (*51*), the frost flower and surface snow samples collected at Site A were characterized by a $\Delta^{199}Hg/\Delta^{201}Hg$ ratio of 1.26 ± 0.10 (1 s.e.). Therefore, it is unlikely that adsorption of RGM to the frost flowers caused MIF either via the MIE or the NFS effect. Instead, it is likely that the Hg in the wet frost flowers at Site A exhibited positive MIF prior to adsorption.

There are at least two processes that could produce the Hg that was adsorbed to the frost flowers as they grew: (1) oxidation of background atmospheric GEM or (2) oxidation of GEM emitted from the snowpack surface during photochemical reduction reactions. The oxidation of atmospheric GEM to RGM and subsequent complete deposition of Hg from the atmospheric boundary layer should not cause MIF of Hg isotopes. During the AMDE that began on March 14, 2009, atmospheric GEM concentrations dropped to less than 0.1 ng/m^3 (Figure 4.4). Due to mass balance, such complete Hg deposition should result in preservation of the isotopic composition of atmospheric GEM in the deposited Hg (*14*). Background TGM collected in Barrow, AK in June 2008 did not display positive $\Delta^{199}Hg$ values ($\Delta^{199}Hg$ = -0.11 and -0.22 ± 0.08‰, 2 s.d. (*14*)). Based on this evidence, we argue that complete depletion of atmospheric Hg during AMDEs results in deposition of Hg that does not display positive MIF.

However, if atmospheric depletion of Hg is not complete and oxidation of GEM to RGM during AMDEs causes positive MIF, background atmospheric Hg deposited during AMDEs might display positive MIF. Several studies have investigated the reactions that result in the oxidation of GEM to RGM during AMDEs (*1, 4, 8, 15, 52*). Although this oxidation may occur through several reaction pathways, kinetic and thermodynamic studies, ab initio calculations, and measured atmospheric halogen concentrations during AMDEs indicate that gaseous atomic Br is one of the most significant oxidizing agents (*1, 4, 8, 9, 53, 54*). GEM oxidation by gaseous Br may proceed according to reactions such as the following:

$$Hg^0 + Br \rightarrow HgBr \quad (3)$$

$$HgBr + Br \rightarrow HgBr_2 \quad (4)$$

Although sunlight is necessary to photolytically produce atomic Br from Br_2, the gas-phase oxidation of Hg^0 by Br (reaction 3) is not a directly photochemically mediated radical pair reaction (*1, 2, 23, 55, 56*). It is possible, however, that the radical pair intermediates in reaction 4 may be relatively long-lived. Therefore, we cannot discount the possibility that reaction 4 may cause MIF via the MIE. However, as discussed previously, because GEM is nearly completely depleted from the atmosphere during AMDEs, it is not likely that deposited RGM retains a significant MIF signature.

Based on these arguments, it is unlikely that RGM produced via oxidation of background atmospheric GEM during the AMDE on March 14, 2009 displayed positive MIF. However, as described above, Hg in wet frost flowers growing at Site A displayed significant positive Δ^{199}Hg values. We infer that RGM deposited to local surface snows was photochemically reduced and reemitted, subsequently locally reoxidized (either by

gaseous halogens or heterogeneously on the frost flowers), and adsorbed to the growing frost flowers (*15*). Sherman et al. (*14*) observed extreme negative Δ^{199}Hg values in snow samples collected during an AMDE in March 2006. To determine the cause of this fractionation, the authors filled a flux chamber with drifted snow that displayed negative Δ^{199}Hg values (Figure 4.5). By exposing the snow to sunlight and collecting the emitted GEM, the authors determined that photochemical reduction of Hg in the snow caused the preferential emission of the odd-mass-number isotopes of Hg as GEM (*14*). Relative to the Hg originally in the snow, this resulted in more negative Δ^{199}Hg values in the snow after photochemical reduction and less negative Δ^{199}Hg values in the emitted GEM (Figure 4.5) (*14*). Although the authors were able to measure the preferential emission of the odd-mass-number isotopes of Hg during this experiment, they did not observe the retention of this Hg in local snow or any other reservoir (*14*).

We suggest that frost flowers may adsorb a portion of the Hg that is reemitted from surface snow and locally reoxidized. These crystals thereby represent a complementary isotopic reservoir to surface snow. As shown in Figure 4.5, if this process occurred in a manner similar to that observed by Sherman et al. (*14*), we would expect the Δ^{199}Hg value of GEM emitted from the collected surface snow samples was positive (expected Δ^{199}Hg ≈ 3.4‰ based on $\Delta^{199}\alpha_{\text{snow-air}} = 0.99660$ (*14*)). As photochemical reduction continued, we expect that Δ^{199}Hg values in the surface snow and emitted GEM decreased (Figure 4.5). The reoxidation and adsorption of this Hg to the frost flowers through time would have caused Δ^{199}Hg values in the ice crystals to decrease as Hg was added to them (Figure 4.5).

It is difficult to estimate when the frost flowers began accumulating Hg and how the rate of Hg adsorption changed through time. Based on the Δ^{199}Hg values measured in frost flowers collected at Site A on March 14, 2009, it is likely that the frost flowers began accumulating Hg after the local surface snow had already lost some Hg. The deposition velocity of RGM depends on a number of factors that may have changed throughout the study period including the meteorology (e.g., wind speed and temperature) and surface properties of the RGM species (*15*). In addition, as the frost flowers grew and their chemical composition and physical properties changed (*32, 33*), their ability to scavenge Hg may have also changed. Because this system is very complex, it is not currently possible to quantitatively model the isotopic evolution of the frost flowers and corresponding surface snow without making an unreasonable number of simplifying assumptions.

In contrast to the frost flowers collected at Site A, frost flowers collected at Site B on March 20, 2009 were characterized by negative δ^{202}Hg values (mean = -0.29 ± 0.01‰), negative Δ^{199}Hg values (Δ^{199}Hg = -0.36 and -0.28, 2 s.d. = 0.18‰) and lower Hg concentrations (mean = 49.7 ± 2.1 ng/L). The difference in frost flower δ^{202}Hg values between Sites A and B probably reflects spatial variations in Hg isotopic composition among snow samples which has been observed previously but is not well understood (*14*). We suggest that there are several possible explanations for the observed negative Δ^{199}Hg values in the frost flowers at Site B including (1) adsorption of isotopically distinct Hg relative to that adsorbed to frost flowers at Site A, (2) photochemical reduction of Hg from the frost flowers, or (3) continued accumulation of Hg emitted from the snowpack surface coupled with deposition of vapor phase condensate. We cannot

rule out the possibility that Hg initially deposited to the frost flowers collected at Site B was different isotopically than Hg initially deposited to frost flowers growing at Site A. However, this seems unlikely because the crystals growing at both sites were part of one large frost flower field (*32*). It is possible that photochemical reduction and loss of Hg from the frost flowers could have occurred at Site B after AMDE conditions ended on March 16, 2009. If the Hg bonding environment in these ice crystals is similar to that of Hg in surface snow, we expect that photochemical reduction of Hg from the frost flowers would cause the preferential loss of the odd-mass-number isotopes of Hg and could have resulted in the observed negative Δ^{199}Hg values. However, because frost flowers contain high concentrations of Br (*29, 31, 32*), it is possible that Hg that is reduced and emitted from the ice crystals may be rapidly reoxidized and readsorbed (*15, 17*). We think it is most likely that frost flowers at Site B continued to accumulate Hg emitted from the local surface snowpack after the dry frost flowers were collected at Site A on March 16. Continued adsorption of this Hg by the frost flowers at Site B could have resulted in the observed negative Δ^{199}Hg values in these samples. After the AMDE ended and atmospheric GEM concentrations returned to background values, water vapor containing little to no Hg may have condensed on the frost flowers at Site B. This would have resulted in decreased Hg concentrations but would not have modified the Hg isotopic composition of the frost flowers.

4.6 Conclusions

The fate of Hg deposited during AMDEs in Polar Regions is a question of scientific interest. Based on analysis of Hg stable isotopes in frost flowers collected

during an AMDE in March 2009, we suggest that Hg accumulating on the crystals was originally deposited to local surface snow. A portion of this Hg was reduced during photochemical reactions, reemitted as GEM, and subsequently locally reoxidized and adsorbed onto the frost flowers. This process likely occurs repeatedly throughout Polar Regions on refreezing sea ice leads during the spring AMDE season. A thinner, more dynamic Arctic sea ice cover is expected in the future (*57, 58*). This sea ice will likely have more open leads and may yield more new ice and frost flowers. The results of this study suggest that frost flowers may, at least temporarily, aid in the local retention of AMDE-deposited Hg. Ultimately, an increase in conditions that favor frost flower growth in the Arctic may cause an increase in Hg flux to sea ice and to the Arctic Ocean.

Acknowledgments

Funding for L. S. Sherman was provided by a National Defense Science and Engineering Graduate Fellowship (DOD-ONR) and the University of Michigan Graham Environmental Sustainability Institute. Funding for J. D. Blum and laboratory support was provided by the John D. MacArthur Professorship at the University of Michigan. Funding for sample collection and research conducted by T. A. Douglas was supported by the U.S. National Science Foundation and the National Aeronautic and Space Administration. Field logistics in Barrow, AK were provided by the Barrow Arctic Science Consortium and were partially funded by Environment Canada and the Canadian IPY program. We thank two anonymous reviewers for comments that greatly improved this manuscript.

References

(1) Goodsite, M. E.; Plane, J. M. C.; Skov, H.; A theoretical study of the oxidation of Hg^0 to $HgBr_2$ in the troposphere. *Environ. Sci. Technol.* **2004,** *38*, 1772-1776.

(2) Brooks, S. B.; Saiz-Lopez, A.; Skov, H.; Lindberg, S. E.; Plane, J. M. C.; Goodsite, M. E.; The mass balance of mercury in the springtime arctic environment. *Geophys. Res. Lett.* **2006,** *33* (13), L13812.

(3) Schroeder, W. H.; Anlauf, K. G.; Barrie, L. A.; Lu, J. Y.; Steffen, A.; Arctic springtime depletion of mercury. *Nature* **1998,** *394*, 331-332.

(4) Lindberg, S. E.; Brooks, S.; Lin, C.-J.; Scott, K. J.; Landis, M. S.; Stevens, R. K.; Goodsite, M.; Richter, A.; Dynamic oxidation of gaseous mercury in the troposphere at polar sunrise. *Environ. Sci. Technol.* **2002,** *36*, 1245-1256.

(5) Skov, H.; Christensen, J. H.; Goodsite, M. E.; Heidam, N. Z.; Jensen, B.; Wahlin, P.; Geernaert, G.; Fate of elemental mercury in the Arctic during atmospheric mercury depletion episodes and the load of atmospheric mercury to the Arctic. *Environ. Sci. Technol.* **2004,** *38* (8), 2373-2382.

(6) Lu, J. Y.; Schroeder, W. H.; Barrie, L. A.; Steffen, A.; Magnification of atmospheric mercury deposition to polar regions in springtime: The link to tropospheric ozone depletion chemistry. *Geophys. Res. Lett.* **2001,** *28* (17), 3219-3222.

(7) Steffen, A.; Schroeder, W. H.; Edwards, G.; Banic, C.; Mercury throughout polar sunrise 2002. *J. Phys. IV* **2003,** *107*, 1267-1270.

(8) Ariya, P. A.; Khalizov, A.; Gidas, A.; Reactions of gaseous mercury with atomic and molecular halogens: Kinetics, product studies, and atmospheric implications. *J. Phys. Chem. A* **2002,** *106*, 7310-7320.

(9) Shepler, B. C.; Peterson, K. A.; Mercury monoxide: A systematic investigation of its ground electronic state. *The Journal of Physical Chemistry A* **2003,** *107* (11), 1783-1787.

(10) Temme, C.; Einax, J. W.; Ebinghaus, R.; Schroeder, W. H.; Measurements of atmospheric mercury species at a coastal site in the Antarctic and over the South Atlantic Ocean during polar summer. *Environ. Sci. Technol.* **2003,** *37*, 22-31.

(11) Gauchard, P.-A.; Aspmo, K.; Temme, C.; Steffen, A.; Ferrari, C.; Berg, T.; Strom, J.; Kaleschke, L.; Dommergue, A.; Bahlmann, E.; Magand, O.; Planchon, F.; Ebinghaus, R.; Banic, C.; Nagorski, S.; Baussand, P.; Boutron, C.; Study of the origin of atmospheric mercury depletion events recorded in Ny-lesund, Svalbard, spring 2003. *Atmos. Environ.* **2005,** *39* (39), 7620-7632.

(12) Johnson, K. P.; Blum, J. D.; Keeler, G. J.; Douglas, T. A.; Investigation of the deposition and emission of mercury in arctic snow during an atmospheric mercury depletion event. *Journal of Geophysical Research* **2008,** *113*, D17304.

(13) Douglas, T. A.; Sturm, M.; Simpson, W. R.; Brooks, S.; Lindberg, S. E.; Perovich, D. K.; Elevated mercury measured in snow and frost flowers near Arctic sea ice leads. *Geophys. Res. Lett.* **2005,** *32*.

(14) Sherman, L. S.; Blum, J. D.; Johnson, K. P.; Keeler, G. J.; Barres, J. A.; Douglas, T. A.; Mass-independent fractionation of mercury isotopes in Arctic snow driven by sunlight. *Nature Geoscience* **2010,** *3* (3), 173-177.

(15) Skov, H.; Brooks, S. B.; Goodsite, M. E.; Lindberg, S. E.; Meyers, T. P.; Landis, M. S.; Larsen, M. R. B.; Jensen, B.; McConville, G.; Christensen, J.; Fluxes of reactive gaseous mercury measured with a newly developed method using relaxed eddy accumulation. *Atmos. Environ.* **2006,** *40* (28), 5452-5463.

(16) Kirk, J. L.; St. Louis, V. L.; Sharp, M. J.; Rapid reduction and reemission of mercury deposited into snowpacks during atmospheric mercury depletion events at Churchill, Manitoba, Canada. *Environ. Sci. Technol.* **2006,** *40*, 7590-7596.

(17) Poulain, A. J.; Lalonde, J. D.; Amyot, M.; Shead, J. A.; Raofie, F.; Ariya, P. A.; Redox transformations of mercury in an Arctic snowpack at springtime. *Atmos. Environ.* **2004,** *38*, 6763-6774.

(18) Steffen, A.; Schroeder, W.; Bottenheim, J.; Narayan, J.; Fuentes, J. D.; Atmospheric mercury concentrations: measurements and profiles near snow and ice surfaces in the Canadian Arctic during Alert 2000. *Atmos. Environ.* **2002,** *36*, 2653-2661.

(19) Lalonde, J.; Poulain, A. J.; Amyot, M.; The role of mercury redox reactions in snow on snow-to-air mercury transfer. *Environ. Sci. Technol.* **2002,** *36*, 174-178.

(20) Larose, C.; Dommergue, A.; De Angelis, M.; Cossa, D.; Averty, B.; Marusczak, N.; Soumis, N.; Schneider, D.; Ferrari, C.; Springtime changes in snow chemistry lead to new insights into mercury methylation in the Arctic. *Geochim. Cosmochim. Acta* **2010,** *74*, 6263-6275.

(21) Dommergue, A.; Ferrari, C. P.; Gauchard, P.-A.; Boutron, C. F.; The fate of mercury species in a sub-arctic snowpack during snowmelt. *Geophys. Res. Lett.* **2003,** *30* (12).

(22) Barrie, L. A.; Bottenheim, J. W.; Schnell, R. C.; Crutzen, P. J.; Rasmussen, R. A.; Ozone destruction and photochemical reactions at polar sunrise in the lower Arctic atmosphere. *Nature* **1988,** *334*, 138-141.

(23) Fan, S.-M.; Jacob, D. J.; Surface ozone depletion in Arctic spring sustained by bromine reactions on aerosols. *Nature* **1992,** *359*, 522-524.

(24) Simpson, W. R.; Alvarez-Aviles, L.; Douglas, T. A.; Sturm, M.; Domine, F.; Halogens in the coastal snow pack near Barrow, Alaska: Evidence of active bromine air-snow chemistry during springtime. *Geophys. Res. Lett.* **2005,** *32*.

(25) Simpson, W. R.; Carlson, D.; Honninger, G.; Douglas, T. A.; Sturm, M.; Perovich, D.; Platt, U.; First-year sea-ice contact predicts bromine monoxide (BrO) levels at Barrow, Alaska better than potential frost flower contact. *Atmospheric Chemistry and Physics* **2007,** *7*, 621-627.

(26) Yang, X.; Pyle, J. A.; Cox, R. A.; Theys, N.; Van Roozendael, M.; Snow-sourced bromine and its implications for polar tropospheric ozone. *Atmospheric Chemistry and Physics* **2010,** *10*, 7763-7773.

(27) Piot, M.; von Glasow, R.; The potential importance of frost flowers, recycling on snow, and open leads for ozone depletion events. *Atmospheric Chemistry and Physics* **2008,** *8* (9), 2437-2467.

(28) Kaleschke, L.; Richter, A.; Burrows, J.; Afe, O.; Heygster, G.; Notholt, J.; Rankin, A. M.; Roscoe, H. K.; Hollwedel, J.; Wagner, T.; Jacobi, H.-W.; Frost flower on sea ice as a source of sea salt and their influence on tropospheric halogen chemistry. *Geophys. Res. Lett.* **2004,** *31* (L16114).

(29) Rankin, A. M.; Wolff, E. W.; Martin, S.; Frost flowers: Implications for tropospheric chemistry and ice core interpretation. *Journal of Geophysical Research* **2002,** *107* (D23).

(30) Martin, S.; Yu, Y.; Drucker, R.; The temperature dependence of frost flower growth on laboratory sea ice and the effect of the flowers on infrared observations of the surface. *Journal of Geophysical Research* **1996,** *101* (C5), 12111-12125.

(31) Perovich, D.; Richter-Menge, J. A.; Surface characteristics of lead ice. *Journal of Geophysical Research* **1994,** *99* (C8), 16341-16350.

(32) Douglas, T. A.; Domine, F.; Barrett, M.; Anastasio, C.; Beine, H. J.; Bottenheim, J.; Grannas, A.; Houdier, S.; Netcheva, S.; Rowland, G.; Staebler, R.; Steffen, A.; Frost flowers growing in the Arctic ocean-atmosphere-sea ice-snow interface: Part 1: Chemical composition and formation history. *Journal of Geophysical Research Atmospheres* **2012,** *117*, D00R09.

(33) Domine, F.; Taillandier, A. S.; Simpson, W. R.; Severin, K.; Specific surface area, density and microstructure of frost flowers. *Geophys. Res. Lett.* **2005,** *32* (L13502).

(34) Andreas, E. L.; Guest, P. S.; Persson, P. O. G.; Fairall, C. W.; Horst, T. W.; Moritz, R. E.; Semmer, S. R.; Near-surface water vapor over polar sea ice is always near ice saturation. *Journal of Geophysical Research* **2002,** *107* (C10).

(35) Douglas, T. A.; Sturm, M.; Simpson, W. R.; Blum, J. D.; Alvarez-Aviles, L.; Keeler, G. J.; Perovich, D. K.; Biswas, A.; Johnson, K.; Influence of snow and ice crystal formation and accumulation on mercury deposition to the Arctic. *Environ. Sci. Technol.* **2008,** *42*, 1542-1551.

(36) Point, D.; Sonke, J. E.; Day, R. D.; Roseneau, D. G.; Hobson, K. A.; Vander Pol, S. S.; Moors, A. J.; Pugh, R. S.; Donard, O. F. X.; Becker, P. R.; Methylmercury photodegradation influenced by sea-ice cover in Arctic marine ecosystems. *Nature Geoscience* **2011,** *4*, 188-194.

(37) Blum, J. D.; Bergquist, B. A.; Reporting the variations in the natural isotopic composition of mercury. *Anal. Bioanal. Chem.* **2007,** *388* (2), 353-359.

(38) Kritee, K.; Blum, J. D.; Johnson, M. W.; Bergquist, B. A.; Barkay, T.; Mercury stable isotope fractionation during reduction of Hg(II) to Hg(0) by mercury resistant microorganisms. *Environ. Sci. Technol.* **2007,** *41*, 1889-1895.

(39) Bergquist, B. A.; Blum, J. D.; Mass-dependent and mass-independent fractionation of Hg isotopes by photo-reduction in aquatic systems. *Science* **2007,** *318* (5849), 417-420.

(40) Zheng, W.; Hintelmann, H.; Mercury isotope fractionation during photoreduction in natural water is controlled by its Hg/DOC ratio. *Geochim. Cosmochim. Acta* **2009,** *73*, 6704-6715.

(41) Zheng, W.; Foucher, D.; Hintelmann, H.; Mercury isotope fractionation during volatilization of Hg(0) from solution into the gas phase. *J. Anal. Atomic Spectro.* **2007,** *22*, 1097-1104.

(42) Zheng, W.; Hintelmann, H.; Isotope fractionation of mercury during its photochemical reduction by low-molecular-weight organic compounds. *J. Phys. Chem. A* **2010,** *114* (12), 4246-4253.

(43) Estrade, N.; Carignan, J.; Sonke, J. E.; Donard, O. F. X.; Mercury isotope fractionation during liquid-vapor evaporation experiments. *Geochim. Cosmochim. Acta* **2009,** *73*, 2693-2711.

(44) Buchachenko, A. L.; Magnetic isotope effect: Nuclear spin control of chemical reactions. *J. Phys. Chem.* **2001,** *105* (44), 9995-10011.

(45) Turro, N. J.; Influence of nuclear spin on chemical reactions: Magnetic isotope and magnetic field effects. *Proceedings of the National Academy of Sciences* **1983,** *80*, 609-621.

(46) Ebinghaus, R.; Kock, H. H.; Schmolke, S. R.; Measurements of atmospheric mercury with high time resolution: Recent applications in environmental research and monitoring. *Fresenius J. Anal. Chem.* **2001,** *371*, 806-815.

(47) Olson, M. L.; Cleckner, L. B.; Hurley, J. P.; Krabbenhoft, D. P.; Heelan, T. W.; Resolution of matrix effects on analysis of total and methyl mercury in aqueous samples from the Florida Everglades. *Fresenius J. Anal. Chem.* **1997,** *358* (3), 392-398.

(48) Bergquist, B. A.; Blum, J. D.; The odds and evens of mercury isotopes: Applications of mass-dependent and mass-independent isotope fractionation. *Elements* **2009,** *5*, 353-357.

(49) Schauble, E. A.; Role of nuclear volume in driving equilibrium stable isotope fractionation of mercury, thallium, and other very heavy elements. *Geochim. Cosmochim. Acta* **2007,** *71*, 2170-2189.

(50) Zheng, W.; Hintelmann, H.; Nuclear field shift effect in isotope fractionation of mercury during abiotic reduction in the absence of light. *The Journal of Physical Chemistry A* **2010,** *114* (12), 4238-4245.

(51) York, D.; Least-squares fitting of a straight line. *Can. J. Phys.* **1966,** *44*, 1076-1086.

(52) Calvert, J. G.; Lindberg, S. E.; A modeling study of the mechanism of the halogen-ozone-mercury homogeneous reactions in the troposphere during the polar spring. *Atmos. Environ.* **2003,** *37*, 4467-4481.

(53) Khalizov, A. F.; Viswanathan, B.; Larregaray, P.; Ariya, P. A.; A theoretical study on the reactions of Hg with halogens: Atmospheric implications. *The Journal of Physical Chemistry A* **2003,** *107* (33), 6360-6365.

(54) Xie, Z.-Q.; Sander, R.; Poschl, U.; Slemr, F.; Simulation of atmospheric mercury depletion events (AMDEs) during polar springtime using the MECCA box model. *Atmospheric Chemistry and Physics* **2008,** *8*, 13197-13233.

(55) Barrie, L.; Platt, U.; Arctic tropospheric chemistry: An overview. *Tellus (B Chem. Phys. Meteorol.)* **1997,** *49*, 450-454.

(56) Foster, K. L.; Plastridge, R. A.; Bottenheim, J. W.; Shepson, P. B.; Finlayson-Pitts, B. J.; Spicer, C. W.; The role of Br_2 and BrCl in surface ozone destruction at polar sunrise. *Science* **2001,** *291*, 471-474.

(57) Rothrock, D. A.; Percival, D. B.; Wensnahan, M.; The decline in arctic sea-ice thickness: Separating the spatial, annual, and interannual variability in a quarter century of submarine data. *Journal of Geophysical Research* **2008,** *113*, C05003.

(58) Haas, C.; Pfaffling, A.; Hendricks, S.; Rabenstein, L.; Etienne, J.-L.; Rigor, I.; Reduced ice thickness in Arctic Transpolar Drift favors rapid ice retreat. *Geophys. Res. Lett.* **2008,** *35*, L17501.

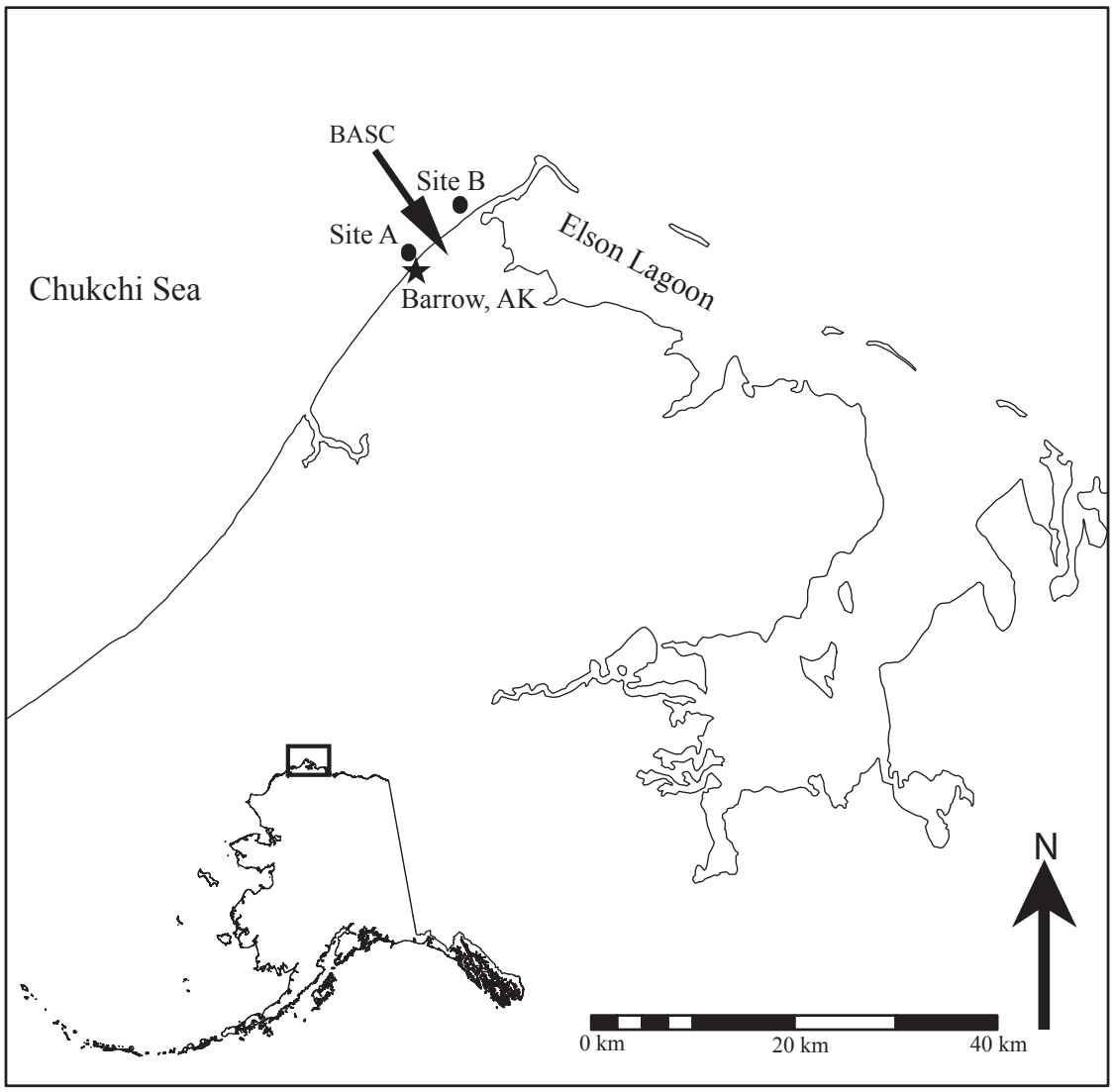


Figure 4.1 Map of frost flower sampling area near Barrow, AK with inset map of Alaska. Frost flower sampling locations (Site A: 71.306433N, 156.807159W and Site B: 71.35385N, 156.688171W) are shown as black dots, the location of Barrow, AK is shown as a star, and the location of Barrow Arctic Science Consortium (BASC) is indicated with an arrow.

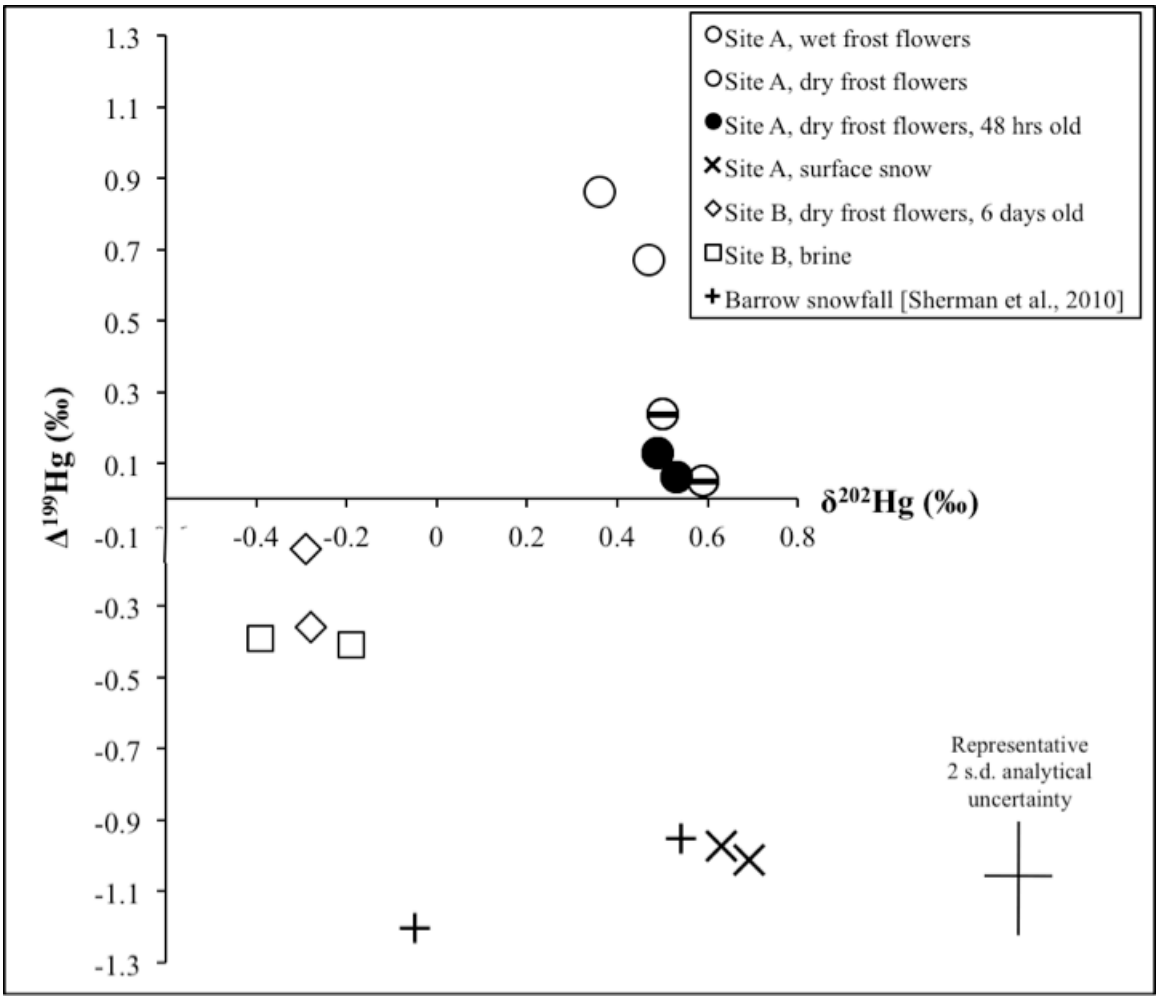


Figure 4.2 Isotopic composition (δ^{202}Hg versus Δ^{199}Hg) of frost flower, surface snow, and brine samples. Wet frost flowers and surface snow samples were collected at Site A on 3/14/09, dry frost flowers were collected at Site A on 3/14/09 and 3/16/09, and dry frost flowers and brine samples were collected at Site B on 3/20/09. Snowfall samples collected near Barrow, AK in March 2006 by Sherman et al. (*14*) are shown as black pluses. Representative sample analytical uncertainty (2 s.d.) is shown.

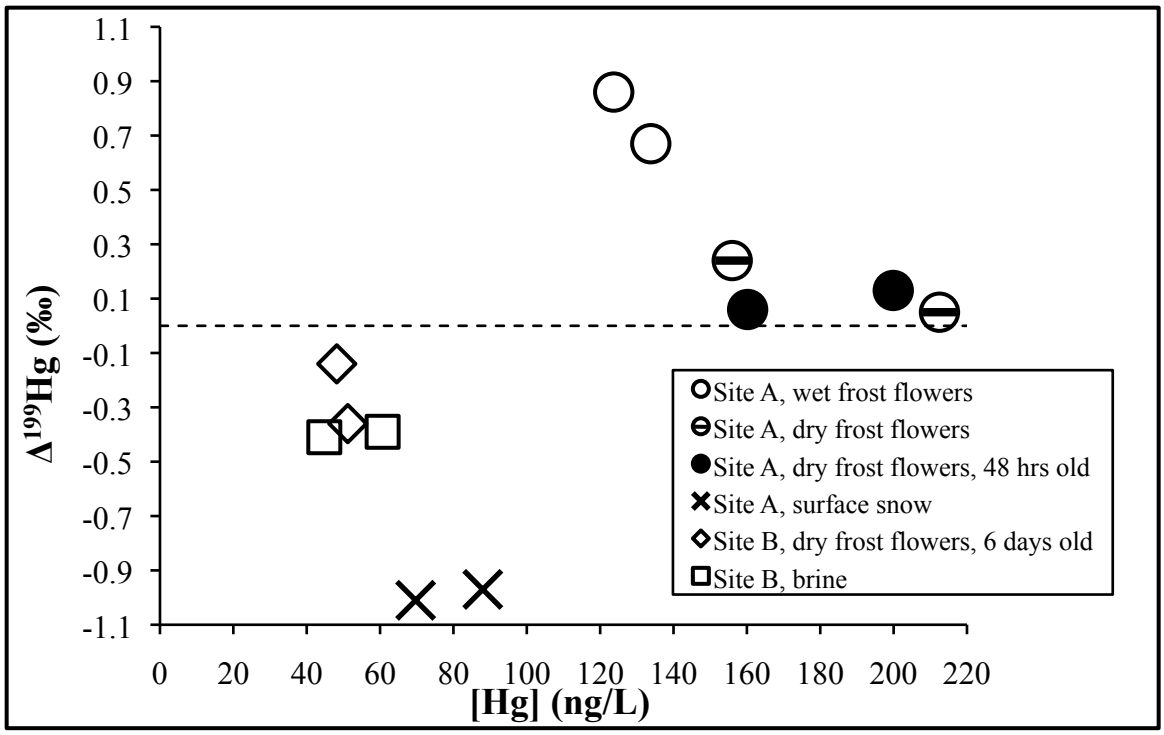


Figure 4.3 Mercury concentration (ng/L) versus Δ^{199}Hg (‰) for frost flower, surface snow, and brine samples. Wet frost flowers and surface snow samples were collected at Site A on 3/14/09, dry frost flowers were collected at Site A on 3/14/09 and 3/16/09, and dry frost flowers and brine samples were collected at Site B on 3/20/09. Horizontal dashed line depicts the 0 values for the y-axis.

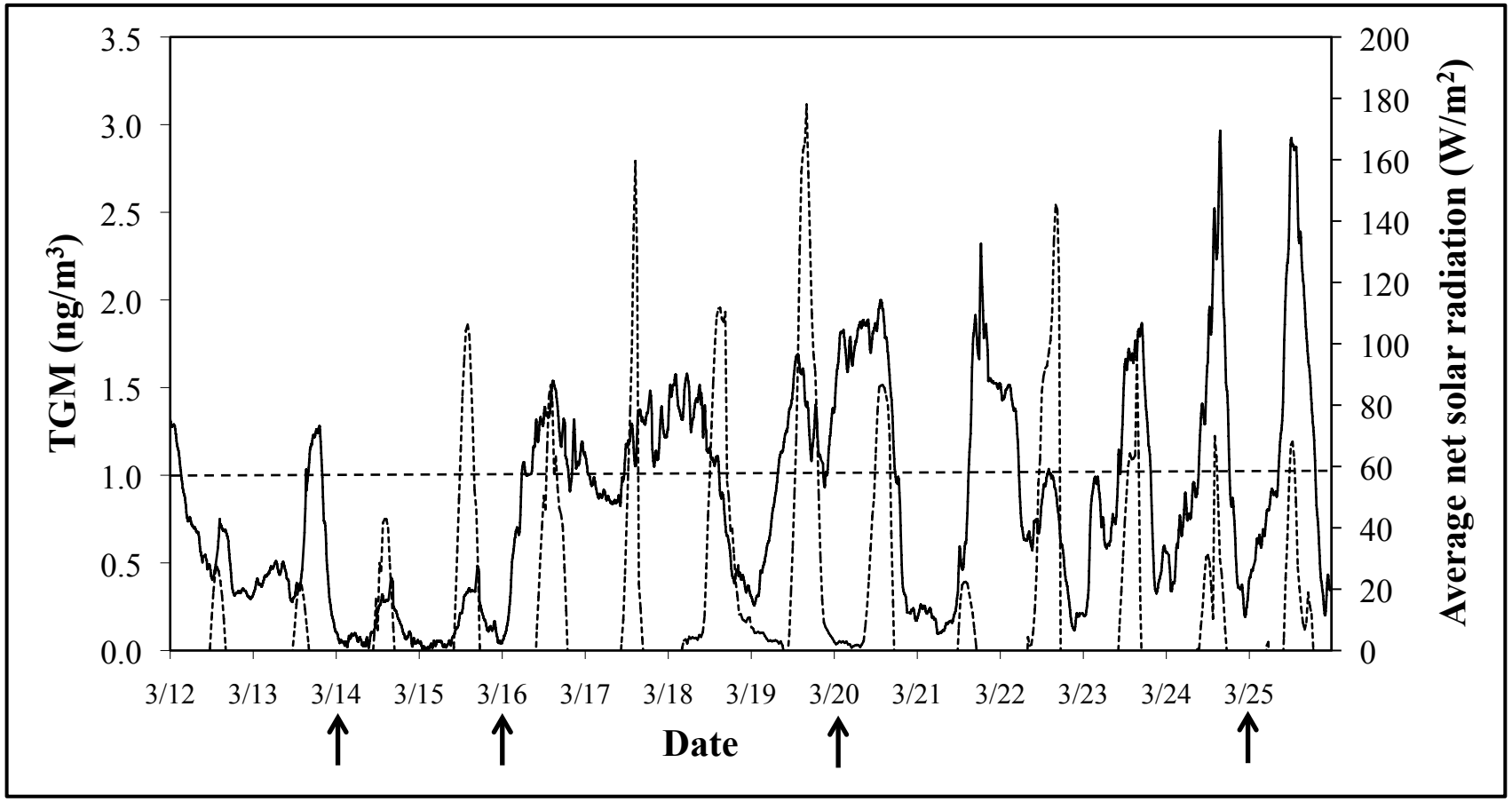


Figure 4.4 Atmospheric TGM concentrations were measured continuously using a Tekran 2537A at the Barrow Arctic Science Consortium (BASC) located ~4 km north of Barrow, AK. Thirty minute averaged TGM concentrations (ng/m^3, solid black line) and hourly average net solar radiation (W/m^2, dotted black line) from March 12, 2009 through March 25, 2009 are shown. AMDE conditions are characterized by TGM concentrations less than 1.0 ng/m^3 (shown by horizontal dashed line). Sample collection dates are indicated by black arrows (Site A: 3/14/09 and 3/16/09, Site B: 3/20/09 and 3/25/09).

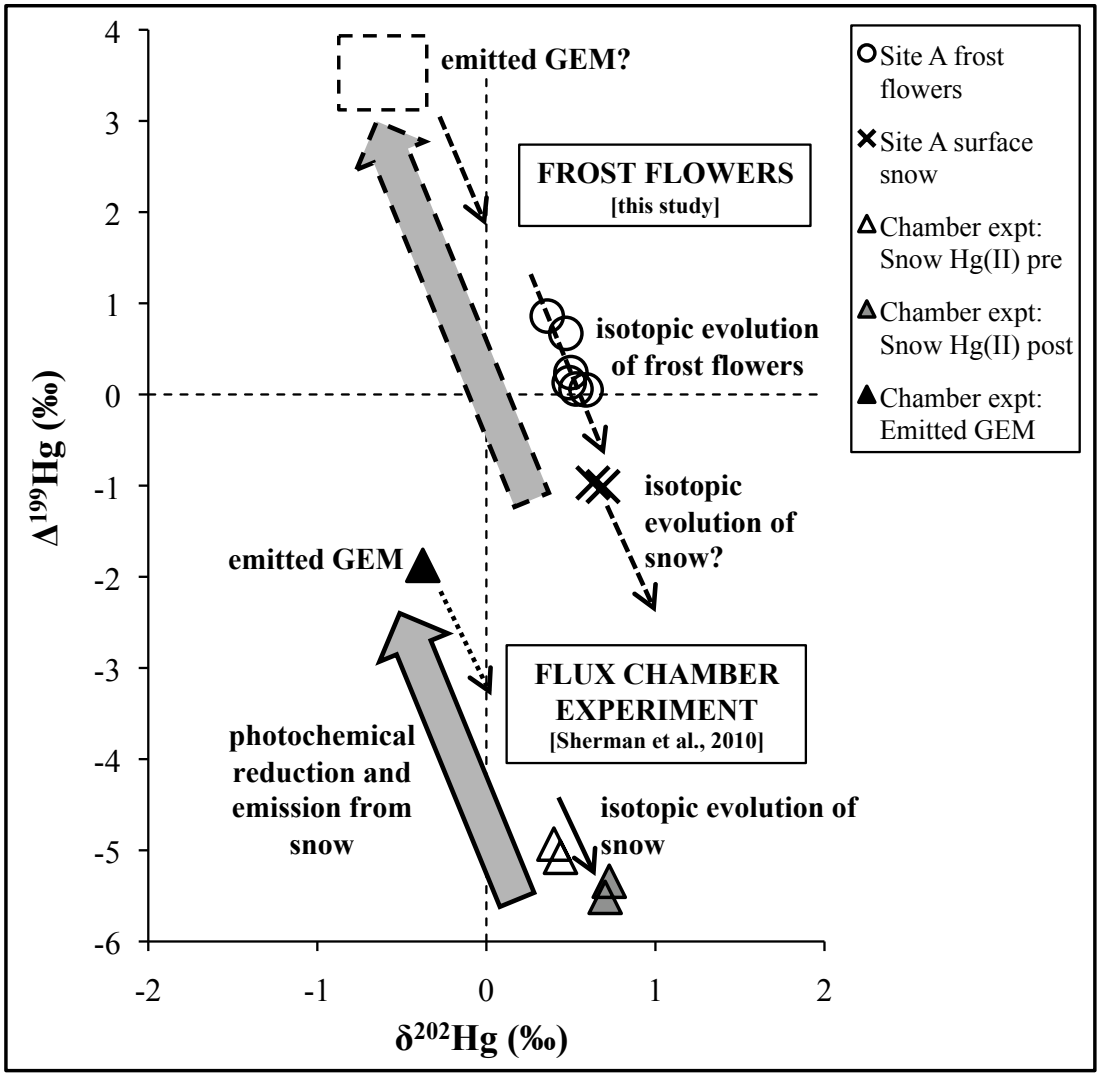


Figure 4.5 Hypothesized isotopic evolution of frost flower samples, surface snow, and emitted GEM. Symbols for frost flower and surface snow samples collected at Site A during this study are shown in the figure legend. Samples collected during a flux chamber experiment conducted by Sherman et al. (*14*) are shown as triangles where drifted snow originally placed in the chamber are open triangles, snow after the experiment are grey triangles, and emitted GEM is a black triangle. Fractionation observed during this experiment is shown as a large solid grey arrow. Hypothesized fractionation occurring during photochemical reduction and emission of Hg from snow during this study is shown as a large dashed grey arrow and the hypothesized isotopic composition of GEM initially emitted by the surface snow is shown as a dashed box. Dashed lines depict the 0 values for both axes.

Table 4.1 Mercury concentrations in frost flower, surface snow, and brine samples. Reported Hg concentrations represent averages of replicate measurements. The MDL for these measurements was 0.76 ng/L and all sample replicates were within 11.8% relative percent difference (RPD) (mean RPD = 2.79 ± 2.88%, n = 40).

Sample type	Collection Location	Collection Date	[Hg] (ng/L)
Wet frost flowers	Site A	3/14/09	124
Wet frost flowers	Site A	3/14/09	134
Wet frost flowers	Site A	3/14/09	136
Dry frost flowers	Site A	3/14/09	128
Dry frost flowers	Site A	3/14/09	156
Dry frost flowers	Site A	3/14/09	127
Dry frost flowers	Site A	3/14/09	164
Dry frost flowers	Site A	3/14/09	213
Dry frost flowers, 48 hrs old	Site A	3/16/09	200
Dry frost flowers, 48 hrs old	Site A	3/16/09	160
Surface snow	Site A	3/14/09	82.3
Surface snow	Site A	3/14/09	92.8
Surface snow	Site A	3/14/09	114
Surface snow	Site A	3/14/09	69.7
Surface snow	Site A	3/14/09	88.0
Brine	Site A	3/14/09	38.5
Brine	Site A	3/14/09	41.4
Brine	Site A	3/14/09	44.5
Dry frost flowers	Site B	3/20/09	51.2
Dry frost flowers	Site B	3/20/09	48.2
Dry frost flowers	Site B	3/20/09	55.4
Dry frost flowers	Site B	3/20/09	42.5
Surface snow	Site B	3/20/09	11.5
Surface snow	Site B	3/20/09	11.3
Brine	Site B	3/20/09	44.8
Brine	Site B	3/20/09	60.7
Frost flowers	1 km S of Site B	3/25/09	91.0
Frost flowers	1 km S of Site B	3/25/09	73.3
Brine	1 km S of Site B	3/25/09	15.9
Brine	1 km S of Site B	3/25/09	16.1

Table 4.2 Mercury isotopic compositions of standards and samples. Presented isotope ratios for the UM-Almadén secondary standard are averages of analytical session averages from January 2010 through March 2011 ("n" is the total number of analytical sessions). Presented isotope ratios for procedural standards are averages of analytical session averages ("n" is the number of processed standards). Number of analysis for samples are the total number of times the sample was analyzed in a single analytical session. Analytical uncertainties for the UM-Almadén standard and procedural standards are 2 s.d. of analytical session averages. Analytical uncertainties presented for limited samples that were measured more than once in a given analytical session are 2 s.d. of analytical session averages. Maximum sample analytical uncertainty for a given isotope ratio is the largest of the uncertainty (2 s.d.) measured in the UM-Almadén standard or procedural standards.

Sample type	Collection Location	Collection Date	[Hg] (ng/L)	n	δ^{202}Hg (‰)	2σ (‰)	δ^{201}Hg (‰)	2σ (‰)	δ^{200}Hg (‰)	2σ (‰)	δ^{199}Hg (‰)	2σ (‰)	Δ^{201}Hg (‰)	2σ (‰)	Δ^{200}Hg (‰)	2σ (‰)	Δ^{199}Hg (‰)	2σ (‰)
UM-Almadén standard				36	-0.58	0.07	-0.48	0.09	-0.28	0.07	-0.17	0.08	-0.04	0.06	0.01	0.05	-0.02	0.07
NIST SRM 3133 (snow process std)				3	0.04	0.03	0.04	0.05	-0.03	0.09	-0.03	0.12	0.01	0.03	-0.05	0.11	-0.04	0.13
Wet frost flowers	Site A	3/14/09	124	1	0.36		0.74		0.11		0.95		0.47		-0.07		0.86	
Wet frost flowers	Site A	3/14/09	134	1	0.47		0.74		0.13		0.79		0.39		-0.10		0.67	
Dry frost flowers	Site A	3/14/09	156	2	0.50	0.02	0.46	0.02	0.21	0.12	0.37	0.10	0.09	0.02	-0.04	0.12	0.24	0.10
Dry frost flowers	Site A	3/14/09	213	2	0.59	0.14	0.32	0.10	0.24	0.02	0.20	0.02	-0.12	0.02	-0.06	0.08	0.05	0.00
Dry frost flowers, 48 h old	Site A	3/16/09	200	1	0.49		0.34		0.17		0.26		-0.02		-0.07		0.13	
Dry frost flowers, 48 h old	Site A	3/16/09	160	1	0.53		0.42		0.10		0.19		0.02		-0.17		0.06	
Surface snow	Site A	3/14/09	69.7	1	0.69		-0.48		0.24		-0.83		-1.00		-0.11		-1.01	
Surface snow	Site A	3/14/09	88.0	1	0.63		-0.40		0.3		-0.81		-0.88		-0.02		-0.97	
Dry frost flowers	Site B	3/20/09	51.2	1	-0.28		-0.61		-0.23		-0.43		-0.40		-0.09		-0.36	
Dry frost flowers	Site B	3/20/09	48.2	1	-0.29		-0.35		-0.30		-0.35		-0.14		-0.16		-0.28	
Brine	Site B	3/20/09	60.7	1	-0.39		-0.53		-0.40		-0.49		-0.23		-0.20		-0.39	
Brine	Site B	3/20/09	44.8	1	-0.19		-0.48		-0.11		-0.46		-0.33		-0.01		-0.41	

CHAPTER 5

Investigation of local mercury deposition from a coal-fired power plant using mercury isotopes[1]

Abstract

Coal combustion accounts for approximately two-thirds of global anthropogenic mercury (Hg) emissions. Enhanced deposition of Hg can occur close to coal-fired utility boilers (CFUBs), but it is difficult to link specific point sources with local deposition. Measurement of Hg stable isotope ratios in precipitation holds promise as a tool to assist in the identification of local Hg deposition related to anthropogenic emissions. We collected daily event precipitation samples in close proximity to a large CFUB in Crystal River, Florida. Precipitation samples collected in Crystal River were isotopically distinct and displayed large negative δ^{202}Hg values (mean = -2.56‰, 1 s.d = 1.10‰, n = 28). In contrast, precipitation samples collected at other sites in FL that were not greatly impacted by local coal combustion were characterized by δ^{202}Hg values close to 0‰ (mean = 0.07‰, 1 s.d. = 0.17‰, n = 13). These results indicate that, depending on factors such as powdered coal isotopic composition and efficiency of Hg removal from flue gas, Hg deposited near CFUBs can be isotopically distinct. As this tool is further refined through future studies, Hg stable isotopes may eventually be used to quantify local deposition of Hg emitted by large CFUBs.

[1] Sherman, L. S., Blum, J. D., Keeler, G. J., Demers, J. D., Dvonch, J. T. Investigation of local mercury deposition from a coal-fired power plant using mercury isotopes. *Environmental Science and Technology* **2012**, *46*, 382-390.

5.1 Introduction

Mercury (Hg) is a bioaccumulative neurotoxin that can enter aquatic ecosystems via atmospheric deposition (*1, 2*). Complex atmospheric Hg chemistry and the mixing of emissions from local, regional, and long-range sources make it challenging to directly trace Hg pollution from sources to receptor sites. Gaseous elemental Hg (GEM) has a relatively long atmospheric residence time and can be transported regionally and globally, whereas reactive gaseous Hg (RGM) and fine particle-bound Hg ($Hg_{(p)}$) are more water soluble and particle reactive (*3, 4*). As a result, these forms of Hg are rapidly scavenged from the atmosphere and deposited to surface environments (*5, 6*). Mercury deposition near point sources and urban areas can be enhanced because RGM and $Hg_{(p)}$ are often emitted in higher relative proportions from anthropogenic sources (*7-11*). However, the relative contribution to Hg deposition from local, regional, and long-range sources is location-specific and depends on a number of factors including the types and quantities of local and regional sources, atmospheric transport patterns, atmospheric oxidants, and local meteorology (*9, 12, 13*).

Multivariate receptor models based on ratios of trace element co-pollutants in combination with meteorological data have been used to quantify the relative impact of local sources on Hg deposition (*9, 11, 13-16*). A number of studies utilized these techniques to investigate Hg deposition in Florida (FL), U.S.A. (*9, 13, 15, 17, 18*). Elevated levels of Hg have been found across FL in freshwater fish (*19, 20*), wading birds (*21*), and precipitation (*13, 22*). Mercury concentrations in FL precipitation can be an order of magnitude greater than those in the urban midwestern U.S.A. (*12, 13, 23*), especially during the summer months (*13, 24*). In the 1990s, researchers found that local

sources of Hg including coal-fired utility boilers (CFUBs), oil-fired utility boilers, municipal and medical waste incinerators, and cement manufacturing facilities contributed significantly to Hg deposition in south FL (*9, 13, 15*). Recent regulations on emissions from municipal and medical waste incinerators have significantly reduced Hg emissions from those sources (*25-27*). Despite these emissions reductions, Hg wet deposition remains elevated across FL, and the current relative impact of local versus long-range transported emissions is not well understood.

The measurement of Hg stable isotope ratios in atmospheric samples has the potential to assist in the identification of Hg emissions from local point sources (*28-32*). This study represents the first use of Hg stable isotope ratios to investigate near-source Hg deposition resulting from coal combustion. This research was performed in collaboration with a study conducted to understand current Hg deposition patterns across FL and provide Hg Total Maximum Daily Load estimates.

5.1.1 Mercury stable isotopes

There are seven stable isotopes of Hg (196, 198, 199, 200, 201, 202, and 204 amu) and isotopic variation has been documented in reservoirs including fossil fuels (*30*) and the atmosphere (*28, 29*). Mercury isotope ratios are reported using delta notation as

$$\delta^{xxx}\text{Hg}\ (‰) = ([(^{xxx}\text{Hg}/^{198}\text{Hg})_{sample}/(^{xxx}\text{Hg}/^{198}\text{Hg})_{SRM\ 3133}] - 1) * 1000 \quad (1)$$

where ^{xxx}Hg is an isotope of Hg and SRM 3133 is a NIST Hg standard (*33*). Mercury isotopes can undergo mass-dependent fractionation (MDF) during processes such as photochemical reduction and evasion from aqueous solutions (*34, 35*). Following previous work we report MDF of Hg isotopes using δ^{202}Hg (*36*). Mercury isotopes can

also undergo mass-independent fractionation (MIF). A relatively small amount of MIF (<~0.5‰) can be caused by differences in nuclear charge radii between the isotopes (the nuclear field shift effect) (*34, 37-39*). A greater magnitude of MIF can occur during spin-selective photochemical reactions involving radical pairs (the magnetic isotope effect) in which the even and odd-mass-number isotopes react at different rates (*29, 40-42*). MIF is reported as the deviation of a measured delta value from that theoretically predicted to result due to kinetic MDF according to the equation:

$$\Delta^{xxx}Hg = \delta^{xxx}Hg - (\delta^{202}Hg * \beta) \quad (2)$$

where β is equal to 0.252 for ^{199}Hg, 0.502 for ^{200}Hg, and 0.752 for ^{201}Hg (*33*).

5.2 Experimental

5.2.1 Site descriptions

During July 2009 daily-event precipitation samples were collected at four sites (designated N, NE, S, and E) surrounding the CFUB in Crystal River, FL at distances of 5.0 to 10.6 km (Figure 5.1 and Table 5.SI-1). These sites and the CFUB were located in close proximity to the Gulf of Mexico coast. As depicted in Figure 5.1, the only significant point source of Hg emissions (>1 kg of Hg per year) within ~50 km of the Crystal River area is the CFUB. Additionally, according to the 2005 U.S. EPA National Emissions Inventory (NEI), the Crystal River CFUB is the largest point source of total Hg emissions in FL and emitted a total of ~300 kg of Hg per year during the period of our study (*8*). It is important to consider the speciation of these emissions because RGM and $Hg_{(p)}$ species are readily deposited near point sources and air pollution control devices (APCDs) can impact Hg speciation. For example, selective catalytic reduction

units (SCRs) promote oxidation of GEM to reactive species (*43*) that are efficiently removed from the flue gas in wet flue-gas desulfurization units or electrostatic precipitators (*43, 44*). For this reason, CFUBs with SCRs and flue-gas desulfurization units are predicted to release a lower percentage of Hg as RGM than those without these APCDs (Table 5.SI-2). In contrast, because the Crystal River CFUB had only limited APCDs in July 2009, an estimated 68% of the Hg emissions from the CFUB were RGM species (Table 5.SI-2) (*8*). Because the Crystal River CFUB is a large point source of RGM emissions isolated from other emissions sources, the area surrounding the utility was a good location to isolate and measure the isotopic composition of locally deposited Hg emitted by a CFUB.

Between July and September 2009 daily event precipitation samples were also collected at nine other sites across FL (Figure 5.1 and Table 5.SI-1). These sites were located near a variety of anthropogenic Hg sources and, depending on meteorological conditions and source characteristics, Hg deposition at these sites may have been influenced by a mixture of local sources and non-local, long-range transported Hg. It is possible that local coal combustion may have impacted samples collected at several of the sites including TPA and UCF. However, not only do the CFUBs near those sites emit much less total Hg than the Crystal River CFUB, but also, due to their APCDs, it is estimated that only ~8% of their Hg emissions are RGM species (Table 5.SI-2). We do not expect, therefore, that these sites were influenced by local coal combustion to the same degree as the Crystal River sites. The Sand Key Park (SDK) site was chosen because it was located on the Gulf of Mexico coast, and during specific meteorological

conditions, Hg deposition at that site was primarily composed of non-local, long-range transported Hg.

5.2.2 Sample collection

Precipitation samples were collected daily using manually deployed tripods (~2 m above ground level) with sampling trains that were similar to those previously deployed in automated collectors (*11, 22, 45*). Tipping bucket rain gauges (R. M. Young) were mounted on the tripods. At each of the four Crystal River sites, three Hg sampling trains were deployed per event to ensure collection of sufficient Hg for isotope analyses (see Supporting Information). These sites were maintained daily from 7/4/09 through 7/24/09; after 7/24/09 samples were collected only at the NE site. Two field blanks were collected at each site during the course of the study (see Supporting Information).

Five coal samples were obtained from the Pennsylvania State University Coal Sample Bank. These coal samples were from the same regions in eastern Kentucky (KY) and West Virginia (WV), but not necessarily the same mines, as those that supplied coal to the Crystal River CFUB during July 2009 (*46*) (Table 5.SI-2).

5.2.3 Meteorological analysis

The precipitation events included in this study were analyzed meteorologically using GRLevel2Analyst software (*47*) with archived NEXRAD Level II radar data (*48*) (see Supporting Information). Using these data, we measured a variety of parameters including storm motion, maximum rainfall intensity, maximum echo top height, and average precipitating cell size at 5-min intervals throughout each event. We

characterized surface wind direction using surface meteorological maps (*49*) and air sounding data (*5*). Air mass transport to the sites was additionally modeled using the NOAA Hybrid Single-Particle Lagrangian Integrated Trajectory (HYSPLIT) model (*50*). The hour of maximum precipitation was used as the start time for each back trajectory, and trajectories were calculated using starting heights of 500 and 1000 m above ground level.

5.2.4 Sample processing and analysis

After collection, precipitation samples were oxidized to a concentration of 1% BrCl (v/v) and stored in a cold room for four months. Mercury concentrations were then measured in the field blanks and a subset of the samples by atomic absorption spectrometry (AAS; MA-2000, Nippon Instruments) (see Supporting Information). The method detection limit (MDL) for these analyses was 0.82 ng/L (3 s.d. of blank analyses) and all sample replicates were within 8.1% relative percent difference (RPD) (mean RPD = 2.0 ± 1.9%, 1 s.d., n = 78). The Crystal River field blanks contained an average of 0.39 ng of Hg (1 s.d. = 0.46 ng, n = 8) while field blanks collected at the other sites in FL contained an average of 0.07 ng of Hg (1 s.d. = 0.10 ng, n = 43). The field blanks collected at the Crystal River sites may be somewhat higher because equipment limitations only allowed cleaning of the funnels and adapters in 5% HNO_3 for 4-8 h compared to 24 h at the other sites. However, the Hg in the Crystal River field blanks represents only a small percentage of the average amount of Hg contained in precipitation samples collected at those sites (mean = 1.8%, 1 s.d. = 1.8%, n = 8) and this amount of

contamination could not have significantly influenced the isotopic compositions of the samples (see Supporting Information).

Mercury in the precipitation samples with sufficient mass for isotopic analyses (i.e., >8 ng) was concentrated into acidic 1% $KMnO_4$ solutions (w/w, Alfa Aesar). Each sample was poured into a 2 L Pyrex bottle and 0.3 mL of 30% $NH_2OH \cdot HCl$ was added and allowed to react for 30 min. A peristaltic pump was then used to add 100 ml of 5% $SnCl_2$ at a rate of 10 ml/min. Mercury-free air was pulled through the sample and carried the resulting GEM into the trapping solution at a rate of 0.7 L/min for four h. Procedural standards (NIST SRM 3133) and blanks were processed in the same manner (see Supporting Information). Each of the four sample replicates were processed by separating the total sample volume in half and processing the two splits in parallel. After transfer into the $KMnO_4$ solutions, final Hg concentrations were measured by AAS and used to determine Hg concentrations in the original precipitation samples. Mercury in procedural standards was consistently recovered completely in the final solutions (mean = 94%, 1 s.d. = 6%, n = 23; see Supporting Information).

Mercury in the coal samples was thermally released and concentrated into 1% $KMnO_4$ solutions according to previously reported methods (*30*). Briefly, the samples were crushed to a fine powder, weighed into ceramic boats, and combusted over 5.75 h in a two-stage quartz tube furnace in which the temperature of the first furnace was incrementally increased to 550°C while the second furnace was held at 1000°C. The resulting GEM was swept by O_2 gas into the $KMnO_4$ solution. Procedural standards (NIST SRM 1632c) and blanks were processed using the same methods. Mercury in

procedural standards was consistently recovered completely in the final solutions (mean = 94%, 1 s.d. = 5%, n = 7; see Supporting Information).

Mercury isotopic compositions were measured using continuous-flow cold vapor generation MC-ICP-MS (Nu Instruments) according to previously published methods (*33, 40*). We estimate the maximum sample analytical uncertainty as 2 s.d. of the measurement of the isotope ratio in procedural standards (e.g., δ^{202}Hg uncertainty = 0.13‰, 2 s.d). Replicate analyses of the UM-Almadén secondary standard (n = 37) and precipitation sample replicates (n = 4) were reproducible within this uncertainty (Table 5.SI-4).

5.3 Results and discussion

5.3.1 Precipitation events

To better interpret the results of our isotopic analyses, we analyzed the meteorological conditions during each precipitation event at Crystal River (Table 5.SI-3). The observed precipitation events fell broadly into two categories based on meteorological conditions. We further characterized the events in "Event Group 1" into three sub-categories, 1A, 1B, and 1C as follows. During the first week of the study (7/4/09 to 7/9/09) and on 7/20/09 (Table 5.SI-3, Event Group 1A), slow-moving cold and stationary fronts persisted over northern FL and southern Georgia. Predominantly westerly winds transported air masses onshore from over the Gulf of Mexico and westerly and southwesterly surface winds transported emissions from the CFUB over the collection sites. These events were characterized by large convective cells that covered the entire study area and resulted in precipitation at all of the Crystal River sites. The

events on 7/17/09 and 7/18/09 (Table 5.SI-3, Event Group 1B) similarly were related to the presence of a cold front over southern Georgia and were characterized by westerly surface winds. In contrast to the earlier events, during the events on 7/17/09 and 7/18/09, large isolated precipitating convective cells (~6 to 10 km in diameter) passed over the CFUB and only resulted in precipitation at some of the sites. Finally, the event on 7/12/11 (Table 4.SI-3, Event Group 1C) was characterized by a local high pressure system and a north-south band of convective precipitating cells (~26 km in north-south length) that moved inland from the west over the CFUB and impacted the NE and E sites. In general, the Group 1 precipitation events (7/4/09 to 7/20/09) were characterized by persistent cold and stationary fronts over northern FL and central Georgia, westerly/southwesterly storm motion and surface winds, and large convective precipitating cells that often impacted the entire study area. Under these conditions, RGM emitted by the CFUB was likely incorporated into cloud droplets (*24*), and because the precipitating cells were larger in diameter than the distance between the collection sites, this Hg was likely deposited at all of the Crystal River collection sites.

The precipitation events on 7/30/09 and 7/31/09 ("Event Group 2") were meteorologically different than the preceding events (Table 5.SI-3). The event on 7/30/09 was not related to a frontal system. During that event, convective cells formed over central FL and were transported into the Crystal River area by southeasterly winds. Southerly surface winds transported emissions from the Crystal River CFUB to the north. On 7/31/09, precipitating cells were transported into the area from the northwest and southerly surface winds similarly transported the CFUB emissions to the north. Especially on 7/30/09 it is unlikely that local emissions from the Crystal River CFUB

were incorporated into the precipitating cells that impacted the NE site. We hypothesize that Hg deposited during these events at the NE site was transported to the area from non-local sources.

We also analyzed the meteorological conditions during events sampled at the Sand Key Park (SDK) site on the Gulf of Mexico coast (Figure 5.1). On 7/26/09, southwesterly onshore flow transported air masses to the area that had spent the previous two days over the Gulf of Mexico. Convective heating caused the formation of offshore cells that moved inland and caused precipitation at the site. Given these conditions and the coastal location of the SDK site, Hg deposited during this event was primarily of non-local origin and transported from over the Gulf of Mexico.

5.3.2 Mercury concentrations

Mercury concentrations in precipitation are presented in Table 5.SI-4. Mercury concentrations in samples collected in Crystal River that were analyzed for Hg isotopic composition ranged from 4.0 to 130 ng/L and concentrations in samples collected at the other sites that were analyzed for Hg isotopic composition ranged from 18 to 69 ng/L. Volume-weighted mean (VWM) sample Hg concentrations at each of the Crystal River sites were calculated by dividing the total amount of Hg deposited by the total volume of precipitation. The VWM concentrations for the four sites were 41 ng/L (N), 27 ng/L (NE), 44 ng/L (E) and 51 ng/L (S). These VWM concentrations are relatively high compared to those reported by previous studies conducted during the summer in south FL (13-27 ng/L) (*22*) and those measured at the FL Mercury Deposition Network sites in July 2009 (15-26 ng/L) (*51*). The lower VWM Hg concentration at the NE site and

higher VWM concentration at the S site may be partly explained by differences in total precipitation amount collected at these sites during individual events. To assess this relationship, precipitation depth (cm) was regressed against the logarithm of Hg concentrations (Figure 5.2, see Supporting Information). As shown in Figure 5.2, the slope of the relationship between precipitation depth and Hg concentration is negative (slope = -0.21 ± 0.03, 1 s.e.; t = -6.62, $p < 0.0001$, $r^2 = 0.63$, n = 28) and 63% of the variation in concentration is explained by differences in precipitation depth (*52*). Although the high volume sample collected at the NE site on 7/4/09 falls outside of the range of the rest of the data, it had little influence on the slope estimate (slope without NE 7/4/09 = -0.19 ± 0.04, 1 s.e.; t = -4.40, $p = 0.0002$, $r^2 = 0.44$, n = 27). Similar relationships between Hg concentration and precipitation amount have been observed in previous studies (*13, 14, 22, 23, 53*). Several of these studies suggest that at locations impacted to varying degrees by Hg from local sources, variations in Hg concentration are largely controlled by the magnitude of local source impacts and not by differences in precipitation amount (*11, 13*). The correlation between Hg concentration and precipitation depth in the Crystal River samples suggests that variations in Hg concentration were not caused by varying impacts from the local CFUB. Instead, based on meteorological analyses, high Hg concentrations, and Hg isotopic analyses, we argue that this correlation resulted because of deposition of Hg from the CFUB at all of the collection sites.

5.3.3 Mercury isotopic compositions

Complete isotopic data are presented in Table 5.SI-4. As depicted in Figure 5.3,

precipitation samples collected in Crystal River were characterized by negative δ^{202}Hg values as low as -4.37 ± 0.13‰, 2 s.d. (mean = -2.56‰, 1 s.d = 1.10‰, n = 28) and slightly positive Δ^{199}Hg values (mean = 0.32‰, 1 s.d = 0.12‰, n = 28). In contrast, precipitation collected at the other sites in FL did not exhibit large negative δ^{202}Hg values (mean = 0.07‰, 1 s.d. = 0.17‰, n = 13) and had a wider range of Δ^{199}Hg values (mean = 0.15‰, 1 s.d = 0.25‰, n = 13). All of the precipitation samples exhibited slight positive Δ^{200}Hg values (mean = 0.11‰, 1 s.d. = 0.07‰, n = 41) that were similar in magnitude to those reported for Midwest precipitation (*28*) (see Supporting Information).

Four of the five coal samples from mines similar to those that supplied the Crystal River CFUB also displayed negative δ^{202}Hg values as low as -1.32 ± 0.13‰, 2 s.d. (mean = -0.74‰, 1 s.d. = 0.69‰, n = 5) but exhibited negative Δ^{199}Hg values (mean = -0.23‰, 1 s.d = 0.08‰, n = 5). These samples did not display MIF of ^{200}Hg (mean Δ^{200}Hg = 0‰, 1 s.d. = 0.02‰, n = 5).

The magnitude of the negative δ^{202}Hg values measured in samples collected in Crystal River greatly exceeds that previously reported for atmospheric samples (*28, 29, 54*). With the exception of the two precipitation samples collected at the NE site on 7/30/09 and 7/31/09 (Table 5.SI-3, Event Group 2), all of the Crystal River samples exhibited δ^{202}Hg values lower than -1.10‰ and there are no clear differences between the four Crystal River collection sites in terms of isotopic composition (Figure 5.3). This is likely due to the fact that large precipitating cells covered the study area during these events and all of the collection sites were similarly impacted by emissions from the CFUB.

5.3.3.1 Factors influencing Hg isotopic compositions

The Hg isotopic composition of any particular precipitation sample is the result of mixing of Hg from different sources combined with the effects of in-source and post-emission fractionation (*28*). Here we address these factors and their potential influence on the observed Hg isotopic compositions of the collected precipitation samples.

5.3.3.1.1 Source isotopic composition

Mercury deposited in precipitation at the Crystal River sites was a mixture of local CFUB-emitted Hg and Hg from non-local sources. During the Event Group 1 precipitation events (7/4/09 through 7/20/09), storm motion was primarily from the west and any non-local Hg deposited at the collection sites was transported to the area from over the Gulf of Mexico. To estimate the isotopic composition of this Hg, we analyzed Hg in precipitation collected at the SDK site on 7/26/09. On the basis of meteorological analyses, Hg deposited during that event was primarily non-local and transported from over the Gulf of Mexico. This sample was characterized by a slightly positive δ^{202}Hg value (0.13 ± 0.13‰, 2 s.d.). Therefore, it is unlikely that the large negative δ^{202}Hg values observed in Crystal River precipitation are due to the influence of non-local Hg transported from over the Gulf of Mexico. Instead, we argue that local deposition of Hg emitted by the Crystal River CFUB resulted in the observed negative δ^{202}Hg values.

The isotopic composition of Hg emitted by a CFUB could be affected by several factors including (1) original source coal isotopic composition, (2) coal cleaning, and (3) in-system fractionation within the power plant. Although we did not have access to coal burned at the Crystal River CFUB during the sampling period, coal samples from mines in the same region as those that supplied coal to the CFUB displayed negative δ^{202}Hg

values and negative Δ^{199}Hg values. Biswas et al. (*30*) measured similarly negative δ^{202}Hg values (mean = -1.23‰, 1 s.d. = 0.29‰, n = 6) and slightly negative Δ^{199}Hg values (mean = -0.13‰, 1 s.d = 0.01‰, n = 2) in other Appalachian coals. Assuming that these values represent the isotopic composition of the original bulk source coal delivered to the Crystal River CFUB in July 2009, additional negative MDF and positive MIF of Hg are required to produce the observed precipitation Hg isotopic compositions.

Coal cleaning prior to combustion may result in powdered coal that displays lower δ^{202}Hg values than the original bulk source coal. To reduce sulfur concentrations, high sulfur Appalachian coals are generally cleaned at the mine prior to shipment using fluidized density separation (*55*). During this process, denser minerals such as Hg-rich sulfides sink and are removed (*55*). Secondary coal cleaning is also conducted at many CFUBs (including the Crystal River CFUB) wherein the more coarse and dense sulfides are rejected at the coal pulverizer during crushing (*56-59*). Because a large percentage of Hg in coal is associated with sulfides (*55, 60*), these processes can remove a significant amount of Hg from the original source coal (*55*). A recent study of coals from the Illinois basin found that sulfide-associated Hg had much higher δ^{202}Hg values (mean = -0.11‰, 1 s.d. = 0.05‰, n = 3) than Hg associated with coexisting organic matter (mean = -1.46‰, 1 s.d. = 0.34‰, n = 21) (*61*). Removal of sulfides through coal cleaning may, therefore, result in the preferential removal of the heavier isotopes of Hg and produce powdered coal with a lower δ^{202}Hg value than the original bulk source coal.

5.3.3.1.2 In-system fractionation

Essentially all of the Hg liberated during coal combustion is expected to be GEM (*59*). As the flue gas leaves the boiler and enters the APCDs, it cools to ~130°C and

some portion of the GEM is oxidized to RGM through gas-phase reactions or via heterogeneous reactions on particles (*43, 59*). The reactive Hg species can subsequently be removed to varying degrees by the APCDs (*43, 59*). MDF of heavy metals (including Zn, Cd, and Hg) has been observed at similarly high temperatures during industrial and volcanic processes (*54, 62-65*). Zambardi et al. (*54*) observed MDF of Hg isotopes in volcanic fumerole emissions and found that downwind of the vents, oxidized plume $Hg_{(p)}$ displayed higher $\delta^{202}Hg$ values (-0.11 ± 0.18‰, 2 s.d.) than total gaseous Hg (-1.74 ± 0.36‰, 2 s.d.) (*54*). The authors hypothesized that this was due to the preferential equilibrium oxidation of the heavy isotopes of Hg (*54*). If a similar process occurs in CFUB flue gas, the heavier isotopes of Hg would be progressively oxidized, adsorbed onto particles and removed in electrostatic precipitators and baghouses (*43, 59*). This process would result in MDF of Hg isotopes such that the Hg remaining in the flue gas would exhibit progressively lower $\delta^{202}Hg$ values relative to the powdered coal that was combusted. Unfortunately, because we cannot determine the Hg removal efficiency from the flue gas at the Crystal River CFUB and because we do not know the exact isotopic composition of the powdered coal that was combusted, we are not able to model this fractionation process.

5.3.3.1.3 Post-emission atmospheric fractionation

In addition to source isotopic composition and in-system fractionation, post-emission atmospheric processes may cause additional MDF and MIF. To our knowledge, the effects of atmospheric reactions on Hg isotopes have not been studied (*36*). However, once emitted to the atmosphere RGM is strongly scavenged by aqueous droplets (*3*). Thus we do not expect that significant secondary MDF effects RGM emitted by the

Crystal River CFUB prior to deposition. It is, however, possible that atmospheric processes could have played a role in modifying the observed Δ^{199}Hg values in the precipitation samples. The Crystal River precipitation samples displayed higher Δ^{199}Hg values (~0.5‰) than the representative source coal samples (mean coal Δ^{199}Hg = -0.24‰, 1 s.d = 0.09‰, n = 5; mean precipitation Δ^{199}Hg = 0.32‰, 1 s.d = 0.12‰, n = 28). Although this magnitude of MIF could have occurred in the power plant system during reactions influenced by the nuclear field shift (NFS) effect (*34*), it is more likely that photochemical reactions in the atmosphere caused the observed positive MIF.

Gratz et al. (*28*) hypothesized that a difference between near-zero Δ^{199}Hg values in total gaseous Hg (mean = -0.09‰, 1 s.d = 0.09‰, n = 7) and positive Δ^{199}Hg values observed in Midwest precipitation (mean = 0.30‰, 1 s.d = 0.14‰, n = 20) could be the result of the magnetic isotope effect (MIE) occurring during photochemical reduction and evasion of Hg from cloud droplets. In experimental studies, the MIE has been demonstrated to result in a Δ^{199}Hg/Δ^{201}Hg ratio between 1.0 and 1.3 (*34, 40*). In contrast, the NFS effect has been theoretically calculated and experimentally demonstrated to result in a higher Δ^{199}Hg/Δ^{201}Hg ratio between 1.6 and 2.5 (*34, 37, 38, 66, 67*). Precipitation samples collected during this study were characterized by Δ^{199}Hg/Δ^{201}Hg ratios within error of 1.0 (Crystal River samples = 1.05 ± 0.14, 1 s.e.; other precipitation samples = 1.12 ± 0.11, 1 s.e. (*68*); Figure 5.4). This suggests that the MIE occurring during photochemical processes in the atmosphere is at least partially responsible for the observed Δ^{199}Hg values in the precipitation samples.

This study of Hg deposited in precipitation across the state of FL provides evidence that Hg isotopes may be useful as a tool to help identify locally deposited Hg

emitted by large CFUBs. We hypothesize that the isotopic composition of source coal, coal cleaning, and processes inherent to the removal of Hg from the flue gas stream caused the emission of Hg with extreme negative δ^{202}Hg values from the Crystal River CFUB. It is likely that the isotopic composition of Hg emissions varies between CFUBs depending on a number of factors such as powdered coal isotopic composition, thermal profile of the power plant system, properties of particles in the flue gas, type of APCDs, and efficiency of Hg removal by APCDs. It is also likely that local Hg deposition near other types of anthropogenic point sources is isotopically different than that measured near the Crystal River CFUB. Future measurements of the Hg isotopic composition of powdered coal and flue gas emissions, percentage of RGM in emissions, and efficiency of Hg removal by APCDs would enable more quantitative estimates of the contribution of local coal combustion to Hg deposition. Additionally, future measurements of the isotopic composition of dry deposited Hg may help to further quantify the impact of anthropogenic point sources on local Hg deposition. In areas surrounding large CFUBs such as Crystal River, FL, the anomalous Hg isotope signature of local CFUB emissions may be useful in tracing the impact of this pollution on local ecosystems.

Acknowledgements

This manuscript is dedicated to the memory of co-author Dr. Gerald J. Keeler and would not have been possible without his inspiration and devotion to scientific research. Funding for this research was provided by a National Defense Science and Engineering Graduate Fellowship (DOD-ONR), the University of Michigan (GESI Graduate Fellowship and Turner Grant), and by the Florida Department of Environmental

Protection (Contract No. SP673). The authors acknowledge the NOAA Air Resources Laboratory for the HYSPLIT transport and dispersion model accessed via the READY website. We thank K. Morin, C. McKendree, and R. Del Valle in Crystal River and M.W. Johnson, J.A. Barres, L. Gratz, F. Marsik, N. Hall, and the members of BEIGL for their assistance. This manuscript was significantly improved by comments from four anonymous reviewers.

References

(1) Mergler, D.; Anderson, H. A.; Chan, L. H. M.; Mahaffey, K. R.; Murray, M.; Sakamoto, M.; Stern, A. H.; Methylmercury exposure and health effects in humans: A worldwide concern. *Ambio* **2007,** *36* (1), 3-11.

(2) Hammerschmidt, C. R., Fitzgerald, W.F.; Methylmercury in Freshwater Fish Linked to Atmospheric Mercury Deposition. *Environ. Sci. Technol.* **2006,** *40*, 7764-7770.

(3) Lin, C.-J.; Pehkonen, S. O.; The chemistry of atmospheric mercury: A review. *Atmos. Environ.* **1999,** *33*, 2067-2079.

(4) Schroeder, W. H., Munthe, J.; Atmospheric mercury - An overview. *Atmos. Environ.* **1998,** *32* (5), 809-822.

(5) Mason, R. P.; Sheu, G.-R.; Role of the ocean in the global mercury cycle. *Global Biogeochem. Cycles* **2002,** *16* (4), 1-14.

(6) Lindberg, S.; Bullock, R.; Ebinghaus, R.; Engstrom, D.; Feng, X.; Fitzgerald, W.; Pirrone, N.; Prestbo, E.; Seigneur, C.; A synthesis of progress and uncertainties in attributing the sources of mercury in deposition. *Ambio* **2007,** *36* (1), 19-32.

(7) Landis, M. S.; Vette, A. F.; Keeler, G. J.; Atmospheric mercury in the Lake Michigan Basin: Influence of the Chicago/Gary urban area. *Environ. Sci. Technol.* **2002,** *36*, 4508-4517.

(8) U.S. Environmental Protection Agency, **2005**. *National Emissions Inventory for Mercury Point Sources in the State of Florida*. access via http://www.epa.gov/ttn/chief/net/2005inventory.html#inventorydata. Accessed November 15, 2010.

(9) Dvonch, J. T.; Graney, J. R.; Keeler, G. J.; Stevens, R. K.; Use of elemental tracers to source apportion mercury in south Florida precipitation. *Environ. Sci. Technol.* **1999,** *33*, 4522-4527.

(10) Lohman, K.; Seigneur, C.; Edgerton, E.; Jansen, J.; Modeling mercury in power plant plumes. *Environ. Sci. Technol.* **2006,** *40*, 3848-3854.

(11) White, E. M.; Keeler, G. J.; Landis, M. S.; Spatial variability of mercury wet deposition in eastern Ohio: Summertime meteorological case study analysis of local source influences. *Environ. Sci. Technol.* **2009,** *43*, 4946-4953.

(12) Keeler, G. J.; Landis, M. S.; Norris, G. A.; Christianson, E. M.; Dvonch, J. R.; Sources of mercury wet deposition in eastern Ohio, USA. *Environ. Sci. Technol.* **2006,** *40*, 5874-5881.

(13) Dvonch, J. T.; Keeler, G. J.; Marsik, F. J.; The influence of meteorological conditions on the wet deposition of mercury in southern Florida. *JApMe* **2005,** *44*, 1421-1435.

(14) Landis, M. S., Vette, A.F., Keeler, G.J.; Atmospheric mercury in the Lake Michigan Basin: Influence of the Chicago/Gary urban area. *Environ. Sci. Technol.* **2002,** *36*, 4508-4517.

(15) Graney, J. R.; Dvonch, J. T.; Keeler, G. J.; Use of multi-element tracers to source apportion mercury in south Florida aerosols. *Atmos. Environ.* **2004,** *38* (12), 1715-1726.

(16) Pancras, J. P.; Vedantham, R.; Landis, M. S.; Norris, G. A.; Ondov, J. M.; Application of EPA Unmix and nonparametric wind regression on high time resolution trace elements and speciated mercury in Tampa, Florida aerosol. *Environ. Sci. Technol.* **2011,** *45* (8), 3511-3518.

(17) Guentzel, J. L.; Landing, W. M.; Gill, G. A.; Pollman, C. D.; Processes influencing rainfall deposition of mercury in Florida. *Environ. Sci. Technol.* **2001,** *35*, 863-873.

(18) Landing, W. M.; Perry Jr., J. J.; Guentzel, J. L.; Gill, G. A.; Pollman, C. D.; Relationships between the atmospheric deposition of trace elements, major ions, and mercury in Florida: The FAMS project (1992-1993). *Water, Air, Soil Pollut.* **1995,** *80*, 343-352.

(19) Hand, J.; Friedemann, M.; Mercury, largemouth bass, and water quality: A preliminary report. Florida Department of Environmental Regulation **1990**.

(20) Axelrad, D. M.; Atkeson, T. D.; Lange, T.; Pollman, C. D.; Gilmour, C. C.; Orem, W. H.; Mendelssohn, I. A.; Frederick, P. C.; Krabbenhoft, D. P.; Aiken, G. R.; Rumbold, D. G.; Scheidt, D. J.; Kalla, P. I.; Mercury monitoring, research and environmental assessment in South Florida. South Florida Environmental Report **2007**.

(21) Frederick, P. C.; Spalding, M. G.; Dusek, R.; Wading birds as bioindicators of mercury contamination in Florida: Annual and geographic variation. *Environ. Toxicol. Chem.* **2002,** *21* (1), 163-167.

(22) Dvonch, J. T.; Graney, J. R.; Marsik, F. J.; Keeler, G. J.; Stevens, R. K.; An investigation of source-receptor relationships for mercury in south Florida using event precipitation data. *Sci. Tot. Environ.* **1998,** *213*, 95-108.

(23) Hoyer, M.; Burke, J.; Keeler, G.; Atmospheric sources, transport and deposition of mercury in Michigan: Two years of event precipitation. *Water, Air, Soil Pollut.* **1995,** *80*, 199-208.

(24) Asman, W. A. H.; Parameterization of below-cloud scavenging of highly soluble gases under convective conditions. *Atmos. Environ.* **1995,** *29* (12), 1359-1368.

(25) Atkeson, T. D.; Pollman, C. D.; Axelrad, D. M., Recent trends in mercury emissions, deposition, and biota in the Florida Everglades: A monitoring and modeling analysis. In *Dynamics of Mercury Pollution on Regional and Global Scales: Atmospheric Processes and Human Exposures Around the World*, Pirrone, N., Mahaffey, K.R., Ed. Springer: **2005**; pp 637-655.

(26) U.S. Environmental Protection Agency, *Mercury Study Report to Congress Volume 2*. Office of Air Quality Planning and Standards, Office of Research and Development: Washington, DC, **1997**.

(27) Lantern Corporation, *Trends of Anthropogenic Mercury Mass Flows and Emissions in Florida*. Final Report: Clayton, M.O., **2002**. pp 1-74.

(28) Gratz, L. E.; Keeler, G. J.; Blum, J. D.; Sherman, L. S.; Isotopic composition and fractionation of mercury in Great Lakes precipitation and ambient air. *Environ. Sci. Technol.* **2010,** *44*, 7764-7770.

(29) Sherman, L. S.; Blum, J. D.; Johnson, K. P.; Keeler, G. J.; Barres, J. A.; Douglas, T. A.; Mass-independent fractionation of mercury isotopes in Arctic snow driven by sunlight. *Nature Geoscience* **2010,** *3* (3), 173-177.

(30) Biswas, A.; Blum, J. D.; Bergquist, B. A.; Keeler, G. J.; Zhouqing, X.; Natural mercury isotope variation in coal deposits and organic soils. *Environ. Sci. Technol.* **2008,** *42* (22), 8303-8309.

(31) Estrade, N.; Carignan, J.; Donard, O. F. X.; Isotope tracing of atmospheric mercury sources in an urban area of northeastern France. *Environ. Sci. Technol.* **2010,** *44* (16), 6062-6067.

(32) Foucher, D.; Ogrinc, N.; Hintelmann, H.; Tracing mercury contamination from the Idrija mining region (Slovenia) to the Gulf of Trieste using Hg isotope ratio measurements. *Environ. Sci. Technol.* **2008,** *43* (1), 33-39.

(33) Blum, J. D.; Bergquist, B. A.; Reporting the variations in the natural isotopic composition of mercury. *Anal. Bioanal. Chem.* **2007,** *388* (2), 353-359.

(34) Zheng, W.; Hintelmann, H.; Mercury isotope fractionation during photoreduction in natural water is controlled by its Hg/DOC ratio. *Geochim. Cosmochim. Acta* **2009,** *73*, 6704-6715.

(35) Zheng, W.; Foucher, D.; Hintelmann, H.; Mercury isotope fractionation during volatilization of Hg(0) from solution into the gas phase. *J. Anal. Atomic Spectro.* **2007,** *22*, 1097-1104.

(36) Bergquist, B. A.; Blum, J. D.; The odds and evens of mercury isotopes: Applications of mass-dependent and mass-independent isotope fractionation. *Elements* **2009,** *5*, 353-357.

(37) Estrade, N.; Carignan, J.; Sonke, J. E.; Donard, O. F. X.; Mercury isotope fractionation during liquid-vapor evaporation experiments. *Geochim. Cosmochim. Acta* **2009,** *73*, 2693-2711.

(38) Schauble, E. A.; Role of nuclear volume in driving equilibrium stable isotope fractionation of mercury, thallium, and other very heavy elements. *Geochim. Cosmochim. Acta* **2007,** *71*, 2170-2189.

(39) Bigeleisen, J.; Nuclear size and shape effects in chemical reactions. Isotope chemistry of the heavy elements. *J. Am. Chem. Soc.* **1996,** *118*, 3676-3680.

(40) Bergquist, B. A.; Blum, J. D.; Mass-dependent and mass-independent fractionation of Hg isotopes by photo-reduction in aquatic systems. *Science* **2007,** *318* (5849), 417-420.

(41) Buchachenko, A. L.; Magnetic isotope effect: Nuclear spin control of chemical reactions. *J. Phys. Chem.* **2001,** *105* (44), 9995-10011.

(42) Zheng, W.; Hintelmann, H.; Isotope fractionation of mercury during its photochemical reduction by low-molecular-weight organic compounds. *J. Phys. Chem. A* **2010,** *114* (12), 4246-4253.

(43) Srivastava, R. K.; Hutson, N.; Martin, B.; Princiotta, F.; Staudt, J.; Control of mercury emissions from coal-fired electric utility boilers. *Environ. Sci. Technol.* **2006,** *40* (5), 1385-1393.

(44) Niksa, S.; Helble, J. J.; Fujiwara, N.; Kinetic modeling of homogeneous mercury oxidation: The importance of NO and H_2O in predicting oxidation in coal-derived systems. *Environ. Sci. Technol.* **2001,** *35*, 3701-3706.

(45) Landis, M. S.; Keeler, G. J.; Critical evaluation of a modified automatic wet-only precipitation collector for mercury and trace element determinations. *Environ. Sci. Technol.* **1997,** *31*, 2610-2615.

(46) U.S. Energy Information Administration, **2009-2011**. *Monthly Utility and Nonutility Fuel Receipts and Fuel Quality Data, EIA-923*. access via http://www.eia.doe.gov/cneaf/electricity/page/eia423.html. Accessed January 20, 2012.

(47) Granato, T. C.; Pietz, R. I.; Gschwind, J.; Lue-Hing, C.; Mercury in soils and crops from fields receiving high cumulative sewage sludge applications: Validation of U.S. EPA's risk assessment for human ingestion. *Water, Air, Soil Pollut.* **1995,** *80*, 1119-1127.

(48) National Climatic Data Center, **2009**. *National Oceanographic and Atmospheric Administration Satellite and Information Service*. access via http://has.ncdc.noaa.gov/pls/plhas/has.dsselect. Accessed October 15, 2009.

(49) Unisys. Unisys Weather Website. access via http://weather.unisys.com/archive/index.php. Accessed

(50) Draxler, R. R.; Rolph, G. D. HYSPLIT (HYbrid Single-Particle Langrangian Integrated Trajectory) Model, **2010**. *National Oceanic and Atmospheric Science Administration, Air Resources Laboratory*. access via http://ready.arl.noaa.gov/HYSPLIT.php. Accessed August 1, 2010.

(51) *Mercury Deposition Network*; National Atmospheric Deposition Program, Illinois State Water Survey: Champaign, IL, **2009**; access via http://nadp.sws.uiuc.edu/maps/.

(52) *SAS OnlineDoc*. Cary, North Carolina, **1999**.

(53) Keeler, G. J.; Gratz, L. E.; Al-Wali, K.; Long-term atmospheric mercury wet deposition at Underhill, Vermont. *Ecotoxicology* **2005,** *14*, 71-83.

(54) Zambardi, T.; Sonke, J. E.; Toutain, J. P.; Sortino, F.; Shinohara, H.; Mercury emissions and stable isotopic compositions at Vulcano Island (Italy). *Earth. Planet. Sci. Lett.* **2009,** *277*, 236-243.

(55) Toole-O'Neil, B.; Tewalt, S. J.; Finkelman, R. B.; Akers, D. J.; Mercury concentration in coal -- unraveling the puzzle. *Fuel* **1999,** *78*, 47-54.

(56) Mardon, S. M.; Hower, J. C.; Impact of coal properties on coal combustion by-product quality: Examples from a Kentucky power plant. *International Journal of Coal Geology* **2004,** *59*, 153-169.

(57) Abel, W. T.; Zulkoski, M.; Gauntlett, G. J.; Dry separation of pyrite from coal. *Industrial and Engineering Chemistry Product Research and Development* **1972,** *11* (3), 342-347.

(58) Progress Energy Crystal River Energy Complex, **2010**. *Process Flow Diagram for Coal Combustion Products and Non-Combustion Waste Products*. access via http://publicfiles.dep.state.fl.us/siting/outgoing/PEF_CREC/3rd_Revised_CCP_Plan/Figure%202_APR10.pdf. Accessed May 1, 2011.

(59) Hower, J. C.; Senior, C. L.; Suuberg, E. M.; Hurt, R. H.; Wilcox, J. L.; Olson, E. S.; Mercury capture by native fly ash carbons in coal-fired power plants. *Prog. Energy Combust. Sci.* **2010,** *36*, 510-529.

(60) Kolker, A.; Senior, C. L.; Quick, J. C.; Mercury in coal and the impact of coal quality on mercury emissions from combustion systems. *Appl. Geochem.* **2006,** *21*, 1821-1836.

(61) Lefticariu, L.; Blum, J. D.; Gleason, J. D.; Mercury isotopic evidence for multiple mercury sources in coal from the Illinois Basin. *Environ. Sci. Technol.* **2011,** *45* (4), 1724-1729.

(62) Cloquet, C.; Carignan, J.; Libourel, G.; Isotopic composition of Zn and Pb atmospheric depositions in an urban/periurban area of northeastern France. *Environ. Sci. Technol.* **2006,** *40* (21), 6594-6600.

(63) Cloquet, C.; Carignan, J.; Libourel, G.; Sterckeman, T.; Perdrix, E.; Tracing source pollution in soils using cadmium and lead isotopes. *Environ. Sci. Technol.* **2006,** *40* (8), 2525-2530.

(64) Toutain, J.-P.; Sonke, J.; Munoz, M.; Nonell, A.; Polve, M.; Viers, J.; Freydier, R.; Sortino, F.; Joron, J.-L.; Sumarti, S.; Evidence for Zn isotopic fractionation at Merapi volcano. *Chem. Geol.* **2008,** *253* (1-2), 74-82.

(65) Smith, C. N.; Kesler, S. E.; Klaue, B.; Blum, J. D.; Mercury isotope fractionation in fossil hydrothermal systems. *Geology* **2005,** *33* (10), 825-828.

(66) Ghosh, S.; Xu, Y.; Humayun, M.; Odom, L.; Mass-independent fractionation of mercury isotopes in the environment. *Geochem. Geophys. Geosyst.* **2008,** *9*, Q03004, doi: 10.1029/2007/GC001827.

(67) Zheng, W.; Hintelmann, H.; Nuclear field shift effect in isotope fractionation of mercury during abiotic reduction in the absence of light. *The Journal of Physical Chemistry A* **2010,** *114* (12), 4238-4245.

(68) York, D.; Least-squares fitting of a straight line. *Can. J. Phys.* **1966,** *44*, 1076-1086.

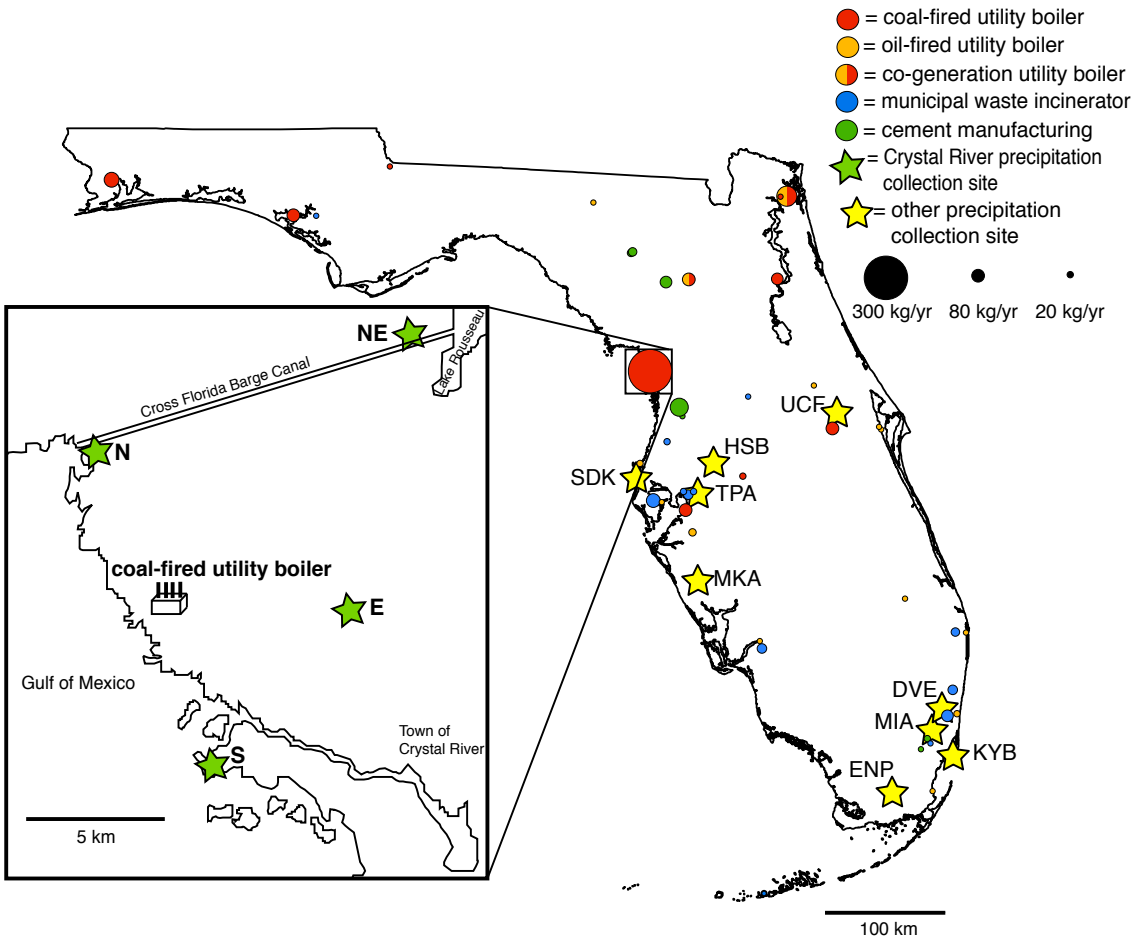


Figure 5.1 Map of Hg emissions sources and sample collection sites with inset showing sites surrounding Crystal River utility. Symbols for point sources are scaled linearly (with respect to radius) according to total estimated Hg emissions relative to the largest source (*8*). Only sources emitting >1 kg of Hg per year are shown. Precipitation collection sites surrounding the Crystal River CFUB (green stars) are labeled as N, NE, S, and E. The other precipitation collection sites are shown as yellow stars.

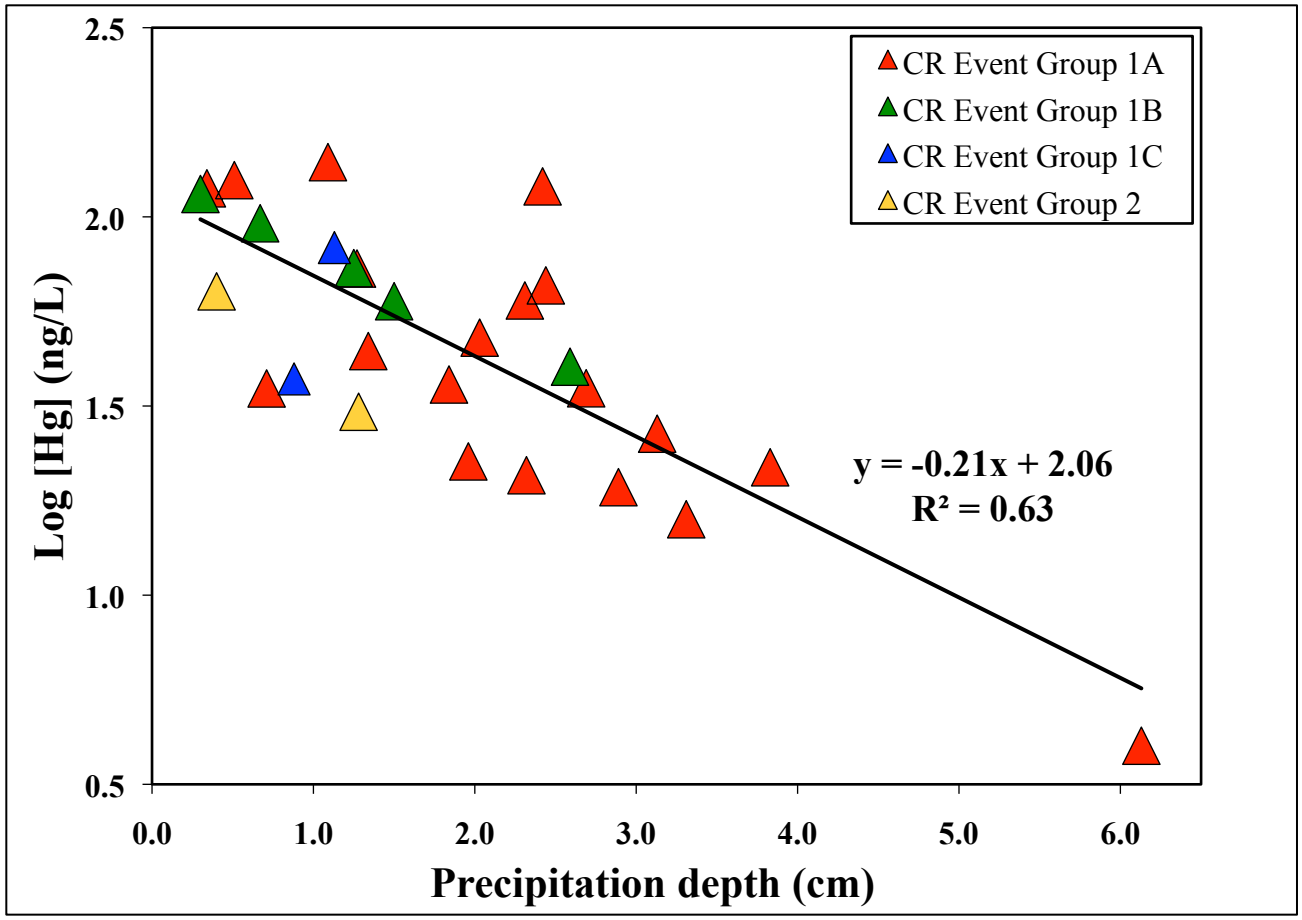


Figure 5.2 Precipitation depth (cm) versus log Hg concentration (ng/L). Precipitation samples collected at sites in Crystal River, FL are shown as triangles. Precipitation events are colored according to Event Group: Event Group 1A (red triangles) includes events from 7/4/09 to 7/9/09 and 7/20/09, Event Group 1B (green triangles) includes the events on 7/17/09 and 7/18/09, Event Group 1C (blue triangles) represents the event on 7/12/09, and Event Group 2 (yellow triangles) includes the events on 7/30/09 and 7/31/09. A linear regression through all of the data points is shown.

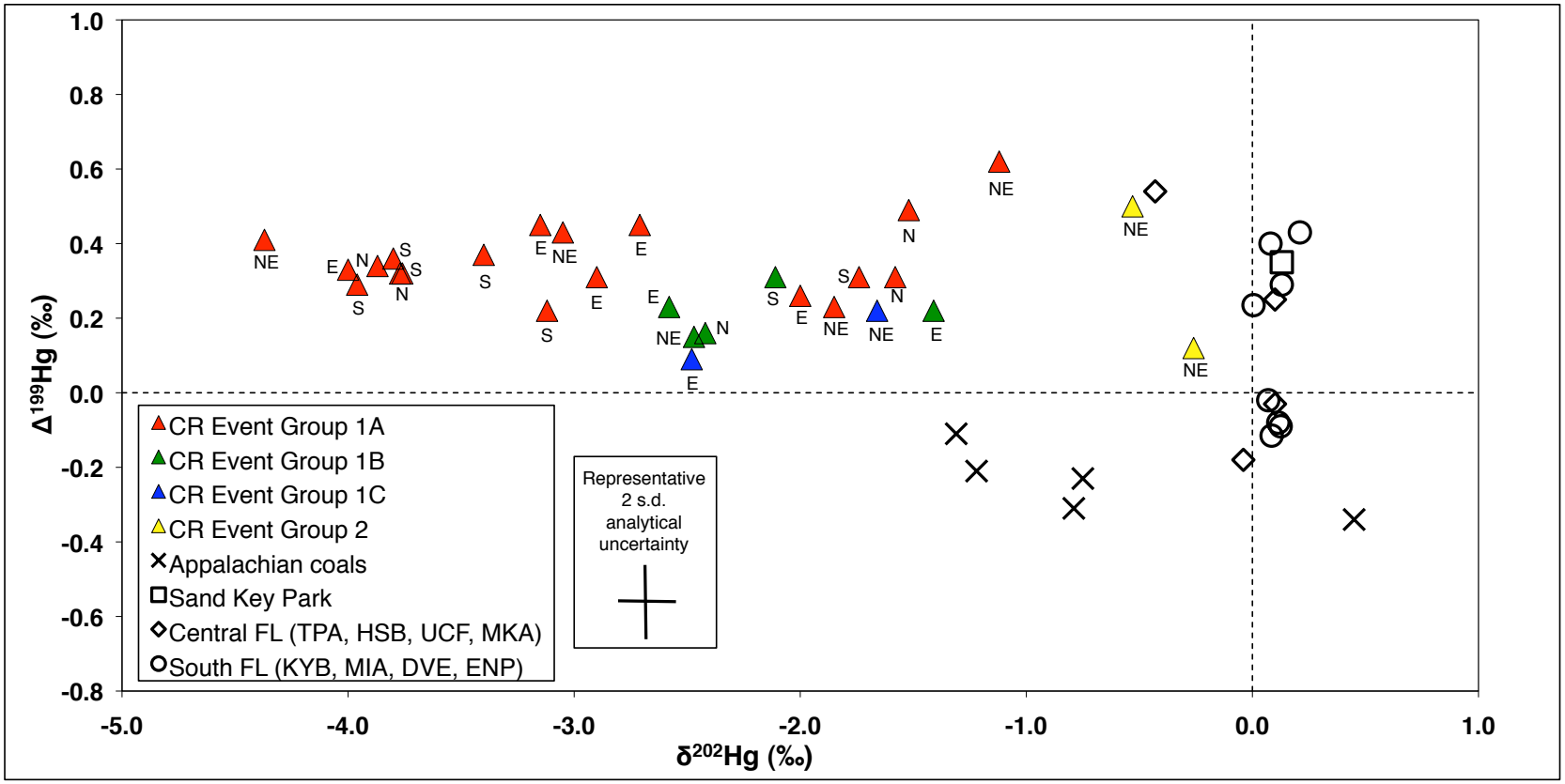


Figure 5.3 δ^{202}Hg (‰) versus Δ^{199}Hg (‰) measured in precipitation and coal samples. Precipitation samples collected at sites in Crystal River, FL are shown as solid triangles and secondarily labeled by collection site location (N, NE, S, E). Precipitation events are grouped according to Event Group (1A = 7/4/09 to 7/9/09 and 7/20/09; 1B = 7/17/09 and 7/18/09; 1C = 7/12/09; 2 = 7/30/09 and 7/31/09). Precipitation samples collected at other sites are shown as open symbols where the Sand Key Park sample is a square, central FL site samples are diamonds, and south FL site samples are circles. Representative Appalachian coal samples are shown as black crosses. Precipitation sample analytical uncertainty based on replicate analyses of procedural standards (2 s.d.) is depicted. Black dashed lines depict the zero values for both axes.

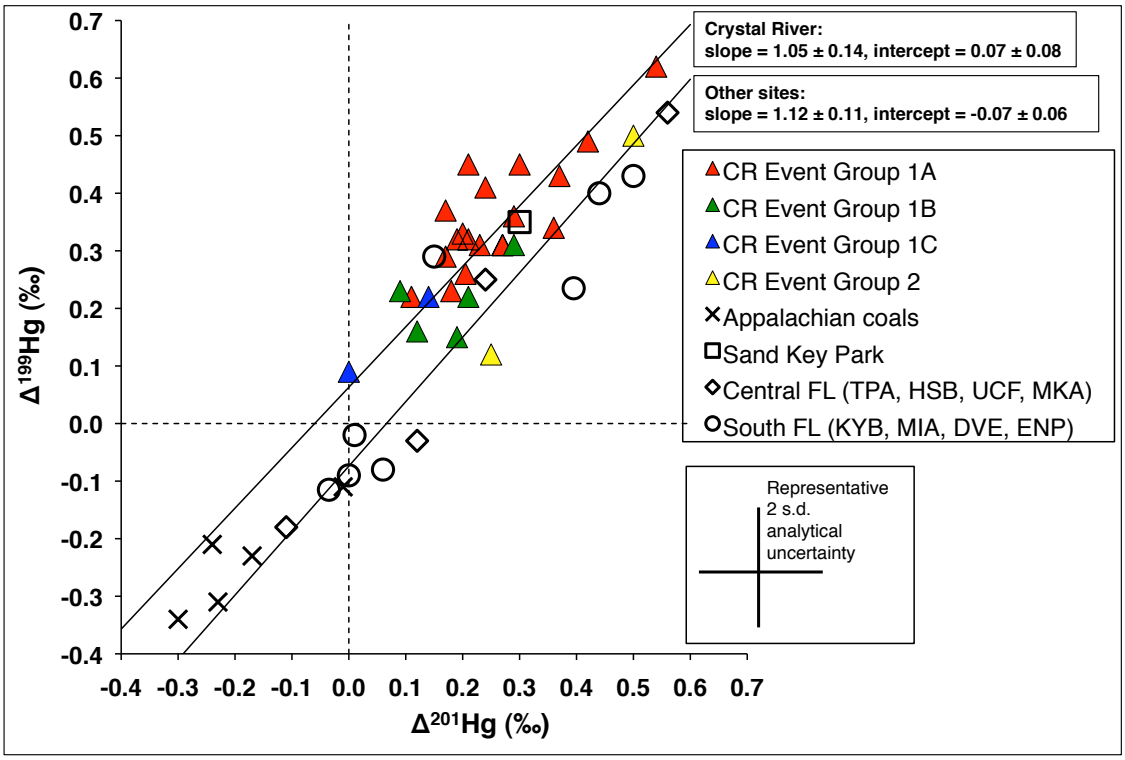


Figure 5.4 Δ^{201}Hg (‰) versus Δ^{199}Hg (‰) in precipitation and coal samples. Precipitation samples collected at sites in Crystal River, FL are shown as solid triangles. Precipitation events are grouped according to Event Group (1A = 7/4/09 to 7/9/09 and 7/20/09; 1B = 7/17/09 and 7/18/09; 1C = 7/12/09; 2 = 7/30/09 and 7/31/09). Precipitation samples collected at other sites are shown as open symbols where the Sand Key Park sample is a square, central FL site samples are diamonds, and south FL site samples are circles. Representative Appalachian coal samples are shown as black crosses. Δ^{199}Hg/Δ^{201}Hg ratios calculated for samples collected in Crystal River and samples collected at the other sites using York regressions (*68*) are shown as solid lines. Representative sample analytical uncertainty for precipitation samples based on replicate analyses of procedural standards (2 s.d.) is depicted. Black dashed lines depict the zero values for both axes.

5.4 Supplemental information

5.4.1 Experimental

5.4.1.1 Sample collection

All sample collection materials were acid-cleaned prior to use (*1*). Precipitation samples were collected using glass funnels into fluorinated polyethylene bottles containing 20 mL of 0.8% HCl (v/v, Suprapur). Between sample collections, all funnels and adapters were soaked in 5% HNO_3 (v/v, Fisher, Trace Metal Grade) and then rinsed thoroughly with deionized water prior to redeployment. At the Crystal River sites, it was not possible to clean and deploy sampling trains daily at all four sites unless precipitation abated for at least six hours. As a result, in two cases (7/7/09-7/8/09 and 7/8/09-7/9/09) precipitation from more than one day was collected as a single sample. These samples were included in this analysis because the precipitating storms were of similar character throughout each sampling period (Table 5.SI-3).

Two field blanks were collected at each of the sites during the course of the study. To collect each field blank, the sampling train was first cleaned and deployed as if to collect a sample. Then ~300 ml of deionized water was poured through the funnel and collected in a fluorinated polyethylene bottle as a sample.

5.4.1.2 Meteorological analysis

Radar data from Tampa, FL (KTBW) was used to analyze events at the Crystal River sites and those at the other central FL sites. Radar data from Miami, FL (KAMX) was used to analyze events at the south FL sites. Radar data from Orlando, FL (KMCO) was used to analyze the event at the University of Central Florida (UCF) site.

5.4.1.3 Statistical analyses

The relationship between Hg concentration and precipitation depth (cm) for samples collected in Crystal River was assessed using linear regression (Figure 5.2). Mercury concentrations were log-transformed in order to satisfy assumptions of linearity and homoscedasticity of variance for statistical analysis. The statistical significance of the slope of this relationship was assessed using PROC GLM (*2*). In addition, the relationships between precipitation sample Δ^{199}Hg and Δ^{201}Hg values were analyzed using York regressions (*3*).

5.4.1.4 Sample processing and analysis

After collection, precipitation samples (>30 ml in volume) were oxidized to a concentration of 1% BrCl (v/v) and stored in a dark cold room for four months. It has been previously documented that aqueous samples can be difficult to analyze for Hg concentrations because BrCl is not always sufficient to release Hg that is strongly bound to ligands (*4*). To determine whether this was a consideration for these precipitation samples, after four months of oxidation, 5 ml aliquots of a subset of the Crystal River samples (n = 18) were treated with ultraviolet (UV) light for four to eight days in closed quartz tubes. Procedural standards (50 pg of NIST SRM 3133 in 5 ml of 1% BrCl (v/v)) and blanks were treated with UV light in the same manner.

The UV treated samples, a smaller subset of the same precipitation samples not treated with UV light (n = 10), and the field blanks collected in Crystal River were analyzed for Hg concentrations by atomic absorption spectrometry (AAS) following $SnCl_2$ reduction (MA-2000, Nippon Instruments) (*5*). The method detection limit (MDL)

for these analyses was 0.82 ng/L (3 s.d. of blank analyses) and all sample replicates were within 8.1% relative percent difference (RPD) (mean RPD = 2.0 ± 1.9%, 1 s.d., n = 78). Mercury in the UV procedural standards was consistently recovered completely (mean = 103%, 1 s.d. = 7%, n = 5) and Hg concentrations in the UV procedural blanks were at the MDL (mean = 0.83 ng/L, 1 s.d. = 1.0 ng/L, n = 4). Mercury concentrations in the precipitation samples with and without UV treatment were the same within analytical error (mean RPD = 4.1 ± 3.7%, 1 s.d., n = 10). These results suggest that after four months of oxidation, UV treatment did not release additional Hg from the Crystal River precipitation samples.

After these analyses, precipitation samples with sufficient Hg (i.e. >8 ng of Hg) were further processed for isotopic analysis as described in the text. Mercury was separated from the samples by $SnCl_2$ reduction and concentrated into $KMnO_4$ solutions. Concentrations were measured in these final $KMnO_4$ solutions by AAS (Table 5.SI-4). Mercury in procedural standards processed in the same manner as samples was consistently recovered completely in the final solutions (mean = 94%, 1 s.d. = 6%, n = 23; see discussion below). Precipitation sample concentrations measured by processing large volume samples for isotopic analysis were considered the best measure of Hg concentrations in the precipitation samples. It is important to note that the purpose of this study was not to quantify long-term trends in deposition at the Crystal River sites or to compare Hg deposition at the Crystal River sites to the other sites in FL. Due to the fact that samples were only collected at the sites for one month and only samples containing >8 ng of Hg could be analyzed for isotopic composition, we are unable to accurately quantify long-term Hg deposition in Crystal River.

5.4.1.5 Field blanks

Over the course of the study, two field blanks were collected at each of the four Crystal River sites. Mercury in those field blanks resulted both from the deionized water poured through the funnels and any Hg still remaining in the sampling train after cleaning. To determine the amount of Hg that was potentially added to each precipitation sample from the sampling train, we subtracted the amount of Hg measured in the deionized water from the total amount of Hg contained in each field blank. As discussed in the text, we found that the Crystal River field blanks contained slightly more Hg (mean = 0.39 ng per blank, 1 s.d. = 0.46 ng, n = 8) than field blanks collected at other sites in FL (mean = 0.07 ng per blank, 1 s.d. = 0.10 ng, n = 43). However, the amount of Hg in the Crystal River field blanks represent an average of only 1.8% (1 s.d. = 1.8%, n = 8) of the Hg contained in the precipitation samples. Although there was not enough Hg in the field blanks to analyze them isotopically, we can estimate the affect of this amount of potential contamination on the isotopic composition of the precipitation samples. First, we estimate that ~1.8% of the Hg in a given Crystal River precipitation sample was due to contamination and assume that prior to addition of the contamination, this sample was isotopically similar to samples collected at the non-Crystal River sites (i.e., mean δ^{202}Hg = 0.07‰). If the δ^{202}Hg value of the contamination was similar to that measured in the most negative Crystal River sample (i.e, δ^{202}Hg = -4.37‰), the measured δ^{202}Hg value of the precipitation sample would decrease by only ~0.01‰. In fact, to produce precipitation with a δ^{202}Hg value equivalent to the average value measured in the Crystal River samples (i.e., δ^{202}Hg = -2.56‰), the δ^{202}Hg value of the contamination would need to be approximately -146‰. Prior to this study, the lowest δ^{202}Hg value observed in a

natural sample was approximately -3‰ (*6*). We are confident, therefore, that the small amount of potential Hg contamination in the Crystal River precipitation samples could not have resulted in the observed negative δ^{202}Hg values.

5.4.1.6 Procedural standards

During the course of this study, 23 precipitation procedural standards (NIST SRM 3133) and 12 procedural blanks were processed and analyzed in the laboratory in the same manner as the precipitation samples. Seven coal procedural standards (NIST SRM 1632c) and five blanks were also combusted and analyzed in the same manner as the coal samples. All of the procedural blanks contained negligible amounts of Hg that was attributable to small quantities of Hg in the oxidizing 1% $KMnO_4$ solutions (mean = 0.32 ng of Hg per solution, 1 s.d. = 0.21 ng, n = 17).

The precipitation procedural standards consisted of a known amount of Hg standard (25 ng or 50 ng of NIST SRM 3133) in 1% BrCl (v/v); the coal standards similarly consisted of a known amount of Hg standard (~150 ng of NIST SRM 1632c). After processing, Hg recoveries in these procedural standards were determined based on the amount of Hg that was processed and the measured Hg concentration in the final $KMnO_4$ trap solutions. For precipitation standards, Hg recoveries were between 81 and 100% (mean = 94%, 1 s.d. = 6%, n = 23). For coal standards, Hg recoveries were between 86 and 99% (mean = 94%, 1 s.d. = 5%, n = 7). The small amount of Hg loss from some of these standards did not cause systematic isotopic fractionation. However, these procedural standards were more variable in isotopic composition than the secondary analytical UM-Almadén standard that was measured several times during each analytical

session (Table 5.SI-4). For this reason, sample analytical uncertainty for each isotope ratio is estimated as 2 s.d. of the same ratio measured in the relevant procedural standards between analytical sessions.

5.4.2 Results and discussion

5.4.2.1 MIF of ^{200}Hg

Many of the precipitation samples collected during this study displayed small positive MIF of ^{200}Hg (Δ^{200}Hg up to 0.23 ± 0.10‰, 2 s.d.; mean = 0.11‰, 1 s.d. = 0.07‰, n = 41). Precipitation samples collected in Crystal River and precipitation samples collected at the other sites across FL displayed similar Δ^{200}Hg values that are comparable to those observed by Gratz et al. (*7*) in Midwest precipitation. In contrast, none of the coal samples analyzed during this study displayed significant MIF of ^{200}Hg (mean Δ^{200}Hg = -0.02‰, 1 s.d. = 0.03‰, n = 5). As noted by Gratz et al. (*7*), because MIF is measured as the deviation from the predicted δ^{202}Hg value based on kinetic MDF, anomalies of ^{198}Hg, ^{200}Hg or ^{202}Hg could cause the observed MIF. Although MIF of ^{200}Hg has now been observed in precipitation samples from multiple locations, the mechanism (or mechanisms) producing this fractionation is not understood. The magnetic isotope effect only produces MIF of the odd-mass-number isotopes of Hg because the even-mass-number isotopes have zero nuclear spin and do not exhibit nuclear magnetic moments (*6, 8, 9*). Additionally, although the nuclear field shift effect can cause MIF of the even-mass-number isotopes of Hg, this mechanism is not predicted to produce measureable MIF of ^{200}Hg relative to ^{202}Hg or ^{198}Hg (*8, 10*). It is possible that the observed small positive MIF of ^{200}Hg could be due to another mechanism acting in

the atmosphere such as photochemical self-shielding (*11, 12*). Future research is needed to better understand the atmospheric reactions and physical mechanisms that result in the observation of positive MIF of ^{200}Hg in precipitation samples.

References

(1) White, E. M.; Keeler, G. J.; Landis, M. S.; Spatial variability of mercury wet deposition in eastern Ohio: Summertime meteorological case study analysis of local source influences. *Environ. Sci. Technol.* **2009,** *43*, 4946-4953.

(2) *SAS OnlineDoc*. Cary, North Carolina, **1999**.

(3) York, D.; Least-squares fitting of a straight line. *Can. J. Phys.* **1966,** *44*, 1076-1086.

(4) Olson, M. L.; Cleckner, L. B.; Hurley, J. P.; Krabbenhoft, D. P.; Heelan, T. W.; Resolution of matrix effects on analysis of total and methyl mercury in aqueous samples from the Florida Everglades. *Fresenius J. Anal. Chem.* **1997,** *358* (3), 392-398.

(5) U.S. Environmental Protection Agency, *Method 1631, Revision E: Mercury in Water by Oxidation, Purge and Trap, and Cold Vapor Atomic Fluorescence Spectrometry (EPA-821/R-02-019)*. Office of Water, Office of Science and Technology, Engineering and Analysis Division: Washington, DC, **2002**.

(6) Bergquist, B. A.; Blum, J. D.; The odds and evens of mercury isotopes: Applications of mass-dependent and mass-independent isotope fractionation. *Elements* **2009,** *5*, 353-357.

(7) Gratz, L. E.; Keeler, G. J.; Blum, J. D.; Sherman, L. S.; Isotopic composition and fractionation of mercury in Great Lakes precipitation and ambient air. *Environ. Sci. Technol.* **2010,** *44*, 7764-7770.

(8) Malinovsky, D.; Vanhaecke, F.; Mass-independent isotope fractionation of heavy elements measured by MC-ICPMS: A unique probe in environmental sciences. *Anal. Bioanal. Chem.* **2011,** *400*, 1619-1624.

(9) Buchachenko, A. L.; Magnetic isotope effect: Nuclear spin control of chemical reactions. *J. Phys. Chem.* **2001,** *105* (44), 9995-10011.

(10) Schauble, E. A.; Role of nuclear volume in driving equilibrium stable isotope fractionation of mercury, thallium, and other very heavy elements. *Geochim. Cosmochim. Acta* **2007,** *71*, 2170-2189.

(11) Navon, O.; Wasserburg, G. J.; Self-shielding in O_2--a possible explanation for oxygen isotopic anomalies in meteorites? *Earth. Planet. Sci. Lett.* **1985,** *73* (1), 1-16.

(12) Mead, C.; Anbar, A. D.; Lyons, J. R.; Johnson, T. M. *Mass-independent fractionation of mercury isotopes in compact fluorescent light bulbs*, Amercian Geophysical Union, Fall Meeting, San Francisco, CA, **2010**.

(13) U.S. Environmental Protection Agency, **2005**. *National Emissions Inventory for Mercury Point Sources in the State of Florida*. access via http://www.epa.gov/ttn/chief/net/2005inventory.html#inventorydata. Accessed November 15, 2010.

(14) U.S. Energy Information Administration, **2009-2011**. *Monthly Utility and Nonutility Fuel Receipts and Fuel Quality Data, EIA-923*. access via http://www.eia.doe.gov/cneaf/electricity/page/eia423.html. Accessed January 20, 2012.

(15) Granato, T. C.; Pietz, R. I.; Gschwind, J.; Lue-Hing, C.; Mercury in soils and crops from fields receiving high cumulative sewage sludge applications: Validation of U.S. EPA's risk assessment for human ingestion. *Water, Air, Soil Pollut.* **1995,** *80*, 1119-1127.

(16) National Climatic Data Center, **2009**. *National Oceanographic and Atmospheric Administration Satellite and Information Service*. access via http://has.ncdc.noaa.gov/pls/plhas/has.dsselect. Accessed October 15, 2009.

(17) Pacyna, E. G.; Pacyna, J. M.; Steenhuisen, F.; Wilson, S.; Global anthropogenic mercury emission inventory for 2000. *Atmos. Environ.* **2006,** *40*, 4048-4063.

(18) Mason, R. P.; Sheu, G.-R.; Role of the ocean in the global mercury cycle. *Global Biogeochem. Cycles* **2002,** *16* (4), 1-14.

Table 5.SI-1 Precipitation collection sites in Crystal River and in other FL locations with site descriptions, site IDs, and site locations (i.e., nearest city).

Site Description	Site ID	Site Location	Latitude	Longitude
Crystal River north site	CR-N	Crystal River, FL	28.996244	-82.732936
Crystal River northeast site	CR-NE	Crystal River, FL	29.024867	-82.616650
Crystal River south site	CR-S	Crystal River, FL	28.906583	-82.689982
Crystal River east site	CR-E	Crystal River, FL	28.948333	-82.639728
University of Central Florida	UCF	Orlando, FL	28.592025	-81.190122
Hillsborough River State Park	HSB	Thonotosassa, FL	28.144017	-82.228100
agricultural field	TPA	Palm River-Clair Mel, FL	27.913433	-82.375111
Sand Key Park	SDK	Clearwater, FL	27.959938	-82.824514
Myakka River State Park	MKA	Sarasota, FL	27.222362	-82.297135
Florida Atlantic University - Davie Campus	DVE	Davie, FL	26.085378	-80.240689
Florida Department of Transportation site, US 27N	MIA	Miami, FL	25.899258	-80.382706
Bill Baggs Cape Florida State Park	KYB	Key Biscayne, FL	25.671941	-80.157363
Everglades National Park	ENP	Homestead, FL	25.389637	-80.680012

Table 5.SI-2. Characteristics of the coal-fired power plants in FL emitting >1 kg of Hg per year (*13*). Analysis includes coal purchases made by each plant from January 2009 through July 2009 (*14*). Emissions controls and modeled estimates of Hg speciation are based on the 2005 U.S. EPA National Emissions Inventory (*13*). Abbreviations: FGD = flue gas desulfurization units, SNCR = selective non-catalytic reduction units, SCR = selective catalytic reduction units.

Facility ID	Location	Coal purchased: Location and Percent (%)	SO_2 controls	NO_x controls	PM controls	Estimated Percent RGM	Estimated Percent $Hg_{(p)}$	Estimated Percent GEM
Crystal River Energy Complex	Crystal River, FL	KY (75%), WV (18%), VA (7%)	NONE	low NOx burners	ESP	68	6	26
Northside Generating Station	Jacksonville, FL	Columbia (92%), WV (8%)	dual alkali	SCR	ESP	8	0	92
James F. Crist Generating Plant	Pensacola, FL	WV (47%), UT (28%), Columbia (9%), CO (9%), KY (8%)	NONE	SNCR	ESP	68	6	26
Big Bend Power Station	Apollo Beach, FL	IL (58%), Columbia (42%)	wet lime FGD	other	ESP	8	0	92
Curtis H. Stanton Energy Center	Orlando, FL	KY (87%), WV (13%)	wet lime FGD	low NOx burners	ESP	8	0	92
Lansing Smith Generating Plant	Lynn Haven, FL	WV (42%), CO (22%), Columbia (13%), UT (13%), KY (9%)	NONE	low NOx burners	ESP	68	6	26
Seminole Electric Cooperative Inc.	Palatka, FL	KY (98%), IL (2%)	wet lime FGD	low NOx burners	ESP	8	0	92
Deerhaven Generating Station	Gainesville, FL	WV (85%), KY (15%)	dry lime FGD	SCR	ESP	58	5	37
Lakeland McIntosh Power Plant	Lakeland, FL	KY (55%), Columbia (25%), WV (19%), PA (2%)	wet lime FGD	low NOx burners	ESP	8	0	92
Herbert Scholz Generating Plant	Sneads, FL	KY (100%)	NONE	NONE	ESP	68	6	26
Cedar Bay Cogeneration Inc.	Jacksonville, FL	KY (98%), WV (2%)	wet lime FGD	SNCR	baghouse	28	42	30
St John River Power Park	Jacksonville, FL	Columbia (90%), WV (7%), KY (3%), PA (1%)	dry lime FGD	SNCR	baghouse	*NO DATA AVAILABLE*		

Table 5.SI-3 Meteorological characteristics of precipitation events. Events in Crystal River are grouped according to meteorological conditions as follows: Event Group 1A includes events from 7/4/09 to 7/9/09 and 7/20/09, Event Group 1B includes the events on 7/17/09 and 7/18/09, Event Group 1C represents the event on 7/12/09, and Event Group 2 includes the events on 7/30/09 and 7/31/09. The time of maximum precipitation (EDT) is based on rain gauge data (measured in Crystal River at the NE site). All wind and storm motion directions are denoted according to the point of origin of the wind. Storm motion, surface wind direction, maximum echo top height, and storm characteristics were determined using GRLevel2Analyst software (*15*) with NEXRAD Level II radar data (*16*), surface meteorological maps (*17*), and upper air soundings (*18*).

Precipitation event date	Precipitation event group	Impacted sites	Time of max precipitation (EDT)	Storm motion	Surface wind direction	Max echo top height (km)	Notes
7/4/09	1A	N, NE, S, E	1:35	W/NW	W	14	stationary front over northern FL; convective precipitating cells over entire study area
7/6/09	1A	N, NE, S, E	13:45	W	W/SW	12	cold front over central GA; convective precipitating cells over entire study area
7/7-7/8/09	1A	N, S, E	15:00 (7/7); 10:45 (7/8)	W	W/SW	9 (7/7); 11 (7/8)	stationary front over central GA/northern FL; convective precipitating cells over entire study area
7/8-7/9/09	1A	N, NE, S, E	17:45 (7/8); 6:00 (7/9) & 19:05 (7/9)	W/SW	SW	7 (7/8); 11 (7/9)	stationary front over central GA/northern FL; convective precipitating cells over entire study area
7/12/09	1C	NE, E	11:40	W	W	6	high pressure system; N-S trending band of convective precipitating cells (average cell diameter = 6.5 km) with light winds aloft
7/17/09	1B	NE, S, E	12:30	WSW	W	11	cold front over central GA; isolated convective precipitating cells (average cell diameter = 6.5 km)
7/18/09	1B	N, E	10:00	WSW	SW	12	cold front over central GA; cluster of convective precipitating cells (average cell diameter = 10 km)
7/20/09	1A	N, NE, S, E	1:10	W	WNW	10	stationary/cold front over northern FL; convective precipitating cells over entire study area
7/30/09	2	NE *(only operational site)*	20:20	SE	S	11	cells formed over central FL; convective precipitating cells over entire study area
7/31/09	2	NE *(only operational site)*	21:30	NW	S	8.5	cold front over northern GA; cluster of isolated convective precipitating cells (average cell diameter = 6 km)
7/26/09	--	Sand Key Park	8:30 & 19:00	SW	SW	9	air mass transport from over Gulf of Mexico, convective precipitating cells (average cell diameter = 6 km)

Table 5.SI-4 Mercury concentrations and isotopic compositions of standards and samples. Crystal River (CR) samples are listed according to site location (N, NE, S, E). Number of analyses for the UM-Almadén standard is the total number of analytical sessions from May 2009 to June 2010 and presented isotope ratios are averages of analytical session averages. Numbers of analyses for procedural standards are the total number of processed standards and presented isotope ratios are averages of analytical session averages. Analytical uncertainties for the UM-Almadén standard and procedural standards are 2 s.d. of analytical session averages.

Sample Type	Site ID	Precip. Date	Precip. Event Group	[Hg] (ng/L)	Precip. depth (cm)	n	δ^{202}Hg (‰)	2σ (‰)	δ^{201}Hg (‰)	2σ (‰)	δ^{200}Hg (‰)	2σ (‰)	δ^{199}Hg (‰)	2σ (‰)	Δ^{201}Hg (‰)	2σ (‰)	Δ^{200}Hg (‰)	2σ (‰)	Δ^{199}Hg (‰)	2σ (‰)
UM-Almadén standard						37	-0.58	0.07	-0.48	0.09	-0.28	0.07	-0.17	0.08	-0.04	0.06	0.01	0.05	-0.02	0.07
NIST SRM 3133 (precipitation procedural std)						23	-0.01	0.13	-0.03	0.16	-0.01	0.12	-0.02	0.11	-0.02	0.11	0.00	0.10	-0.02	0.10
NIST SRM 1632c (coal procedural std)						7	-1.86	0.13	-1.44	0.10	-0.93	0.07	-0.49	0.04	-0.04	0.03	0.01	0.03	-0.02	0.04
Precipitation	CR-N	7/4/09	1A	23	1.96	1	-3.87		-2.56		-1.85		-0.64		0.36		0.09		0.34	
Precipitation	CR-NE	7/4/09	1A	4.0	6.13	1	-1.12		-0.30		-0.37		0.34		0.54		0.19		0.62	
Precipitation	CR-S	7/4/09	1A	120	0.34	1	-3.12		-2.24		-0.16		-0.57		0.11		-0.03		0.22	
Precipitation	CR-E	7/4/09	1A	19	2.89	1	-3.15		-2.17		-1.45		-0.34		0.21		0.13		0.45	
Precipitation	CR-N	7/6/09	1A	16	3.31	1	-1.52		-0.72		-0.60		0.11		0.42		0.16		0.49	
Precipitation	CR-NE	7/6/09	1A	36	1.84	1	-3.05		-1.92		-1.37		-0.34		0.37		0.17		0.43	
Precipitation	CR-S	7/6/09	1A	48	2.03	1	-3.40		-2.38		-1.61		-0.49		0.17		0.10		0.37	
Precipitation	CR-E	7/6/09	1A	21	2.32	1	-2.71		-1.74		-1.21		-0.23		0.30		0.15		0.45	
Precipitation	CR-N	7/7-7/8/09	1A	22	3.83	1	-1.58		-0.92		-0.68		-0.09		0.27		0.11		0.31	
Precipitation	CR-S	7/7-7/8/09	1A	130	0.51	1	-3.96		-2.81		-2.02		-0.71		0.17		-0.03		0.29	
Precipitation	CR-E	7/7-7/8/09	1A	35	2.69	1	-2.90		-1.95		-1.35		-0.42		0.23		0.11		0.31	
Precipitation	CR-S	7/7-7/8/09	1A	27	3.13	1	-1.74		-1.04		-0.77		-0.13		0.27		0.11		0.31	
Precipitation	CR-N	7/8-7/9/09	1A	120	2.42	1	-3.76		-2.64		-1.84		-0.62		0.19		0.05		0.32	
Precipitation	CR-NE	7/8-7/9/09	1A	73	1.27	1	-4.37		-3.05		-2.16		-0.70		0.24		0.04		0.41	
Precipitation	CR-S	7/8-7/9/09	1A	44	1.34	1	-3.80		-2.57		-1.80		-0.59		0.29		0.11		0.36	
Precipitation	CR-E	7/8-7/9/09	1A	140	1.09	1	-4.00		-2.81		-1.97		-0.68		0.20		0.04		0.33	
Precipitation	CR-NE	7/12/09	1C	37	0.88	1	-1.66		-1.11		-0.69		-0.19		0.14		0.14		0.22	
Precipitation	CR-E	7/12/09	1C	83	1.13	1	-2.48		-1.86		-1.22		-0.53		0.00		0.02		0.09	
Precipitation	CR-NE	7/17/09	1B	60	1.50	1	-2.47		-1.67		-1.16		-0.48		0.19		0.08		0.15	
Precipitation	CR-S	7/17/09	1B	73	1.25	1	-2.11		-1.30		-0.85		-0.14		0.29		0.21		0.31	
Precipitation	CR-E	7/17/09	1B	40	2.59	1	-1.41		-0.85		-0.61		-0.45		0.21		0.10		0.22	

Precipitation	CR-N	7/18/09	1B	96	0.67	1	-2.42		-1.70		-1.13		-0.42		0.12		0.08		0.16	
Precipitation	CR-E	7/18/09	1B	120	0.30	1	-2.58		-1.85		-1.32		-0.50		0.09		-0.03		0.23	
Precipitation	CR-NE	7/20/09	1A	35	0.71	1	-1.85		-1.21		-0.83		-0.63		0.18		0.10		0.23	
Precipitation	CR-S	7/20/09	1A	60	2.31	2	-3.77	0.08	-2.62	0.06	-1.74	0.06	-0.24	0.13	0.21	0.01	0.15	0.01	0.32	0.11
Precipitation	CR-E	7/20/09	1A	66	2.44	1	-1.91		-1.28		-0.96		-0.25		0.15		0.00		0.24	
Precipitation	CR-E REP	7/20/09	1A	66	--	1	-2.09		-1.31		-0.91		0.06		0.26		0.14		0.28	
Precipitation	CR-NE	7/30/09	2	31	1.28	1	-0.26		0.05		-0.04		0.37		0.25		0.09		0.12	
Precipitation	CR-NE	7/31/09	2	64	0.40	1	-0.53		0.10		-0.09		0.42		0.50		0.17		0.50	
Precipitation	SDK	7/26/09		27	3.48	1	0.13		0.40		0.26		0.38		0.30		0.19		0.35	
Precipitation	TPA	9/1/09		21	3.92	1	0.10		0.31		0.15		0.27		0.24		0.10		0.25	
Precipitation	HSB	7/29/09		35	2.54	1	0.10		0.20		0.29		0.00		0.12		0.23		-0.03	
Precipitation	UCF	8/12/09		23	4.06	1	-0.43		0.23		0.02		0.43		0.56		0.23		0.54	
Precipitation	MKA	7/25/09		61	2.13	1	-0.04		-0.14		0.05		-0.19		-0.11		0.07		-0.18	
Precipitation	KYB	7/25/09		25	3.98	1	0.21		0.66		0.24		0.48		0.50		0.14		0.43	
Precipitation	MIA	7/18/09		63	4.35	1	0.12		0.08		0.16		-0.09		-0.01		0.10		-0.12	
Precipitation	MIA REP	7/18/09		67	--	1	0.13		0.11		0.22		-0.03		0.01		0.16		-0.06	
Precipitation	DVE	9/1/09		20	3.83	1	0.13		0.25		0.27		0.32		0.15		0.20		0.29	
Precipitation	ENP	7/5/09		30	4.37	1	0.08		0.50		0.22		0.01		0.44		0.18		0.40	
Precipitation	ENP	7/9/09		55	2.16	1	0.11		0.15		0.15		-0.05		0.06		0.09		-0.08	
Precipitation	ENP	7/13/09		20	1.07	1	0.07		0.07		0.10		0.32		0.01		0.07		-0.02	
Precipitation	ENP	7/15/09		18	4.16	1	0.10		0.55		0.27		0.15		0.47		0.22		0.30	
Precipitation	ENP REP	7/15/09		18	--	1	-0.09		0.25		0.08		-0.08		0.32		0.13		0.17	
Precipitation	ENP	7/19/09		70	1.71	1	0.14		0.07		0.10		-0.11		-0.03		0.03		-0.11	
Precipitation	ENP REP	7/19/09		69	--	1	0.03		-0.01		0.08		0.06		-0.04		0.06		-0.12	
Coal	Upper Kittanning seam; Barbour, WV					2	-1.32	0.22	-1.01	0.23	-0.65	0.05	-0.44	0.05	-0.02	0.06	0.02	0.06	-0.11	0.00
Coal	Elkhorn #3 seam; Floyd, KY					2	-0.81	0.01	-0.84	0.01	-0.41	0.03	-0.51	0.00	-0.23	0.00	-0.01	0.02	-0.31	0.00
Coal	Pond Creek seam; Pike, KY					1	0.41		0.03		0.18		-0.21		-0.28		-0.03		-0.31	

Coal	Stockton-Lewiston seam; Kanawha, WV	2	-0.76	0.00	-0.73	0.07	-0.38	0.04	-0.42	0.03	-0.16	0.07	0.00	0.04	-0.23	0.03
Coal	Blend 4 seams; Raleigh, WV	2	-1.24	0.03	-1.14	0.03	-0.61	0.06	-0.52	0.13	-0.21	0.01	0.01	0.04	-0.21	0.13

CHAPTER 6

Mercury stable isotopes in sediments and largemouth bass (*Micropterus salmoides*) from Florida lakes[1]

Abstract

Humans and wildlife can be exposed to hazardous levels of mercury (Hg) through the consumption of high trophic level fish with elevated concentrations of monomethylmercury (MeHg). Studies have shown that increased atmospheric deposition of Hg often leads to increased MeHg concentrations in aquatic organisms. However, depending on the ecosystem characteristics, reductions in Hg emissions may not always lead to immediate decreases in fish MeHg concentrations. Measurements of natural abundance Hg stable isotope ratios may enable a better understanding of these complex relationships. To gain insight into the sources of Hg to sport fish in central Florida, we measured the Hg isotopic composition of surface sediments and largemouth bass from freshwater lakes. We found that fish collected from lakes located near the large Crystal River coal-fired power plant did not display evidence of anomalous negative δ^{202}Hg values that were observed in nearby precipitation. This suggests that Hg recently deposited from the atmosphere is not preferentially methylated and bioaccumulated in these lakes relative to previously deposited Hg accumulated in the lake sediments. We also observed significant positive Δ^{199}Hg values in the fish that were correlated with the

[1] Sherman, L. S., Blum, J. D. Mercury stable isotopes in sediments and largemouth bass (*Micropterus salmoides*) from Florida lakes. *Science of the Total Environment* **in review**.

light penetration depth. This indicates that a significant amount of photochemical degradation of MeHg (up to ~40%) occurred prior to uptake of the remaining MeHg into the food webs. These results suggest that depending on physical lake characteristics and biogeochemical factors, decreased atmospheric Hg deposition may not lead to immediate short-term reductions in fish MeHg concentrations. Instead, recovery of some freshwater fish populations to baseline MeHg concentrations may take decades to centuries.

Abbreviations

MeHg, monomethylmercury; Hg, mercury; UV, ultraviolet; DOC, dissolved organic carbon; FL, Florida; MDF, mass-dependent fractionation; MIF, mass-independent fractionation; FDEP, Florida Department of Environmental Protection; CFUB, coal-fired utility boiler; CVAFS, cold vapor atomic fluorescence spectrometry; U.S. EPA, U.S. Environmental Protection Agency; UM BEIGL, University of Michigan Biogeochemistry and Environmental Isotope Geochemistry Laboratory; AAS, atomic absorption spectrometry; VPDB, Vienna Pee Dee Belemnite; METAALICUS, Mercury Experiment to Assess Atmospheric Loading in Canada and the United States

6.1 Introduction

Monomethylmercury (MeHg) is a neurotoxin that threatens human and wildlife health mainly through the consumption of aquatic organisms with elevated MeHg concentrations (*1-4*). In aquatic systems, inorganic mercury (Hg) is methylated to MeHg, which is subsequently bioaccumulated (*5*), often reaching concentrations that exceed recommended human consumption levels (0.1 μg/kg body weight/day) in high trophic

level fish (*2, 6*). Elevated levels of MeHg can also result in decreased reproductive success, central nervous system damage, and deleterious behavioral changes in piscivorous birds, fish, and mammals (*3, 4, 7, 8*).

Depending on lake characteristics, Hg can be methylated both biotically and abiotically in surface sediments (*9, 10*), biotically within low oxygen zones in the water column (*11*), abiotically in the water column (*12, 13*) and within periphyton and algal mats (*14, 15*). MeHg can also be produced in nearby wetlands and transported to freshwater lakes (*16*). In most oxygenated, well-mixed freshwater lakes, sulfate-reducing bacteria at the oxic/anoxic boundary layer in surface sediments account for the majority of biotic, in-lake methylation (*17-23*). After it is produced, MeHg can be demethylated biotically (*24-26*) and abiotically during photochemical reactions involving visible and ultraviolet (UV) radiation (*27-30*). A number of factors can impact MeHg production and degradation such as lake acidity (*10, 31, 32*), nutrient concentration (*31, 33*), dissolved organic carbon (DOC) concentration and composition (*9, 34, 35*), sulfide and sulfate concentration (*9, 36*), and light intensity and depth of light penetration (*28, 37*). MeHg that is not degraded can be taken up by benthic organisms (*38*) or exported into the overlying water column and enter the pelagic food web (*5, 39*). Unlike inorganic Hg, MeHg is rapidly assimilated into the tissues of organisms and is not readily excreted (*5, 40*). As a result, MeHg bioaccumulates through food webs and in most cases nearly all (>90%) of the Hg in fish muscle tissue is MeHg (*41-46*).

Concentrations of MeHg in freshwater fish are controlled by a number of variables including supply of bioavailable MeHg, physical water body characteristics, food web structure, and fish characteristics such as feeding strategy, age, and growth rate

(*23, 31, 39, 43, 47-49*). Recent studies indicate that the amount of Hg that is deposited from the atmosphere to a water body can significantly influence fish MeHg concentrations (*50-53*). However, the relationships between Hg deposition and MeHg concentrations in fish are complex and there are a number of variables that can influence the formation, degradation, and bioaccumulation of MeHg (*23, 39*). Although some studies suggest that decreased atmospheric deposition of Hg may result in rapid reductions in freshwater fish MeHg concentrations (*53, 54*), lake sediments contain accumulated Hg that may continue to be methylated. As a result, depending on the characteristics of the system, fish MeHg concentrations may remain elevated for decades to centuries after atmospheric Hg deposition decreases (*23, 39, 52, 55-57*). It is necessary to better characterize these relationships to more accurately predict and assess the impacts of Hg emissions regulations on fish MeHg concentrations.

Elevated concentrations of Hg in precipitation, fish, and other wildlife have been observed across the state of Florida (FL; U.S.A.) for more than two decades (*31, 58-64*). Largemouth bass are common sport fish in FL, but due to their high MeHg concentrations, the FL Department of Health currently maintains largemouth bass limited consumption advisories for more than 325 water bodies in FL (*65*). In addition, the FL Department of Health recommends that women of childbearing age restrict consumption of largemouth bass to 170 g (6 oz.) per month from all untested lakes (*65*). Although MeHg concentrations in largemouth bass have recently decreased in some parts of FL (such as the Water Conservation Areas in south FL; *60*), these trends do not appear to be consistent across the state.

Recent studies have demonstrated that measurement of natural abundance Hg stable isotope ratios in environmental samples can be used to characterize the sources of Hg to fish populations and to better understand Hg cycling within aquatic systems (*66-69*). There are seven stable isotopes of Hg (196 - 204 amu) and mercury stable isotope ratios are reported using delta notation:

$$\delta^{xxx}Hg\ (‰) = ([(^{xxx}Hg/^{198}Hg)_{sample}/(^{xxx}Hg/^{198}Hg)_{SRM\ 3133}] - 1) * 1000 \quad (1)$$

where ^{xxx}Hg is an isotope of Hg and SRM 3133 is a NIST Hg standard (*70*). Mass-dependent fractionation (MDF) of Hg isotopes occurs during a number of biotic and abiotic processes including methylation (*71, 72*) and MeHg degradation (*73, 74*). Mercury stable isotopes can also undergo mass-independent fractionation (MIF), which is reported as the deviation of a measured isotope ratio from that theoretically predicted to result due to MDF:

$$\Delta^{xxx}Hg = \delta^{xxx}Hg - (\delta^{202}Hg * \beta) \quad (2)$$

For kinetic reactions, β is equal to 0.252 for ^{199}Hg, 0.502 for ^{200}Hg, and 0.752 for ^{201}Hg (*70*). A high degree of MIF can occur due to the magnetic isotope effect during photochemical reactions that involve the formation of long-lived radical pairs (*74-76*). Only the odd-mass-number isotopes of Hg have unpaired nuclear spin and are magnetic. As a result, during these reactions, radical pairs involving odd-mass-number isotopes of Hg recombine at different rates than those involving even-mass-number isotopes of Hg. This process has been shown experimentally to occur during the photochemical degradation of MeHg in aquatic solutions containing DOC and result in a $\Delta^{199}Hg/\Delta^{201}Hg$ ratio of 1.36 ± 0.02 (2 s.e.) (*74*). A number of recent studies have observed significant positive MIF in fish along with similar $\Delta^{199}Hg/\Delta^{201}Hg$ ratios of between ~1.2 and ~1.3

(*66-68, 74, 77-80*). It has been hypothesized that photochemical demethylation of MeHg in the water column prior to incorporation of the remaining MeHg into the food web causes the observation of MIF of Hg isotopes in fish (*66-69, 74, 78-80*).

6.2 Materials and methods

6.2.1 Sample collection

Water samples, sediments and largemouth bass were collected between October 2008 and December 2011 by the FL Department of Environmental Protection (FDEP) and the FL Fish and Wildlife Conservation Commission in collaboration with a statewide study conducted to understand Hg deposition patterns and model Hg concentrations in fish populations. Water samples, sediments, and largemouth bass were collected from 20 lakes in central FL (Figure 6.1). Five of these lakes (Lake Rousseau, Little Lake Henderson, Lake Davis, Lake Panasoffkee, and Lake Bonable) were located within 50 km of one of the largest anthropogenic point sources of Hg in FL, the 2267 MW Crystal River coal-fired utility boiler (CFUB). Of these lakes, four are located in the Withlacoochee River watershed (Figure 6.1). This large watershed (5440 km^2) contains numerous lakes and wetlands that are hydrologically connected to the Withlacoochee River (*81*). The closest lake to the Crystal River CFUB, Lake Rousseau (L1557), is a damned lake at the downstream end of the Withlacoochee River. One of the other large lakes in the watershed, Lake Tsala Apopka, is comprised of connected lakes, including Little Lake Henderson (L732) and Lake Davis (L72), in which water levels and flow are maintained using control structures (*81*).

Water quality parameters including light penetration depth and pH were measured in each lake. Light penetration depth was measured manually at approximately the deepest part of the lake using a secchi disk attached to a rope marked with 0.1 m increments. Over the course of the study, light penetration depths were measured one to three times in each lake. Water samples were collected using trace metal-clean techniques (*82, 83*) from the open surface water of each lake and taken to the FDEP Central Laboratory for analysis. These samples were collected at 1.0 m depth below the water surface except in lakes that were less than 1 m deep or when equipment constraints did not allow sampling at depth (Table 6.1). Water sampling equipment rinse blanks (deionized water) were collected throughout the field sampling campaign (n = 22) and these blanks generally did not contain detectable amounts of total Hg or MeHg (see Section 6.5.1). Total Hg concentrations were determined using cold vapor atomic fluorescence spectrometry (CVAFS) according to U.S. Environmental Protection Agency (U.S. EPA) Method 1631-E (*84*). MeHg concentrations were determined using CVAFS after ethylation, gas chromatographic separation, and pyrolysis according to a modified version of U.S. EPA Method 1630 (*85, 86*). Alkalinity (as mg of $CaCO_3$ per liter) was determined with an automatic titration instrument (PC-Titrate) and DOC concentrations were measured using a total organic carbon analyzer (Shimadzu TOC-V).

Sediments (upper 8 to 10 cm) were collected from each lake with a Ponar dredge using trace metal-clean methods. Three dredge samples were taken in each lake from the location of deepest water depth. These samples were homogenized together into pre-washed high-density polyethylene bottles (I-CHEM) and kept frozen at -25°C until analysis at the University of Michigan Biogeochemistry and Environmental Isotope

Geochemistry Laboratory (UM BEIGL). The dredge was cleaned between samples with deionized water. Five dredge rinse blanks (deionized water) were collected after cleaning and these blanks did not contain detectable quantities of Hg.

Adult largemouth bass (>178 mm in length) were collected from each lake using electro-fishing methods. Fish length, weight, sex, and age (determined using sagittal otoliths; *87*) were recorded (Table 6.SI-1). Right-side dorsal muscle fillets were taken from each individual using trace metal-clean methods. We did not measure fish MeHg concentrations during this study. However, as discussed previously, it is likely that >90% of the Hg in the fish muscle was MeHg (*41, 45*). The fish samples were stored frozen at -25°C until they were shipped to the UM BEIGL.

6.2.2 Sample processing

The Hg isotopic compositions of sediment samples from all 20 lakes and largemouth bass from a subset of the lakes (n = 11) were analyzed (Figure 6.1). The 11 lakes for fish analyses were chosen based on their locations and water quality characteristics to represent a wide variety of conditions. Two fish each from Mill Dam Lake (L440) and Lake Kerr (L374) and three fish from each of the other lakes were analyzed for Hg isotopes. Over the course of the study, replicate analyses (total Hg concentration and Hg isotopic composition) were made of individual fish (n = 10) and sediment samples (n = 3).

To prepare the samples, the frozen sediments and fish were freeze-dried for 48 to 72 hours (Virtis Sentry Freezemobile 12SL). The dry samples were then homogenized and ground to a fine powder using an alumina ball mill mixer (SPEX). Between samples

the ball mill was cleaned by repeatedly grinding silica sand that had been baked at 750°C for 8 hours to remove any Hg. Small aliquots of baked silica sand (50-60 mg) were also processed periodically between samples and analyzed as grinding blanks using atomic absorption spectrometry (AAS; MA-2000, Nippon Instruments). The ground silica sand blanks did not contain significant amounts of Hg (mean = 86 pg of Hg per grinding blank, 1 s.d. = 42 pg, n = 4). After grinding, the samples were weighed into ceramic boats and Hg in the samples was thermally released using previously published methods (*88*). Briefly, each sample was placed in a two-stage furnace where the temperature of the first furnace was incrementally increased to 750°C and the second furnace was maintained at 1000°C. The released $Hg^0_{(g)}$ was carried in a stream of Hg-free O_2 and bubbled into 25 g of acidic 1% (w/w) $KMnO_4$ solution ($KMnO_4$ in 1.8M trace metal grade H_2SO_4). To concentrate the Hg and separate it from any combustion products present in these solutions, the Hg was subsequently transferred into secondary 1% $KMnO_4$ solutions. To do this, the primary solutions were first reduced with 2% (w/w) of 30% $NH_2OH \cdot HCl$ and then divided into 5 ml aliquots. Mercury in each aliquot was reduced with 0.3 ml of 20% $SnCl_2$ and 0.3 ml of 50% H_2SO_4 and then bubbled into a secondary 1% $KMnO_4$ solution using a modified autosampler. Mercury concentrations were measured in these final solutions by AAS and used to determine total Hg concentrations in the sediments and fish tissue samples. Mercury standards (NIST SRM 3133) measured during concentration analyses were replicable to within ± 5%.

Procedural standards and blanks were processed using the same methods. Over the course of this study, six sediment procedural standards (NIST SRM 1944), 16 fish procedural standards (seven CRM DORM-3 and nine ERM CE-464), and nine procedural

blanks were analyzed. All of the procedural blanks contained negligible amounts of Hg attributable almost entirely to Hg in the 1% $KMnO_4$ solutions (mean = 0.02 ng of Hg per g solution, 1 s.d. = 0.02 ng Hg per g solution, n = 9). Mercury recoveries in the procedural standards were determined after processing based on the amount of Hg that was originally combusted and the measured Hg concentration in the final 1% $KMnO_4$ solution. For the sediment standards, mean Hg recovery was 95% (1 s.d. = 15%, n = 6); for the DORM-3 fish standards, mean Hg recovery was 90% (1 s.d. = 10%, n = 7); for the ERM CE-464 fish standards, mean Hg recovery was 96% (1 s.d. = 9.9%, n = 9).

6.2.3 Stable isotope ratio analyses

Mercury stable isotope ratios were measured in samples and standards using cold-vapor multi-collector inductively-coupled plasma mass spectrometry (Nu Instruments) according to previously published methods (*70, 74*). The <100% yields during combustion and purification for some of the procedural standards did not cause any systematic isotope fractionation. However, the measured isotopic compositions of these procedural standards were more variable than those of the secondary UM Almadén standard that was measured ~5 times during each analytical session. For this reason, sample analytical uncertainty for each isotope ratio is estimated as 2 s.d. of the same ratio measured in the relevant procedural standards. Mercury isotope ratios measured in replicate fish (n = 10) and sediment samples (n = 3) were reproducible within these uncertainties (Table 6.SI-1).

Carbon ($\delta^{13}C$, relative to VPDB) and nitrogen ($\delta^{15}N$, relative to air N_2) stable isotope ratios were also measured in the largemouth bass samples at the University of

Michigan Stable Isotope Laboratory. Approximately 700 μg of powdered material per sample was loaded into tin weigh boats. The samples were analyzed using an elemental combustion system (Costech ECS 4010) coupled to an isotope ratio mass spectrometer (Finnigan Delta V Plus). International standards (IAEA 600, IAEA-CH-6, IAEA N_2 and USGS 25) were used to normalize on a per-run basis and maintain precision of $\delta^{13}C$ and $\delta^{15}N$ values of better than ± 0.12‰ (1 s.d.).

6.3 Results and discussion

6.3.1 Water quality parameters

Water quality measurements for the studied lakes are shown in Table 6.1. Florida generally has warm wet summers and cooler dry winters. As a result, characteristics of these lakes can vary seasonally (*89*) and the measurements made during this study may not represent average yearly conditions. The studied lakes are generally shallow, well mixed, and fully oxic. Although it is possible that some Hg methylation occurs in the water column of these lakes or in periphyton and algal mats, because these lakes are not stratified and are fully oxic it is likely that the majority of in-lake Hg methylation occurs in the surface sediments. The lakes were highly variable with respect to pH (4.81 to 9.60) and alkalinity (<0.65 mg/L to 140 mg/L; method detection limit = 0.65 mg/L). They contained low to moderately high concentrations of total Hg (0.22 to 5.8 ng/L; method detection limit = 0.10 ng/L), low to moderately high concentrations of MeHg (<0.022 ng/L to 0.510 ng/L; method detection limit = 0.022 ng/L), and relatively high concentrations of DOC (1.9 mg/L to 33 mg/L; method detection limit = 1 mg/L). Although we did not measure UV penetration in these lakes, it is likely correlated with

(but more rapidly attenuated than) visible light because UV light is more readily absorbed by DOC in surface waters (*30, 90, 91*). Previous studies have observed that light penetration depths in FL lakes are seasonally variable with the greatest transparency observed during the dry season (November through February) when algal biomass and suspended particulate matter concentrations are diminished (*92*). The light penetration depths presented in Table 6.1 were measured during the same season in which the sediments and fish were collected. We found that these light penetration depths were negatively correlated with DOC concentration (slope = -0.05 ± 0.02, 1 s.e.; $p = 0.01$; $r^2 = 0.31$; $n = 20$). In lakes with high light penetration and low DOC concentrations, it is likely that rates of photochemical demethylation of MeHg are enhanced (*27, 28, 93*).

6.3.2 Mercury concentrations

Previous studies have measured sediment accumulation rates in FL wetlands of between 0.16 cm/yr and 0.33 cm/yr (*94, 95*). Similar accumulation rates (up to 0.40 cm/yr) have been measured in organic-rich FL lake sediments (*95-97*). Based on these accumulation rates, we expect that the upper 10 cm of sediment in the study lakes represents accumulation over the past ~25 and ~60 years. However, it is likely that sediment accumulation rates in these shallow lakes are spatially and temporally variable as a result of sediment redistribution, mixing, and focusing into deeper areas (*96, 98*). Therefore, although it is likely that the sampled sediments represent accumulation of less than 100 years, it is possible that they contain a mixture of pre-anthropogenic and anthropogenic Hg.

Sediment total Hg concentrations are reported as dry weight concentrations and fish total Hg concentrations are reported as wet weight concentrations (Table 6.SI-1). Total Hg concentrations in replicate sediment and fish samples generally agreed within analytical uncertainty (mean relative percent difference = 8.6%, 1 s.d. = 7.8%, n = 13). Total Hg concentrations in sediment samples ranged from 31.3 ng/g to 307 ng/g (mean = 153 ng/g, 1 s.d = 81.9 ng/g, n = 20) (Table 6.SI-1). These concentrations are similar to those measured previously in FL (*55, 99*). A study of sediment cores from the FL Everglades indicated that historic sediments (pre-1900) generally had Hg concentrations of <100 ng/g whereas recent sediments (post-1985) had Hg concentrations of >100 ng/g (and up to 400 ng/g) (*99*). Although lake sediments collected during this study may contain a mixture of pre-anthropogenic and anthropogenic Hg, most of the sediments had Hg concentrations elevated above these background levels (i.e., >100 ng/g) and likely include significant amounts of anthropogenic Hg (*99-101*).

Total Hg concentrations in fish tissue samples ranged from 43.7 ng/g to 1190 ng/g (mean = 361 ng/g, 1 s.d. = 291 ng/g, n = 31) (Table 6.SI-1). Fish analyzed during this study do not necessarily represent the range or average Hg concentrations in adult largemouth bass in the study lakes. However, the Hg concentrations measured during this study are similar to those previously observed in FL largemouth bass (*31, 58, 59*). There are no clear correlations between total Hg or MeHg concentrations in water, sediments, or fish from these lakes. Total Hg concentrations in the lake sediments are not correlated with total Hg concentrations in the water column. In addition, total Hg concentrations in fish are not correlated with total Hg concentrations in the sediments, total Hg concentrations in the water, or MeHg concentrations in the water. However,

because only a limited number of samples were analyzed from each lake, these samples may not be fully representative of average total Hg or MeHg concentrations.

6.3.3 Carbon and nitrogen isotope ratios

Carbon and nitrogen isotope ratios in the fish tissue samples are presented in the supplemental information (Table 6.SI-1). Carbon isotope ratios are often used to determine the carbon source to the base of a food web (*102*). In contrast, because nitrogen isotope ratios increase by ~3‰ per trophic level, $\delta^{15}N$ values are often used to estimate consumer trophic position (*103-105*). Measured $\delta^{13}C$ values in the largemouth bass ranged from -16.2 to -30.0‰ (mean = -24.5‰, 1 s.d. = 3.8‰, n = 31) and $\delta^{15}N$ values ranged from 7.88 to 16.3‰ (mean = 11.8‰, 1 s.d. = 2.1‰, n = 31). Largemouth bass collected from the same lakes displayed similar $\delta^{13}C$ and $\delta^{15}N$ values and within lake isotopic variability ($\delta^{13}C$: mean 1 s.e. = 0.56‰; $\delta^{15}N$: mean 1 s.e. = 0.22‰) was less than between lake isotopic variability ($\delta^{13}C$: mean 1 s.e. = 1.13‰; $\delta^{15}N$: mean 1 s.e. = 0.63‰). It is possible that some of the variability between individuals in a given lake is due to differences in tissue lipid content (*106, 107*) or due to differences in individual fish feeding behavior (*105, 108*). Largemouth bass are opportunistic top predators that generally eat a variety of small aquatic invertebrates when they are young but switch to a diet of crayfish, larger invertebrates, and other fish as adults (*47, 109, 110*). As a result, older largemouth bass may be feeding on a higher proportion of benthic organisms and at a higher effective trophic level than younger largemouth bass. However, overall the largemouth bass $\delta^{15}N$ values were not correlated with fish length ($p = 0.28$, $r^2 = 0.04$), fish age ($p = 0.66$, $r^2 = 0.01$), or total Hg concentration ($p = 0.11$, $r^2 = 0.08$) (Table 6.SI-1).

Therefore, it is not likely that ontogenetic dietary shifts leading to differences in effective trophic level can explain the between lake variability in $\delta^{15}N$ values. Instead, it is more likely that the variations in $\delta^{15}N$ values are due to differences in $\delta^{15}N$ at the base of the food web. Similarly, it is likely that differences in $\delta^{13}C$ values between lakes are a result of differences in the carbon isotopic composition at the base of the food webs (*105*).

6.3.4 Mercury stable isotope ratios

The proportion of atmospheric Hg deposition at a given location that results from local, regional, and long-range emissions is location-specific (*111-113*) but a number of studies have observed enhanced Hg deposition near point sources and urban areas (*101, 112, 114-116*). In July 2009, Sherman et al. (2012) found that Hg emitted by the Crystal River CFUB was deposited locally in precipitation and displayed anomalous negative $\delta^{202}Hg$ values (mean = -2.56‰, 1 s.d = 1.10‰, n = 28). Following sample collection for the Sherman et al. (2012) study, in 2009 and 2010, selective catalytic reduction units and flue gas desulfurization units were installed on two of the Crystal River CFUB's four units (*117*). Although these air pollution control devices are known to decrease Hg emissions (*118*), Hg emissions from the CFUB estimated by the U.S. EPA Toxic Release Inventory did not change significantly between 2009 and 2011 (*119*). In addition, coal combusted at the CFUB was sourced from mines in the same regions of Kentucky and West Virginia from 2009 to 2011 (*120*). Therefore, although we were not able to collect precipitation near the CFUB after July 2009, the isotopic composition of combusted coal powder likely remained relatively constant and we suggest that reactive Hg emitted by

the CFUB and deposited locally in precipitation likely displayed extreme negative δ^{202}Hg values similar to those observed by Sherman et al. (2012) throughout this study.

To investigate the relationship between Hg emitted by the Crystal River CFUB and Hg in lake sediments and largemouth bass, we divided the study lakes into two categories: those located close to the CFUB (<50 km away, 5 lakes; fish were analyzed from three of these lakes) and those located farther from the CFUB (>50 km away, 15 lakes; fish were analyzed from eight of these lakes). Although the spatial distribution of Hg deposition near a point source depends on a number of factors, we hypothesize that reactive Hg species emitted by the CFUB are more likely to be deposited to lakes within 50 km of the utility than to those located farther away (*101, 111-113*). We used these samples to 1) assess whether Hg recently deposited from the atmosphere was preferentially methylated and bioaccumulated compared to previously deposited Hg accumulated in lake sediments and 2) explore the influence of physical lake characteristics and biogeochemical processes on the Hg isotopic compositions of largemouth bass. The Hg isotopic compositions of all analyzed samples and standards are presented in the supplemental information (Table 6.SI-1).

6.3.4.1 Lakes closer to (<50 km) the Crystal River CFUB

Results of the Mercury Experiment to Assess Atmospheric Loading in Canada and the United States (METAALICUS) spike isotope addition study suggest that recently deposited Hg can be rapidly methylated and bioaccumulated in aquatic food webs (*53*). If these results are applicable to the FL lakes, we hypothesized that Hg emitted by the Crystal River CFUB and deposited to the nearby lakes would be preferentially

methylated and bioaccumulate up the food web to the largemouth bass. Further, assuming that the extreme negative δ^{202}Hg values observed in precipitation collected near the Crystal River CFUB (*88*) are representative of Hg recently deposited from the atmosphere, we hypothesized that the largemouth bass collected from lakes close to the CFUB would display evidence of those negative δ^{202}Hg values. Based on the average δ^{202}Hg values of sediments from these lakes (mean = -0.84‰, 1 s.d. = 0.19‰, n = 5) and precipitation (mean = -2.56‰, 1 s.d = 1.10‰, n = 28; Sherman et al., 2012), isotopic mass balance can be used to estimate the expected δ^{202}Hg values in the fish depending on the proportion of Hg in the fish that is derived from recent atmospheric deposition. For example, if only ~2% of the Hg in the fish was derived from recent atmospheric deposition, δ^{202}Hg values in these fish would be ~0.05‰ lower than sediment δ^{202}Hg values. This amount of deviation would not be distinguishable from analytical variability. However, if ~10% to ~30% of the Hg in the fish was derived from recent atmospheric deposition, δ^{202}Hg values in the fish would be ~0.25 to ~0.55‰ lower than sediment δ^{202}Hg values. Deviations of this magnitude would be distinguishable from analytical uncertainty and from the isotopic variability between individual fish.

We did not observe lower δ^{202}Hg values in fish compared to sediments in these lakes that we could attribute to recent deposition of Hg emitted by the Crystal River CFUB. Sediments from lakes close to the CFUB had δ^{202}Hg values ranging from -1.11 to -0.63‰ (± 0.12‰, 2 s.d.; mean = -0.84‰, 1 s.d. = 0.19‰, n = 5). Δ^{199}Hg values in these sediments were close to 0‰ (mean = 0.00‰, 1 s.d. = 0.17‰, n = 5). A similar lack of MIF of Hg isotopes in lake and coastal sediments has been observed in previous studies (*67-69, 121*). Largemouth bass from these lakes displayed δ^{202}Hg values ranging from -

0.57 to -0.22‰ (± 0.15‰, 2 s.d.; mean = 0.09‰, 1 s.d. = 0.38‰, n = 9) and Δ^{199}Hg values from 0.52 to 0.97‰ (± 0.07‰, 2 s.d.; mean = 0.67‰, 1 s.d. = 0.16‰, n = 9). As shown in Figure 6.2, these Hg isotopic compositions were similar to those of sediments and fish collected from the lakes located >50 km from the Crystal River CFUB.

There are several possible explanations for the lack of lower δ^{202}Hg values in fish collected from lakes located near the Crystal River CFUB. First, it is possible that the negative δ^{202}Hg values measured in precipitation during July 2009 near the Crystal River CFUB (*88*) were not representative of Hg deposition in the area. However, as described previously, because estimated Hg emissions and the origin of the combusted coal did not change throughout the study period, we suggest that these values are a good estimate of the isotopic composition of Hg emitted by the CFUB and deposited locally. Second, it is possible that MDF occurring in the water column (e.g., due to adsorption to DOC or suspended particles or due to photochemical reduction) or through biotic processes in the sediments (e.g., methylation and demethylation) may have altered and somewhat obscured the negative δ^{202}Hg values (*71, 73, 74*). However, it is likely that these processes occur to a similar degree in the lakes both near to and far from the CFUB. Therefore, even if these processes obscured the lower δ^{202}Hg values, a measurable offset between fish from the two areas would have been preserved.

Finally, it is most likely in these lakes that recently deposited Hg is not preferentially methylated and bioaccumulated compared to previously accumulated Hg in the sediments. This further supports our assertion, based on physical lake characteristics, that water column methylation is not a large source of MeHg in these lakes. Previous studies have similarly found that although a portion of recently deposited Hg can be

rapidly methylated and enter food webs, the large reservoir of previously deposited Hg in surface sediments can provide a significant source of MeHg to the ecosystem (*39, 52, 56*). If we assume that the sediment sample collected in Lake Rousseau is representative of surface sediments throughout the lake, we can estimate the relative percentages of recently deposited and historically deposited Hg in the sediments. Based on measurements made at a nearby Mercury Deposition Network site (FL05), average annual deposition of Hg during the study period (2008 to 2011) was 14.3 $\mu g/m^3$ (1 s.d. = 1.0 $\mu g/m^3$) (*122*). Assuming a dry sediment density of ~1 g/cm^3 (*123, 124*), this amount of annual Hg deposition directly to the lake surface represents only ~0.1% of the total Hg in the upper 10 cm of sediments in Lake Rousseau. Therefore, annual atmospheric Hg deposition likely represents a very small percentage of the total Hg in surface sediments of these lakes. This may be especially true for lakes with large watersheds such as the Withlacoochee River watershed that do not receive all of their Hg from direct atmospheric deposition (*23, 57*). It is likely that Hg transported through the watershed in association with suspended solids and sediments provides an influx of previously deposited Hg to these lakes (*125-127*). Our data suggest that in these lakes recently deposited Hg mixes with previously deposited Hg in the sediments (some of which has been transported through the watershed) and that a portion of this Hg is methylated and enters the food web.

6.3.4.2 Lakes farther from (>50 km) the Crystal River CFUB

In addition to understanding the sources of Hg to largemouth bass in these lakes, the data collected in this study can be used to explore the influence of physical lake

characteristics and biogeochemical processes on Hg isotopes in fish. Sediments from lakes >50 km from Crystal River, FL had δ^{202}Hg values ranging from -1.19 to -0.46‰ (± 0.12‰, 2 s.d.; mean = -0.72‰, 1 s.d. = 0.25‰, n = 15) and Δ^{199}Hg values close to 0‰ (mean = -0.05‰, 1 s.d. = 0.13‰, n = 15). In contrast to the sediments, δ^{202}Hg values of fish from these lakes ranged from -0.60 to 0.68‰ (± 0.15‰, 2 s.d.; mean = 0.09‰, 1 s.d. = 0.38‰, n = 22) and Δ^{199}Hg values ranged from 0.18 to 4.43‰ (± 0.07‰, 2 s.d.; mean = 1.35‰, 1 s.d. = 1.22‰, n = 22) (Figure 6.2). Similar Hg isotope ratios in fish from lakes and coastal environments have been observed in previous studies (*67-69, 74, 121*). Largemouth bass Hg isotopic compositions were less variable within each lake than between lakes, especially with respect to Δ^{199}Hg values (within lake 1 s.e. of Δ^{199}Hg values = 0.21‰; between lake 1 s.e. of mean Δ^{199}Hg values = 0.48‰). This suggests that lake characteristics and/or processes occurring within each lake largely control the observed MIF.

There have been two hypotheses proposed to explain the positive Δ^{199}Hg values observed in fish populations: 1) *in vivo* MIF occurring in organisms leads to the observation of increasing Δ^{199}Hg with increasing trophic level (*77, 128*) or 2) photochemical demethylation of MeHg prior to uptake into organisms causes MIF and this isotopic signature is retained during trophic transfer (*69, 74, 78-80*). Das et al. (*77*) observed a correlation between Δ^{199}Hg values and trophic level (based on δ^{15}N values) in a freshwater lake in FL and concluded that MIF likely occurs during metabolic processes within the fish (*77*). However, no experimentally studied biotic processes have been shown to produce MIF of Hg isotopes (*71, 73, 129*) and theoretical calculations suggest that biochemical processes are unlikely to produce MIF of Hg isotopes (*73*). Natural

processes that cause MIF in the absence of light have been shown to produce only <~0.3‰ of fractionation (*130-133*). In addition, recent experimental studies by Kwon et al. (*78*) demonstrated that no MIF occurs during trophic transfer of MeHg from food to fish. Finally, as has been observed in previous studies, Δ^{199}Hg values measured in largemouth bass tissues during this study do not correlate with trophic position based on δ^{15}N values (*67, 69, 79*). Therefore we suggest that it is unlikely that the observed positive Δ^{199}Hg values in the largemouth bass were caused by *in vivo* MIF.

It appears most likely that photochemical demethylation of MeHg resulted in the observed positive Δ^{199}Hg values in the largemouth bass. According to this scenario, after MeHg is produced, a portion of it is photochemically demethylated in the water column before the remaining MeHg is taken up by organisms. Bergquist and Blum (*74*) conducted photochemical demethylation experiments using natural sunlight in aqueous solutions containing 1 mg/L and 10 mg/L of DOC and observed that the Δ^{199}Hg/Δ^{201}Hg ratio of MeHg remaining in the solution was 1.36 ± 0.02, 2 s.e. (*74*). As shown in Figure 6.3, based on a York regression (*134*), we observed a comparable Δ^{199}Hg/Δ^{201}Hg ratio in the largemouth bass samples (1.30 ± 0.01, 1 s.e., n = 31). These data support the hypothesis that photochemical degradation of MeHg prior to incorporation of remaining MeHg into the food web resulted in the observed positive MIF in the fish.

If photochemical degradation of MeHg is responsible for the MIF, then Δ^{199}Hg values of the largemouth bass should be related to the magnitude of photochemical demethylation. It is also possible that an increased degree of photochemical demethylation could result in a measurable depletion of MeHg from the water column. As discussed previously, more photochemical demethylation of Hg occurs in lakes with

greater light penetration depths and lower concentrations of DOC (*90, 91*). As shown in Figure 6.4a, light penetration depth in these FL lakes is positively correlated to Δ^{199}Hg values measured in the largemouth bass (slope = 0.88 ± 0.16, 1 s.e.; $p < 0.0001$; $r^2 = 0.51$, n = 31). In addition, as shown in Figure 6.4b (on a log-log scale) DOC concentrations are negatively correlated with Δ^{199}Hg values in the fish (slope = -0.45 ± 0.12, 1 s.e.; $p = 0.0007$; $r^2 = 0.33$, n = 31). Finally, although Δ^{199}Hg values in the largemouth bass are only weakly correlated to the percent MeHg in the water column ($p = 0.10$, $r^2 = 0.89$, n = 31), the highest Δ^{199}Hg values (greater than 1.5‰) only occurred in fish from lakes with low percent MeHg (<5%). Although photochemical demethylation has been proposed by several previous studies to explain MIF observed in fish, correlations between MIF, light penetration depth, and DOC concentration have not been previously reported.

Some lakes show significant deviations from the correlations of MIF in the largemouth bass with light penetration depth and DOC concentration. This variability may be due to seasonal differences in light penetration depth and differences in the relationship between DOC concentration and UV radiation absorption (*90*) caused by variations in DOC composition. The fish from Lake Rousseau (L1557) do not fall on the correlation line between DOC concentration and Δ^{199}Hg values defined by fish from the other lakes. If data from Lake Rousseau are excluded, this correlation is stronger (slope = 0.80 ± 0.12, 1 s.e.; $p < 0.0001$; $r^2 = 0.68$, n = 28). This may be due to variations in the character of DOC in Lake Rousseau, which is located at the downstream end of the large Withlacochee River watershed. Additionally, the observed Δ^{199}Hg values in largemouth bass from Lake Kerr (L374) are higher than expected based on light penetration depth. Lake Kerr is a deep lake in which light penetration depth can be up to 4.2 m (*124*). If the

average annual light penetration depth in Lake Kerr is greater than that measured during this study, increased photochemical demethylation could have resulted in the observed high Δ^{199}Hg values in the largemouth bass.

In addition to the observed variability between the lakes, in some cases individual fish collected from a given lake display varying magnitudes of MIF. These variations may be partly due to differing rates of MeHg elimination and differences in individual fish feeding habit (*43, 49, 135*). As described previously, because the diets of largemouth bass generally switch from aquatic invertebrates to crayfish, larger invertebrates, and other fish as they age (*47, 109, 110*), it is possible that older largemouth bass may be feeding on more benthic organisms than younger largemouth bass. This could result in older largemouth bass accumulating more MeHg from the benthic food web that has not been photochemically demethylated to the same degree as the MeHg in the water column and, therefore, displays lower Δ^{199}Hg values. For example, the one-year-old largemouth bass from Mill Dam Lake (L440) displayed a significantly higher Δ^{199}Hg value (individual 810001, Δ^{199}Hg = 3.25‰ ± 0.15‰, 2 s.d.) than the two-year-old largemouth bass from the same lake (individual 810005, Δ^{199}Hg = 1.49‰ ± 0.15‰, 2 s.d.). These differences in feeding habit could also partially explain the observation of similar Δ^{199}Hg values between individuals from lakes with different light penetration depths. However, as described previously, because Δ^{199}Hg values are not correlated to fish age ($p = 0.79$, $r^2 = 0.00$), it does not appear that these differences in feeding habit are present in all of the lakes.

Based on the observed Δ^{199}Hg values in the largemouth bass we can estimate the proportion of MeHg that was degraded in each of the lakes due to photochemical

demethylation. Although DOC concentrations were variable, the lakes contained 13.5 mg/L of DOC on average (1 s.d. = 9.4 mg/L, n = 20) (Table 6.1). If we assume that experiments conducted with 10 mg/L of DOC in solution (*74*) are applicable to these FL lakes, we estimate that between ~4% (Lake Thonotassa, L1790) and ~40% (Lake Kerr, L374) of the MeHg in these lakes was photochemical degraded (see Section 6.5.3 for calculations). Point et al. (*79*) suggested that the ratio of MeHg to DOC could affect the relationship between photochemical demethylation and MIF of Hg isotopes and extrapolated Bergquist and Blum's (2007) experimental data to lower MeHg/DOC ratios. Application of the calculations made by Point et al. (*79*) using MeHg/DOC ratios observed in these FL lakes only negligibly lowers our estimates of the percentage of photochemical demethylation to between ~4 and ~37% (Section 6.5.3).

By using the Δ^{199}Hg values to estimate the amount of MDF that occurred in the water column due to photochemical demethylation, we can estimate the amount of MDF that occurred prior to this in the sediments before the MeHg was exported to the water column. Bergquist and Blum (*74*) observed that photochemical demethylation of MeHg resulted in fractionation such that the ratio of Δ^{199}Hg/δ^{202}Hg of MeHg remaining in an aqueous solution as the experiment progressed was 4.8 ± 0.33 (1 s.e.). Assuming that this experiment is relevant to these natural lakes, we can use these data to estimate the δ^{202}Hg values of MeHg in the lake sediments based on the Hg isotopic compositions of the largemouth bass. We additionally assume that no MIF occurs during trophic transfer and that the isotopic compositions of largemouth bass reflect that of MeHg in the water column prior to entry into the food web. Based on the average isotopic composition of largemouth bass from each lake and the Δ^{199}Hg/δ^{202}Hg relationship observed by

Bergquist and Blum (2007), we back-calculated the isotopic composition of MeHg in the sediments prior to photochemical demethylation in the water column. These estimated sediment MeHg δ^{202}Hg values are consistently offset from the measured bulk sediment δ^{202}Hg values by an average of 0.45‰ (1 s.d. = 0.19‰, n = 11) (Figure 6.5a). The estimated sediment MeHg δ^{202}Hg values are also positively correlated with the measured bulk sediment δ^{202}Hg values (slope = 0.89 ± 0.32, 1 s.e.; p = 0.02; r^2 = 0.47, n = 11) (Figure 6.5b). Gehrke et al. (*66*) observed a similar offset (0.60 ± 0.16‰, 1 s.d.) between bulk sediment δ^{202}Hg values and estimated sediment MeHg δ^{202}Hg values based on the isotopic compositions of young-of-year fish in San Francisco Bay, California. The measured bulk sediment δ^{202}Hg values and estimated sediment MeHg δ^{202}Hg values in Lake Davis (L72) are offset to a lesser degree (0.07‰). In contrast to the other lakes, Lake Davis is one of the shallowest lakes in FL and it was covered with a 10-20 cm thick floc layer during sample collection. It is possible that these characteristics resulted in atypical MDF in the sediments of this lake. If Lake Davis is excluded, the correlation between measured sediment δ^{202}Hg values and estimated sediment MeHg δ^{202}Hg values is stronger (slope = 0.99 ± 0.25, 1 s.e.; p = 0.004; r^2 = 0.67, n = 10).

The observed offset between measured bulk sediment and estimated sediment MeHg δ^{202}Hg values (based on the isotopic compositions of the largemouth bass) is likely due to a balance between biotic methylation and demethylation in surface sediments. Experimental studies have demonstrated that the light isotopes of Hg are preferentially methylated and demethylated during biotic processes (*71, 73, 74*). The similarity among the lakes in the offset between measured bulk sediment and estimated sediment MeHg δ^{202}Hg values may suggest that similar rates of methylation and demethylation occur in

lake sediments throughout the region. However, we cannot rule out the possibility that δ^{202}Hg values measured in the bulk sediment samples are not representative of the relatively small fraction of bioavailable Hg in sediments that can be methylated (*136, 137*). If bioavailable Hg has higher δ^{202}Hg values than that measured in the bulk sediments, the observed offset in δ^{202}Hg values between the bulk sediment and our estimated values for MeHg in the sediments may not reflect net fractionation due to biotic methylation and demethylation.

6.4 Conclusions

Mercury isotope ratios measured in sediments and largemouth bass from freshwater lakes in central FL suggest that recently deposited atmospheric Hg is not preferentially methylated and bioaccumulated compared to previously accumulated Hg in lake sediments. Furthermore, the Hg isotope data suggest that the majority of the MeHg in largemouth bass is ultimately derived from Hg previously deposited in the lake sediments. We hypothesize that processes occurring in the sediments such as microbial methylation and demethylation cause MDF such that MeHg which is exported to the water column has δ^{202}Hg values ~0.45‰ higher than bulk sediments. Once in the water column, photochemical demethylation causes significant MIF of the odd-mass-number isotopes of Hg and degradation of a significant portion of the MeHg before the remaining MeHg is incorporated into the food web. The Δ^{199}Hg values of fish tissues are correlated with light penetration depth and DOC concentration and reflect the proportion of MeHg that was photochemically demethylated in each lake.

The results of this study suggest that reductions in atmospheric deposition of Hg to FL lakes may not rapidly result in decreased MeHg concentrations in largemouth bass because the primary source of Hg to the fish is Hg accumulated in the sediments rather than Hg recently deposited to the water column. It is important to consider that the magnitude and timing of changes in fish MeHg concentrations in response to changes in atmospheric deposition are influenced by physical lake characteristics, ecosystem properties, and fish physiological characteristics (*23, 39, 56, 57*). In lakes with small watersheds that are dominated by direct atmospheric Hg input, fish may respond rapidly to reductions in Hg deposition (*53*). However, in lakes fed by large watersheds, previously deposited Hg can inflow into the lake long after it is deposited from the atmosphere and continuously add to the reservoir of Hg in the sediments that is available for methylation. Therefore, in many lakes, declines in fish MeHg concentrations may be prolonged for decades to centuries after Hg deposition reductions occur.

Acknowledgements

Funding for this research was provided by the University of Michigan (Graham Environmental Sustainability Institute Graduate Fellowship and Turner Grant) and by the Florida Department of Environmental Protection (Contract No. SP673). We thank G. White, T. Seal, and M. Thompson at the FDEP and T. Lange at the FL Fish and Wildlife Conservation Commission for their assistance with sample collection, water quality parameter analyses, and information about Florida lake ecosystems. We also thank K. C. Lohmann, L. Wingate, and members of the UM BEIGL for their assistance with isotope

analyses. This manuscript was greatly improved by comments from three anonymous reviewers.

References

(1) Clarkson, T. W.; Magos, L.; The toxicology of mercury and its chemical compounds. *Crit. Rev. Toxicol.* **2006,** *36*, 609-662.

(2) Mergler, D.; Anderson, H. A.; Chan, L. H. M.; Mahaffey, K. R.; Murray, M.; Sakamoto, M.; Stern, A. H.; Methylmercury exposure and health effects in humans: A worldwide concern. *Ambio* **2007,** *36* (1), 3-11.

(3) Evers, D. C.; Savoy, L. J.; DeSorbo, C. R.; Yates, D. E.; Hanson, W.; Taylor, K. M.; Siegel, L. S.; Cooley Jr., J. H.; Bank, M. S.; Major, A.; Munney, K.; Mower, B. F.; Vogel, H. S.; Schoch, N.; Pokras, M.; Goodale, M. W.; Fair, J.; Adverse effects from environmental mercury loads on breeding common loons. *Ecotoxicology* **2008,** *17*, 69-81.

(4) Scheuhammer, A. M.; Meyer, M. W.; Sandheinrich, M. B.; Murray, M. W.; Effects of environmental methylmercury on the health of wild birds, mammals, and fish. *Ambio: A Journal of the Human Environment* **2007,** *36* (1), 12-19.

(5) Mason, R. P.; Reinfelder, J. R.; Morel, F. M. M.; Bioaccumulation of mercury and methylmercury. *Water, Air, Soil Pollut.* **1995,** *80*, 915-921.

(6) U.S. Environmental Protection Agency, **2012**. *Mercury: Human Exposure*. access via http://www.epa.gov/hg/exposure.htm. Accessed March 25, 2012.

(7) Wolfe, M. F.; Schwarzbach, S.; Sulaiman, R. A.; Effects of mercury on wildlife: A comprehensive review. *Environmental Toxicology and Chemistry* **1997,** *17* (2), 146-160.

(8) Adams, D. H.; Sonne, C.; Basu, N.; Dietz, R.; Nam, D.-H.; Leifsson, P. S.; Jensen, A. L.; Mercury contamination in spotted seatrout, *Cynoscion nebulosus*: An assessment of liver, kidney, blood, and nervous system health. *Science of the Total Environment* **2010,** *408*, 5808-5816.

(9) Ullrich, S. M.; Tanton, T. W.; Abdrashitova, S. A.; Mercury in the aquatic environment: A review of factors affecting methylation. *Critical Reviews in Environmental Science and Technology* **2001,** *31* (3), 241-293.

(10) Gilmour, C. C.; Henry, E. A.; Mercury methylation in aquatic systems affected by acid deposition. *Environmental Pollution* **1991,** *71*, 131-169.

(11) Eckley, C. S.; Hintelmann, H.; Determination of mercury methylation potentials in the water column of lakes across Canada. *Science of the Total Environment* **2006,** *368* (1), 111-125.

(12) Celo, V.; Lean, D. R. S.; Scott, S. L.; Abiotic methylation of mercury in the aquatic environment. *Science of the Total Environment* **2006,** *368*, 126-137.

(13) Siciliano, S. D.; O'Driscoll, N. J.; Tordon, R.; Hill, J.; Beauchamp, S.; Lean, D. R. S.; Abiotic production of methylmercury by solar radiation. *Environmental Science and Technology* **2005,** *39*, 1071-1077.

(14) Cleckner, L. B.; Gilmour, C. C.; Hurley, J. P.; Krabbenhoft, D. P.; Mercury methylation in periphyton of the Florida Everglades. *Limnology and Oceanography* **1999,** *44*, 1815-1825.

(15) Desrosiers, M.; Planas, D.; Mucci, A.; Mercury methylation in the epilithon of boreal shield aquatic ecosystems. *Environmental Science and Technology* **2006,** *40*, 1540-1546.

(16) Branfireun, B. A.; Krabbenhoft, D. P.; Hintelmann, H.; Hunt, R. J.; Hurley, J. P.; Rudd, J. W. M.; Speciation and transport of newly deposited mercury in a boreal forest wetland: A stable mercury isotope approach. *Water Resources Research* **2005,** *41*, W06016.

(17) Korthals, E. T.; Winfrey, M. R.; Seasonal and spatial variations in mercury methylation and demethylation in an oligotrophic lake. *Applied and Environmental Microbiology* **1987,** *53* (10), 2397-2404.

(18) Berman, M.; Bartha, R.; Levels of chemical versus biological methylation of mercury in sediments. *Bulletin of Environmental Contamination and Toxicology* **1986,** *36*, 401-404.

(19) Benoit, J. M.; Gilmour, C. C.; Heyes, A.; Mason, R. P.; Miller, C. L., Geochemical and biological controls over methylmercury production and degradation in aquatic ecosystems. In *Biogeochemistry of Environmentally Important Trace Elements*, Cai, Y.; Braids, O. C., Eds. American Chemical Society: Washington, DC, **2003**; Vol. 835, pp 262-297.

(20) Compeau, G. C.; Bartha, R.; Sulface-reducing bacteria: Principal methylators of mercury in anoxic estuarine sediment. *Applied and Environmental Microbiology* **1985,** *50* (2), 498-502.

(21) Fleming, E. J.; Mack, E. E.; Green, P. G.; Nelson, D. C.; Mercury methylation from unexpected sources: Molybdate-inhibited freshwater sediments and an iron-reducing bacterium. *Applied and Environmental Microbiology* **2006,** *72* (1), 457-464.

(22) Krabbenhoft, D. P.; Gilmour, C. C.; Benoit, J. M.; Babiarz, C. L.; Andren, A. W.; Hurley, J. P.; Methyl mercury dynamics in littoral sediments of a temperate

seepage lake. *Canadian Journal of Fisheries and Aquatic Sciences* **1998,** *55* (4), 835-844.

(23) Munthe, J. A.; Bodaly, R. A.; Branfireun, B. A.; Driscoll, C. T.; Gilmour, C. C.; Harris, R.; Horvat, M.; Lucotte, M.; Malm, O.; Recovery of mercury-contaminated fisheries. *Ambio* **2007,** *36* (1), 33-44.

(24) Marvin-DiPasquale, M.; Agee, J.; McGowan, C.; Oremland, R. S.; Thomas, M.; Krabbenhoft, D.; Gilmour, C. C.; Methyl-mercury degradation pathways: A comparison among three mercury-impacted ecosystems. *Environmental Science and Technology* **2000,** *34* (23), 4908-4916.

(25) Robinson, J. B.; Tuovinen, O. H.; Mechanisms of microbial resistance and detoxification of mercury and organomercury compounds: Physiological, biochemical, and genetic analyses. *Microbiological Reviews* **1984,** *48* (2), 95-124.

(26) Marvin-DiPasquale, M. C.; Oremland, R. S.; Bacterial methylmercury degradation in Florida Everglades peat sediment. *Environmental Science and Technology* **1998,** *32* (17), 2556-2563.

(27) Sellers, P.; Kelly, C. A.; Rudd, J. W. M.; MacHutchon, A. R.; Photodegradation of methylmercury in lakes. *Nature* **1996,** *380*, 694-697.

(28) Lehnherr, I.; St. Louis, V. L.; Importance of ultraviolet radiation in the photodemethylation of methylmercury in freshwater ecosystems. *Environmental Science and Technology* **2009,** *43*, 5692-5698.

(29) Hammerschmidt, C. R.; Fitzgerald, W. F.; Photodecomposition of methylmercury in an Arctic Alaskan lake. *Environmental Science and Technology* **2006,** *40* (4), 1212-1216.

(30) Black, F. J.; Poulin, B. A.; Flegal, A. R.; Factors controlling the abiotic photo-degradation of monomethylmercury in surface waters. *Geochimica et Cosmochimica Acta* **2012,** *84*, 492-507.

(31) Lange, T. R.; Royals, H. E.; Connor, L. L.; Influence of water chemistry on mercury concentration in largemouth bass from Florida lakes. *Transactions of the American Fisheries Society* **1993,** *122*, 74-84.

(32) Xun, L.; Campbell, N. E. R.; Rudd, J. W. M.; Measurements of specific rates of net methyl mercury production in the water column and surface sediments of acidified and circumneutral lakes. *Canadian Journal of Fisheries and Aquatic Sciences* **1987,** *44*, 750-757.

(33) Kelly, E. N.; Schindler, D. W.; St. Louis, V. L.; Donald, D. B.; Vladicka, K. E.; Forest fire increases mercury accumulation by fishes via food web restructuring

and increased mercury inputs. *Proceedings of the National Academy of Sciences* **2006,** *103*, 19380-19385.

(34) Miskimmin, B. M.; Rudd, J. W. M.; Kelly, C. A.; Influence of dissolved organic carbon, pH, and microbial respiration rates on mercury methylation and demethylation in lake water. *Canadian Journal of Fisheries and Aquatic Sciences* **1992,** *49*, 17-22.

(35) Zhang, T.; Hsu-Kim, H.; Photolytic degradation of methylmercury enhanced by binding to natural organic ligands. *Nature Geoscience* **2010,** *3*, 473-476.

(36) Gilmour, C. C.; Henry, E. A.; Mitchell, R.; Sulfate stimulation of mercury methylation in freshwater sediments. *Environmental Science and Technology* **1992,** *26* (11), 2281-2287.

(37) Burns, D. A.; Riva-Murray, K.; Bradley, P. M.; Aiken, G. R.; Brigham, M. E.; Landscape controls on total and methyl Hg in the upper Hudson River basin, New York, USA. *Journal of Geophysical Research* **2012,** *117*, G01034.

(38) Boudou, A.; Ribeyre, F., Mercury in the food web: Accumulation and transfer mechanisms. In *Metal Ions in Biological Systems*, Sigel, A.; Sigel, H., Eds. Marcel Dekker, Inc.: New York, **1997**; Vol. 34.

(39) Orihel, D. M.; Paterson, M. J.; Blanchfield, P. J.; Bodaly, R. A.; Gilmour, C. C.; Hintelmann, H.; Temporal changes in the distribution, methylation, and bioaccumulation of newly deposited mercury in an aquatic ecosystem. *Environmental Pollution* **2008,** *154*, 77-88.

(40) Mason, R. P.; Reinfelder, J. R.; Morel, F. M. M.; Uptake, toxicity, and trophic transfer of mercury in a coastal diatom. *Environ. Sci. Technol.* **1996,** *30* (6), 1835-1845.

(41) Grieb, T. M.; Driscoll, C. T.; Gloss, S. P.; Schofield, C. L.; Bowie, G. L.; Porcella, D. B.; Factors affecting mercury accumulation in fish in the upper Michigan peninsula. *Environmental Toxicology and Chemistry* **1990,** *9*, 919-930.

(42) Wang, W.-X.; Wong, R. S. K.; Bioaccumulation kinetics and exposure pathways of inorganic mercury and methylmercury in a marine fish, the sweetlips *Plectorhinchus gibbosus*. *Marine Ecology Progress Series* **2003,** *261*, 257-268.

(43) Trudel, M.; Rasmussen, J. B.; Modeling the elimination of mercury by fish. *Environmental Science and Technology* **1997,** *31* (6), 1716-1722.

(44) Pickhardt, P. C.; Stepanova, M.; Fisher, N. S.; Contrasting uptake routes and tissue distributions of inorganic and methylmercury in mosquitofish (*Gambusia affinis*)

and redear sunfish (*Lepomis microlophus*). *Environmental Toxicology and Chemistry* **2006,** *25* (8), 2132-2142.

(45) Bloom, N. S.; On the chemical form of mercury in edible fish and marine invertebrate tissue. *Canadian Journal of Fisheries and Aquatic Sciences* **1992,** *49* (5), 1010-1017.

(46) Pentreath, R. J.; The accumulation of mercury from food by the plaice, *Pleuronectes platessa* L. *Journal of Experimental Marine Biology and Ecology* **1976,** *25* (1), 51-65.

(47) MacRury, N. K.; Graeb, B. D. S.; Johnson, B. M.; Clements, W. H.; Comparison of dietary mercury exposure in two sympatric top predator fishes, largemouth bass and northern pike: A bioenergetics modeling approach. *Journal of Aquatic Ecosystem Stress and Recovery* **2002,** *9* (3), 137-147.

(48) Ward, S. M.; Neumann, R. M.; Seasonal variations in concentrations of mercury in axial tissue of largemouth bass. *North American Journal of Fisheries Management* **1999,** *19*, 89-96.

(49) Trudel, M.; Rasmussen, J. B.; Bioenergetics and mercury dynamics in fish: a modelling perspective. *Canadian Journal of Fisheries and Aquatic Sciences* **2006,** *63*, 1890-1902.

(50) Hammerschmidt, C. R.; Fitzgerald, W. F.; Methylmercury in freshwater fish linked to atmospheric mercury deposition. *Environmental Science and Technology* **2006,** *40*, 7764-7770.

(51) Hammerschmidt, C. R.; Fitzgerald, W. F.; Methylmercury in mosquitoes related to atmospheric mercury deposition and contamination. *Environmental Science and Technology* **2005,** *39*, 3034-3039.

(52) Paterson, M. J.; Blanchfield, P. J.; Podemski, C.; Hintelmann, H. H.; Gilmour, C. C.; Harris, R.; Ogrinc, N.; Rudd, J. W. M.; Sandilands, K. A.; Bioaccumulation of newly deposited mercury by fish and invertebrates: an enclosure study using stable mercury isotopes. *Canadian Journal of Fisheries and Aquatic Sciences* **2006,** *63* (10), 2213-2224.

(53) Harris, R. C.; Rudd, J. W. M.; Amyot, M.; Babiarz, C. L.; Beaty, K. G.; Blanchfield, P. J.; Bodaly, R. A.; Branfireun, B. A.; Gilmour, C. C.; Graydon, J. A.; Heyes, A.; Hintelmann, H.; Hurley, J. P.; Kelly, C. A.; Krabbenhoft, D. P.; Lindberg, S. E.; Mason, R. P.; Paterson, M. J.; Podemski, C. L.; Robinson, A.; Sandilands, K. A.; Southworth, G. R.; St. Louis, V. L.; Tate, M. T.; Whole-ecosystem study shows rapid fish-mercury response to changes in mercury deposition. *Proceedings of the National Academy of Sciences* **2007,** *104* (42), 16586-16591.

(54) Hrabik, T. R.; Watras, C. J.; Recent declines in mercury concentration in a freshwater fishery: Isolating the effects of de-acidification and decreased atmospheric mercury deposition in Little Rock Lake. *Science of the Total Environment* **2002,** *297* (1,Äì3), 229-237.

(55) Kannan, K.; Smith, R. G.; Lee, R. F.; Windom, H. L.; Heitmuller, P. T.; Macauley, J. M.; Summers, J. K.; Distribution of total mercury and methyl mercury in water, sediment, and fish from south Florida estuaries. *Archives of Environmental Contamination and Toxicology* **1998,** *34*, 109-118.

(56) Sunderland, E. M.; Dalziel, J.; Heyes, A.; Branfireun, B. A.; Krabbenhoft, D. P.; Gobas, F. A. P. C.; Response of a macrotidal estuary to changes in anthropogenic mercury loading between 1850 and 2000. *Environmental Science and Technology* **2010,** *44* (5), 1698-1704.

(57) Knightes, C. D.; Sunderland, E. M.; Barber, M. C.; Johnston, J. M.; Ambrose, R. B. J.; Application of ecosystem-scale fate and bioaccumulation models to predict fish mercury response times to changes in atmospheric deposition. *Environmental Toxicology and Chemistry* **2009,** *28*, 881-893.

(58) Hand, J.; Friedemann, M., Mercury, largemouth bass, and water quality: A preliminary report. Florida Department of Environmental Regulation: Talahassee, FL, **1990**.

(59) Lange, T. R.; Royals, H. E.; Connor, L. L.; Mercury accumulation in largemouth bass (*Micropterus salmoides*) in a Florida Lake. *Archives of Environmental Contamination and Toxicology* **1994,** *27* (4), 466-471.

(60) Axelrad, D. M.; Lange, T.; Gabriel, M. C.; Aiken, G. R.; Brandon, A.; Cunningham, M. W.; DeBusk, T.; Dierberg, F.; Donner, B. A.; Frederick, P.; Gilmour, C.; Harris, R.; Jansen, D.; Krabbenhoft, D. P.; McCray, J. M.; Orem, W. H.; Oronato, D. P.; Pollman, C. D.; Rumbold, D. G.; White, G.; Wright, A. L.; Ye, R., 2011 South Florida Environmental Report: Chapter 3B Mercury and Sulfur Monitoring, Research and Environmental Assessment in South Florida. South Florida Water Management District: **2011**; Vol. I, p 53.

(61) Dvonch, J. T.; Keeler, G. J.; Marsik, F. J.; The influence of meteorological conditions on the wet deposition of mercury in southern Florida. *JApMe* **2005,** *44*, 1421-1435.

(62) Dvonch, J. T.; Graney, J. R.; Marsik, F. J.; Keeler, G. J.; Stevens, R. K.; An investigation of source-receptor relationships for mercury in south Florida using event precipitation data. *Sci. Total Environ.* **1998,** *213*, 95-108.

(63) Frederick, P. C.; Spalding, M. G.; Dusek, R.; Wading birds as bioindicators of mercury contamination in Florida: Annual and geographic variation. *Environ. Toxicol. Chem.* **2002,** *21* (1), 163-167.

(64) Royals, H. E.; Lange, T.; Mercury in Florida fish and wildlife. *Florida Wildlife* **1990,** *44* (2), 3-6.

(65) Florida Department of Health, **2012**. *Your Guide to Eating Fish Caught in Florida*. access via http://www.myfloridaeh.com/medicine/fishconsumptionadvisories/index.html. Accessed January 5, 2012.

(66) Gehrke, G. E.; Blum, J. D.; Slotton, D. G.; Greenfield, B. K.; Mercury isotopes link mercury in San Francisco Bay forage fish to surface sediments. *Environmental Science and Technology* **2011,** *45* (4), 1264-1270.

(67) Gantner, N.; Hintelmann, H.; Zheng, W.; Muir, D. C.; Variations in stable isotope fractionation of Hg in food webs of Arctic lakes. *Environmental Science and Technology* **2009,** *43*, 9148-9154.

(68) Perrot, V.; Epov, V. N.; Pastukhov, M. V.; Grebenshchikova, V. I.; Zouiten, C.; Sonke, J. E.; Husted, S.; Donard, O. F. X.; Amouroux, D.; Tracing sources and bioaccumulation of mercury in fish of Lake Baikal - Angara River using Hg isotopic composition. *Environmental Science and Technology* **2010,** *44* (21), 8030-8037.

(69) Senn, D. B.; Chesney, E. J.; Blum, J. D.; Bank, M. S.; Maage, A.; Shine, J. P.; Stable isotope (N, C, Hg) study of methylmercury sources and trophic transfer in the northern Gulf of Mexico. *Environ. Sci. Technol.* **2010,** *44* (5), 1630-1637.

(70) Blum, J. D.; Bergquist, B. A.; Reporting the variations in the natural isotopic composition of mercury. *Anal. Bioanal. Chem.* **2007,** *388* (2), 353-359.

(71) Rodriguez-Gonzalez, P.; Epov, V. N.; Bridou, R.; Tessier, E.; Guyoneaud, R.; Monperrus, M.; Amouroux, D.; Species-specfic stable isotope fractionation of mercury during Hg(II) methylation by an anaerobic bacteria (*Desulfobulbus propionicus*) under dark conditions. *Environ. Sci. Technol.* **2009**.

(72) Malinovsky, D.; Vanhaecke, F.; Mass-independent isotope fractionation of heavy elements measured by MC-ICPMS: A unique probe in environmental sciences. *Anal. Bioanal. Chem.* **2011,** *400*, 1619-1624.

(73) Kritee, K.; Barkay, T.; Blum, J. D.; Mass dependent stable isotope fractionation of mercury during *mer* mediated microbial degradation of monomethylmercury. *Geochimica et Cosmochimica Acta* **2009,** *73*, 1285-1296.

(74) Bergquist, B. A.; Blum, J. D.; Mass-dependent and mass-independent fractionation of Hg isotopes by photo-reduction in aquatic systems. *Science* **2007,** *318* (5849), 417-420.

(75) Turro, N. J.; Influence of nuclear spin on chemical reactions: Magnetic isotope and magnetic field effects. *Proceedings of the National Academy of Sciences* **1983,** *80*, 609-621.

(76) Buchachenko, A. L.; Magnetic isotope effect: Nuclear spin control of chemical reactions. *J. Phys. Chem.* **2001,** *105* (44), 9995-10011.

(77) Das, R.; Salters, V. J. M.; Odem, A. L.; A case for in vivo mass-independent fractionation of mercury isotopes in fish. *Geochemistry Geophysics Geosystems* **2009,** *10*, Q11012.

(78) Kwon, S. Y.; Blum, J. D.; Carvan, M. J.; Basu, N.; Head, J. A.; Madenjian, C. P.; David, S. R.; Absence of fractionation of mercury isotopes during trophic transfer of methylmercury to freshwater fish in captivity. *Environmental Science and Technology* **2012,** *46* (14), 7527-7534.

(79) Point, D.; Sonke, J. E.; Day, R. D.; Roseneau, D. G.; Hobson, K. A.; Vander Pol, S. S.; Moors, A. J.; Pugh, R. S.; Donard, O. F. X.; Becker, P. R.; Methylmercury photodegradation influenced by sea-ice cover in Arctic marine ecosystems. *Nature Geoscience* **2011,** *4*, 188-194.

(80) Laffont, L.; Sonke, J. E.; Maurice, L.; Hintelmann, H.; Pouilly, M.; Bacarreza, Y. S.; Perez, T.; Behra, P.; Anomalous mercury isotopic compositions of fish and human hair in the Bolivian Amazon. *Environ. Sci. Technol.* **2009,** *43*, 8985-8990.

(81) U.S. Department of the Interior/U.S. Geological Survey, *Surface-water and groundwater interactions along the Withlacoochee River, West-Central Florida; Scientific Investigations Report 2009-5124*. **2009**.

(82) Hurley, J. P.; Shafer, M. M.; Cowell, S. E.; Overdier, J. T.; Hughes, P. E.; Armstrong, D. E.; Trace metal assessment of Lake Michigan tributaries using low-level techniques. *Environ. Sci. Technol.* **1996,** *30*, 2093-2098.

(83) Gill, G. A.; Fitzgerald, W. F.; Mercury sampling of open ocean waters at the picomolar level. *Deep Sea Research (Part A, Oceanographic Research Papers)* **1985,** *32* (3), 287-297.

(84) U.S. Environmental Protection Agency, *Method 1631, Revision E: Mercury in Water by Oxidation, Purge and Trap, and Cold Vapor Atomic Fluorescence Spectrometry (EPA-821/R-02-019)*. Office of Water, Office of Science and Technology, Engineering and Analysis Division: Washington, DC, **2002**.

(85) U.S. Environmental Protection Agency, *Method 1630: Methyl Mercury in Water by Distillation, Aqueous Ethylation, Purge and Trap, and Cold Vapor Atomic Fluorescence Spectrometry*. Office of Water, Office of Science and Technology, Engineering and Analysis Division: Washington, DC, **1998**.

(86) Bloom, N.; Determination of picogram levels of methylmercury by aqueous phase ethylation, followed by cryogenic gas chromatography with cold vapour atomic fluorescence detection. *Canadian Journal of Fisheries and Aquatic Sciences* **1989,** *46*, 1131-1140.

(87) Taubert, B. D.; Tranquilli, J. A.; Verification of the formation of annuli in otoliths of largemouth bass. *Transactions of the American Fisheries Society* **1982,** *111* (4), 531-534.

(88) Sherman, L. S.; Blum, J. D.; Keeler, G. J.; Demers, J. D.; Dvonch, J. T.; Investigation of local mercury deposition from a coal-fired power plant using mercury isotopes. *Environ. Sci. Technol.* **2012,** *46* (1), 382-390.

(89) Griffith, G. E.; Canfield, D. E. J.; Horsburgh, C. A.; Omernik, J. M.; Lake Regions of Florida. *U.S. Environmental Protection Agency* **1997**, EPA/R-97/127.

(90) Morris, D. P.; Zagarese, H.; Williamson, C. E.; Balseiro, E. G.; Hargreaves, B. R.; Modenutti, B.; Moeller, R.; Queimalinos, C.; The attenuation of solar UV radiation in lakes and the role of dissolved organic carbon. *Limnology and Oceanography* **1995,** *40* (8), 1381-1391.

(91) Amyot, M.; Mierle, G.; Lean, D.; McQueen, D. J.; Effect of solar radiation on the formation of dissolved gaseous mercury in temperate lakes. *Geochimica et Cosmochimica Acta* **1997,** *61* (5), 975-987.

(92) Brown, C. D.; Canfield, D. E. J.; Bachmann, R. W.; Hoyer, M. V.; Seasonal patterns of chlorophyll, nutrient concentrations and secchi depth transparency in Florida lakes. *Journal of Lake and Reservoir Management* **1998,** *14* (1), 60-76.

(93) Krabbenhoft, D. P.; Olson, M. L.; Dewild, J. F.; Clow, D. W.; Striegl, R. G.; Dornblaser, M. M.; VanMetre, P.; Mercury loading and methylmercury production and cycling in high-altitude lakes from the western United States. *Water, Air, and Soil Pollution: Focus* **2002,** *2* (2), 233-249.

(94) Craft, C. B.; Richardson, C. J.; Peat accretion and N, P, and organic C accumulation in nutrient-enriched and unenriched Everglades peatlands. *Ecological Applications* **1993,** *3* (3), 446-458.

(95) Brenner, M.; Schelske, C. L.; Keenan, L. W.; Historical rates of sediment and nutrient accumulation in marshes of the Upper St. Johns River Basin, Florida, U.S.A. *Journal of Paleolimnology* **2001,** *26* (3), 241-257.

(96) Brezonik, P. L.; Engstrom, D. R.; Modern and historic accumulation rates of phosphorus in Lake Okeechobee, Florida. *Journal of Paleolimnology* **1998,** *20*, 31-46.

(97) Binford, M. W.; Brenner, M.; Engstrom, D. R., Temporal sedimentation patterns in the nearshore littoral of Lago Huiñaimarca. In *Lake Titicaca, a Synthesis of Limnological Knowledge*, Dejoux, C.; Iltis, A., Eds. Kluwer Academic Publishers: Norwell, MA, **1992**.

(98) Whitmore, T. J.; Brenner, M.; Schelske, C. L.; Highly variable sediment distribution in shallow, wind-stressed lakes: a case for sediment-mapping surveys in paleolimnological studies. *Journal of Paleolimnology* **1996,** *15*, 207-221.

(99) Rood, B. E.; Gottgens, J. F.; Delfino, J. J.; Earle, C. D.; Crisman, T. L.; Mercury accumulation trends in Florida Everglades and savannas marsh flooded soils. *Water, Air, Soil Pollut.* **1995,** *80* (981-990).

(100) Fitzgerald, W. F.; Engstrom, D. R.; Mason, R. P.; Nater, E. A.; The case for atmospheric mercury contamination in remote areas. *Environ. Sci. Technol.* **1998,** *32*, 1-7.

(101) Dvonch, J. T.; Graney, J. R.; Keeler, G. J.; Stevens, R. K.; Use of elemental tracers to source apportion mercury in south Florida precipitation. *Environ. Sci. Technol.* **1999,** *33*, 4522-4527.

(102) DeNiro, M. J.; Epstein, S.; Influence of diet on the distribution of carbon isotopes in animals. *Geochimica et Cosmochimica Acta* **1978,** *42*, 495-506.

(103) Peterson, B. J.; Fry, B.; Stable isotopes in ecosystem studies. *Annual Reviews in Ecology and Systematics* **1987,** *18*, 293-320.

(104) Fry, B.; Stable isotope diagrams of freshwater food webs. *Ecology* **1991,** *72* (6), 2293-2297.

(105) Fry, B.; Mumford, P. L.; Tam, F.; Fox, D. D.; Warren, G. L.; Havens, K. E.; Steinman, A. D.; Trophic position and individual feeding histories of fish from Lake Okeechobee, Florida. *Canadian Journal of Fisheries and Aquatic Sciences* **1999,** *56* (4), 590-600.

(106) Focken, U.; Becker, K.; Metabolic fractionation of stable carbon isotopes: Implications of different proximate compositions for studies of the aquatic food webs using $\delta^{13}C$ data. *Oecologia* **1998,** *115*, 337-343.

(107) Gaye-Siessegger, J.; Focken, U.; Muetzel, S.; Abel, H.; Becker, K.; Feeding level and individual metabolic rate affect $\delta^{13}C$ and $\delta^{15}N$ values in carp: Implications for food web studies. *Oecologia* **2004,** *138*, 175-183.

(108) Gu, B.; Schelske, C. L.; Hoyer, M. V.; Stable isotopes of carbon and nitrogen as indicators of diet and trophic structure of the fish community in a shallow hypereutrophic lake. *Journal of Fish Biology* **1996,** *49*, 1233-1243.

(109) Soupir, C. A.; Brown, M. L.; Kallemeyn, L. W.; Trophic ecology of largemouth bass and northern pike in allopatric and sympatric assemblages in northern boreal lakes. *Canadian Journal of Zoology* **2000,** *78* (10), 1759-1766.

(110) Wheeler, A. P.; Allen, M. S.; Habitat and diet partitioning between shoal bass and largemouth bass in the Chipola River, Florida. *Transactions of the American Fisheries Society* **2003,** *132* (3), 438-449.

(111) Lindberg, S.; Bullock, R.; Ebinghaus, R.; Engstrom, D.; Feng, X.; Fitzgerald, W.; Pirrone, N.; Prestbo, E.; Seigneur, C.; A synthesis of progress and uncertainties in attributing the sources of mercury in deposition. *Ambio* **2007,** *36* (1), 19-32.

(112) White, E. M.; Keeler, G. J.; Landis, M. S.; Spatial variability of mercury wet deposition in eastern Ohio: Summertime meteorological case study analysis of local source influences. *Environ. Sci. Technol.* **2009,** *43*, 4946-4953.

(113) Expert Panel on Mercury Atmospheric Processes, *Mercury Atmospheric Processes: A Synthesis Report, TR-104214*. Tampa, FL, **1994**.

(114) Landis, M. S.; Vette, A. F.; Keeler, G. J.; Atmospheric mercury in the Lake Michigan Basin: Influence of the Chicago/Gary urban area. *Environ. Sci. Technol.* **2002,** *36*, 4508-4517.

(115) U.S. Environmental Protection Agency, **2005**. *National Emissions Inventory for Mercury Point Sources in the State of Florida*. access via http://www.epa.gov/ttn/chief/net/2005inventory.html - inventorydata. Accessed November 15, 2010.

(116) Lohman, K.; Seigneur, C.; Edgerton, E.; Jansen, J.; Modeling mercury in power plant plumes. *Environ. Sci. Technol.* **2006,** *40*, 3848-3854.

(117) U.S. Environmental Protection Agency, **2012**. *Clean Air Markets - Data and Maps*. access via http://camddataandmaps.epa.gov/gdm/index.cfm. Accessed January 20, 2012.

(118) Srivastava, R. K.; Hutson, N.; Martin, B.; Princiotta, F.; Staudt, J.; Control of mercury emissions from coal-fired electric utility boilers. *Environ. Sci. Technol.* **2006,** *40* (5), 1385-1393.

(119) U.S. Environmental Protection Agency, **2009-2011**. *Toxic Release Inventory Explorer*. access via http://iaspub.epa.gov/triexplorer/tri_release.chemical. Accessed January 20, 2012.

(120) U.S. Energy Information Administration, **2009-2011**. *Monthly Utility and Nonutility Fuel Receipts and Fuel Quality Data, EIA-923*. access via http://www.eia.doe.gov/cneaf/electricity/page/eia423.html. Accessed January 20, 2012.

(121) Gehrke, G. E.; Blum, J. D.; Marvin-DePasquale, M.; Sources of mercury to San Francisco Bay surface sediment as revealed by mercury stable isotopes. *Geochimica et Cosmochimica Acta* **2010,** *75* (3), 691-705.

(122) National Atmospheric Deposition Program, **2012**. *Mercury Deposition Network*. access via http://nadp.sws.uiuc.edu/MDN/. Accessed March 05, 2012.

(123) Davis, M. B.; Ford, M. S.; Sediment focusing in Mirror Lake, New Hampshire. *Limnology and Oceanography* **1982,** *27* (1), 137-150.

(124) St. Johns River Water Management District, **2011**. *Lake Kerr: Water quality*. access via http://www.floridaswater.com/watershedfacts/factPages/KER.html. Accessed March 15, 2012.

(125) Hurley, J. P.; Benoit, J. M.; Babiarz, C. L.; Shafer, M. M.; Andren, A. W.; Sullivan, J. R.; Hammond, R.; Webb, D. A.; Influences of watershed characteristics on mercury levels in Wisconsin Rivers. *Environmental Science and Technology* **1995,** *29*, 1867-1875.

(126) Babiarz, C. L.; Andren, A. W.; Total concentrations of mercury in Wisconsin (USA) lakes and rivers. *Water, Air and Soil Pollution* **1994,** *83*, 173-183.

(127) Brigham, M. E.; Wentz, D. A.; Aiken, G. R.; Krabbenhoft, D. P.; Mercury cycling in stream ecosystems. 1. Water column chemistry and transport. *Environmental Science and Technology* **2009,** *43*, 2720-2725.

(128) Jackson, T. A.; Whittle, D. M.; Evans, M. S.; Muir, D. C. G.; Evidence for mass-independent and mass-dependent fractionation of the stable isotopes of mercury by natural processes in aquatic ecosystems. *Appl. Geochem.* **2008,** *23* (3), 547-571.

(129) Kritee, K.; Blum, J. D.; Johnson, M. W.; Bergquist, B. A.; Barkay, T.; Mercury stable isotope fractionation during reduction of Hg(II) to Hg(0) by mercury resistant microorganisms. *Environ. Sci. Technol.* **2007,** *41*, 1889-1895.

(130) Estrade, N.; Carignan, J.; Sonke, J. E.; Donard, O. F. X.; Mercury isotope fractionation during liquid-vapor evaporation experiments. *Geochim. Cosmochim. Acta* **2009,** *73*, 2693-2711.

(131) Zheng, W.; Hintelmann, H.; Mercury isotope fractionation during photoreduction in natural water is controlled by its Hg/DOC ratio. *Geochim. Cosmochim. Acta* **2009,** *73*, 6704-6715.

(132) Zheng, W.; Hintelmann, H.; Isotope fractionation of mercury during its photochemical reduction by low-molecular-weight organic compounds. *J. Phys. Chem. A* **2010,** *114* (12), 4246-4253.

(133) Ghosh, S.; Schauble, E. A.; Couloume, G. L.; Blum, J. D.; Bergquist, B. A.; Estimation of nuclear volume dependent fractionation of mercury isotopes in equilibrium liquid-vapor evaporation experiments. *Chem. Geol.* **2012**.

(134) York, D.; Least-squares fitting of a straight line. *Can. J. Phys.* **1966,** *44*, 1076-1086.

(135) Rice, J. A.; Breck, J. E.; Bartell, S. M.; Kitchell, J. F.; Evaluating the constraints of temperature, activity and consumption on growth of largemouth bass. *Environmental Biology of Fishes* **1983,** *9* (3), 263-275.

(136) Marvin-DePasquale, M.; Lutz, M. A.; Brigham, M. E.; Krabbenhoft, D. P.; Aiken, G. R.; Orem, W. H.; Hall, B. D.; Mercury cycling in stream ecosystems. 2. Benthic methylmercury production and bed sediment - pore water partitioning. *Environmental Science and Technology* **2009,** *43*, 2726-2732.

(137) Bloom, N. S.; Preus, E.; Katon, J.; Hiltner, M.; Selective extractions to assess the biogeochemically relevant fraction of inorganic mercury in sediments and soils. *Analytica Chimica Acta* **2003,** *479*, 233-248.

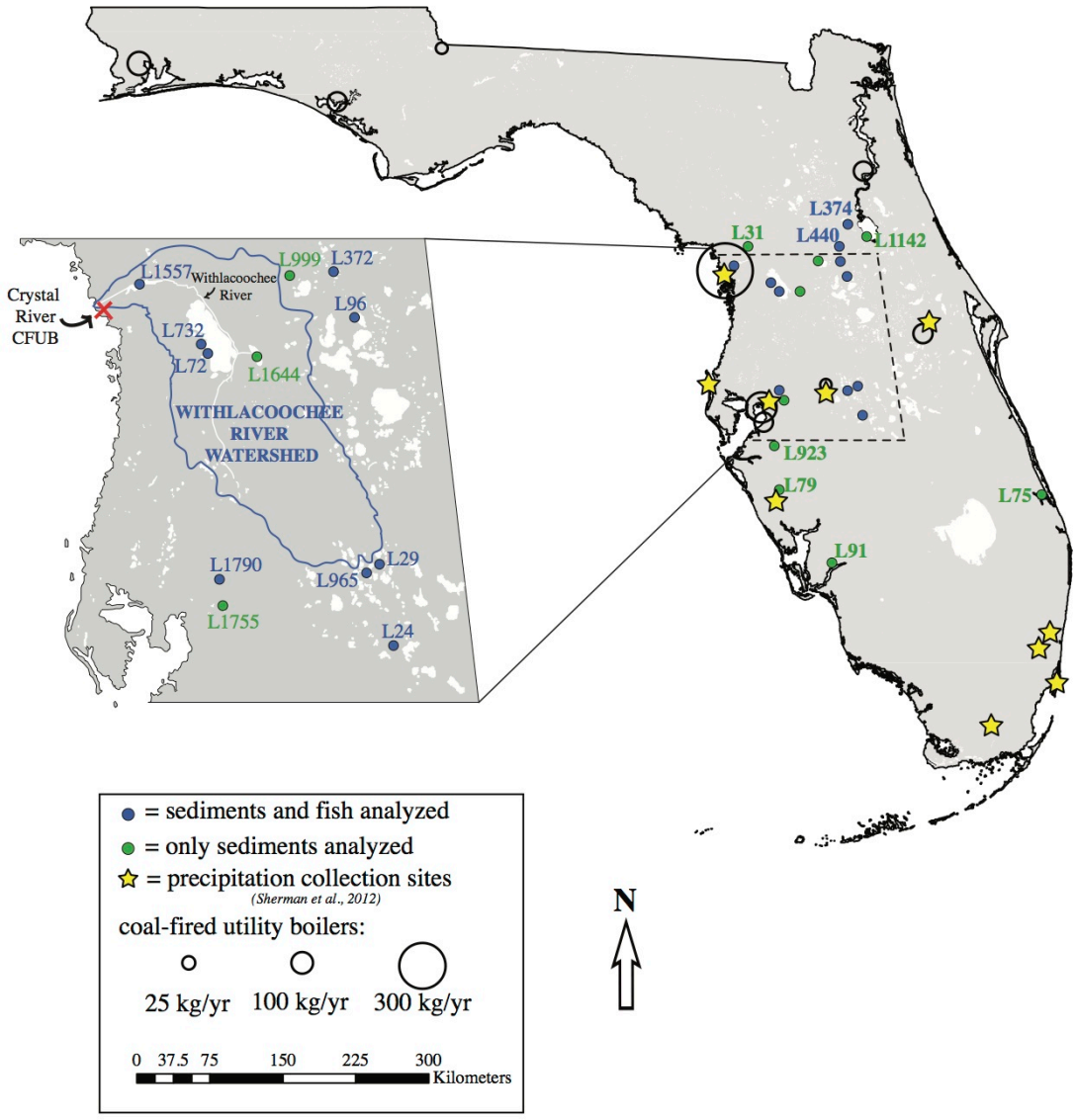


Figure 6.1 Map of sample collection sites. Freshwater lakes across FL are shown in white. Lakes from which sediments and fish were collected are shown as blue dots and lakes from which only sediments were collected are shown as green dots. Coal-fired utility boilers are shown as black circles scaled linearly (with respect to radius) relative to the largest source according to total estimated Hg emissions (*115*). Precipitation collection sites from Sherman et al. (*88*) are shown as yellow stars. Inset shows an enlarged area with the Withlacoochee River watershed outlined in blue. The coal-fired utility boiler at Crystal River, FL is shown as a red cross.

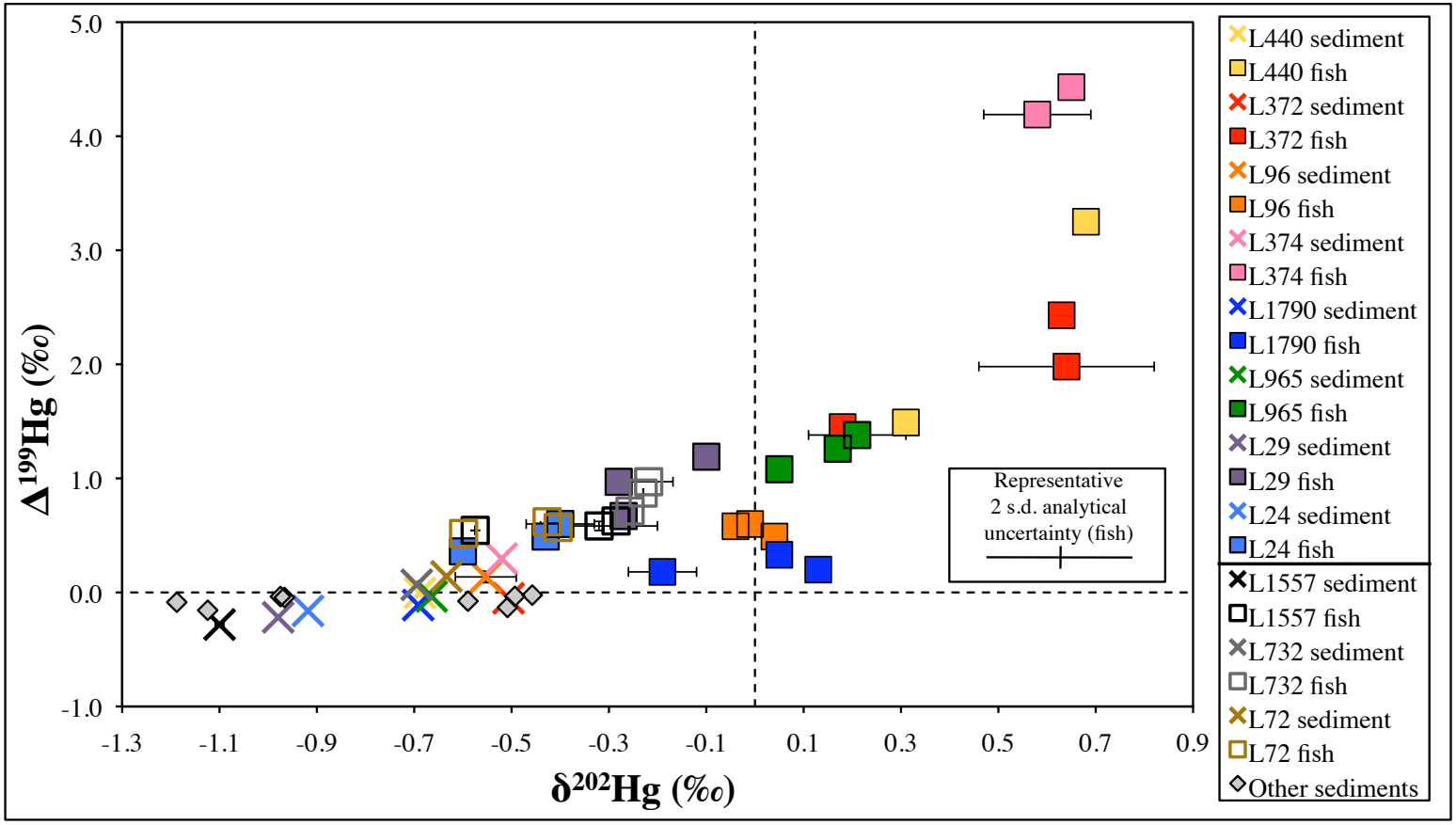


Figure 6.2 Mercury isotopic composition of sediment and largemouth bass samples. Sediment samples from lakes in which fish were not collected are shown as grey diamonds; sediment samples from lakes in which fish were collected are shown as colored crosses; largemouth bass from lakes located <50 km of Crystal River are shown as open colored squares; largemouth bass from lakes located >50 km from Crystal River, FL are shown as filled colored squares. Error bars on individual symbols are 1 s.d. of replicate sample analyses. Representative 2 s.d. analytical uncertainty for largemouth bass samples (based on measurement of procedural standards) is shown. Dashed lines depict the 0 values for both axes.

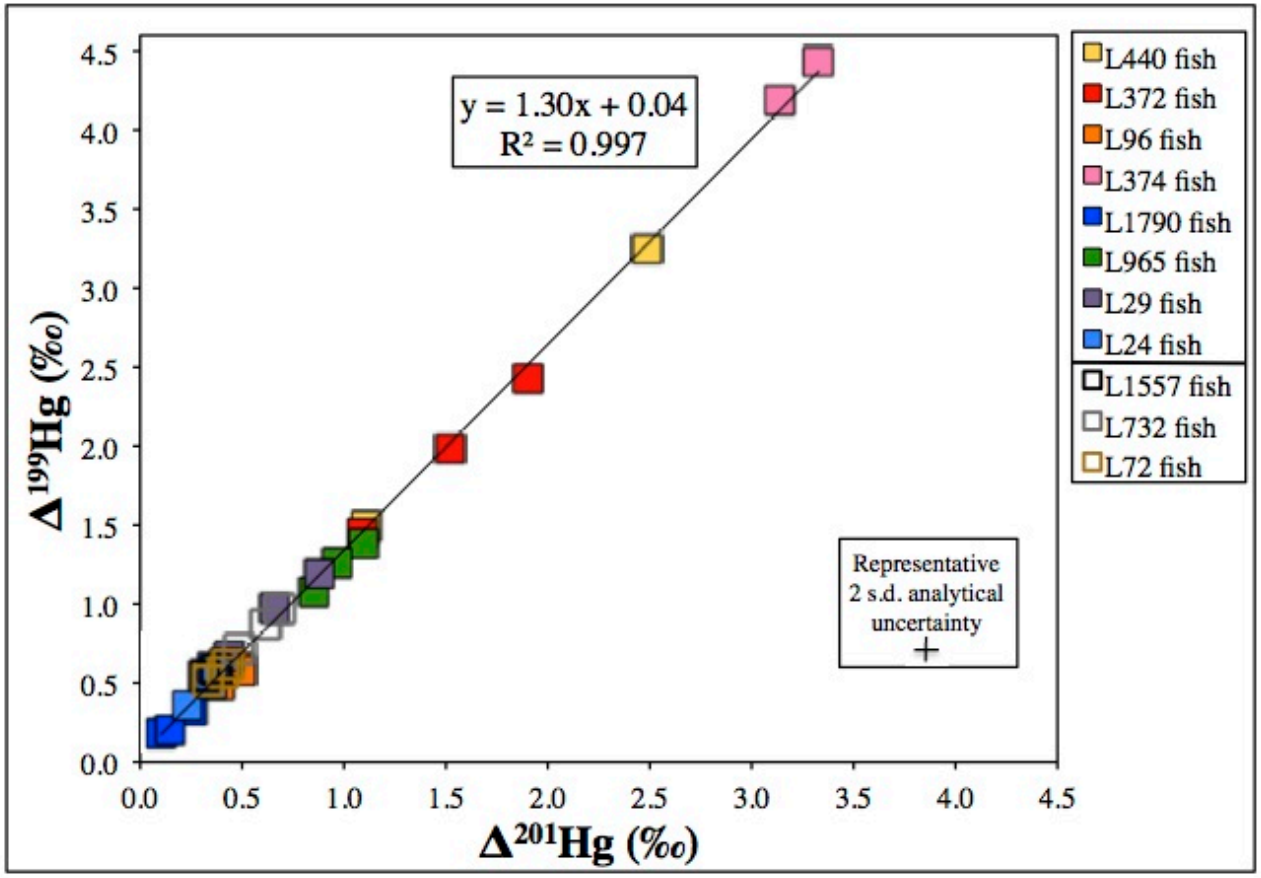
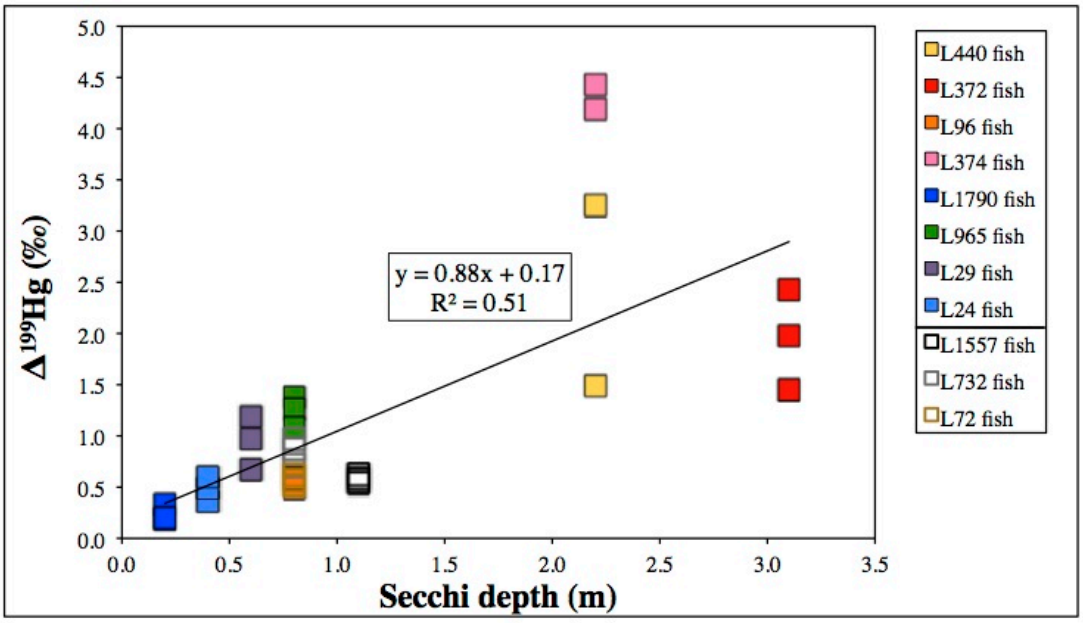


Figure 6.3 Mass-independent fractionation of Hg in largemouth bass. Δ^{199}Hg versus Δ^{201}Hg measured in the largemouth bass samples. Fish from lakes located <50 km of Crystal River are shown as open colored squares; fish from lakes located >50 km from Crystal River, FL are shown as filled colored squares. On the basis of a York regression (*134*), the Δ^{199}Hg/Δ^{201}Hg ratio in the fish is 1.30 ± 0.03 (2 s.e., n = 31). Representative 2 s.d. analytical uncertainty based on measurement of procedural standards is shown.

Figure 6.4 Light penetration depth and DOC concentration versus MIF in largemouth bass. Largemouth bass from lakes located <50 km of Crystal River are shown as open colored squares; fish from lakes located >50 km from Crystal River, FL are shown as filled colored squares. **a.** Light penetration depth (m) was measured as secchi depth. Solid line shows a linear regression model including fish from all of the lakes (slope = 0.88 ± 0.16, 1 s.e.; $p < 0.0001$, $r^2 = 0.51$, $n = 31$). **b.** Solid line shows a linear regression model through the log-transformed data including fish from all of the lakes (slope = -0.45 ± 0.12, 1 s.e.; $p = 0.0007$, $r^2 = 0.33$, $n = 31$). Horizontal dashed line shows the 0 values for the y-axis.

a.


y = 0.88x + 0.17
R² = 0.51
Δ199Hg (‰)
Secchi depth (m)
L440 fish
L372 fish
L96 fish
L374 fish
L1790 fish
L965 fish
L29 fish
L24 fish
L1557 fish
L732 fish
L72 fish

b.

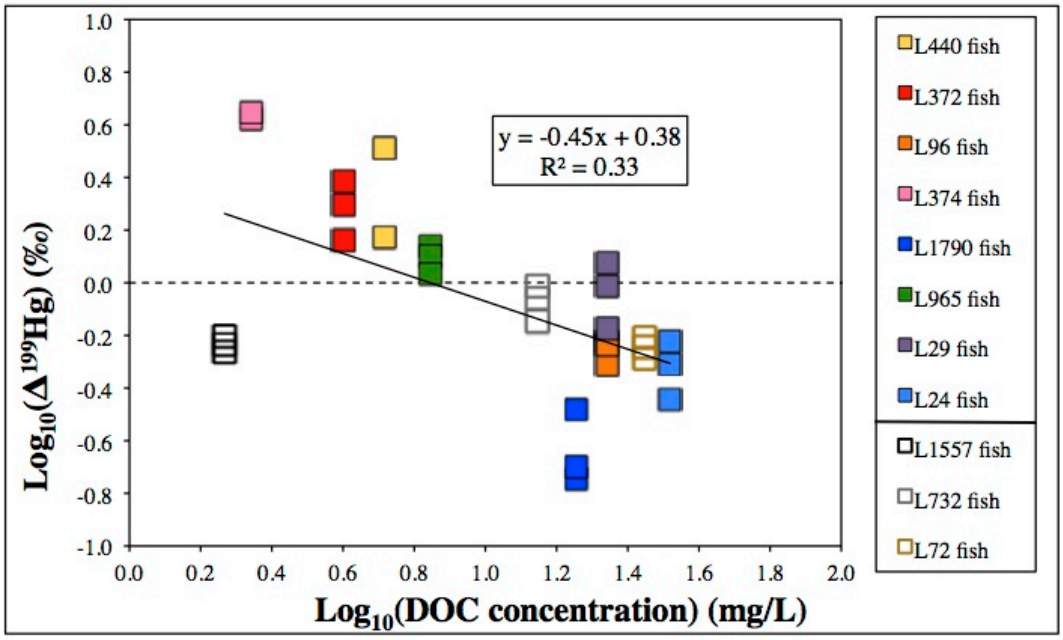
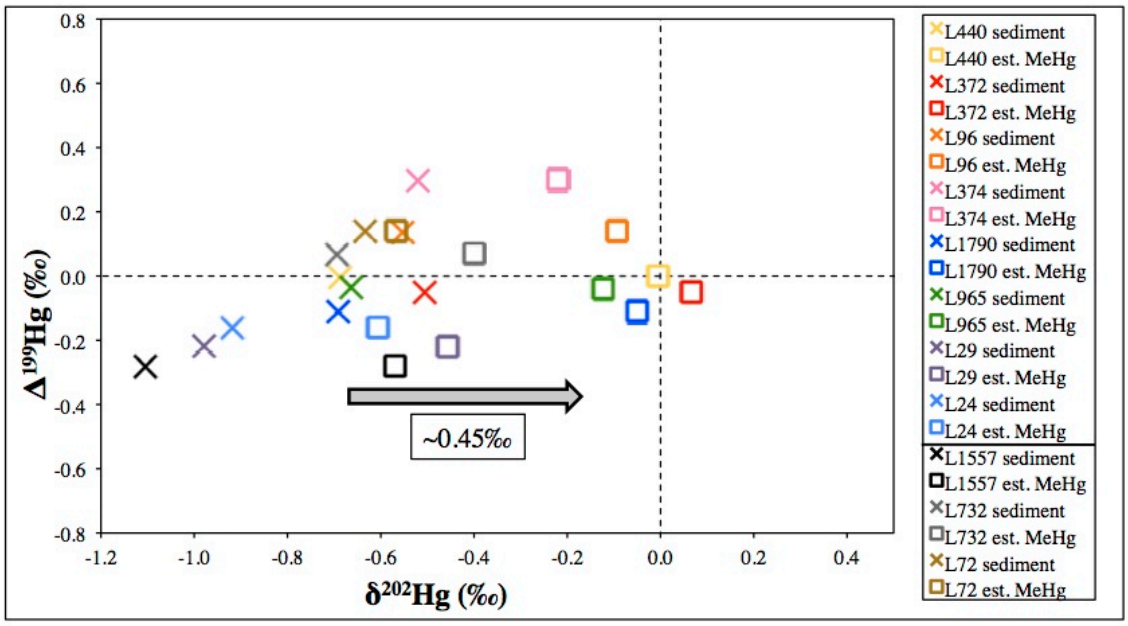

y = -0.45x + 0.38
R² = 0.33
Log10(Δ199Hg) (‰)
Log10(DOC concentration) (mg/L)
L440 fish
L372 fish
L96 fish
L374 fish
L1790 fish
L965 fish
L29 fish
L24 fish
L1557 fish
L732 fish
L72 fish

Figure 6.5 Bulk sediment isotopic composition versus estimated sediment MeHg isotopic composition. Bulk sediment and estimated sediment MeHg isotopic compositions (based on isotopic compositions of largemouth bass) are shown for all of the study lakes. **a.** Sediment samples are shown as colored crosses; estimated sediment MeHg isotopic compositions are shown as open colored squares. Arrow shows average offset between bulk sediment δ^{202}Hg values and estimated MeHg δ^{202}Hg values (mean = 0.45‰, 1 s.d. = 0.19‰, n = 11). **b.** Solid line shows a linear regression between bulk sediment δ^{202}Hg values and estimated sediment MeHg δ^{202}Hg values for all of the lakes (slope = 0.89 ± 0.32, 1 s.e.; p = 0.02; r^2 = 0.47, n = 11).

a.


0.8
0.6
0.4
0.2
0.0
-0.2
-0.4
-0.6
-0.8
-1.2
-1.0
-0.8
-0.6
-0.4
-0.2
0.0
0.2
0.4
Δ199Hg (‰)
δ202Hg (‰)
~0.45‰
L440 sediment
L440 est. MeHg
L372 sediment
L372 est. MeHg
L96 sediment
L96 est. MeHg
L374 sediment
L374 est. MeHg
L1790 sediment
L1790 est. MeHg
L965 sediment
L965 est. MeHg
L29 sediment
L29 est. MeHg
L24 sediment
L24 est. MeHg
L1557 sediment
L1557 est. MeHg
L732 sediment
L732 est. MeHg
L72 sediment
L72 est. MeHg

b.

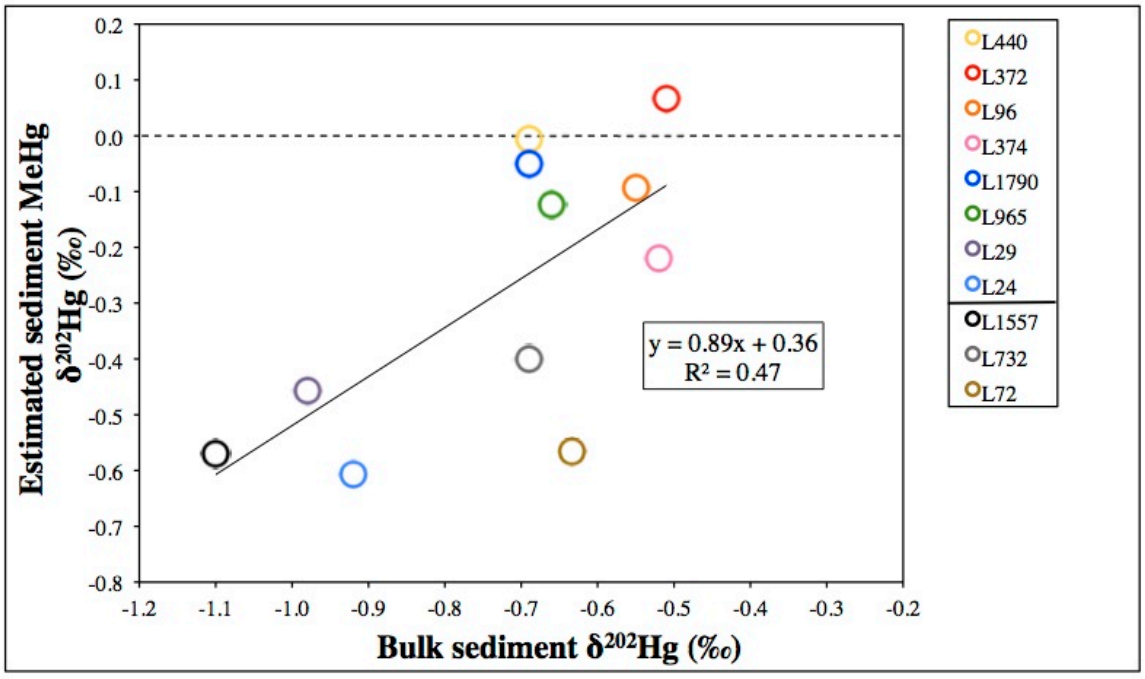

0.2
0.1
0.0
-0.1
-0.2
-0.3
-0.4
-0.5
-0.6
-0.7
-0.8
-1.2
-1.1
-1.0
-0.9
-0.8
-0.7
-0.6
-0.5
-0.4
-0.3
-0.2
Estimated sediment MeHg δ202Hg (‰)
Bulk sediment δ202Hg (‰)
y = 0.89x + 0.36
R² = 0.47
L440
L372
L96
L374
L1790
L965
L29
L24
L1557
L732
L72

Table 6.1 Water quality parameters. Secchi depth and pH were measured in each lake in the months listed. The other water quality parameters were measured by the FDEP using samples collected in the months listed. Measured values that were below the detection limit are listed as BDL.

Lake Name	Lake ID	Latitude	Longitude	Secchi depth (m)	Month of Secchi depth measurement	Water Quality Parameters						
						Month collected	Depth of collection (m)	pH	Total Hg (ng/L)	MeHg (ng/L)	Alkalinity (mg/L)	DOC (mg/L)
Lake Rousseau	L1557	29.00887	-82.61299	1.1	Oct-09	May-09	1.0	8.57	0.43	0.063	110	1.9
Little Lake Henderson	L732	28.84820	-82.32872	0.8	Oct-09	Jun-09	0.1	8.53	0.59	0.041	78	14
Lake Davis	L72	28.82011	-82.28797	0.8	Dec-09	Apr-09	0.1	7.47	4.2	0.054	130	28
Mill Dam Lake	L440	29.17978	-81.83547	2.2	May-09	Apr-09	1.0	6.60	0.68	0.030	2.8	5.2
Lake Catherine	L372	29.06480	-81.83386	3.1	Jul-09	Apr-09	1.0	4.81	1.5	0.069	BDL	4.0
Lake Yale	L96	28.91937	-81.74389	0.8	Jul-09	May-09	1.0	8.14	1.6	0.510	130	22
Lake Kerr	L374	29.35686	-81.80095	2.2	May-09	Apr-09	1.0	5.68	1.2	0.028	BDL	2.2
Lake Thonotosassa	L1790	28.05846	-82.27894	0.2	May-09	May-09	1.0	9.60	1.3	0.120	78	18
Lake Hartridge	L965	28.05174	-81.74613	0.8	Apr-10	Jun-09	0.1	9.43	0.58	0.072	52	7.0
Lake Henry	L29	28.09272	-81.66759	0.6	Oct-08	Oct-08	1.0	6.64	3.8	0.120	5.8	22
Lake Gordon	L24	27.85550	-81.62766	0.4	Nov-08	Nov-08	1.0	5.65	0.22	0.230	3.3	33
Lake Panasoffkee	L1644	28.8065	-82.12954	0.5	Dec-09	Jun-09	0.1	9.42	0.54	0.069	140	8.6
Bonable Lake	L31	29.13827	-82.52339	0.2	Dec-09	May-09	1.0	5.64	5.2	0.130	1.2	5.2
Smith Lake	L999	29.06373	-81.9909	2.6	Dec-09	May-09	1.0	6.44	0.78	0.026	2.3	6.2
Lake George	L1142	29.21389	-81.58574	0.6	Oct-09	Aug-09	1.0	7.27	4.6	0.170	44	24
Lake Hooker	L1755	27.980611	-82.263498	0.1	Jun-10	Mar-10	0.5	6.94	2.7	0.110	28	21
Parrish Lake	L923	27.61008	-82.31187	1.4	Jun-10	Aug-09	1.0	6.88	0.58	BDL	7.2	8.6
Lake Myakka	L79	27.26883	-82.28832	0.6	Feb-10	Dec-08	0.5	7.78	5.8	0.080	40	21
Arrowhead Lake	L91	26.70894	-81.89515	0.7	Apr-10	Feb-09	1.0	9.12	0.60	0.074	97	4.4
Unnamed Lake	L75	27.21826	-80.24818	1.3	Jan-10	Feb-09	1.0	7.42	0.99	0.085	60	14

6.5 Supplemental information

6.5.1 Water quality parameters

Total Hg and MeHg concentrations in the water quality samples were determined at the FDEP Central Laboratory. Procedural blanks run during these analyses were consistently at or below the method detection limit (MDL) both for total Hg (MDL = 0.10 ng/L; mean blank = 0.11 ng/L, 1 s.d. = 0.03 ng/L, n = 21) and MeHg (MDL = 0.022 ng/L; mean blank = 0.022 ng/L, 1 s.d. = 0 ng/L, n = 21). Analytical sample replicates differed by an average of 5.7% relative percent difference in total Hg concentration (n = 22) and an average of 6.2% relative percent difference in MeHg concentration (n = 21).

Total Hg concentrations in 19 of 22 water sampling equipment blanks were below the MDL (mean = 0.15 ng/L, 1 s.d. = 0.14 ng/L, n = 22). Of the three blanks that had concentrations above the MDL, only one was above the practical quantification limit of 0.4 ng/L. MeHg concentrations in 16 of 21 field equipment blanks were below the MDL (mean = 0.026 ng/L, 1 s.d. = 0.014 ng/L, n = 21) and all of the blanks were below the practical quantification limit of 0.088 ng/L.

6.5.2 Supplemental data

Table 6.SI-1 Complete concentration and isotopic data. Lakes from which both sediments and largemouth bass were analyzed are listed first (n = 11); lakes from which only sediments were analyzed are listed below the bold line (n = 9). The number of analyses for the UM-Almadén standard is the total number of analytical sessions from January 2011 to January 2012 and isotope ratios given are averages of the mean value for each session. The number of analyses given for procedural standards is the total number of processed standards and the isotope ratios given are averages of the mean value for each session. Analytical uncertainties for the UM-Almadén standard and procedural standards are 2 s.d. of analytical session averages. Analytical uncertainties for samples are 2 s.d. of multiple analyses within one analytical session.

Standard Name														n	δ^{202}Hg (‰)	2σ (‰)	δ^{201}Hg (‰)	2σ (‰)	δ^{200}Hg (‰)	2σ (‰)	δ^{199}Hg (‰)	2σ (‰)	Δ^{201}Hg (‰)	2σ (‰)	Δ^{200}Hg (‰)	2σ (‰)	Δ^{199}Hg (‰)	2σ (‰)
UM Almadén standard														61	-0.57	0.05	-0.46	0.05	-0.28	0.03	-0.16	0.04	-0.03	0.02	0.01	0.02	-0.02	0.03
NIST SRM 1944 (sediment procedural standard)														6	-0.44	0.12	-0.34	0.08	-0.22	0.05	-0.10	0.04	-0.01	0.05	0.00	0.03	0.01	0.04
CRM DORM-3 (fish procedural standard)														7	0.48	0.15	1.84	0.13	0.32	0.07	1.94	0.06	1.48	0.04	0.08	0.02	1.82	0.06
ERM CE-464 (fish procedural standard)														9	0.68	0.06	2.48	0.03	0.43	0.05	2.57	0.08	1.97	0.03	0.09	0.04	2.40	0.07
Lake Name	**Lake ID**	**Latitude**	**Longitude**	**Month sediment collected**	**Sediment ID**	**Month fish collected**	**Fish ID**	**Fish length (mm)**	**Fish age (yr)**	**Fish sex**	**Total Hg (ng/g)**	**δ^{13}C (‰)**	**δ^{15}N (‰)**	**n**	**δ^{202}Hg (‰)**	**2σ (‰)**	**δ^{201}Hg (‰)**	**2σ (‰)**	**δ^{200}Hg (‰)**	**2σ (‰)**	**δ^{199}Hg (‰)**	**2σ (‰)**	**Δ^{201}Hg (‰)**	**2σ (‰)**	**Δ^{200}Hg (‰)**	**2σ (‰)**	**Δ^{199}Hg (‰)**	**2σ (‰)**
Lake Rousseau	L1557	29.00887	-82.61299	Oct-09	L1557 sed Rep 1						208			2	-1.10	0.21	-1.09	0.20	-0.49	0.13	-0.55	0.16	-0.26	0.04	0.06	0.02	-0.27	0.10
					L1557 sed Rep 2						211			2	-1.11	0.03	-1.08	0.06	-0.50	0.00	-0.57	0.03	-0.25	0.08	0.06	0.02	-0.29	0.04
						Dec-11	1211045 Rep 1	334	no data	M	43.7	-27.0	13.7	2	-0.41	0.06	0.08	0.02	-0.11	0.01	0.51	0.02	0.38	0.06	0.10	0.02	0.61	0.03
							1211045 Rep 2				55.7			2	-0.24	0.01	0.19	0.03	-0.04	0.00	0.49	0.04	0.37	0.02	0.08	0.01	0.55	0.05
							1211046	382	no data	M	204	-26.3	14.0	2	-0.57	0.06	-0.12	0.03	-0.20	0.02	0.40	0.00	0.32	0.02	0.09	0.05	0.54	0.01
							1211047	455	no data	F	163	-26.8	14.3	2	-0.29	0.20	0.21	0.24	-0.06	0.16	0.55	0.14	0.42	0.09	0.09	0.06	0.63	0.09
Little Lake Henderson	L732	28.84820	-82.32872	Oct-09	L732 sed						256			2	-0.69	0.14	-0.40	0.01	-0.27	0.01	-0.11	0.06	0.12	0.10	0.08	0.09	0.07	0.10
						Dec-11	1211048 Rep 1	318	no data	M	499	-26.8	10.9	2	-0.18	0.05	0.55	0.09	0.01	0.09	0.92	0.05	0.69	0.05	0.11	0.07	0.97	0.04
							1211048 Rep 2				412			2	-0.25	0.04	0.48	0.04	-0.02	0.04	0.91	0.05	0.67	0.07	0.10	0.02	0.97	0.04
							1211049	305	no data	M	524	-29.4	11.1	2	-0.26	0.07	0.29	0.03	-0.04	0.01	0.65	0.07	0.48	0.08	0.09	0.05	0.71	0.06
							1211050	345	no data	M	531	-28.0	11.2	2	-0.23	0.01	0.44	0.05	0.00	0.05	0.81	0.04	0.61	0.05	0.11	0.04	0.87	0.04
Lake Davis	L72	28.82011	-82.28797	Dec-09	L72 sed						71.2			2	-0.63	0.02	-0.34	0.04	-0.20	0.02	-0.02	0.02	0.13	0.03	0.12	0.03	0.14	0.03
						Dec-11	1211051	326	no data	F	494	-28.2	10.2	2	-0.43	0.12	0.11	0.16	-0.10	0.05	0.51	0.16	0.43	0.07	0.11	0.01	0.62	0.13
							1211052	406	no data	F	559	-28.5	10.1	2	-0.60	0.01	-0.12	0.07	-0.20	0.10	0.37	0.05	0.33	0.06	0.10	0.10	0.52	0.05
							1211053	420	no data	M	672	-27.8	10.7	2	-0.40	0.02	0.11	0.06	-0.09	0.03	0.47	0.01	0.41	0.07	0.12	0.04	0.57	0.00
Mill Dam Lake	L440	29.17978	-81.83547	May-09	L440 sed						192			2	-0.69	0.02	-0.59	0.05	-0.18	0.05	-0.18	0.01	-0.08	0.04	0.17	0.04	0.00	0.00
						Aug-10	810001	196	1	M	120	-26.9	12.7	2	0.68	0.09	3.00	0.08	0.50	0.10	3.42	0.08	2.49	0.02	0.16	0.14	3.25	0.11
							810005	250	2	F	386	-27.1	13.0	2	0.31	0.04	1.34	0.08	0.31	0.15	1.57	0.10	1.11	0.05	0.15	0.13	1.49	0.09
Lake Catherine	L372	29.06480	-81.83386	Jul-09	L372 sed						214			2	-0.51	0.06	-0.44	0.03	-0.11	0.08	-0.18	0.03	-0.06	0.07	0.15	0.11	-0.05	0.01
						Aug-10	610036	416	5	M	1190	-25.1	13.3	2	0.18	0.11	1.22	0.13	0.25	0.04	1.49	0.03	1.09	0.04	0.16	0.02	1.45	0.06
							710043	187	1	M	562	-30.0	16.0	2	0.63	0.02	2.38	0.07	0.51	0.03	2.59	0.09	1.90	0.05	0.19	0.02	2.43	0.08
							710049 Rep 1	290	4	M	1150	-29.4	16.3	2	0.68	0.03	2.03	0.07	0.53	0.07	2.14	0.14	1.52	0.04	0.19	0.05	1.97	0.13

							710049 Rep 2				1150			2	0.65	0.09	2.01	0.06	0.49	0.11	2.16	0.11	1.52	0.01	0.16	0.07	2.00	0.09
							710049 Rep 3				1090			2	0.59	0.09	1.97	0.09	0.47	0.06	2.13	0.02	1.53	0.16	0.18	0.02	1.98	0.05
Lake Yale	L96	28.91937	-81.74389	Jul-09	L96 sed Rep 1						222			2	-0.51	0.01	-0.26	0.11	-0.10	0.01	0.04	0.03	0.13	0.12	0.15	0.02	0.17	0.03
					L96 sed Rep 2						226			2	-0.60	0.02	-0.32	0.09	-0.15	0.09	-0.05	0.11	0.13	0.08	0.15	0.10	0.10	0.11
						Aug-10	910049	204	1	F	199	-22.0	13.1	2	0.04	0.17	0.42	0.13	0.13	0.02	0.50	0.03	0.39	0.00	0.11	0.07	0.49	0.02
							910051	219	1	M	211	-21.4	14.1	2	-0.01	0.13	0.48	0.16	0.14	0.15	0.60	0.13	0.48	0.06	0.14	0.09	0.60	0.10
							910054 Rep 1	223	1	M	162	-21.7	13.6	2	-0.02	0.24	0.48	0.18	0.14	0.07	0.58	0.13	0.50	0.00	0.16	0.05	0.58	0.07
							910054 Rep 2				168			2	-0.05	0.00	0.45	0.01	0.13	0.04	0.56	0.05	0.49	0.01	0.15	0.04	0.57	0.05
Lake Kerr	L374	29.35686	-81.80095	May-09	L374 sed						148			2	-0.52	0.04	-0.26	0.06	-0.11	0.01	0.17	0.07	0.13	0.03	0.15	0.03	0.30	0.06
						Aug-10	810036 Rep 1	178	1	M	287	-27.8	13.2	2	0.66	0.03	3.61	0.03	0.52	0.03	4.36	0.14	3.11	0.01	0.19	0.01	4.20	0.13
							810036 Rep 2				299			2	0.50	0.10	3.54	0.22	0.43	0.09	4.31	0.27	3.16	0.15	0.18	0.05	4.18	0.25
							810037	193	1	M	192	-28.2	13.1	2	0.65	0.14	3.82	0.09	0.47	0.10	4.60	0.11	3.33	0.02	0.14	0.03	4.43	0.07
Lake Thonotosassa	L1790	28.05846	-82.27894	Jan-10	L1790 sed						123			2	-0.69	0.02	-0.63	0.01	-0.24	0.02	-0.29	0.10	-0.11	0.03	0.11	0.00	-0.11	0.09
						Aug-10	810019 Rep 1	282	1	F	no data	-19.6	7.98	2	-0.24	0.00	-0.07	0.00	-0.06	0.04	0.12	0.02	0.11	0.00	0.06	0.04	0.18	0.02
							810019 Rep 2				72.4			2	-0.14	0.09	-0.02	0.17	0.02	0.04	0.14	0.16	0.09	0.11	0.10	0.00	0.18	0.13
							810023	291	1	M	48.5	-16.9	7.88	2	0.13	0.09	0.25	0.15	0.17	0.06	0.23	0.14	0.15	0.09	0.10	0.02	0.20	0.12
							810026	315	2	M	75.3	-16.2	7.90	2	0.05	0.03	0.29	0.02	0.11	0.00	0.34	0.01	0.25	0.00	0.08	0.01	0.33	0.02
Lake Hartridge	L965	28.05174	-81.74613	Apr-10	L965 sed						161			2	-0.66	0.02	-0.50	0.03	-0.22	0.04	-0.20	0.01	0.00	0.02	0.11	0.03	-0.04	0.01
						Mar-10	309135	311	2	M	181	-21.1	11.0	2	0.17	0.10	1.09	0.16	0.22	0.13	1.30	0.09	0.97	0.09	0.14	0.08	1.26	0.06
							309141	365	4	M	384	-21.9	11.0	2	0.05	0.12	0.89	0.13	0.16	0.15	1.09	0.07	0.85	0.04	0.13	0.09	1.08	0.04
							309142 Rep 1	365	4	M	313	-21.3	10.7	2	0.28	0.05	1.32	0.03	0.23	0.08	1.46	0.04	1.11	0.00	0.09	0.10	1.39	0.03
							309142 Rep 2				294			2	0.13	0.11	1.18	0.14	0.20	0.12	1.41	0.03	1.08	0.06	0.13	0.07	1.38	0.00
Lake Henry	L29	28.09272	-81.66759	Apr-10	L29 sed						307			2	-0.98	0.03	-0.94	0.05	-0.37	0.09	-0.46	0.19	-0.20	0.07	0.12	0.10	-0.22	0.19
						Oct-08	1008237 Rep 1	202	0	F	81.3	-25.3	10.0	2	-0.08	0.03	0.83	0.05	0.08	0.07	1.19	0.03	0.90	0.03	0.12	0.06	1.21	0.04
							1008237 Rep 2				76.2			2	-0.11	0.07	0.78	0.11	0.03	0.01	1.15	0.01	0.86	0.16	0.09	0.02	1.18	0.02
							1008242	260	1	M	233	-23.1	10.4	2	-0.27	0.05	0.23	0.20	-0.01	0.01	0.60	0.02	0.44	0.17	0.12	0.04	0.67	0.03
							1008248	332	3	M	871	-23.5	10.3	2	-0.28	0.05	0.45	0.10	-0.02	0.12	0.91	0.02	0.66	0.14	0.12	0.10	0.97	0.00
Lake Gordon	L24	27.85550	-81.62766	Jun-10	L24 sed						275			2	-0.92	0.15	-0.81	0.08	-0.35	0.10	-0.39	0.09	-0.12	0.03	0.11	0.03	-0.16	0.05
						Nov-08	1108063	223	0	M	226	-19.4	11.2	2	-0.60	0.07	-0.22	0.05	-0.19	0.01	0.21	0.01	0.23	0.10	0.11	0.02	0.36	0.01
							1108067	365	3	M	310	-21.1	10.5	2	-0.43	0.02	0.03	0.02	-0.10	0.08	0.39	0.05	0.35	0.04	0.11	0.09	0.49	0.05
							1108073 Rep 1	421	3	F	301	-22.6	11.2	2	-0.45	0.11	0.00	0.04	-0.13	0.03	0.46	0.09	0.34	0.12	0.10	0.03	0.57	0.06
							1108073 Rep 2				314			2	-0.36	0.12	0.11	0.06	-0.08	0.07	0.54	0.00	0.38	0.03	0.10	0.01	0.63	0.03
Lake Panasoffkee	L1644	28.8065	-82.12954	Dec-09	L1644 sed						69.6			2	-0.81	0.13	-0.50	0.06	-0.28	0.07	-0.09	0.07	0.10	0.04	0.13	0.01	0.11	0.04

Bonable Lake	L31	29.13827	-82.52339	Dec-09	L31 sed			31.3		1	-0.97		-0.78		-0.37		-0.29		-0.06		0.12		-0.04	
Smith Lake	L999	29.06373	-81.9909	Dec-09	L999 sed Rep 1			232		2	-0.46	0.08	-0.45	0.12	-0.07	0.11	-0.17	0.08	-0.10	0.06	0.16	0.07	-0.06	0.06
					L999 sed Rep 2			195		2	-0.53	0.03	-0.51	0.03	-0.07	0.04	-0.15	0.07	-0.12	0.01	0.19	0.03	-0.01	0.07
Lake George	L1142	29.21389	-81.58574	Oct-09	L1142 sed			155		2	-0.97	0.15	-0.82	0.25	-0.45	0.19	-0.28	0.16	-0.09	0.14	0.04	0.11	-0.04	0.12
Lake Hooker	L1755	27.980611	-82.263498	Jun-10	L1755 sed			140		2	-1.19	0.01	-0.98	0.01	-0.49	0.09	-0.39	0.02	-0.08	0.01	0.11	0.09	-0.09	0.02
Parrish Lake	L923	27.61008	-82.31187	Jun-10	L923 sed			65.1		2	-0.51	0.12	-0.51	0.10	-0.15	0.07	-0.26	0.02	-0.13	0.01	0.10	0.01	-0.13	0.01
Lake Myakka	L79	27.26883	-82.28832	Feb-10	L79 sed			97.4		2	-1.12	0.02	-1.01	0.02	-0.49	0.04	-0.44	0.07	-0.17	0.00	0.08	0.02	-0.16	0.08
Arrowhead Lake	L91	26.70894	-81.89515	Apr-10	L91 sed			80		2	-0.46	0.10	-0.39	0.04	-0.15	0.11	-0.14	0.01	-0.05	0.03	0.08	0.06	-0.02	0.04
Unnamed Lake	L75	27.21826	-80.24818	Jan-10	L75 sed			28.9		1	-0.59		-0.56		-0.17		-0.22		-0.12		0.12		-0.08	

6.5.3. Photochemical demethylation calculations

We hypothesize that the observed MIF (expressed as $\Delta^{199}Hg$) in the largemouth bass tissue is due to photochemical demethylation of MeHg in the water column prior to uptake of the remaining MeHg into the food web. We estimated the percent photochemical demethylation in each lake in two ways as described below: 1) using data from Bergquist and Blum (2007) and 2) using calculations made by Point et al. (*1*) and assuming that the magnitude of MIF is affected by the MeHg/DOC ratio in the water column.

1) In the FL lakes the average DOC concentration was 13.5 mg/L (1 s.d. = 9.4 mg/L, n = 20). Using data from photochemical demethylation experiments with 10 mg/L DOC presented by Berquist and Blum (2007), we calculated the expected relationship between $\Delta^{199}Hg$ and the fraction of MeHg remaining in the aqueous system according to:

$$10^3 * \ln[(10^{-3}\Delta^{199}Hg_t + 1)/(10^{-3}\Delta^{199}Hg_i + 1)] = S * \ln(f) \quad (1)$$

where

S = slope (see below)

f = fraction of MeHg remaining in the reactor

$\Delta^{199}Hg_i$ = initial $\Delta^{199}Hg$ value (assume $\Delta^{199}Hg_i = 0$)

$\Delta^{199}Hg_t$ = $\Delta^{199}Hg$ value at a given time

S is calculated by plotting $10^3 * \ln[(10^{-3}\Delta^{199}Hg_t + 1)/(10^{-3}\Delta^{199}Hg_i + 1)]$ versus ln(f) for the relevant photochemical demethylation experiment (*2*). For the 10 mg/L DOC photochemical demethylation experiment, S = -7.82.

To apply this experiment to the FL lakes we then assumed that the measured bulk sediment $\Delta^{199}Hg$ values represent the $\Delta^{199}Hg$ values of MeHg in the sediments prior to

photochemical demethylation in the water column. We calculated the average percent MeHg that was photochemically demethylated in each lake according to:

$$\ln(f) = \{10^3 * \ln[10^{-3}(\Delta^{199}Hg_{avg.fish} - \Delta^{199}Hg_{sediment}) + 1]\}/S \quad (2)$$

The results of these calculations are shown in Table 6.SI-2.

2) We also estimated percent photochemical demethylation of MeHg in these lakes according to calculations made by Point et al. (*1*). Assuming that the ratio of MeHg to DOC affects the magnitude of resulting MIF, Point et al. (2011) extrapolated the experiments conducted by Bergquist and Blum (2007) to lower MeHg/DOC ratios. According to Point et al. (2011), the best-fit fractionation factor for $\Delta^{199}Hg$ was:

$$10^3 \ln\alpha_{\Delta 199Hg} = -8.7 * 0.999985^{(MeHg/DOC)} \quad (3)$$

This fractionation factor can be rearranged to calculate an S for each lake that can be used in Eq. (2) such that:

$$S = 10^3 * (e^{(z/1000)} - 1) \quad (4)$$

where

$$z = 10^3 \ln\alpha_{\Delta 199Hg} = -8.7 * 0.999985^{(MeHg/DOC)}$$

The estimated percent photochemical demethylation of MeHg in the FL lakes based on these calculations are shown in Table 6.SI-2.

References

(1) Point, D.; Sonke, J. E.; Day, R. D.; Roseneau, D. G.; Hobson, K. A.; Vander Pol, S. S.; Moors, A. J.; Pugh, R. S.; Donard, O. F. X.; Becker, P. R.; Methylmercury photodegradation influenced by sea-ice cover in Arctic marine ecosystems. *Nature Geoscience* **2011,** *4*, 188-194.

(2) Bergquist, B. A.; Blum, J. D.; Mass-dependent and mass-independent fractionation of Hg isotopes by photo-reduction in aquatic systems. *Science* **2007,** *318* (5849), 417-420.

Table 6.SI-2 Estimated percent photochemical demethylation of MeHg from FL lakes. Percent photochemical demethylation of MeHg prior to incorporation of the remaining MeHg into the food web was calculated for each lake using two methods as described.

Lake Name	Lake ID	Average fish Δ^{199}Hg (‰)	Sediment Δ^{199}Hg (‰)	1) Percent photochemical demethylation *(based on Bergquist and Blum, 2007)*	2) Percent photochemical demethylation *(based on Point et al., 2011)*
Lake Rousseau	L1557	0.58	-0.28	10.4	9.4
Little Lake Henderson	L732	0.85	0.07	9.5	8.6
Lake Davis	L72	0.57	0.14	5.3	4.8
Mill Dam Lake	L440	2.37	0.00	26.1	23.9
Lake Catherine	L372	1.95	-0.05	22.5	20.6
Lake Yale	L96	0.56	0.14	5.2	4.7
Lake Kerr	L374	4.31	0.30	40.1	37.0
Lake Thonotosassa	L1790	0.24	-0.11	4.4	4.0
Lake Hartridge	L965	1.24	-0.04	15.1	13.7
Lake Henry	L29	0.94	-0.22	13.8	12.5
Lake Gordon	L24	0.48	-0.16	7.9	7.1

CHAPTER 7

Conclusions

Mercury (Hg) has been used for centuries in precious metal extraction, industrial production, and consumer products (e.g., batteries and lighting) (*1*). More recently, the toxicity of Hg and monomethylmercury (MeHg) have become widely recognized. A great deal of scientific research is now devoted to understanding Hg biogeochemical cycling and determining the factors that result in high levels of MeHg in fish species. Until recent decades, many of these studies were plagued by contamination during sample collection or in analytical laboratories. Development of trace metal clean sample collection and processing techniques (such as the "clean hands" method (*2*) and bottle cleaning procedures (*3, 4*)) and Hg-free laboratories has enabled the accurate measurement of very low concentrations of Hg and MeHg in a variety of environmental samples.

Despite the magnitude of research conducted to date, significant gaps exist in our knowledge of Hg biogeochemistry and environmental cycling. Recent advances in multi-collector inductively-coupled plasma mass spectrometry now allow precise measurement of natural abundance Hg stable isotope ratios. As a result of these analytical improvements and advances in techniques to purify and concentrate Hg from samples, the field of Hg isotope geochemistry has expanded significantly over the course of this dissertation. Not only can Hg isotopes be used to trace sources of Hg into the

environment, but they can also be used to better understand biogeochemical processes that result in isotope fractionation. Although many important questions remain, the research presented here adds to our current understanding of Hg biogeochemical cycling.

7.1 Summary of key findings

7.1.1 Methodological advancements

Throughout the course of this dissertation, a number of important advancements have been achieved in sample collection and processing techniques. These improvements are the result of the collaborative efforts of many individuals from the University of Michigan Biogeochemistry and Environmental Isotope Geochemistry Laboratory and the University of Michigan Air Quality Laboratory. We have greatly expanded the types of samples that can be analyzed for Hg isotopes and increased the efficiency with which samples can be processed. These advances will allow future studies to probe new questions by analyzing greater numbers of complex environmental samples.

The study presented in Chapter 2 represents one of the first to measure natural abundance Hg isotopes in water samples. Previous studies employed artificially enriched Hg isotope spikes to trace Hg in aquatic systems (*5*) or high concentrations of Hg in experimental aqueous solutions to observe fractionation (*6*). However, to understand Hg cycling in natural aquatic systems and characterize Hg fractionation during reactions occurring in those systems, it is necessary to measure natural abundance Hg isotope ratios in low concentration water samples. We first developed a purge-and-trap method to release and concentrate Hg from relatively high concentration hydrothermal water samples (*7*). Subsequently, we advanced our techniques to enable concentration and

measurement of Hg isotopes in large volume, very low concentration precipitation samples (e.g., snow and rain) (*8-10*). Using these methods, we are now able to fully recover Hg both in procedural standards and samples. Also, we consistently achieve very low procedural blank concentrations that are due almost entirely to the reagent blank in the oxidizing trap solutions.

We have also developed techniques to collect and analyze total gaseous Hg samples. By pulling ambient air through multiple gold traps with vacuum pumps, we are able to collect enough Hg for duplicate isotopic analyses in a 24 h period. We developed a slow thermal desorption profile to release the Hg from these gold traps and capture it in oxidizing solutions. We are now able to consistently recover Hg from gaseous samples and procedural standards.

Finally, we have improved our ability to release, concentrate, and measure Hg isotopes in solid samples. This process has been iterative and involved developing thermal desorption profiles that result in the slow and complete release of Hg from each sample type. Consistent measurement of Hg concentrations and isotope ratios in procedural standards has allowed us to perfect these methods. We are now able to consistently recover, concentrate, and analyze Hg isotopes in a variety of environmental samples including sediments, rocks, plants, water filters, fish tissues, insects, and human hair and urine.

7.1.2 Mercury stable isotope fractionation

Research presented in this dissertation has helped to identify and characterize a number of processes that cause fractionation of Hg isotopes. First, as described in

Chapter 2, loss of Hg from hydrothermal fluids can cause mass-dependent fractionation (MDF) of Hg isotopes (*7*). We observed that the light isotopes of Hg were preferentially lost from a hydrothermal pool in the Yellowstone Plateau volcanic field as the hydrothermal waters travelled from the vent to the outflow channel. This fractionation was characterized using a Rayleigh-type fractionation model with $^{202/198}\alpha_{r/p} = 1.00059 \pm 0.00016$ (1 s.d.). We hypothesize that this MDF was primarily due to volatilization of $Hg^0_{(g)}$ from the hydrothermal water and secondarily due to co-precipitation of Hg with siliceous sinter.

Second, as observed in Chapter 5, the heavy isotopes of Hg can be preferentially removed prior to the emission of Hg from a coal-fired power plant (*10*). Mercury deposited in precipitation near the large Crystal River, Florida coal-fired power plant exhibited extreme negative δ^{202}Hg values. On the basis of the proximity of the sites to the power plant, meteorological conditions, and estimated speciation of Hg emissions from the power plant, we hypothesize that Hg emitted by the power plant also displayed extreme negative δ^{202}Hg values. Appalachian coal similar to that purchased by the power plant displayed somewhat negative δ^{202}Hg values. We point out that the removal of sulfides with high δ^{202}Hg values prior to combustion would result in coal powder with lower δ^{202}Hg values. Additionally, adsorption of Hg to particles and removal by air pollution control devices may result in the preferential loss of the heavy isotopes of Hg from the flue gas. These processes likely resulted in the extreme negative δ^{202}Hg values observed in Hg emitted by the Crystal River coal-fired power plant.

Third, as described in Chapters 3 and 4, photochemical reduction and loss of Hg from snow can cause a large degree of mass-independent fractionation (MIF), likely as a

result of the magnetic isotope effect (*8*). We conducted a flux chamber experiment in which we exposed surface snow to sunlight and measured the Hg isotopic composition of the snow before and after exposure as well as the isotopic composition of $Hg^0_{(g)}$ that was emitted from the snow. Photochemical reduction of Hg in the surface snow caused the preferential reduction and emission of the odd-mass-number isotopes of Hg as $Hg^0_{(g)}$. This resulted in more negative Δ^{199}Hg values in the snow and a less negative Δ^{199}Hg value in the emitted $Hg^0_{(g)}$. Snowfall, surface snow, and drifted snow samples similarly displayed negative Δ^{199}Hg values and the magnitude of MIF was correlated with the estimated amount of exposure to sunlight for each sample type.

The MIF observed in these samples is especially interesting because it is opposite to that observed during photochemical reduction and loss of Hg from aqueous systems (*6*). Bergquist and Blum (*6*) observed that photochemical reduction of Hg^{2+} from an aqueous solution containing dissolved organic carbon resulted in the preferential retention of the odd-mass-number isotopes of Hg in the solution. In comparison, we observed that the odd-mass-number isotopes were preferentially lost from the surface snow (*8*). This contrast may be due to differences in the composition of oxidized Hg complexes between the aqueous solutions and surface snow. Zheng and Hintelmann (*11*) found that photochemical reduction of Hg by non sulfur-containing organic compounds resulted in the preferential retention of the odd-mass-number isotopes of Hg whereas photochemical reduction of Hg by sulfur-containing organic compounds resulted in the preferential loss of the odd-mass-number isotopes of Hg. They hypothesized that this was due to the generation of radical pairs either in the triplet or singlet state. If radical pairs are generated in the triplet state, triplet to singlet conversion is enhanced by the odd-

mass-number isotopes of Hg and radical pairs that include odd-mass-number isotopes of Hg preferentially recombine and are retained as reactants. In contrast, if radical pairs are generated in the singlet state, singlet to triplet conversion is enhanced by the odd-mass-number isotopes of Hg and the recombination of radical pairs that include odd-mass-number isotopes of Hg becomes spin forbidden. During photochemical reduction reactions, this results in the preferential loss of the odd-mass-number isotopes of Hg as $Hg^0_{(g)}$. It is possible that heterogeneous photochemical reduction reactions in the snow caused radical pairs to be generated in the singlet state. Future research is needed to fully understand the processes resulting in the observed negative MIF in surface snow.

As described in Chapter 5, we have also observed that atmospheric processes can cause MIF of Hg isotopes (*10*). Many of the precipitation samples collected in central Florida displayed positive Δ^{199}Hg values (*10*) that were similar to those observed by Gratz et al. (*12*) in midwestern U.S. precipitation. We hypothesize that photochemical reduction of Hg in cloud droplets may result in the preferential loss of the odd-mass-number isotopes of Hg from the droplets. In addition, many of the precipitation samples collected in Florida and in the midwestern U.S. displayed small positive MIF of ^{200}Hg (*10, 12*). Neither of the mechanisms currently proposed to cause MIF of Hg isotopes (the magnetic isotope effect and the nuclear volume effect) are expected to cause measureable MIF of the even-mass-number isotopes of Hg. It is possible that photochemical self-shielding during atmospheric reactions may play a role in producing MIF of ^{200}Hg (*13, 14*) but further experiments are necessary to understand this phenomenon.

Fourth, as described in Chapter 6, we observed that photochemical demethylation of MeHg in freshwater lakes causes the preferential retention of the odd-mass-number

isotopes of Hg (as MeHg) in the water column (*15*). Bergquist and Blum (*6*) observed that photochemical demethylation of MeHg from an aquatic solution containing dissolved organic carbon resulted in increasingly positive Δ^{199}Hg values in the solution. They hypothesized that this MIF signature was retained and preserved during bioaccumulation through the aquatic food web. We found that light penetration depth in freshwater lakes of central Florida was correlated with Δ^{199}Hg values measured in largemouth bass from the same lakes. These data support the hypothesis that the magnitude of MIF in fish is controlled by the magnitude of photochemical demethylation of MeHg prior to incorporation of the remaining MeHg into the pelagic food web.

Throughout this dissertation, measurement of natural abundance Hg stable isotopes has enabled the characterization of Hg fractionation during environmentally relevant processes. Specifically, we have found that photochemical processes on snow crystals, in aqueous environments, and in the atmosphere can cause significant MDF and MIF of Hg isotopes. It is likely that future studies will continue to use measurement of Hg isotope fractionation to better understand the chemical reactions that control Hg biogeochemical cycling.

7.1.3 Sources and fate of atmospherically deposited Hg

In addition to building greater understanding of the processes that cause Hg fractionation, we have begun to characterize the isotopic composition of Hg emissions and investigated the fate of atmospherically deposited Hg. It is important to note that Hg deposition at a given location is the result of emissions from natural and anthropogenic sources at local, regional, and global scales. A number of factors including local and

regional meteorology, proximity to sources, types of sources, speciation of emissions, and presence of atmospheric oxidants can impact the relative percentage of Hg deposition at a given location that is derived from local, regional, and global sources.

As described in Chapter 2, emissions of $Hg^0_{(g)}$ from hydrothermal systems may be characterized by negative δ^{202}Hg values and slightly positive Δ^{199}Hg values (*7*). Zambardi et al. (*16*) similarly found that emissions of $Hg^0_{(g)}$ from a volcanic fumerole displayed negative δ^{202}Hg values. Although these data are from a limited number of locations, they suggest that natural emissions of $Hg^0_{(g)}$ from volcanic environments may display negative δ^{202}Hg values.

In Polar Regions, Hg deposited during atmospheric mercury depletion events (AMDEs) that remains in the snow until snowmelt likely displays highly negative Δ^{199}Hg values (*8*). If this Hg enters waterbodies and additional MIF does not occur prior to uptake into the food web, this isotopic signature may be preserved in fish and piscivorous mammals. However, as observed in Chapter 4, some of the Hg that is photochemically reduced and lost from the snowpack is reoxidized and captured by nearby ice crystals (*9*). These ice crystals form a complementary isotopic reservoir of Hg. It is possible that Hg remaining in the snow (with negative Δ^{199}Hg values) mixes with Hg in ice crystals (with positive Δ^{199}Hg values) during spring snowmelt. As a result, depending on the mass balance, Hg that is exported to aquatic systems may not display the distinct negative Δ^{199}Hg values observed in surface snow.

Finally, as described above and in Chapter 5 (*10*), the isotopic composition of locally deposited Hg emitted by coal-fired power plants can be isotopically distinct. Biswas et al. (*17*) observed that coal from different regions displayed an approximately

3‰ range in δ^{202}Hg values and suggested that the isotopic composition of emissions from coal-fired power plants could be unique depending on the coal that was combusted. Data presented in Chapter 5 supports this hypothesis. It may be possible for future studies to use the distinct isotopic signature of Hg emitted by coal-fired power plants to quantify local deposition of those emissions. If this becomes possible, Hg isotopes may ultimately be used to enforce or evaluate the effectiveness of Hg emissions regulations such as the new 2011 Mercury and Air Toxics Standards. In addition, if anthropogenic emissions of Hg from different point sources are isotopically distinct, Hg isotopes could be used to better quantify the impact of those emissions on local and regional deposition. This information could be used to better inform new, more effective Hg emissions regulations.

As a follow-up, in Chapter 6 (*15*) we investigated whether the distinct negative δ^{202}Hg values observed in precipitation near the Crystal River, Florida power plant could be used to trace Hg emissions into local fish populations. However, we did not observe any evidence of the extreme negative δ^{202}Hg values in largemouth bass collected from lakes in close proximity to the power plant. Instead, we found that MeHg in the fish was primarily derived from Hg accumulated in lake sediments and that the fish isotopic compositions were influenced by fractionation in the sediments and water column. We suggest that the distinct signature of Hg emitted by the power plant was obscured as a result of mixing with previously deposited Hg in the sediments. These results may have important implications for regulatory assessment and future monitoring studies. Especially in lakes fed by large watersheds, previously deposited Hg can inflow into the lake long after it is deposited from the atmosphere and continuously add to the reservoir of Hg in the sediments that is available for methylation. In these lakes, declines in fish

MeHg concentrations may be prolonged for decades to centuries after Hg deposition reductions occur. Therefore, it is important to consider lake physical characteristics and fish physiology when choosing locations and species as biomonitors to assess the impact of Hg emissions regulations.

7.2 Future work

The research described in this dissertation raises a number of scientifically interesting and important questions that may be addressed by future studies. Specifically, several of the chapters describe Hg fractionation observed in environmental samples, but future work is needed to fully understand the processes and mechanisms resulting in this fractionation. Additionally, we present evidence that anthropogenic sources of Hg can be isotopically distinct. It may ultimately be possible to use Hg isotopes to quantify the amount of local Hg deposition that results from a given point source. However, significant additional research is needed to enable the use of Hg isotopes to meaningfully inform Hg emissions regulations and assess the effectiveness of such policies.

Measurement of Hg isotopes in atmospheric samples may enable greater understanding of atmospheric Hg chemistry and enable the fingerprinting of Hg that is emitted to the atmosphere and transported to deposition sites. Field studies could be coupled with experimental studies and atmospheric chemistry models to understand the relative importance and expected impact of atmospheric reactions on Hg isotopes. This multi-faceted approach could also elucidate the relative importance of different oxidants in global atmospheric Hg cycling. This information could be used to significantly improve the accuracy of Hg transport and deposition models.

Continued research is also needed to characterize the isotopic composition of dry deposited Hg. Both reactive gaseous Hg and fine particulate Hg can be dry deposited but this deposition is very difficult to collect and quantify. Although dry deposition may represent a significant flux of Hg in certain locations, atmospheric Hg models often are unable to estimate its magnitude without unacceptably large uncertainties. It is possible that future studies could use Hg stable isotopes to characterize and better understand the atmospheric reactions that produce dry deposited Hg species. Additionally, if the isotopic composition of this Hg is distinct, Hg isotopes could be used to quantify dry deposition. This research will require the development of methods to successfully capture sufficient quantities of dry deposited Hg without inducing secondary fractionation.

Experimental studies are needed to understand the processes that control the isotopic composition of Hg emitted from anthropogenic point sources such as coal-fired power plants. This information, in turn, may enable the isotopic fingerprinting of Hg emitted by a variety of sources and could ultimately play a role in the enforcement of emissions regulations. We hypothesize in Chapter 5 that the isotopic composition of the original coal, coal cleaning processes, and removal of Hg by air pollution control devices caused the emission of isotopically distinct Hg from a coal-fired power plant. However, we cannot quantify the amount of local Hg deposition that results from these emissions, and we cannot determine whether the observed distinct isotopic signature would be observed in Hg emissions from other coal-fired power plants. Laboratory combustion experiments using coal of known isotopic composition and mock air pollution control devices (e.g., in-line carbon addition and a particle removal system) could be used to

determine the effects of these systems on the isotopic composition of Hg emissions. In addition, combustion of coal of known isotopic composition at a full-scale test power plant and isotopic analysis of the emitted Hg would help to constrain in-system fractionation. This research is necessary in order to expand our findings to other locations and to quantitatively assess the impact of coal combustion on local Hg deposition.

Finally, future studies may use the data presented in this dissertation to begin to trace Hg from natural and anthropogenic sources into sensitive ecosystems. It may be possible to use MIF of Hg isotopes to trace AMDE-deposited Hg into Arctic ecosystems. As discussed previously, this may be complicated both by the retention of $Hg^0_{(g)}$ emitted from the surface snow on nearby ice crystals (*9*) and by photochemical processes in waterbodies (*18*). It may also be possible to trace emissions from anthropogenic sources to local deposition sites and into aquatic ecosystems using Hg isotopes. As demonstrated in Chapter 6, it is possible to use Hg isotopes to determine whether high Hg concentrations in aquatic organisms are the result of recent atmospheric deposition or methylation of accumulated Hg in lake sediments. Further research is needed to determine the relevance of these findings to other locations with different lake and watershed characteristics.

The field of Hg stable isotope geochemistry has expanded rapidly over the course of this dissertation. As Hg purification and analytical techniques are further refined, Hg stable isotopes may become widely utilized in Hg biogeochemical studies. It is likely that Hg isotopes will be used to better understand Hg atmospheric chemistry, including the oxidation/reduction reactions that control the lifetime of Hg in the atmosphere. It is

also likely that Hg isotopes will be used to better understand Hg bioaccumulation, to determine the sources of MeHg to freshwater and marine fish, and to better understand the pathways of human exposure to MeHg. Finally, it is possible that Hg isotopes may be used as a tool to enforce Hg emissions regulations and to determine the effectiveness of those regulations in decreasing local deposition of Hg and reducing concentrations of MeHg in aquatic organisms. Along with studies by many others, research presented in this dissertation has helped to lay the groundwork for this important future research.

References

(1) Fitzgerald, W. F.; Lamborg, C. H., Geochemistry of Mercury in the Environment. In *Treatise on Geochemistry 9*, Holland, H. D., and Turekian, K.K., Ed. Elsevier Oxford, **2003**; Vol. 9, pp 107-148.

(2) U.S. Environmental Protection Agency, *Method 1669: Method for sampling ambient water for the determination of metals at EPA ambient criteria levels*. Office of Water, Office of Science and Technology, Engineering and Analysis Division: Washington, D.C., **1996**.

(3) Hammerschmidt, C. R.; Bowman, K. L.; Tabatchnick, M. D.; Lamborg, C. H.; Storage bottle material and cleaning for determination of total mercury in seawater. *Limnol. Oceanogr. Methods* **2011,** *9*, 426-431.

(4) Landis, M. S.; Keeler, G. J.; Critical evaluation of a modified automatic wet-only precipitation collector for mercury and trace element determinations. *Environ. Sci. Technol.* **1997,** *31*, 2610-2615.

(5) Harris, R. C.; Rudd, J. W. M.; Amyot, M.; Babiarz, C. L.; Beaty, K. G.; Blanchfield, P. J.; Bodaly, R. A.; Branfireun, B. A.; Gilmour, C. C.; Graydon, J. A.; Heyes, A.; Hintelmann, H.; Hurley, J. P.; Kelly, C. A.; Krabbenhoft, D. P.; Lindberg, S. E.; Mason, R. P.; Paterson, M. J.; Podemski, C. L.; Robinson, A.; Sandilands, K. A.; Southworth, G. R.; St. Louis, V. L.; Tate, M. T.; Whole-ecosystem study shows rapid fish-mercury response to changes in mercury deposition. *Proceedings of the National Academy of Sciences* **2007,** *104* (42), 16586-16591.

(6) Bergquist, B. A.; Blum, J. D.; Mass-dependent and mass-independent fractionation of Hg isotopes by photo-reduction in aquatic systems. *Science* **2007,** *318* (5849), 417-420.

(7) Sherman, L. S.; Blum, J. D.; Nordstrom, D. K.; McCleskey, R. B.; Barkay, T.; Vetriani, C.; Mercury isotopic composition of hydrothermal systems in the Yellowstone Plateau volcanic field and Guaymas Basin sea-floor rift. *Earth. Planet. Sci. Lett.* **2009,** *279*, 86-96.

(8) Sherman, L. S.; Blum, J. D.; Johnson, K. P.; Keeler, G. J.; Barres, J. A.; Douglas, T. A.; Mass-independent fractionation of mercury isotopes in Arctic snow driven by sunlight. *Nature Geoscience* **2010,** *3* (3), 173-177.

(9) Sherman, L. S.; Blum, J. D.; Douglas, T. A.; Steffen, A.; Frost flowers growing in the Arctic ocean-atmosphere-sea ice-snow interface: 2. Mercury exchange between the atmosphere, snow, and frost flowers. *Journal of Geophysical Research* **2012,** *117*, D00R10.

(10) Sherman, L. S.; Blum, J. D.; Keeler, G. J.; Demers, J. D.; Dvonch, J. T.; Investigation of local mercury deposition from a coal-fired power plant using mercury isotopes. *Environ. Sci. Technol.* **2012,** *46* (1), 382-390.

(11) Zheng, W.; Hintelmann, H.; Isotope fractionation of mercury during its photochemical reduction by low-molecular-weight organic compounds. *J. Phys. Chem. A* **2010,** *114* (12), 4246-4253.

(12) Gratz, L. E.; Keeler, G. J.; Blum, J. D.; Sherman, L. S.; Isotopic composition and fractionation of mercury in Great Lakes precipitation and ambient air. *Environ. Sci. Technol.* **2010,** *44*, 7764-7770.

(13) Mead, C.; Anbar, A. D.; Lyons, J. R.; Johnson, T. M. *Mass-independent fractionation of mercury isotopes in compact fluorescent light bulbs*, Amercian Geophysical Union, Fall Meeting, San Francisco, CA, **2010**.

(14) Navon, O.; Wasserburg, G. J.; Self-shielding in O_2--a possible explanation for oxygen isotopic anomalies in meteorites? *Earth. Planet. Sci. Lett.* **1985,** *73* (1), 1-16.

(15) Sherman, L. S.; Blum, J. D.; Mercury stable isotopes in sediments and largemouth bass (*Micropterus salmoides*) from Florida lakes. *Science of the Total Environment***, in review**.

(16) Zambardi, T., Sonke, J.E., Toutain, J.P., Sortino, F., Shinohara, H.; Mercury emissions and stable isotopic compositions at Vulcano Island (Italy). *Earth Planet. Sci. Lett.* **2008,** *277*, 236-243.

(17) Biswas, A.; Blum, J. D.; Bergquist, B. A.; Keeler, G. J.; Zhouqing, X.; Natural mercury isotope variation in coal deposits and organic soils. *Environ. Sci. Technol.* **2008,** *42* (22), 8303-8309.

(18) Point, D.; Sonke, J. E.; Day, R. D.; Roseneau, D. G.; Hobson, K. A.; Vander Pol, S. S.; Moors, A. J.; Pugh, R. S.; Donard, O. F. X.; Becker, P. R.; Methylmercury photodegradation influenced by sea-ice cover in Arctic marine ecosystems. *Nature Geoscience* **2011,** *4*, 188-194.